frontiers | Research Topics

Carbon-water-nitrogen processes and mechanisms of agricultural and forest ecosystems under future climate change

Edited by
Yunpu Zheng, Haoran Zhou, Qingpeng Yang and Ming Xu

Published in
Frontiers in Plant Science
Frontiers in Forests and Global Change

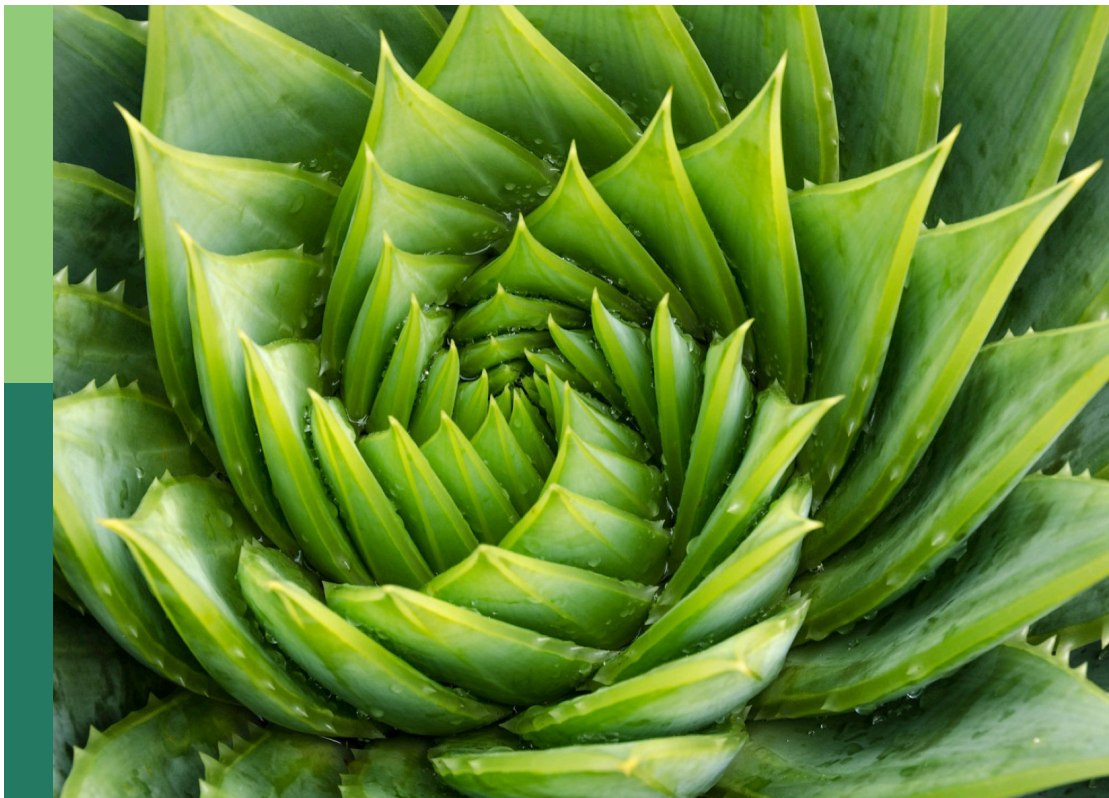

ISSN 1664-8714
ISBN 978-2-8325-4941-4
DOI 10.3389/978-2-8325-4941-4

About Frontiers

Frontiers is more than just an open access publisher of scholarly articles: it is a pioneering approach to the world of academia, radically improving the way scholarly research is managed. The grand vision of Frontiers is a world where all people have an equal opportunity to seek, share and generate knowledge. Frontiers provides immediate and permanent online open access to all its publications, but this alone is not enough to realize our grand goals.

Frontiers journal series

The Frontiers journal series is a multi-tier and interdisciplinary set of open-access, online journals, promising a paradigm shift from the current review, selection and dissemination processes in academic publishing. All Frontiers journals are driven by researchers for researchers; therefore, they constitute a service to the scholarly community. At the same time, the *Frontiers journal series* operates on a revolutionary invention, the tiered publishing system, initially addressing specific communities of scholars, and gradually climbing up to broader public understanding, thus serving the interests of the lay society, too.

Dedication to quality

Each Frontiers article is a landmark of the highest quality, thanks to genuinely collaborative interactions between authors and review editors, who include some of the world's best academicians. Research must be certified by peers before entering a stream of knowledge that may eventually reach the public - and shape society; therefore, Frontiers only applies the most rigorous and unbiased reviews. Frontiers revolutionizes research publishing by freely delivering the most outstanding research, evaluated with no bias from both the academic and social point of view. By applying the most advanced information technologies, Frontiers is catapulting scholarly publishing into a new generation.

What are Frontiers Research Topics?

Frontiers Research Topics are very popular trademarks of the *Frontiers journals series*: they are collections of at least ten articles, all centered on a particular subject. With their unique mix of varied contributions from Original Research to Review Articles, Frontiers Research Topics unify the most influential researchers, the latest key findings and historical advances in a hot research area.

Find out more on how to host your own Frontiers Research Topic or contribute to one as an author by contacting the Frontiers editorial office: frontiersin.org/about/contact

Carbon-water-nitrogen processes and mechanisms of agricultural and forest ecosystems under future climate change

Topic editors

Yunpu Zheng — Hebei University of Engineering, China

Haoran Zhou — Tianjin University, China

Qingpeng Yang — Institute of Applied Ecology, Chinese Academy of Sciences (CAS), China

Ming Xu — Beijing Normal University, Zhuhai, China

Citation

Zheng, Y., Zhou, H., Yang, Q., Xu, M., eds. (2024). *Carbon-water-nitrogen processes and mechanisms of agricultural and forest ecosystems under future climate change*. Lausanne: Frontiers Media SA. doi: 10.3389/978-2-8325-4941-4

Table of contents

frontiers | Frontiers in Plant Science

TYPE Editorial
PUBLISHED 15 May 2024
DOI 10.3389/fpls.2024.1423506

OPEN ACCESS

EDITED AND REVIEWED BY
Sebastian Leuzinger,
Auckland University of Technology, New Zealand

*CORRESPONDENCE
Yunpu Zheng
zhengyunpu@hebeu.edu.cn
Ming Xu
91122020071@bnu.edu.cn

RECEIVED 26 April 2024
ACCEPTED 06 May 2024
PUBLISHED 15 May 2024

CITATION
Zheng Y, Yang Q, Zhou H and Xu M (2024) Editorial: Carbon-water-nitrogen processes and mechanisms of agricultural and forest ecosystems under future climate change. *Front. Plant Sci.* 15:1423506. doi: 10.3389/fpls.2024.1423506

Editorial: Carbon-water-nitrogen processes and mechanisms of agricultural and forest ecosystems under future climate change

Yunpu Zheng[1]*, Qingpeng Yang[2], Haoran Zhou[3] and Ming Xu[4,5]*

[1]School of Water Conservancy and Hydropower, Hebei University of Engineering, Handan, Hebei, China, [2]Institute of Applied Ecology, Chinese Academy of Sciences (CAS), Shenyang, China, [3]School of Earth System Science, Institute of Surface-Earth System Science, Tianjin University, Tianjin, China, [4]BNU-HKUST Laboratory for Green Innovation, Advanced Institute of Natural Sciences, Beijing Normal University at Zhuhai, Zhuhai, China, [5]Guangdong-Hong Kong Joint Laboratory for Carbon Neutrality, Jiangmen Laboratory of Carbon Science and Technology, Jiangmen, China

KEYWORDS

global change, plant growth, carbon sequestration, crop yield, carbon budget, ecosystem structure and function, ecological process models

Editorial on the Research Topic

Carbon-water-nitrogen processes and mechanisms of agricultural and forest ecosystems under future climate change

It is well known that agricultural and forest ecosystems serve as vital carbon sinks in terrestrial ecosystems. Understanding the fundamental processes and mechanisms of ecosystem carbon cycles in face of climate change is critical for quantifying the carbon sinks of terrestrial ecosystems. Ecosystem carbon cycles cannot be separated from water and nitrogen cycles and thus the response and adaptation of carbon-water-nitrogen processes in agricultural and forest ecosystems to climate change demand further studies. This research topic published 10 papers to gain novel insights into the underlying mechanisms and processes of carbon-water-nitrogen interactions in agricultural and forest ecosystems in response to climate change.

Litter decomposition is a pivotal biogeochemical process, which profoundly influences carbon and nitrogen cycling in forest and grassland ecosystems. Climatic factors can significantly impact litter decomposition rates, carbon sequestration, and the emissions of greenhouse gases such as CO_2 and N_2O. Liu et al. conducted a comprehensive meta-analysis of 351 samples from 37 published studies to explore the interactive effects of solar radiation and precipitation on litter decomposition and CO_2 emission on a global scale. They found that the solar radiation significantly increased litter decomposition which was dependent on precipitation regimes. Meanwhile, Li et al. investigated the effects of warming and reclamation on N_2O emission flux through a long-term manipulative warming experiment on the Qinghai-Tibetan Plateau. Their results demonstrated that reclamation amplified the warming effects on N_2O emissions by enhancing soil nitrification and related

enzymatic activities in alpine meadows. Additionally, Lin et al.examined the long-term spatiotemporal variations in aboveground carbon sequestration rates in the eastern Tibetan Plateau using a forest landscape model under different climate change scenarios. Their study highlighted the variability in aboveground carbon sequestration rates across various forest types in response to climate warming.

The escalating frequency and duration of drought events under climate change have prompted heightened scrutiny of their impacts on temporal and spatial variations in evapotranspiration and water use efficiency. Yang et al. analyzed the inter-annual variations of evapotranspiration with eddy covariance fluxes in an urban forest in Beijing, China, revealing that spring and mid-summer droughts primarily drove inter-annual variations in evapotranspiration due to the reduced stomatal conductance. Furthermore, Xu et al. employed the ensemble empirical mode decomposition method to investigate spatial variations and mechanisms influencing the stability of water use efficiency in China. Their findings explored the role of precipitation and soil moisture in promoting stable water use efficiency, with unstable trends primarily driven by positive or negative reversals. In addition, Jiang et al. presented an in-depth analysis of the impact of seasonal drought on root distribution and water utilization patterns of forests in south China. Their findings highlighted the critical role of deep fine roots in utilizing deep soil water during the dry season, constituting a substantial portion of total water consumption.

Leaf photosynthesis, reliant on both photochemical and carboxylation processes, is central to terrestrial carbon fluxes. Accurate estimation of photochemical parameters and maximum carboxylation rates is essential for predicting carbon fluxes of terrestrial ecosystems. The article by Liu et al. found that the inferred values of the photochemical redox parameters varied with leaf macronutrient contents. The work of Li et al. evaluated the relationships between the leaf maximum rate of carboxylation and both leaf N_{area} and photosynthetic pigments of winter wheat in a farmland ecosystem in China. One of the study's notable findings was the strongest correlation between leaf V_{cmax} and leaf Chl_{area}. Their findings suggest that photosynthetic pigment content serves as a predictor for estimating V_{cmax}, offering a novel approach for spatially continuous V_{cmax} estimation and enhancing simulation accuracy in ecological models.

In addition to the above articles from field studies, two papers elucidated the mitigated effects of elevated CO_2 concentrations on environmental stressors such as drought and nutrient deficiency. Based on manipulative experiment with environmental growth chambers, Chang et al. examined the effects of elevated CO_2 concentration and temperature on plant growth and leaf gas exchange of winter wheat along a soil water gradient, and found that elevated CO_2 concentration substantially enhanced leaf photosynthesis by about 30% under water deficiency, suggesting the negative impacts of water deficiency on winter wheat might be partially mitigated by elevated CO_2 concentration. Li et al.reported findings that the plant growth and leaf photosynthesis of annual ryegrass under phosphorus deficiency were enhanced by elevated CO_2 concentration, indicating the impacts of phosphorus deficiency on annual ryegrass may be alleviated by elevated CO_2 concentration under climate change.

This research topic presents the latest studies on how climate change affects the carbon-water-nitrogen processes of agricultural and forest ecosystems. Meanwhile, this research topic highlights the importance and uncertainty of ecosystem functioning in response to climate change. Therefore, fully exploring the potential mechanisms and processes of agriculture and forests to climate change is pivotal to projecting the potential risk of climate change on global grain yield and forest carbon sequestrations.

Author contributions

YZ: Writing – original draft, Writing – review & editing. QY: Writing – review & editing. HZ: Writing – review & editing. MX: Writing – original draft, Writing – review & editing.

Funding

The author(s) declare financial support was received for the research, authorship, and/or publication of this article. Ming Xu was supported by the Special Fund for Science and Technology Innovation Strategy of Guangdong Province, China under Grant No. 2022660500250009604.

Acknowledgments

The editors would like to thank the authors, reviewers, and the Frontiers in Plant Science team, whose efforts have led to the success of this Research Topic.

Conflict of interest

The authors declare that the research was conducted in the absence of any commercial or financial relationships that could be construed as a potential conflict of interest.

Publisher's note

frontiers | Frontiers in Plant Science

TYPE Original Research
PUBLISHED 23 March 2023
DOI 10.3389/fpls.2023.1162160

OPEN ACCESS

EDITED BY
Yunpu Zheng,
Hebei University of Engineering, China

REVIEWED BY
Ruichang Shen,
Nanchang University, China
Gang Fu,
Institute of Geographic Sciences and Natural Resources Research (CAS), China

*CORRESPONDENCE
Hasbagan Ganjurjav
ganjurjav@foxmail.com

SPECIALTY SECTION
This article was submitted to Functional Plant Ecology, a section of the journal Frontiers in Plant Science

RECEIVED 09 February 2023
ACCEPTED 08 March 2023
PUBLISHED 23 March 2023

CITATION
Li Z, Li Y, Hu G, Wu H, Liang Y, Yan J, He S, Ganjurjav H and Gao Q (2023) Reclamation intensifies the positive effects of warming on N_2O emission in an alpine meadow. *Front. Plant Sci.* 14:1162160. doi: 10.3389/fpls.2023.1162160

Reclamation intensifies the positive effects of warming on N_2O emission in an alpine meadow

Zheng Li[1,2], Yan Li[3], Guozheng Hu[1,2], Hongbao Wu[4], Yan Liang[5], Jun Yan[6], Shicheng He[6], Hasbagan Ganjurjav[1,2]* and Qingzhu Gao[1,2]

[1]Institute of Environment and Sustainable Development in Agriculture, Chinese Academy of Agricultural Sciences, Beijing, China, [2]National Agricultural Experimental Station for Agricultural Environment, Nagqu, China, [3]Tianjin Meteorological Bureau, Tianjin, China, [4]College of Resource and Environment, Anhui Science and Technology University, Fengyang, China, [5]Ordos Foresry and Grassland Science Institute, Ordos, China, [6]Nagqu Grassland Station, Nagqu, China

Climatic warming can alter grassland nitrous oxide (N_2O) emissions due to soil property alterations. However, how the reclamation affect grassland N_2O flux under warming conditions remains unclear in alpine meadow ecosystems. We conducted a long-term manipulative warming experiment in a natural alpine meadow and a cultivated grassland on the Qinghai-Tibetan Plateau to explore the separate and interactive effects of warming and reclamation on the soil N_2O emission flux. N_2O fluxes were measured under four treatments including control (CK), warming (W), reclamation (R) and warming under reclamation (WR) from August 2018 to July 2019. We measured the content of soil C, N nutrients and 5 enzymatic activities in 2018 and 2019. Correlation analysis and structural equation modeling were used to clarify how soil N availability and soil enzyme activities affect N_2O emission. Our results indicated that compared to the ambient conditions for the growing and non-growing seasons, soil N_2O flux was significantly increased 59.1% and 152.0% by warming and 28.4% and 142.4% by reclamation, respectively. Compared with W, WR significantly increased N_2O flux by 18.9% and 81.1% during the growing and non-growing seasons, respectively. Soil moisture was negatively correlated to enzymatic activity and N_2O flux. Both warming and reclamation promoted soil nitrification by increasing related enzymatic activities that acted to increase the N_2O flux. Reclamation resulted in a greater sensitivity of the activity of ammonia monooxygenase and hydroxylamine oxidoreductase to warming, thus enhancing the effects of warming on increasing the N_2O flux. Our research indicated that reclamation can additionally increase the effects of warming on N_2O emissions for alpine meadows. Therefore, excessive expansion of arable land should be avoided, and new reclamation sites should be planned scientifically, as warming is expected to intensify in the future.

KEYWORDS

warming, reclamation, alpine meadows, Qinghai-Tibet Plateau, Nitrous Oxide

1 Introduction

Terrestrial ecosystems account for 70% of the global N_2O production (Barnard et al., 2005) and in particular, grasslands cover 35% of the world's land area (Dubois, 2011) and are a primary source of this gas that is released into the atmosphere. Grasslands are facing the dual pressure of warming and reclamation and these changes can affect soil N_2O emissions by altering soil nutrition, temperature, moisture and microbes (Contosta et al., 2011; Abraha et al., 2018).

Warming can alter soil N availability (Elrys et al., 2021; Li et al., 2022a) and associated enzymatic activities (Rich et al., 2003; Wendeborn, 2020) as well as nitrification and denitrification processes. Generally, warming can accelerate soil N cycling, and this results in increased N_2O flux. Warming also increases turnover of soil N and soil microbe activities in ice land grasslands (Séneca et al., 2021) and this increases N loss as N_2O (Robertson and Groffman, 2007). In the Qinghai-Tibetan Plateau (QTP), the annual N_2O flux for the alpine meadows increases gradually with temperature due to the direct positive effects of warming on soil microorganisms and enzymes (Du et al., 2016). However, other studies have reported that warming did not increase N availability and N_2O emissions. For example, a meta-analysis about soil carbon and nitrogen dynamics on the Tibetan Plateau reported insignificant response of soil $NH_4^+ - N$ to warming in the grassland (Zhang et al., 2015). Moreover, a recent study suggested that warming decreased the soil moisture in a relatively wet soil and probably increased O_2 concentrations thereby inhibiting N_2O production through denitrification in an alpine meadow (Wang J. et al., 2021). In contrast, warming did not significantly affect N_2O emission during the first and the second growing season, but stimulated N_2O uptake in the third growing season in a tundra ecosystem on the Chinese Changbai Mountain (Zhou et al., 2016).

Reclamation is a common approach for degraded grassland restoration or forage production and this practice alters soil N and moisture content and soil N_2O emissions (Buchen et al., 2018). Firstly, ploughing increases N input from mineralization of the organic N in plant litter resulting in increased N_2O emission (Drewer et al., 2017). Secondly, minimum tillage increases soil N_2O by increasing soil water-holding capacity that results a decrease in aerobic soil conditions that favors denitrification (Krol et al., 2016). Thirdly, plowing can increase soil pore spaces and air permeability and release trapped gases in soil pore spaces thus increasing soil N_2O flux (Ball et al., 1999; Heincke and Kaupenjohann, 1999). Finally, soil organic matter mineralization can be promoted by reclamation *via* increased soil oxygen consumption thereby again favoring denitrification (Li et al., 2007). For example, a study of 3 Canadian Arctic ecosystems suggested the consumption of soil organic matter facilitated denitrification resulting in increased N_2O production (Paré and Bedard-Haughn, 2013).

The Qinghai–Tibetan Plateau (QTP) is called the "third pole" of the world (Qiu, 2008) due to its high altitude and coldness. The alpine meadow serves as a dominant ecosystem in the QTP (Wang et al., 2014) and an important reservoir of N_2O emissions (Hu et al., 2010). Climate warming has profoundly affected the QTP where air temperature has reached 0.25°C per decade (Yao et al., 2019). The shortage of animal forage and grassland degradation has driven the conversion of some alpine meadows into cultivated grasslands for forage (Gao et al., 2019) and the numbers of converted meadows have dramatically increased in high altitude locations over the recent decades (Yang et al., 2015). There have been numerous recent studies documenting how warming affects N_2O emission flux in the growing season for these areas (Zhu et al., 2015; Chen et al., 2017; Zhao et al., 2017; Wang J. et al., 2021). However, the interactions of warming and reclamation on the soil N_2O emission flux remains unclear.

We used open-top chambers (OTC) to perform a long-term manipulative experiment in a cultivated grassland and a natural alpine meadow on the QTP. We aim to explore whether there are interactive effects of warming and reclamation on grassland N_2O emission and to clarify how soil N availability and soil enzyme activities regulate the responses of N_2O emission to warming and reclamation. We hypothesized that (1) warming and reclamation can affect soil nutrients and increase nitrification enzyme activity to promote N_2O flux; (2) there are significant positive interactions between warming and reclamation on soil N_2O flux.

2 Materials and methods

2.1 Study site

Our experiment was started at 2011 in the Nagqu National Observation and Experimental Station for Agricultural Environment (31.441°N, 92.017°E; 4460 m above sea level), Tibet Autonomous Region, China. The data from the China Meteorological Data Sharing Service System indicated the mean annual temperature (-0.6°C) and the mean annual precipitation (457.6 mm) from 1980 to 2011 in this region. Here, the sedge *Kobresia pygmaea* dominates the alpine meadow as a main grassland type. *Elymus nutans* was used to build cultivated grassland in 2011, when we just plowed the soil of alpine meadow and planted the seeds of *Elymus nutans* without any fertilizer. All the experimental sites were fenced in 2010 and there were no activities of grazing, fertilization or mowing during the experimental period.

2.2 Experiment design

In this experiment, the OTCs (made of solar radiation-transmitting plastic; height 0.45 m; diameter at ground height 1.20 m and diameter at maximum height 0.65 m) were used to simulate climatic warming. The warming experiment began in 2011 with a design including four replicates and four treatments: control (CK), warming (W), reclamation (R) and warming under reclamation (WR). At each of the locations for planted grassland and meadow, there were a total of eight plots. Each test location had a surface area of 2,500 cm^2. The plot diagram and realistic picture were showed in Figure 1. Measurements of soil N_2O flux began in July 2018 and ended in August 2019. After warming, in the growing

10.3389/fpls.2023.1162160

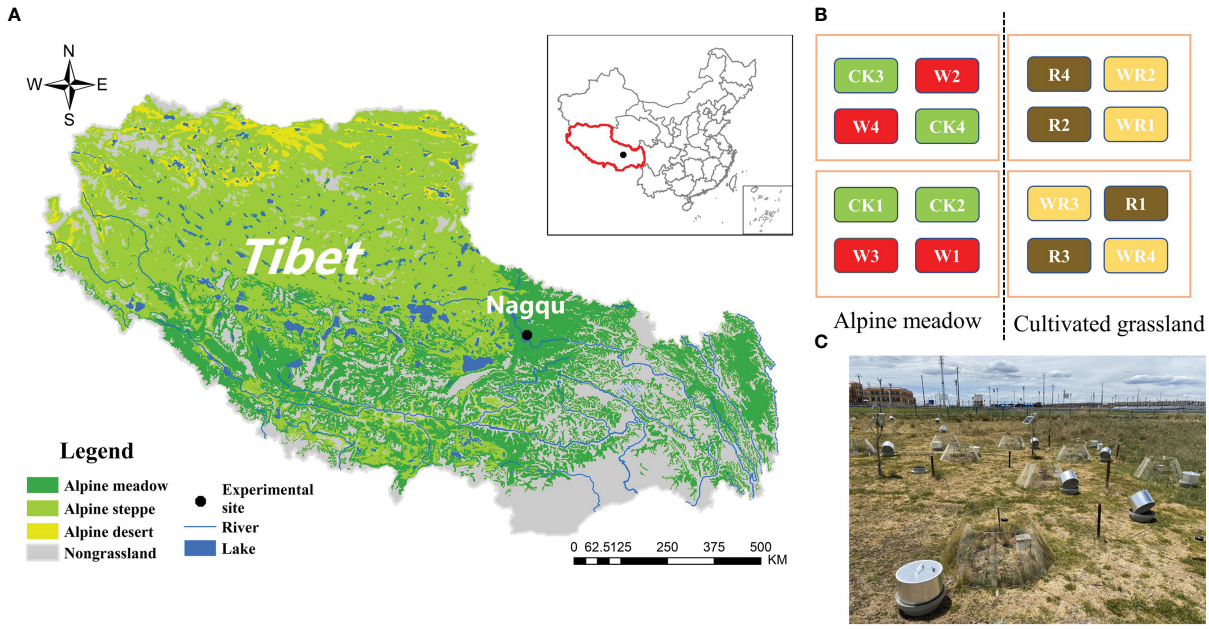

FIGURE 1
The figure of experimental site location **(A)**, plot diagram **(B)** and realistic scene**(C)**.

season, soil temperature (5 cm depth) significantly increased by 1.2 °C and 1.0 °C in the alpine meadow and the cultivated grassland, respectively and soil moisture (5 cm depth) significantly decreased by 5.5% and 2.6%, respectively (Figure 2).

2.3 Microclimates measurements

Throughout the growing season, the EM50 Data Collection System from Decagon Devices, Pullman, WA, USA, was utilized for soil temperature and moisture content measurements at 5 cm depths at 30 min intervals in each plot and site. During the non-growing season, no microclimatic data were gathered.

2.4 N_2O flux measurements

Closed static chamber and gas chromatography were used for the measurement of N_2O emission flux (Yan et al., 2018). To reduce the heating effect of solar radiation during sampling, heat-insulating foam was applied to the exterior of each chamber. Each plot had a cylindrical container with a shaft ring and chamber that was 31.8 cm in diameter and 20 cm high. With a headspace height of 20 cm, the collar's bottom was placed in the ground (5 cm). Each chamber has a fan to guarantee even air distribution and a ventilation duct to maintain equilibrium throughout sampling. Gas samples (30 mL each) were taken at 0, 5, 15, and 30 minutes after the chamber was closed using pre-vacuumed 10 mL air bottles. N_2O fluxes were

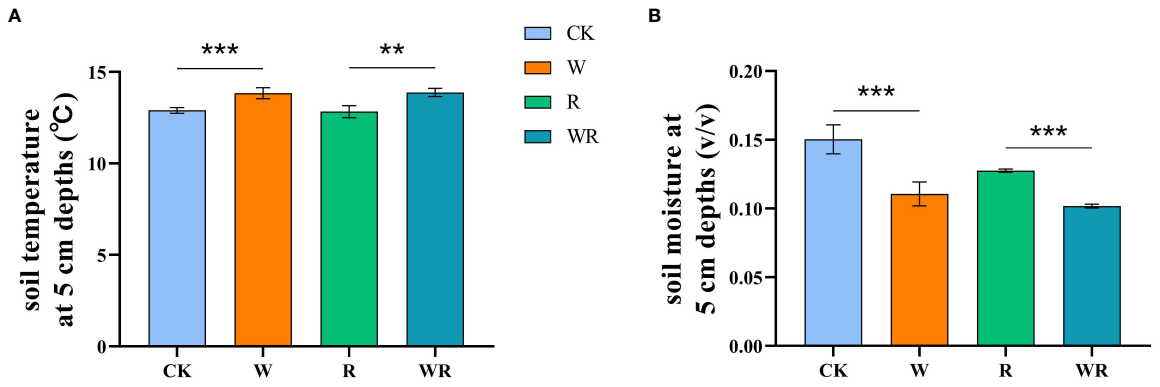

FIGURE 2
Soil temperature (°C) and moisture (v/v) at 5 cm depths under four treatments with the result of t-test. CK, control; W, warming; R, reclamation; WR, warming under reclamation. Mean ± Standard error (n = 4) was shown in the figure. (*0.01< p< 0.05; **0.001< p< 0.01; ***p< 0.001).

sampled on all plots at 11:00 - 13:00 (during this period, the weather in this area is generally clear, and thunderstorms are avoided as much as possible to reduce the influence of weather factors on the experimental determination) once every 15 days in each month during growing season (May to September) and in the middle of each month during non-growing season (October to April). In total, we measured N_2O flux twice in a month during growing season and once in a month during non-growing season. The N_2O flux data for September 2018 were lost. Gas chromatography with a flame ionization detector (Model 4890D; Agilent, Wilmington, TX, USA) was used to quantify N_2O in gas samples. The calculation of N_2O emission flux is as shown below (Yuesi and Yinghong, 2003):

$$F_{N_2O} = \rho \times \frac{P}{P_0} \times \frac{V}{A} \times \frac{\Delta c}{\Delta t} \times \frac{273.15}{273.15 + T}$$

where F_{N_2O} is the N_2O flux (μg $m^{-2}h^{-1}$), ρ (kg/m^3) is the N_2O gas density, P (kPa) is the atmospheric pressure at the time of sampling, P_0 (kPa) is the standard atmospheric pressure, V (m^3) and A (m^2) are the capacity and basal area of the chamber, respectively. $\frac{\Delta c}{\Delta t}$ is the gradient of the linear regression for the gas concentration gradient with time (m^3 m^{-3} h^{-1}), and T is the mean air temperature throughout the sampling period (°C).

We used the average of two daily N_2O emission flux as the monthly N_2O flux for each treatment in the growing season. In the non-growing season, the daily N_2O flux represented the monthly N_2O flux The calculation for the mean N_2O emission fluxes in the growing season (from June to September), non-growing season (from October to May) was the same as used for the monthly N_2O emission fluxes. We took the mean N_2O emission fluxes for each observation day during a particular period as the average N_2O emission flux during that period.

2.5 Soil C and N measurements

A bucket auger (5 cm diameter) was used to collect soil samples of each experimental plot at 0–15 cm depth in mid-Aug 2018 and mid-July 2019. After collecting, the samples were passed through a soil sieve with 2 mm apertures. Soil total C (TC) and total N (TN) contents were determined by A Vario EL III TOC element analyzer (Elementar, Hanau, Germany). Soil organic carbon (SOC) content was determined by the potassium dichromate oxidation method. Soil samples extracted by 2 M KCl (Wei et al., 2014) were used to detect the content of $NH_4^+ - N$ and NO_3^-N by a flow injection auto analyzer (Auto Analyzer 3, Bran Luebbe, Norderstedt, Germany). Dissolved organic nitrogen (DON) was obtained as the difference between the TN and inorganic N (NH_4^+, NO_2^- and NO_3^-) in the filtrate. Inorganic nitrogen was also measured by a flow injection auto analyzer (Auto Analyzer 3, Bran Luebbe) as previously described (Yang J. et al., 2021).

2.6 Soil enzymatic activity measurements

Soil ammonia monooxygenase (AMO), hydroxylamine oxidoreductase (HAO), nitrite reductase (NXR), nitric oxide reductase (NOR) and nitrous oxide reductase (NOS) were measured using enzyme-linked immunosorbent assay (ELISA) commercial kits to determine the related enzyme activities (U/g). The specific function of these enzymes involved in nitrification and denitrification are recorded in the following table (Table 1). In the kit, solid phase antibody was to be combined with enzyme and its labeled antibody to form antibody-antibody-enzyme-labeled antibody complex. After thorough washing and adding specific substrate, this color of complex began to change. The shade of the color was positively correlated with the activity of the sample enzyme. The absorbance (OD value) was measured with an enzyme label at 450nm wavelength, and the concentration of the activity of the sample enzyme was calculated by standard curve (Shanghai Zhuocai Biology).

2.7 Statistical analyses and calculations

The effects of warming, reclamation, sampling day and their interactions on average N_2O emission flux were tested using repeated ANOVA calculations. The average N_2O emission flux under different treatments for the growing and non-growing seasons was calculated using the hoc-posttest with LSD (least significant difference) to examine differences among all treatments. We used two-way ANOVA to measure warming, reclamation and their interactive effects on soil nutrients and enzymatic activities in 2018 and 2019. The response ratio (r), which was computed as r=Ln(T/A) where T was the value under the treatment and A was the value under ambient conditions, was used to quantify the extent of the treatment's impact on soil

TABLE 1 The main enzymes involving in soil nitrification and denitrification and their roles in specific process.

The type of enzyme	Pathway	Process
Ammonia monooxygenase (AMO)	$NH_4^+ - N \rightarrow NH_2OH$	Nitrification
Hydroxylamine oxidoreductase (HAO)	$NH_2OH \rightarrow NOH$	Nitrification
Nitrite reductase (NXR)	$NO_2^- \rightarrow NO$	Denitrification
Nitric oxide reductase (NOR)	$NO \rightarrow N_2O$	Denitrification
Nitrous oxide reductase (NOS)	$N_2O \rightarrow N_2$	Denitrification

"→" means soil nitrogen changes from one form to another.

nutrients and enzyme activity. Values of the response ratio that were positive or negative showed that the therapy had either beneficial or detrimental effects. The t-test was used to determine its significant differences from zero. Linear regression analysis was used to measure the relationships between enzyme activity and N_2O flux in the two types of grassland.

Structural equation modeling (SEM) using Amos25 SSPS software (Amos Development Corporation, IBM, Chicago, Ill, USA) was used to explore the possible causal links between N_2O emission flux and soil environmental variables and soil enzyme activities under warming and reclamation. The indexes of the model were chosen from soil environmental variables and soil enzyme activities that were related to nitrification and denitrification. The N_2O flux under each treatment was the average of N_2O flux in August 2018 and July 2019. We selected the first component (65.0%) of the results of PCA for the activity of AMO, HAO, NXR, NOR and NOS to represent the enzyme activity. If the value of the root mean square (RMESA) deviation was > 0.05, the indexes and related pathways were altered until the value of RMESA was< 0.05, and the model with the lowest AIC value was selected as the best model. Before all analysis, data were checked for normality and homogeneity using F-test.

3 Results

3.1 Changes in soil N_2O emission flux

Warming, reclamation, sampling day and their interactions significantly affected the N_2O emission flux for our experimental areas (p<0.01, Table 2). Overall, the N_2O flux for CK was lower than that for the other treatments (Figure 3A). Warming significantly increased N_2O flux by 59.1% and 152.0% (p<0.01) and reclamation significantly (p<0.01) increased the N_2O flux by 28.4% and 142.4% during growing and non-growing seasons, respectively compared with CK. When compared with W, WR significantly (p<0.01) increased N_2O flux by 18.9% and 81.0% during growing and non-growing seasons, respectively (Figure 3B).

TABLE 2 Results (*df*, *F* and *P*) of repeated measures analysis of variances (RMANOVA) for the separate and interactive effects of warming (W), reclamation (R), sampling day (D) on soil N_2O emission flux.

Model	df	F	P
D	10	2244.33	<0.01
D×W	10	113.21	<0.01
D×R	10	122.97	<0.01
D×W×R	10	33.39	<0.01
W	1	1372.92	<0.01
R	1	815.41	<0.01
W×R	1	16.42	<0.01

3.2 Changes in soil properties

Warming significantly (p<0.001) increased the soil TC and SOC (Table 3), with the response ratio (r) values of 0.08 and 0.06, respectively in the alpine meadow (Figure 4A). Reclamation significantly (p<0.001) decreased the soil TC and SOC (Table 3) with r values of -0.26 and -0.26, respectively in the absence of warming (Figure 4B). Under warming, reclamation significantly (p<0.001) decreased the soil TC and SOC, with r values of -0.41 and -0.37, respectively (Figure 4C). Soil $NH_4^+ - N$ and NO_3^-N content were also significantly (p<0.001) affected by warming (Table 3), with r values of -0.17 and 0.43, respectively (Figure 4A). Compared with CK, reclamation significantly (p<0.01) decreased the soil TN, $NH_4^+ - N$ and NO_3^-N content (Table 3) with r values of -0.07, -0.17 and -0.14, respectively. Under warming, reclamation significantly (p<0.01 and p<0.001) decreased the soil TN, $NH_4^+ - N$ and NO_3^-N content with r values of -0.18, -0.18 and -0.65, respectively (Figure 4C).

3.3 Changes in soil enzymatic activities

Compared with CK, W significantly (p<0.001) increased AMO, HAO, NXR, NOR and NOS activities (Table 3) with r values of 0.17, 0.28, 0.20, 0.29 and 0.57, respectively (Figure 4A). Reclamation significantly increased AMO, HAO, NXR, NOR and NOS activities (Table 3) in the absence of warming with r values of 0.05 (p<0.01), 0.20 (p<0.001), 0.14 (p<0.01), 0.12 (p<0.05) and 0.21 (p<0.001), respectively (Figure 4B). Under warming, reclamation significantly increased AMO, HAO, NXR and NOR with r values of 0.13 (p<0.001), 0.25 (p<0.001), 0.13 (p<0.01) and 0.28 (p<0.001), respectively (Figure 4C).

3.4 Factors affecting soil N_2O emissions

In the natural alpine meadow, AMO and NXR activities were not significantly correlated with N_2O flux. In the cultivated grassland, AMO, HAO, NXR, NOR and NOS activities were all significantly (p<0.05) correlated with N_2O flux. Moreover, after reclamation, the N_2O flux was more sensitive to the activity of HAO (Figure 5).

Structural equation modeling indicated that warming and reclamation did not directly affect the N_2O emission flux. Warming increased soil enzymatic activity (0.58) and decreased soil $NH_4^+ - N$ content (-0.44) and soil moisture (-0.24). Reclamation increased the soil enzymatic activity (0.19) and decreased soil $NH_4^+ - N$ (-0.44). Soil enzymatic activity positively (0.74) affected the soil N_2O flux but was negatively (-0.28) affected by soil moisture. Soil $NH_4^+ - N$ promoted enzymatic activity (0.27) while soil moisture (-0.33) was negatively correlated to soil enzymatic activity (Figure 6A). The standardized total effect of warming and reclamation on the N_2O flux were 0.33 and 0.17, respectively (Figure 6B). Overall, the indirect effects of warming and reclamation *via* changing soil $NH_4^+ - N$ content, soil NO_3^-N content, soil moisture and soil enzymatic activity explained 91.2% of the variance in N_2O emission flux.

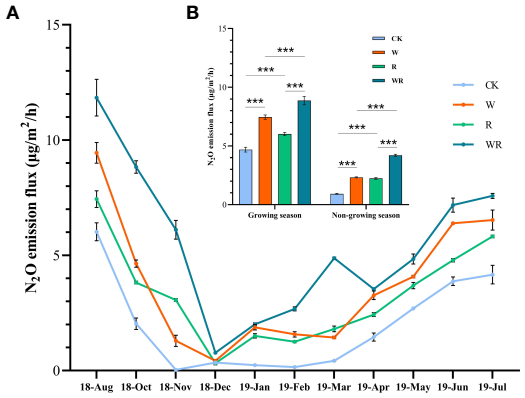

FIGURE 3
Soil N_2O emission flux under warming and reclamation **(A)** during August 2018 and July 2019 and **(B)** different season. CK, control; W, warming; R, reclamation; WR, warming under reclamation. Mean ± Standard error (n = 4) was shown in the figure. (*0.01< p< 0.05; **0.001< p< 0.01; ***p< 0.001).

4 Discussion

4.1 Effects of warming and reclamation on soil nutrients

Increasing temperatures can increase soil carbon and nitrogen cycling in cold ecosystems and warming has increased soil C and N content in the QTP terrestrial ecosystems (Chang et al., 2021; Huai Chen et al., 2013). In our study, warming significantly increased soil TC and SOC in the alpine meadow, which might be explained by the increase of living fine root biomass and root exudation rates under warming, thus promoting C input from root exudates C into the soil (Liu et al., 2022; Wang Q. et al., 2021). Warming can facilitate nitrification (Bai et al., 2013) and directly increase related enzymatic activities by increasing soil temperature (Du et al., 2016). We observed that warming significantly decreased soil $NH_4^+ - N$ while increasing soil NO_3^-N as well as AMO and HAO activities in the alpine meadow (Figure 4A). However, our results were not consistent with the general effects of warming on soil SOC and $NH_4^+ - N$. For an instance, previous studies thought the rough balance of the increase of both plant input and soil microbial respiration by warming led to the insignificant response of C, N contents to the impacts of warming (Zhang et al., 2015). This difference might be explained by discrepant plant and soil microbial composition, even in similar ecosystem. The actual mechanism by which warming affected soil C, N in the alpine meadow should be further investigated.

Generally, conversion of alpine pastureland to artificial grassland decreases soil C and N (Linsler et al., 2013). Firstly, reclamation can destroy the soil macroaggregate (Liu et al., 2014) that is critical to soil nutrient distribution and sequestration rates (Kasper et al., 2009) thus causing the loss of soil C and N (Krol et al., 2016; Zhang et al., 2021). Secondly, cultivation may lead to a loss of soil organic matter in the surface soil layers due to the increase of soil C and N mineralization under tillage (Busari et al., 2016). Our results confirmed that compared with CK, there was a significant decline of soil TC, SOC, TN, $NH_4^+ - N$ and NO_3^-N after reclamation.

4.2 Effects of warming and reclamation on N_2O flux

Soil N content serves as an important factor affecting soil N_2O emissions (Li et al., 2022b). We found that the content of soil $NH_4^+ - N$ and not NO_3^-N, was positively correlated with N_2O flux. Previous studies of relationships between soil N_2O emission and soil moisture have mixed results. A global meta-analysis indicated a strong positive relationship between the effect sizes of N_2O emission and soil moisture (Li et al., 2020) although another study found no significant correlation between soil moisture and N_2O emission in the alpine steppes of the QTP (Yang Y. et al., 2021). However, our results demonstrated that soil moisture was negatively correlated to enzymatic activities and N_2O flux. This was most likely the result of increased activity and abundance of nitrobacteria that resulted from the modest decrease of soil moisture (Liu et al., 2017).

Reclamation also loosens the soil and enhances its total porosity to increase soil oxygen content (Farahani et al., 2022) that could promote nitrification (Wendeborn, 2020) leading to increased soil N_2O production. Significant increases of alpine meadow soil N_2O emissions have been documented following cultivation (Zhang et al., 2017). This was consistent with our study results that indicated reduced soil N_2O fluxes for the control treatment than that under reclamation (Figure 3). Accordingly, we observed the positive effect of reclamation on enzymatic activity in the model (Figure 6).

Agricultural land use can alter the resilience of the ecosystem towards warming such as elevated N_2O emissions demonstrated for the Amazon (Lage Filho et al., 2022). We found a significant interaction of warming and reclamation on N_2O flux primarily due to their interactions with soil moisture. Soil moisture in cultivated grasslands is usually less than that in the natural grassland (Ganjurjav et al., 2018) and it can be reduced further by warming. We observed WR significantly decreased soil moisture compared to W (Figure 4C). Therefore, the decrease of soil moisture by the synergistic effect of warming and reclamation might create suitable environmental conditions for nitrification to

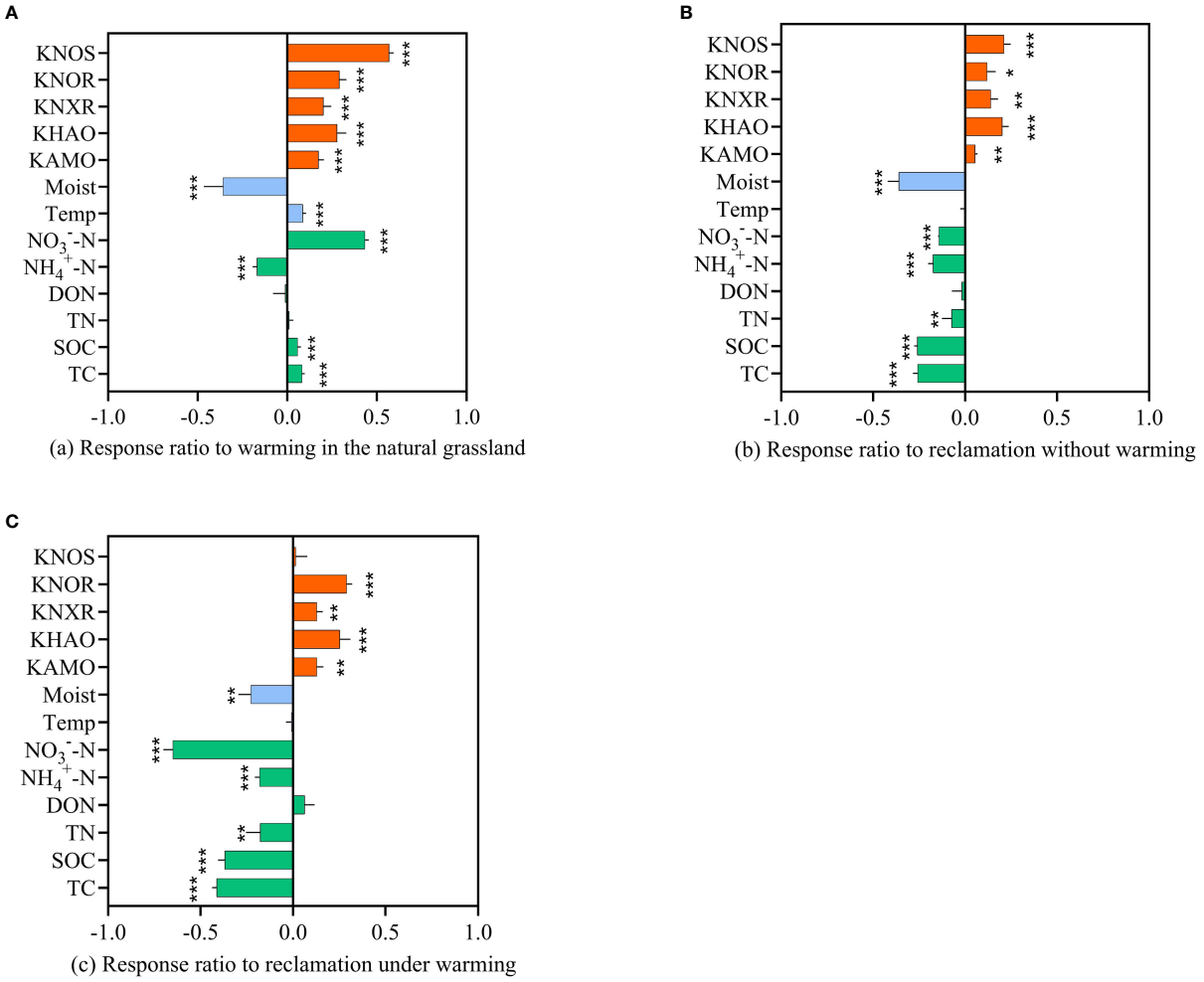

FIGURE 4
Response ratio (r) of soil properties and enzymatic activities under each treatment. **(A)** warming in natural grassland: shows the difference between CK and W, **(B)** reclamation without warming: shows the difference between CK and R, **(C)** reclamation under warming: shows the difference between W and WR. "*" indicates $p < 0.05$, "**" indicates $p < 0.01$, and "***" indicates $p < 0.001$. TC: soil total carbon, SOC: soil dissolved carbon concentration, TN: soil total nitrogen, DON: soil dissolved organic nitrogen, NH4+-N: soil ammonium concentration, NO3– N: soil nitrate concentration, Temp: soil temperature, Moist: soil volumetric moisture, KAMO: enzymatic activity of AMO, KHAO: enzymatic activity of HAO, KNXR: enzymatic activity of NXR, KNOR: enzymatic activity of NOR, KNOS: enzymatic activity of NOS.

increase N_2O emissions that also might serve as a primary contributor for the AMO, and HAO activity increases we found in our study. We confirmed that soil $NH_4^+ - N$, moisture and enzymatic activity were altered by warming and that reclamation promoted nitrification and increased soil N_2O flux.

Soil N_2O is predominantly produced by microbial-mediated nitrification and denitrification (Doltra et al., 2015). In alpine meadows, soil N_2O is primarily produced through nitrification rather than denitrification in the growing season (Du et al., 2016; Yan et al., 2018). In our study, the higher N_2O emission flux under warming and reclamation was primarily derived from the increase of enzymatic activity related to nitrification. During the non-growing season, denitrification is a primary N_2O production process because of snow cover and freezing-thawing can create an anaerobic environment in topsoil (Priemé and Christensen, 2001; Groffman et al., 2006; Risk et al., 2013). For instance, warming massively increased N_2O emissions (101.9%) during the non-growing season in an alpine grassland of the Tianshan (Gong et al., 2021). Analogously, we found that warming significantly increased the average N_2O emission flux during non-growing season in both ambient and reclamation conditions (Figure 3). This may be due to the increased denitrification enzymatic activities and soil nitrogen mineralization rates (Contosta et al., 2011). However, we did not measure soil properties and related enzymatic activities during the off-growing season. The mechanism for soil N_2O flux response to warming and reclamation during the non-growing season still needs further investigation.

4.3 Uncertainties and implications

The primary uncertainty for our experimental design was in the warming chamber since temperature as well as evapotranspiration and gas exchange can be altered in open-top chambers. The rain sheltering effect resulted in lower levels of precipitation reaching the

10.3389/fpls.2023.1162160

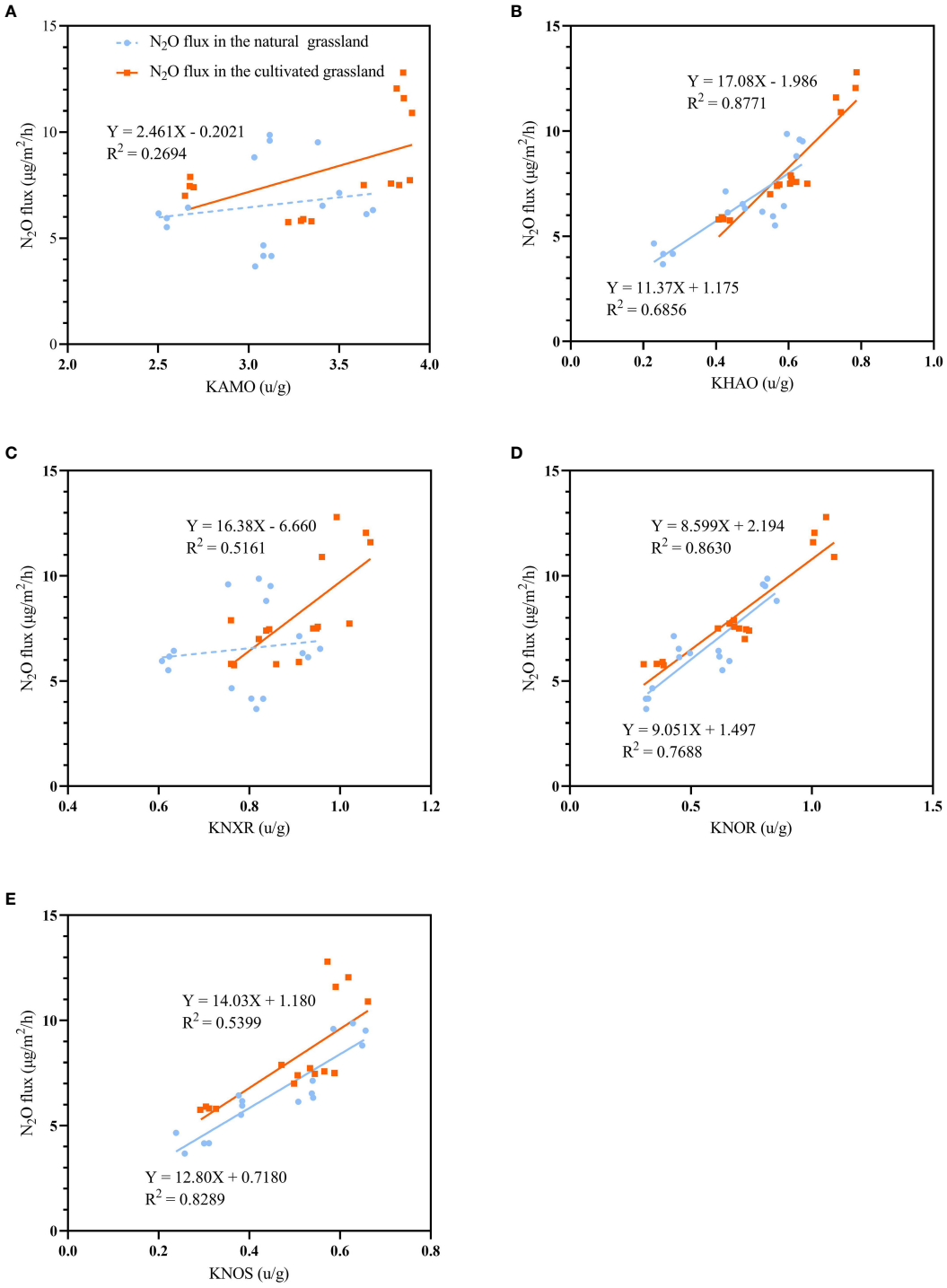

FIGURE 5
Linear regression between N_2O emission flux and enzymatic activity of AMO **(A)**, HAO **(B)**, NXR **(C)**, NOR **(D)** and NOS **(E)** (KAMO, KHAO, KNXR, KNOR, KNOS) in natural alpine meadow (blue dot and line) and cultivated grassland (orange square and line). Solid line indicates $p < 0.05$ and dotted line indicates $p > 0.05$.

warming chambers than for the ambient temperature chambers and could directly affect soil N_2O flux in the chambers. Nevertheless, the above-mentioned methods are acceptable because warming chambers have been widely used in grassland ecosystems to simulate warming (Chen et al., 2016; Zhao et al., 2017). Moreover, we have a tiny database and are unable to undertake automated continuous measurement of soil N_2O flow in warming chambers. It makes it difficult to draw firm conclusions for complete alpine meadow ecosystems on the QTP.

Our results can provide insights for future research and grassland management as follows: (1) despite the increase of enzymatic activities by reclamation and warming, the question of

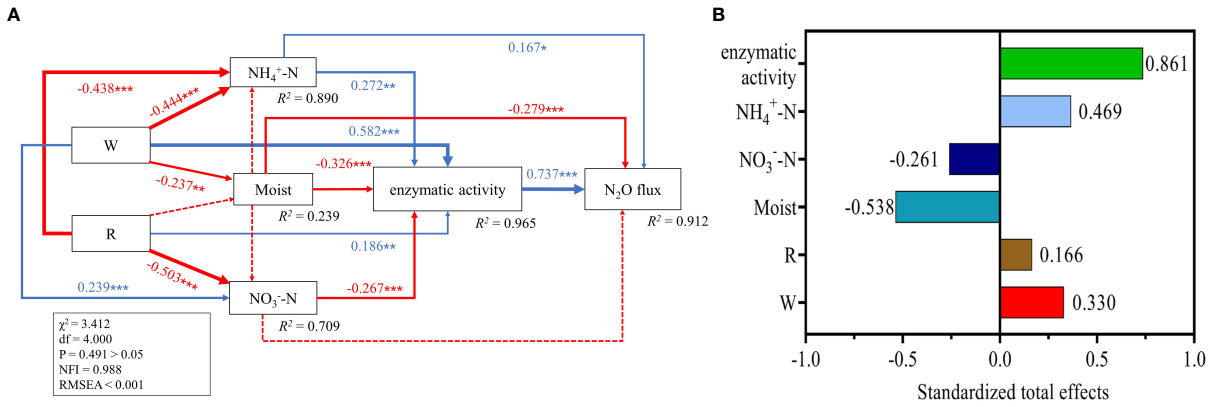

FIGURE 6
Direct and indirect effects of warming (W) and reclamation (R) on N_2O emission flux **(A)**. W, warming; R, reclamation, $NH_4^+ - N$: soil ammonium concentration, NO_3^-N: soil nitrate concentration, Moist: soil volumetric moisture, enzymatic activity: the first principal component of PCA analysis for the activities of AMO, HAO, NXR, NOR and NOS. The arrows' numbers correspond to path coefficients. Beneficial and detrimental correlations are denoted by blue and red arrows, respectively. At the bottom right of boxes, the related *R* square in the model were displayed. "*" tells $p< 0.05$, "**" tells $p< 0.01$, and "***" tells $p< 0.001$. Standardized total effects **(B)** were showed to evaluate the effects of W, R, Moist, $NH_4^+ - N$, NO_3^-N and enzymatic activity on N_2O flux in the model, and the plus or minus of these values represented their positive or negative effects respectively on N_2O flux. The information presented here includes all data gathered throughout treatments and years (n = 32).

whether more soil N will be lost as N_2O or be incorporated by plants requires the isotope tracer technique for an answer; (2) it is necessary to study the mechanism by which reclamation and warming increase the soil N_2O flux during non-growing season; (3) in response to a warming climate, no-tillage seeding may be a better way to improve the productivity of the grassland in alpine meadows due to increased N_2O flux by reclamation in cultivated grasslands.

5 Conclusions

We conducted a long-term manipulative warming experiment in an alpine meadow and a farmed grassland on the QTP and found that both warming and reclamation increased the N_2O emission flux during both the vegetation seasons and off-growing seasons. Reclamation intensified the positive effects of warming on N_2O flux, due to their interaction on the decrease of soil moisture

TABLE 3 Results (*df*, *F* and *P*) of two-way analysis of variances (ANOVA) for the separate and interactive effects of warming (W) and reclamation effects on soil total carbon (TC), soil dissolved carbon concentration (SOC), soil total nitrogen (TN), soil dissolved organic nitrogen (DON), soil ammonium concentration (NH_4^- N), soil nitrate concentration (NO_3N), and the enzymatic activity of AMO, HAO, NXR, NOR and NOS (KAMO, KHAO, KNXR, KNOR, KNOS).

Factors		W				R				W×R			
Year		2018		2019		2018		2019		2018		2019	
variables	df	F	P	F	P	F	P	F	p	F	P	F	P
TC	1	78.56	<0.001	371.92	<0.001	1350.5	<0.001	2011.1	<0.001	1.95	0.188	549.52	<0.001
SOC	1	61.07	<0.001	135.91	<0.001	1026.8	<0.001	930.83	<0.001	6.21	0.028	214.27	<0.001
TN	1	114.25	<0.001	28.17	<0.001	32.11	<0.001	18.41	0.001	7.19	0.020	28.17	<0.001
DON	1	0.08	0.786	11.04	0.006	0.33	0.575	0.42	0.528	1.22	0.292	1.09	0.317
$NH_4^+ - N$	1	70.47	<0.001	258.54	<0.001	99.26	<0.001	216.76	<0.001	3.21	0.098	20.25	0.001
NO_3^-N	1	425.81	<0.001	92.02	<0.001	841.17	<0.001	617.48	<0.001	479.7	<0.001	245.53	<0.001
KAMO	1	426.65	<0.001	115.41	<0.001	87.22	<0.001	22.66	<0.001	46.621	<0.001	0.03	0.857
KHAO	1	107.09	<0.001	347.83	<0.001	41.77	<0.001	243.12	<0.001	26.579	<0.001	0.01	0.909
KNXR	1	104.61	<0.001	35.55	<0.001	105.46	<0.001	1.66	0.222	0.077	0.786	0.13	0.729
KNOR	1	298.19	<0.001	202.79	<0.001	108.96	<0.001	61.49	<0.001	21.039	0.001	30.99	<0.001
KNOS	1	144.37	<0.001	462.15	<0.001	12.56	0.004	8.26	0.014	23.432	<0.001	0.05	0.825

to increase ammonia monooxygenase and hydroxylamine oxidoreductase activities. However, warming, reclamation and their interactions on N_2O flux during non-growing season still needs further investigation. Our results suggest that future research should pay more attention to N_2O emissions from cultivated grasslands and the cultivated grassland in alpine meadow should be scientifically projected to better adapt to a warming climate.

Data availability statement

The original contributions presented in the study are included in the article/supplementary material. Further inquiries can be directed to the corresponding author.

Author contributions

The research was designed by HG and GQ. The experiments were performed by ZL, YLi, HW, YLia, JY, SH. Date analysis and draft writing were conducted by ZL and HG. The manuscript was revised by ZL and HG. All authors contributed to the article and approved the submitted version.

Funding

We appreciate National Natural Science Foundation of China (32171590), the Youth innovation Program of Chinese Academy of Agricultural Sciences (Y2023QC08), and the Central Public interest Scientific Institution Basal Research Fund (BSRF202009) for their financial support

Conflict of interest

The authors declare that the research was conducted in the absence of any commercial or financial relationships that could be construed as a potential conflict of interest.

Publisher's note

References

Abraha, M., Gelfand, I., Hamilton, S. K., Chen, J., and Robertson, G. P. (2018). Legacy effects of land use on soil nitrous oxide emissions in annual crop and perennial grassland ecosystems. *Ecol. Appl.* 28 (5), 1362–1369. doi: 10.1002/eap.1745

Bai, E., Li, S., Xu, W., Li, W., Dai, W., and Jiang, P. (2013). A meta-analysis of experimental warming effects on terrestrial nitrogen pools and dynamics. *New Phytol.* 199 (2), 441–451. doi: 10.1111/nph.12252

Ball, B. C., Scott, A., and Parker, J. P. (1999). Field N_2O, CO_2 and CH_4 fluxes in relation to tillage, compaction and soil quality in Scotland. *Soil Tillage. Res.* 53 (1), 29–39. doi: 10.1016/S0167-1987(99)00074-4

Barnard, R., Leadley, P. W., and Hungate, B. A. (2005). Global change, nitrification, and denitrification: A review. *Global Biogeochem. Cycles.* 19 (1), B1007. doi: 10.1029/2004GB002282

Buchen, C., Lewicka-Szczebak, D., Flessa, H., and Well, R. (2018). Estimating N_2O processes during grassland renewal and grassland conversion to maize cropping using N_2O isotopocules. *Rapid Commun. Mass. Spectromet.* 32 (13), 1053–1067. doi: 10.1002/rcm.8132

Busari, M. A., Salako, F. K., and Tuniz, C. (2016). Stable isotope technique in the evaluation of tillage and fertilizer effects on soil carbon and nitrogen sequestration and water use efficiency. *Eur. J. Agron.* 73, 98–106. doi: 10.1016/j.eja.2015.11.002

Chang, R., Liu, S., Chen, L., Li, N., Bing, H., Wang, T., et al. (2021). Soil organic carbon becomes newer under warming at a permafrost site on the Tibetan plateau. *Soil Biol. Biochem.* 152, 108074. doi: 10.1016/j.soilbio.2020.108074

Chen, J., Luo, Y., Xia, J., Shi, Z., Jiang, L., Niu, S., et al. (2016). Differential responses of ecosystem respiration components to experimental warming in a meadow grassland on the Tibetan plateau. *Agric. For. Meteorol.* 220, 21–29. doi: 10.1016/j.agrformet.2016.01.010

Chen, X., Wang, G., Huang, K., Hu, Z., Song, C., Liang, Y., et al. (2017). The effect of nitrogen deposition rather than warming on carbon flux in alpine meadows depends on precipitation variations. *Ecol. Eng.* 107, 183–191. doi: 10.1016/j.ecoleng.2017.07.018

Chen, H., Zhu, Q., Peng, C., Wu, N., Wang, Y., Fang, X., et al. (2013). The impacts of climate change and human activities on biogeochemical cycles on the qinghai-Tibetan plateau. *Global Change Biol.* 19 (10), 2940–2955. doi: 10.1111/gcb.12277

Contosta, A. R., Frey, S. D., and Cooper, A. B. (2011). Seasonal dynamics of soil respiration and n mineralization in chronically warmed and fertilized soils. *Ecosphere* 2 (3), 1–21. doi: 10.1890/ES10-00133.1

Doltra, J., Olesen, J. E., Báez, D., Louro, A., and Chirinda, N. (2015). Modeling nitrous oxide emissions from organic and conventional cereal-based cropping systems under different management, soil and climate factors. *Eur. J. Agron.* 66, 8–20. doi: 10.1016/j.eja.2015.02.002

Drewer, J., Anderson, M., Levy, P. E., Scholtes, B., Helfter, C., Parker, J., et al. (2017). The impact of ploughing intensively managed temperate grasslands on N_2O, CH_4 and CO_2 fluxes. *Plant Soil* 411 (1), 193–208. doi: 10.1007/s11104-016-3023-x

Du, Y., Guo, X., Cao, G., Wang, B., Pan, G., and Liu De, L.. (2016). Simulation and prediction of nitrous oxide emission by the water and nitrogen management model on the Tibetan plateau. *Biochem. Syst. Ecol.* 65, 49–56. doi: 10.1016/j.bse.2016.02.002

Dubois, O. (2011). *The state of the world's land and water resources for food and agriculture (solaw)* (London: Earthscan).

Elrys, A. S., Wang, J., Metwally, M. A. S., Mohamed, A. S., Cheng, Y., Zhang, J.-B., et al. (2021). Global gross nitrification rates are dominantly driven by soil carbon-to-nitrogen stoichiometry and total nitrogen. *Global Change Biol.* 27 (24), 6512–6524. doi: 10.1111/gcb.15883

Farahani, E., Emami, H., and Forouhar, M. (2022). Effects of tillage systems on soil organic carbon and some soil physical properties. *Land. Degradation. Dev.* 33 (8), 1307–1320. doi: 10.1002/ldr.4221

Ganjurjav, H., Hu, G., Wan, Y., Li, Y., Danjiu, L., and Gao, Q.. (2018). Different responses of ecosystem carbon exchange to warming in three types of alpine grassland on the central qinghai–Tibetan plateau. *Ecol. Evol.* 8 (3), 1507–1520. doi: 10.1002/ece3.3741

Gao, X., Dong, S., Xu, Y., Wu, S., Wu, X., Zhang, X., et al. (2019). Resilience of revegetated grassland for restoring severely degraded alpine meadows is driven by plant and soil quality along recovery time: A case study from the three-river headwater area of qinghai-Tibetan plateau. *Agricult. Ecosyst. Environ.* 279, 169–177. doi: 10.1016/j.agee.2019.01.010

Gong, Y., Yue, P., Li, K., Mohammat, A., and Liu, Y.. (2021). Different responses of ecosystem CO_2 and N_2O emissions and CH_4 uptake to seasonally asymmetric warming in an alpine grassland of the tianshan. *Biogeosciences* 18 (11), 3529–3537. doi: 10.5194/bg-18-3529-2021

Groffman, P. M., Hardy, J. P., Driscoll, C. T., Driscoll, C. T., and Fahey, T. J.. (2006). Snow depth, soil freezing, and fluxes of carbon dioxide, nitrous oxide and methane in a northern hardwood forest. *Global Change Biol.* 12 (9), 1748–1760. doi: 10.1111/j.1365-2486.2006.01194.x

Heincke, M., and Kaupenjohann, M. (1999). Effects of soil solution on the dynamics of N_2O emissions: A review. *Nutrient. Cycling. Agroecosyst.* 55 (2), 133–157. doi: 10.1023/A:1009842011599

Hu, Y., Chang, X., Lin, X., Wang, Y., Wang, S., Duan, J., et al. (2010). Effects of warming and grazing on N_2O fluxes in an alpine meadow ecosystem on the Tibetan plateau. *Soil Biol. Biochem.* 42 (6), 944–952. doi: 10.1016/j.soilbio.2010.02.011

Kasper, M., Buchan, G. D., Mentler, A., and Blum, W. E. H.. (2009). Influence of soil tillage systems on aggregate stability and the distribution of c and n in different aggregate fractions. *Soil Tillage. Res.* 105 (2), 192–199. doi: 10.1016/j.still.2009.08.002

Krol, D. J., Jones, M. B., Williams, M., Richards, K. G., Bourdin, F., and Lanigan, G. J.. (2016). The effect of renovation of long-term temperate grassland on N_2O emissions and n leaching from contrasting soils. *Sci. Total. Environ.* 560-561, 233–240. doi: 10.1016/j.scitotenv.2016.04.052

Lage Filho, N. M., Cardoso, A. S., Azevedo, J., Faturi, C., da Silva, T. C., Domingues, F. N., et al. (2022). Land use, temperature, and nitrogen affect nitrous oxide emissions in Amazonian soils. *Agronomy* 12 (7), 1608. doi: 10.3390/agronomy12071608

Li, X.-G., Wang, Z.-F., Ma, Q.-F., and Li, F.-M.. (2007). Crop cultivation and intensive grazing affect organic c pools and aggregate stability in arid grassland soil. *Soil Tillage. Res.* 95 (1), 172–181. doi: 10.1016/j.still.2006.12.005

Li, Z., Tang, Z., Song, Z., Chen, W., Tian, D., Tang, S., et al. (2022a). Variations and controlling factors of soil denitrification rate. *Global Change Biology.* 28(6), 2133–2145. doi: 10.1111/gcb.16066

Li, Z., Zeng, Z., Song, Z., Tian, D., Huang, X., Nie, S., et al. (2022b). Variance and main drivers of field nitrous oxide emissions: A global synthesis. *J. Cleaner. Product.* 353, 131686. doi: 10.1016/j.jclepro.2022.131686

Li, L., Zheng, Z., Wang, W., Biederman, J. A., Xu, X., Ran, Q., et al. (2020). Terrestrial N_2O emissions and related functional genes under climate change: A global meta-analysis. *Global Change Biol.* 26 (2), 931–943. doi: 10.1111/gcb.14847

Linsler, D., Geisseler, D., Loges, R., Taube, F., and Ludwig, B.. (2013). Temporal dynamics of soil organic matter composition and aggregate distribution in permanent grassland after a single tillage event in a temperate climate. *Soil Tillage. Res.* 126, 90–99. doi: 10.1016/j.still.2012.07.017

Liu, M. -Y., Chang, Q.- R., Qi, Y.- B., Liu, J., and Chen, T.. (2014). Aggregation and soil organic carbon fractions under different land uses on the tableland of the loess plateau of China. *CATENA* 115, 19–28. doi: 10.1016/j.catena.2013.11.002

Liu, R., Hayden, H. L., Suter, H., Hu, H., Lam, S. K., He, J., et al. (2017). The effect of temperature and moisture on the source of N_2O and contributions from ammonia oxidizers in an agricultural soil. *Biol. Fertil. Soils.* 53 (1), 141–152. doi: 10.1007/s00374-016-1167-8

Liu, M., Wen, J.- H., Chen, Y.- M., Xu, W.-J., Wang, Q., Ma, Z.-L., et al. (2022). Warming increases soil carbon input in a sibiraea angustata-dominated alpine shrub ecosystem. *J. Plant Ecol.* 15 (2), 335–346. doi: 10.1093/jpe/rtab101

Paré, M. C., and Bedard-Haughn, A. (2013). Soil organic matter quality influences mineralization and GHG emissions in cryosols: A field-based study of sub- to high Arctic. *Global Change Biol.* 19 (4), 1126–1140. doi: 10.1111/gcb.12125

Priemé, A., and Christensen, S. (2001). Natural perturbations, drying–wetting and freezing–thawing cycles, and the emission of nitrous oxide, carbon dioxide and methane from farmed organic soils. *Soil Biol. Biochem.* 33 (15), 2083–2091. doi: 10.1016/S0038-0717(01)00140-7

Qiu, J. (2008). China: The third pole. *Nature* 454 (7203), 393–396. doi: 10.1038/454393a

Rich, J. J., Heichen, R. S., Bottomley, P. J., Cromack, K., and Myrold, D. D.. (2003). Community composition and functioning of denitrifying bacteria from adjacent meadow and forest soils. *Appl. Environ. Microbiol.* 69 (10), 5974–5982. doi: 10.1128/AEM.69.10.5974-5982.2003

Risk, N., Snider, D., and Wagner-Riddle, C. (2013). Mechanisms leading to enhanced soil nitrous oxide fluxes induced by freeze–thaw cycles. *Can. J. Soil Sci.* 93 (4), 401–414. doi: 10.4141/cjss2012-071

Robertson, G. P., and Groffman, P. M. (2007). "NITROGEN TRANSFORMATIONS," in *Soil microbiology, ecology and biochemistry*, *3rd ed.* Ed. E. A. Paul (San Diego: Academic Press), 341–364.

Séneca, J., Söllinger, A., Herbold, C. W., Pjevac, P., Prommer, J., Verbruggen, E., et al. (2021). Increased microbial expression of organic nitrogen cycling genes in long-term warmed grassland soils. *ISME. Commun.* 1 (1), 69. doi: 10.1038/s43705-021-00073-5

Wang, Q., Chen, L., Xu, H., Ren, K., Xu, Z., Tang, Y., et al. (2021). The effects of warming on root exudation and associated soil n transformation depend on soil nutrient availability. *Rhizosphere* 17, 100263. doi: 10.1016/j.rhisph.2020.100263

Wang, Y., Chen, H., Zhu, Q., Peng, C., Wu, N., Yang, G., et al. (2014). Soil methane uptake by grasslands and forests in China. *Soil Biol. Biochem.* 74, 70–81. doi: 10.1016/j.soilbio.2014.02.023

Wang, J., Luo, Y., Quan, Q., Ma, F., Tian, D., Chen, W., et al. (2021). Effects of warming and clipping on CH_4 and N_2O fluxes in an alpine meadow. *Agric. For. Meteorol.* 297, 108278. doi: 10.1016/j.agrformet.2020.108278

Wei, D., Xu, R., Liu, Y., Wang, Y., and Wang, Y.. (2014). Three-year study of CO_2 efflux and CH_4/N_2O fluxes at an alpine steppe site on the central Tibetan plateau and their responses to simulated n deposition. *Geoderma* 232-234, 88–96. doi: 10.1016/j.geoderma.2014.05.002

Wendeborn, S. (2020). The chemistry, biology, and modulation of ammonium nitrification in soil. *Angewandte. Chemie. Int. Edition.* 59 (6), 2182–2202. doi: 10.1002/anie.201903014

Yan, Y., Ganjurjav, H., Hu, G., Liang, Y., Li, Y., He, S., et al. (2018). Nitrogen deposition induced significant increase of N_2O emissions in an dry alpine meadow on the central qinghai–Tibetan plateau. *Agricult. Ecosyst. Environ.* 265, 45–53. doi: 10.1016/j.agee.2018.05.031

Yang, J., Guo, W., Wang, F., Wang, F., Zhang, L., Zhou, B., et al. (2021). Dynamics and influencing factors of soluble organic nitrogen in paddy soil under different long-term fertilization treatments. *Soil Tillage. Res.* 212, 105077. doi: 10.1016/j.still.2021.105077

Yang, C., Shen, W., and Wang, T. (2015). Spatial-temporal characteristics of cultivated land in Tibet in recent 30 years. *Trans. Chin. Soc. Agric. Eng.* 31 (1), 8.

Yang, Y., Xiao, Y., Li, C., Wang, B., Gao, Y., Zhou, G., et al. (2021). Nitrogen addition, rather than altered precipitation, stimulates nitrous oxide emissions in an alpine steppe. *Ecol. Evol.* 11 (21), 15153–15163. doi: 10.1002/ece3.8196

Yao, T., Xue, Y., Chen, D., Chen, F., Thompson, L., Cui, P., et al. (2019). Recent third pole's rapid warming accompanies cryospheric melt and water cycle intensification and interactions between monsoon and environment: Multidisciplinary approach with observations, modeling, and analysis. *Bull. Am. Meteorol. Soc.* 100 (3), 423–444. doi: 10.1175/BAMS-D-17-0057.1

Yuesi, W., and Yinghong, W. (2003). Quick measurement of CH4, CO2 and N2O emissions from a short-plant ecosystem. *Adv. Atmos. Sci.* 20 (5), 842–844. doi: 10.1007/BF02915410

Zhang, M., Li, D., Wang, X., Abulaiz, M., Yu, P., Li, J., et al. (2021). Conversion of alpine pastureland to artificial grassland altered CO_2 and N_2O emissions by decreasing c and n in different soil aggregates. *PeerJ* 9, e11807. doi: 10.7717/peerj.11807

Zhang, X.-Z., Shen, Z.-X., and Fu, G. (2015). A meta-analysis of the effects of experimental warming on soil carbon and nitrogen dynamics on the Tibetan plateau. *Appl. Soil Ecol.* 87, 32–38. doi: 10.1016/j.apsoil.2014.11.012

Zhang, Z., Zhu, X., Wang, S., Duan, J., Chang, X., Luo, C., et al. (2017). Nitrous oxide emissions from different land uses affected by managements on the qinghai-Tibetan plateau. *Agric. For. Meteorol.* 246, 133–141. doi: 10.1016/j.agrformet.2017.06.013

Zhao, Z., Dong, S., Jiang, X., Liu, S., Ji, H., Li, Y., et al. (2017). Effects of warming and nitrogen deposition on CH_4, CO_2 and N_2O emissions in alpine grassland ecosystems of the qinghai-Tibetan plateau. *Sci. Total. Environ.* 592, 565–572. doi: 10.1016/j.scitotenv.2017.03.082

Zhou, Y., Hagedorn, F., Zhou, C., Jiang, X., Wang, X., Li, M.-H., et al. (2016). Experimental warming of a mountain tundra increases soil CO_2 effluxes and enhances CH_4 and N_2O uptake at changbai mountain, China. *Sci. Rep.* 6 (1), 21108. doi: 10.1038/srep21108

Zhu, X., Luo, C., Wang, S., Zhang, Z., Cui, S., Bao, X., et al. (2015). Effects of warming, grazing/cutting and nitrogen fertilization on greenhouse gas fluxes during growing seasons in an alpine meadow on the Tibetan plateau. *Agric. For. Meteorol.* 214-215, 506–514. doi: 10.1016/j.agrformet.2015.09.008

frontiers | Frontiers in Plant Science

TYPE Original Research
PUBLISHED 04 July 2023
DOI 10.3389/fpls.2023.1225295

OPEN ACCESS

EDITED BY
Haoran Zhou,
Yale University, United States

REVIEWED BY
Yonggang Chi,
Zhejiang Normal University, China
Mingjie Xu,
Shenyang Agricultural University, China

*CORRESPONDENCE
Tao Qi
qitao@hebeu.edu.cn

RECEIVED 19 May 2023
ACCEPTED 19 June 2023
PUBLISHED 04 July 2023

CITATION
Li Y, Wang Q, Fu T, Qiao Y, Hao L and Qi T (2023) Leaf photosynthetic pigment as a predictor of leaf maximum carboxylation rate in a farmland ecosystem.
Front. Plant Sci. 14:1225295.
doi: 10.3389/fpls.2023.1225295

Leaf photosynthetic pigment as a predictor of leaf maximum carboxylation rate in a farmland ecosystem

Yue Li[1], Qingtao Wang[2], Taimiao Fu[2], Yunfeng Qiao[3], Lihua Hao[4] and Tao Qi[2]*

[1]School of Earth Science and Engineering, Hebei University of Engineering, Handan, China, [2]School of Landscape and Ecological Engineering, Hebei University of Engineering, Handan, China, [3]Institute of Geographic Sciences and Natural Resources Research, Chinese Academy of Sciences, Beijing, China, [4]School of Water Conservancy and Hydropower, Hebei University of Engineering, Handan, China

The leaf maximum rate of carboxylation (V_{cmax}) is a key parameter of plant photosynthetic capacity. The accurate estimation of V_{cmax} is crucial for correctly predicting the carbon flux in the terrestrial carbon cycle. V_{cmax} is correlated with plant traits including leaf nitrogen (N_{area}) and leaf photosynthetic pigments. Proxies for leaf chlorophyll (Chl_{area}) and carotenoid contents (Car_{area}) need to be explored in different ecosystems. In this study, we evaluated the relationship between leaf maximum rate of carboxylation (scaled to 25°C; V_{cmax25}) and both leaf N_{area} and photosynthetic pigments (Chl_{area} and Car_{area}) in winter wheat in a farmland ecosystem. Our results showed that V_{cmax25} followed the same trends as leaf Chl_{area}. However, leaf N_{area} showed smaller dynamic changes before the flowering stage, and there were smaller seasonal variations in leaf Car_{area}. The correlation between leaf V_{cmax25} and leaf Chl_{area} was the strongest, followed by leaf Car_{area} and leaf N_{area} (R^2 = 0.69, R^2 = 0.47 and R^2 = 0.36, respectively). The random forest regression analysis also showed that leaf Chl_{area} and leaf Car_{area} were more important than leaf N_{area} for V_{cmax25}. The correlation between leaf V_{cmax25} and N_{area} can be weaker since nitrogen allocation is dynamic. The estimation accuracy of the V_{cmax25} model based on N_{area}, Chl_{area}, and Car_{area} (R^2 = 0.75) was only 0.05 higher than that of the V_{cmax25} model based on Chl_{area} and Car_{area} (R^2 = 0.70). However, the estimation accuracy of the V_{cmax25} model based on Chl_{area} and Car_{area} (R^2 = 0.70) was 0.34 higher than that of the V_{cmax25} model based on N_{area} (R^2 = 0.36). These results highlight that leaf photosynthetic pigments can be a predictor for estimating V_{cmax25}, expanding a new way to estimate spatially continuous V_{cmax25} on a regional scale, and to improve model simulation accuracy.

KEYWORDS

leaf chlorophyll content, leaf carotenoid content, leaf nitrogen content, maximum rate of carboxylation, photosynthetic capacity

1 Introduction

Farmland ecosystems play an important role in the carbon cycle of terrestrial ecosystems (Robertson et al., 2000). However, the carbon flux of farmland ecosystems is one of the main uncertainties in global terrestrial carbon cycle research and is significantly affected by human activities (Lal, 2001; Bondeau et al., 2007; Taylor et al., 2013). High-quality simulations of the carbon budget of farmland ecosystems are beneficial for future projections of climate change and crop yield (Houborg et al., 2015; Bonan and Doney, 2018). Process-based terrestrial biosphere models (TBMs) are effective tools for estimating changes in the ecosystem carbon budget. However, currently there is still significant uncertainty in simulating the impact of climate change on terrestrial carbon flux (Smith and Dukes, 2012; Anav et al., 2015; Li et al., 2018a). Approximately 90% of carbon and water fluxes in biosphere and atmospheric occur through photosynthesis, and the photosynthetic module is an important part of TBMs (Zhu et al., 2016). Photosynthetic rate is a primary source of uncertainty in terrestrial carbon dynamic modelling because of the lack of in-depth research on photosynthesis and field observation data (Dietze, 2014).

To simulate photosynthetic rate, most TBMs used a kinetic enzyme model based on Farquhar–von Caemmerer–Berry (FvCB) (Farquhar et al., 1980; Jin et al., 2023). The maximum rate of carboxylation (V_{cmax}) and the maximum rate of electron transport (J_{max}) are two key photosynthetic parameters in FvCB model. V_{cmax} represents the maximum rate of Ribulose-1,5-Bisphosphate (RuBP) carboxylation catalyzed by Rubisco (ribulose 1,5-bisphosphate carboxylase/oxygenase) enzyme (Quebbeman and Ramirez, 2016). J_{max} is the rate of RuBP regeneration through the electron transport chain (Voncaemmerer and Farquhar, 1981; Sharkey et al., 2007). In process-based models, V_{cmax} plays a critical role in constraining photosynthetic rates (Lebauer et al., 2013). Previously, V_{cmax} was assumed to be a fixed value (at the temperature of 25°C; V_{cmax25}), which varied with plant functional type (PFT) in process-based models (Houborg et al., 2013; Zhang et al., 2014). Nonetheless, there are seasonal variations for V_{cmax25} (Grassi et al., 2005; Medvigy et al., 2013; Alton, 2017; Croft et al., 2017). Even for the same PFT, the difference between species is great (Dillen et al., 2012; Croft et al., 2017). Previous studies have typically used leaf nitrogen content (N) to model the photosynthetic capacity to incorporate spatiotemporal changes in V_{cmax25} (Kattge et al., 2009; Walker et al., 2014). However, it is not possible to accurately retrieve leaf nitrogen content based on remote sensing data (Knyazikhin et al., 2013). Additionally, a relationship between leaf N and V_{cmax25} cannot be applied at large scales or to different PFTs because Rubisco-N, rather than total leaf nitrogen (photosynthetic and nonphotosynthetic nitrogen pools), is more related to V_{cmax25} (Croft et al., 2017; Onoda et al., 2017; Effah et al., 2023). Nonphotosynthetic N pools can complicate the relationships between leaf V_{cmax25} and leaf N.

In recent years, leaf chlorophyll content has been retrieved relatively accurately via remote sensing (Croft et al., 2013), which plays a crucial role in capturing light energy to drive photosynthetic reactions (Yang et al., 2014; Croft et al., 2020; Huang et al., 2023). Leaf chlorophyll can effectively eliminate the influence of nonphotosynthetic N, which refers to changes in the photosynthetic active N pool (Croft et al., 2017). Leaf chlorophyll contents have been adopted to represent photosynthetic capacity in some studies (Houborg et al., 2015; Croft et al., 2017). In farmland ecosystems, Houborg et al. (2013) adopted an intermediate variable (leaf N) to demonstrate a semi- empirical relationship between the leaf V_{cmax25} and chlorophyll content. In temperate deciduous forests, Croft et al. (2017) found a direct correlation between leafV_{cmax25} and leaf Chl_{area}. Luo et al. (2018) incorporated Chl_{leaf} into terrestrial biosphere models to constrain V_{cmax25} based on the relationship between V_{cmax25} and Chl_{leaf} from the work of Croft et al. (2017), and improved the temporal correlations between the measured and the estimated fluxes in a temperate deciduous forest. Strong correlations between the field-measured leaf chlorophyll content and V_{cmax25} have been reported in various PFTs (Qian et al., 2019; Lu et al., 2020; Wang et al., 2020; Qian et al., 2021; Lu et al., 2022; Liu et al., 2023b). Recent studies have found that leaf carotenoid, another major photosynthetic pigment, can improve the estimation precision for V_{cmax25} based on leaf Chl_{area}. Leaf carotenoid content increases the capability of phenological monitoring, particularly in areas where seasonal variations in leaf chlorophyll content are not obvious (Wong et al., 2019). The functional relationship between the photosynthetic pigments (chlorophyll and carotenoid) and V_{cmax25} plays an important role in regional model simulations (Croft and Chen, 2018; Luo et al., 2018; Luo et al., 2019). Therefore, leaf chlorophyll and carotenoid contents should be incorporated into the V_{cmax25} model to improve the accuracy of TBMs in simulating C dynamics (Luo et al., 2019). However, the relationships between leaf pigment content (especially leaf carotenoid content) and $V_{cmax25}$are still unclear. A large-scale spatial mapping of V_{cmax25} requires understanding how these relationships change in different PFTs.

In this study, we estimated the relationships between V_{cmax25} with leaf nitrogen and leaf pigments (chlorophyll and carotenoid) in a farmland ecosystem. Photosynthesis response curves, leaf nitrogen and leaf pigment content (chlorophyll and carotenoid contents) were observed at Yucheng (YC) Ecological Station during the 2021. We also investigated the correlations between V_{cmax25} with leaf nitrogen, chlorophyll and carotenoid contents in a farmland ecosystem. We also analyzed the relationships among these driving variables associated with V_{cmax25} and assessed their relative importance.

2 Materials and methods

2.1 Field site description

We carried out field experiments in Yucheng, Shandong Province, China (36°57′ N,116°38′ E). The station is a wheat producing area in China, which located in a warm temperate zone. The annual average temperature and precipitation are 13.1°C and 610 mm, respectively. The average temperature in January is -3°C, and the average temperature in July is 26.9°C.

Precipitation occurs mainly from June to August, accounting for 69.1% of the total annual precipitation and shows a pattern of spring drought and summer floods (Zhu et al., 2020). The tidal soil is the main soil type in this area. The PH value is 8.0 and the soil organic matter content is 15.0 g kg^{-1}. Mass fraction of soil total nitrogen is 0.64 g kg^{-1} (Hga et al., 2020).

2.2 Measurements of CO_2 response curve

Leaf gas exchange in winter wheat was measured in a 10 × 10m subset area within a larger field. We conducted winter wheat observation experiment from day of the year (DOY) 92 (April 2) to 147 (May 27) in 2021. Leaf samples were randomly selected approximately once every seven days (Table 1). Three to four winter wheat leaf samples were collected weekly during the 2021 growing season. The CO_2 response curves for leaves in winter wheat were measured by a portable gas-exchange system (Li 6400; Li-Cor, Inc., Lincoln, NE, USA).

CO_2 response curves were observed under saturated light conditions. It took about 40 minutes to observe CO_2 response curves. Adjust the photosynthetic photon flux density (PPFD) to 1,500 µmol m^{-2} s^{-1} (saturated light). The flow rate was maintained at 500 mmol s^{-1}, and the relative humidity was set in the range of 40–80% during the measurement period. The air CO_2 concentrations (C_a) gradients are 380, 300, 200, 100, 50, 380, 600, 800, 1,000, and 1,200 µmol CO_2 mol^{-1} air. Leaf samples were acclimated in a 2 × 3 cm^2 leaf cuvette for 20 min at a temperature of 25°C and a CO_2 concentration of 380 µmol CO_2 mol^{-1} before measuring CO_2 response curves. V_{cmax} and J_{max} values were estimated by an Excel tool (www.landflux.org/Tools.php) (Ethier and Livingston, 2004). Arrhenius equation (Equation 1 and Table 2) was used in our study to normalize V_{cmax} and J_{max} to V_{cmax25} and J_{max25} (Sharkey et al., 2007; Sharkey, 2016). The net photosynthetic rate (A_{sat}) was recorded at a PPFD of 1,500 µmol m^{-2} s^{-1} and a CO_2 concentration of 380 µmol mol^{-1}.

$$f(T_k) = k_{25}\exp(c - \Delta H_a/RT_k) \quad (1)$$

TABLE 1 Leaf measurements stages and sample sizes of winter wheat at YC site in 2021.

Measurement DOY	Sample sizes	Growing stages
92 (April 2)	4	Elongation stage (≤95)
96 (April 6)	4	Booting stage (≤117)
105 (April 15)	3	Booting stage (≤117)
119 (April 29)	3	Flowering stage (≤131)
126 (May 6)	3	Flowering stage (≤131)
133 (May 13)	4	Filling stage (≤161)
140 (May 20)	4	Filling stage (≤161)
147 (May 27)	4	Filling stage (≤161)

TABLE 2 Parameters values referring to the temperature responses of leaf photosynthetic capacity.

Parameter	Value at 25°C	c	ΔH_a
V_{cmax}	1	26.355	65.33
J	1	17.710	43.90

1 indicates the value of $f(T_k)/k_{25}$ at 25°C.

where k_{25} and $f(T_k)$ were, respectively, the values at 25°C and leaf surface temperature. c was a scaling constant (Table 2). ΔH_a referred to the activation energy. R was the molar gas constant (0.008314 kJ mol^{-1} K^{-1}). T_k represented the absolute leaf temperature.

2.3 Leaf biochemistry measurements

We conducted leaf biochemical analyses (leaf nitrogen content, N_{area}; leaf chlorophyll content, $Chl_{area;}$ and leaf carotenoid content, Car_{area}) on the same day as leaf A/Ci curves observations. The leaves of winter wheat were sampled from the same locations as for the A/Ci curves observations. For leaf photosynthetic pigment (chlorophyll and carotenoid) and nitrogen analyses, leaf samples were immediately packed in paper bags and were sent to chemistry laboratory. Fresh leaf weight was also recorded in chemistry laboratory. The leaf photosynthetic pigments were extracted using 95% ethanol. A Shimadzu UV-2600 spectrophotometer was used to calculate both leaf chlorophyll and carotenoid contents by measuring the absorbance at 665, 649, and 470 nm (Fargasova and Molnarova, 2010). We used the same leaves as those measured to determine the leaf photosynthetic pigments to calculate leaf nitrogen content. Dry the leaf samples at 80°C for 48 hours until a constant weight. Specific leaf area (SLA) was determined by leaf dry weights and leaf area. We ground the dried leaves into powder by a mixer mill (MM400, RETSCH, Germany). A Vario MAX CN elemental analyzer (Elementar Analyzer system, Hanau, Germany) was used to record leaf nitrogen content.

Fractions of leaf N allocated to photosynthetic components, i.e., active Rubisco (P_R), bioenergetics pools (P_B) and light-harvesting components (P_L), were determined based on V_{cmax}, J_{max} and leaf chlorophyll content, according to the equations reported by Niinemets and Tenhunen (1997).

$$P_R = \frac{V_{cmax}}{6.25 \times V_{cr} \times M_A \times N_{mass}} \quad (2)$$

$$P_B = \frac{J_{max}}{8.06 \times J_{mc} \times M_A \times N_{mass}} \quad (3)$$

$$P_L = \frac{C_C}{C_B \times N_{mass}} \quad (4)$$

where M_A referred to dry leaf mass per unit area (g m^{-2}). C_c was leaf chlorophyll content (mmol g^{-1}). N_{mass} represented nitrogen content per dry leaf mass (g g^{-1}). The C_B value was 2.15 mmol g^{-1}. The values of V_{cr} and J_{mc} were 20.5 µmol CO_2 (g Rubisco)$^{-1}$ s^{-1} and

156 μmol electrons (μmol cyt f)$^{-1}$ s^{-1} at the temperature of 25°C, respectively (Niinemets et al., 1998).

2.4 Data analysis

In the correlation analyses, we used Pearson's correlation coefficients to demonstrate the linear correlation strength between two variables. Pearson correlation coefficient, also known as the Pearson product-moment correlation coefficient, is represented by R in this paper. The following function was used to calculate R:

$$R = \frac{\sum_{i=1}^{n}(x-\bar{x})(y-\bar{y})}{\sqrt{\sum_{i=1}^{n}(x-\bar{x})^2(y-\bar{y})^2}} \quad (5)$$

where n is the sample size, and R is between -1 and +1. The larger the absolute value of R, the stronger the correlation. There may be a positive (R>0) or negative (R<0) correlation between two variables.

The relationships between leaf nitrogen content and leaf photosynthetic pigments (chlorophyll and carotenoid contents) were evaluated by simple linear regressions. We used the statistical package in Origin Pro 9.0 to conduct simple linear regressions. Analysis of variance (ANOVA) was adopted to evaluate the significance of the regression equations. The statistical significance of tests was set at 0.05. The prediction variables, leading to changes in V_{cmax25}, included leaf nitrogen, chlorophyll, carotenoid, and SLA. We adopted random forest regression analysis (Breiman, 2001) to discern the amount of changes in V_{cmax25}. The relative importance of each predictor was evaluated by random forest regression analysis (Delgado-Baquerizo et al., 2017), which can resolve the multicollinearity problems between prediction variables. The percentage increase in the mean square error (% IncMSE) indicates the influence of replacing a predictor with a random variable on the predicted outcome, which represents the effect of predictors on the dependent variable. the original variable was more important when the random variable changed the original variance significantly.Therefore, the higher the %IncMSEof predictor, the more importance it is. Random forest package (randomForest) in R was used in our study to perform the random forest regression (http://www.r-project.org/). Multiple linear regression models were constructed to explore the effects of leaf nitrogen and photosynthetic pigments (chlorophyll and carotenoid) on variations in V_{cmax25}. The performances of the V_{cmax25} models were estimated using the coefficient of determination (R^2) between different leaf trait variables. We used SPSS® version 17.0 (SPSS Inc. Chicago, IL, USA) to perform multiple linear regression analysis in our study.

3 Results

3.1 Seasonal variations in leaf photosynthetic parameters and biochemical parameters

Winter wheat showed large temporal variations in leaf photosynthetic rate and V_{cmax25} in 2021. At the elongation and booting stages, the leaf A_{sat} and V_{cmax25} increased gradually before the flowering stage (on average, 42% and 62% higher on DOY 126 than on DOY 92, respectively), reaching a peak of 28.63 μmol m^{-2} s^{-1} and 133.46 μmol m^{-2} s^{-1}, respectively, at the flowering stage. A_{sat} and V_{cmax25} then declined rapidly during the filling stage (on average, 79% and 190% lower on DOY 147 than on DOY 126, respectively) (Figures 1A, C). Temporal variations in leaf J_{max25} and V_{cmax25} were consistent (Figure 1C). Leaf chlorophyll content had a similar temporal variation to V_{cmax25}, which gradually reached its peak at the flowering stage (on average, 68% higher on DOY 126 than on DOY 92) and rapidly declined at the filling stage (on average, 99% lower on DOY 147 than on DOY 126) (Figure 1B). Leaf A_{sat} and photosynthetic parameters appeared to follow the trends of leaf chlorophyll content. However, there were some differences in the seasonal patterns of leaf chlorophyll, nitrogen, and carotenoid contents. Leaf nitrogen content showed smaller dynamic changes before the flowering stage than leaf Chl_{area} (on average, 26% higher on DOY 126 than on DOY 92) and then declined rapidly at the late stage (on average, 83% lower on DOY 147 than on DOY 126) (Figure 1A). The peak value of leaf Car_{area} was, on average, 48% higher than that of Car_{area} on DOY 92. There were minor changes in leaf Car_{area} after the flowering stage (on average, 33% lower on DOY 147 than on DOY 126) (Figure 1B). Therefore, smaller seasonal changes were showed in leaf Car_{area} compared to leaf Chl_{area} in winter wheat, particularly after the flowering stage.

3.2 Correlation of leaf photosynthetic parameters and leaf traits variables

There were positive correlations between the leaf photosynthetic parameters (A_{sat}, V_{cmax25}, and J_{max25}) and leaf trait variables (N_{area}, Chl_{area}, and Car_{area}) (Figure 2). The correlation coefficient between leaf V_{cmax25} and leaf Chl_{area} was the highest (0.83), followed by leaf Car_{area} (0.68) and leaf N_{area} (0.60), all of which showed significant linear positive correlations ($p<0.001$) (Figure 2). The correlations between Leaf J_{max25} were also significantly correlated with leaf traits variables (N_{area}, Chl_{area}, Car_{area}), with correlation coefficients of 0.55 ($p<0.01$), 0.79 ($p<0.001$), and 0.70 ($p<0.001$), respectively. Correlations were also observed between the three leaf trait variables (Figure 2).

Simple linear regressions were conducted between leaf photosynthetic capacity with leaf nitrogen content, and leaf photosynthetic pigments (Table 3). The resultsindicated that leaf Chl_{area} accounted for 69% and 63% of the temporal variation in V_{cmax25} and J_{max25}, respectively ($p<0.001$). Leaf Car_{area} accounted for 47% and 48% of the temporal variation in V_{cmax25} and J_{max25}, respectively ($p<0.001$). However, there was a weak relationship between leaf N_{area} and leaf photosynthetic capacity. Leaf N_{area} accounted for only 36% and 30% of the temporal variation in V_{cmax25} and J_{max25}, respectively ($p<0.001$) (Table 3). There were certain limitations to estimating V_{cmax25} based on leaf N_{area}.

3.3 Changes in leaf nitrogen allocation

The ratios between leaf Chl_{area} and N_{area} indicate the allocation of leaf nitrogen between the Rubisco and leaf chlorophyll

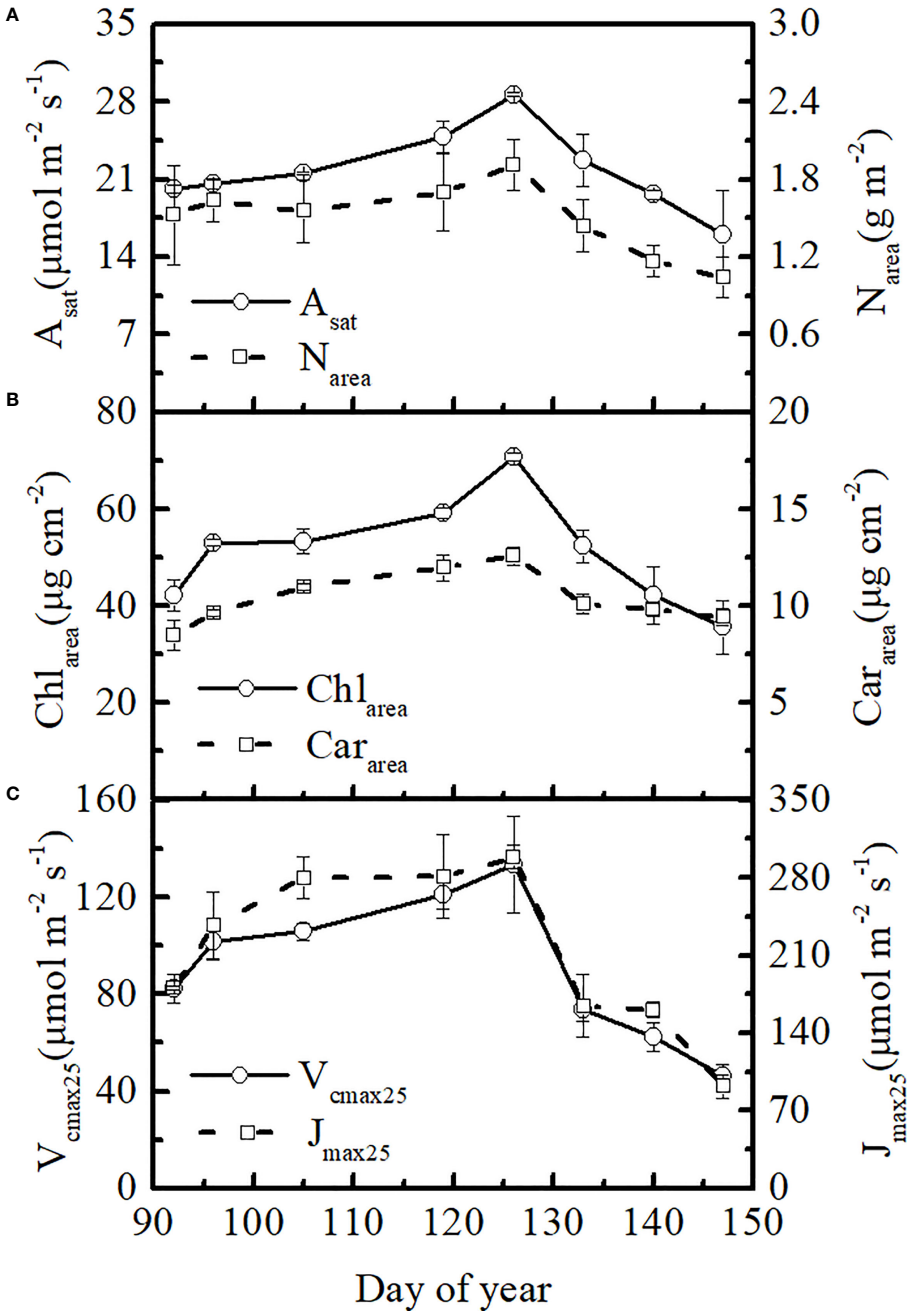

FIGURE 1
Seasonal changes in **(A)** photosynthetic rate and nitrogen content, **(B)** leaf chlorophyll and leaf carotenoid contents, and **(C)** V_{cmax25} and J_{max25} for winter wheat in 2021.

components (Kenzo et al., 2006). There was little seasonal variation in the ratios between leaf Chl_{area} to N_{area} (both units are μg cm^{-2}) after DOY 105 in 2021 (Figure 3A). The leaf Chl_{area}/N_{area} ratios showed a rapidly increasing trend at the beginning stage (DOY 92 and DOY 96). The ratios were 0.23 and 0.32 at DOY 92 and 96, respectively. Leaf Chl_{area}/N_{area} ratios were maintained at approximately 0.36 from DOY 105 to DOY 147 (Figure 3A).

P_R, P_B, and P_L showed seasonal patterns that first increased and then decreased (Figures 3B–D). The growing stage at which leaf P_B reached its highest point in winter wheat differed from that of P_R and P_L. Temporal variations in leaf P_R and P_L were coordinated, reaching their highest points at the flowering stage. In general, changes in leaf N allocation to different N pools were dynamic (Figures 3B–D), which may have led to a weak correlation between leaf nitrogen and V_{cmax25} (Table 3).

3.4 Relationships among leaf nitrogen, chlorophyll and carotenoid contents

A significant linear relationship between leaf nitrogen and leaf chlorophyll contents (R^2 = 0.90, p<0.001) was observed in our study.

10.3389/fpls.2023.1225295

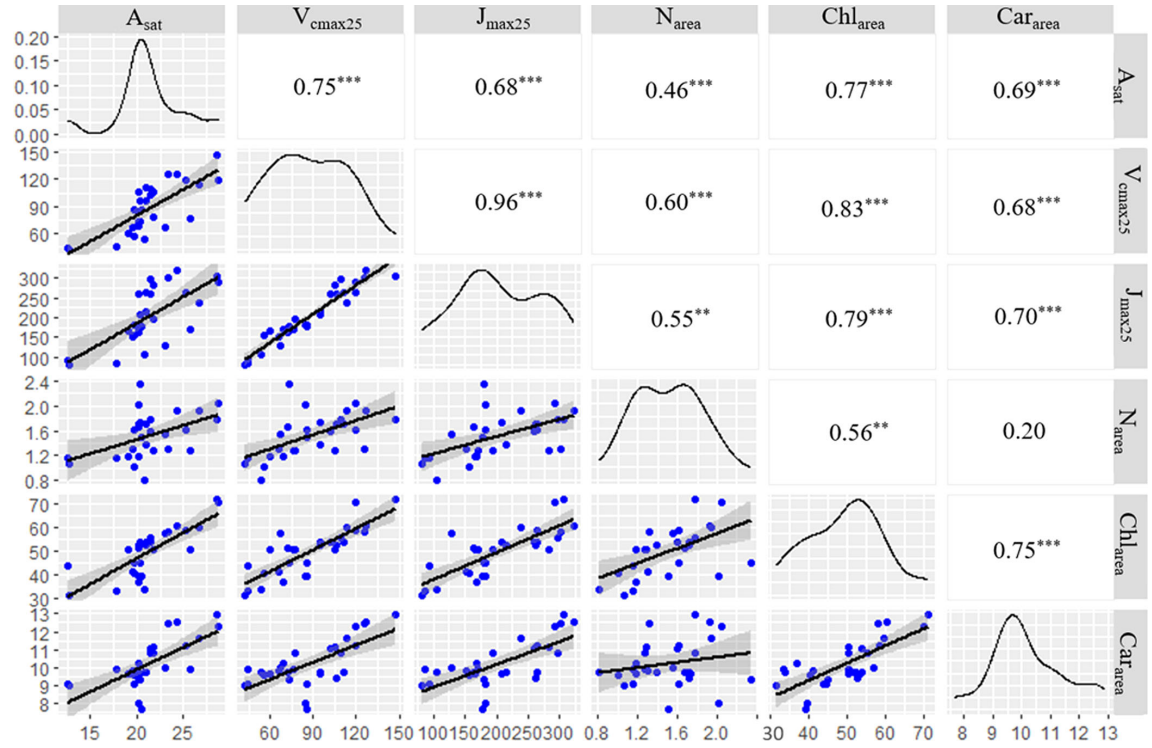

FIGURE 2
Correlation between both leaf photosynthetic rate and leaf photosynthetic capacity with different leaf traits variables. ***, ** and * represent p< 0.001, p< 0.01and p< 0.05, respectively. The caption describes all significant situations of correlation between parameters, including significant correlation (*) and extremely significant correlation (** and ***). The results in Figure 2 showed that the parameters were highly correlated (** and ***) or uncorrelated.

The observations on DOYs 92 and 96 were outside the 95% confidence intervals of the regression (Figure 4A), which may be attributed to the significant variations in nitrogen allocation to the leaf chlorophyll fractions on these two days (Figure 3A). Leaf Chl_{area} was also strongly correlated with Car_{area} (R^2 = 0.71, p=0.005) (Figure 4B). However, a weaker relationship between leaf N_{area} and Car_{area} was observed (R^2 = 0.43, p=0.05) in winter wheat in 2021 (Figure 4C).

3.5 The importance of each prediction variable to V_{cmax25}

We used a random forest regression analysis to evaluate the relative importance of each prediction variable for V_{cmax25}. Leaf Car_{area}, $Chl_{area,}$ and leaf N_{area} were all main prediction variables for V_{cmax25} in our study (Figure 5). Leaf Chl_{area} (%IncMSE = 22.60%) was the most important driver of V_{cmax25}, followed by leaf Car_{area} (%IncMSE was 21.47%), and leaf N_{area} (%IncMSE = 19.08%). The importance of SLA (%IncMSE = 15.66%) to V_{cmax25} was far below the importance of leaf photosynthetic pigment and nitrogen content (Figure 5).

3.6 Optimization of V_{cmax25} model by multiple regression models

Multiple linear regression models were established to improve the accuracy of the V_{cmax25} models using leaf N_{area}, $Chl_{area,}$ and Car_{area} (Equations 6-9). The estimation accuracies of the binary linear regression models for V_{cmax25} (R^2 = 0.72, 0.70, and 0.69, respectively, for f(N_{area}, Chl_{area}), f(Chl_{area}, Car_{area}), and

TABLE 3 Coefficients of determination for simple linear regressions between photosynthetic parameters with both leaf nitrogen and leaf photosynthetic pigment during 2021.

	N_{area}		Chl_{area}		Car_{area}	
	R^2	p	R^2	p	R^2	p
V_{cmax25}	0.36	***	0.69	***	0.47	***
J_{max25}	0.30	***	0.63	***	0.48	***

The caption describes all significant situations of correlation between parameters, including significant correlation (*) and extremely significant correlation (** and ***). The results in Table 3 showed that the parameters were highly correlated (***). ***, ** and * represent p< 0.001, p< 0.01and p< 0.05, respectively.

10.3389/fpls.2023.1225295

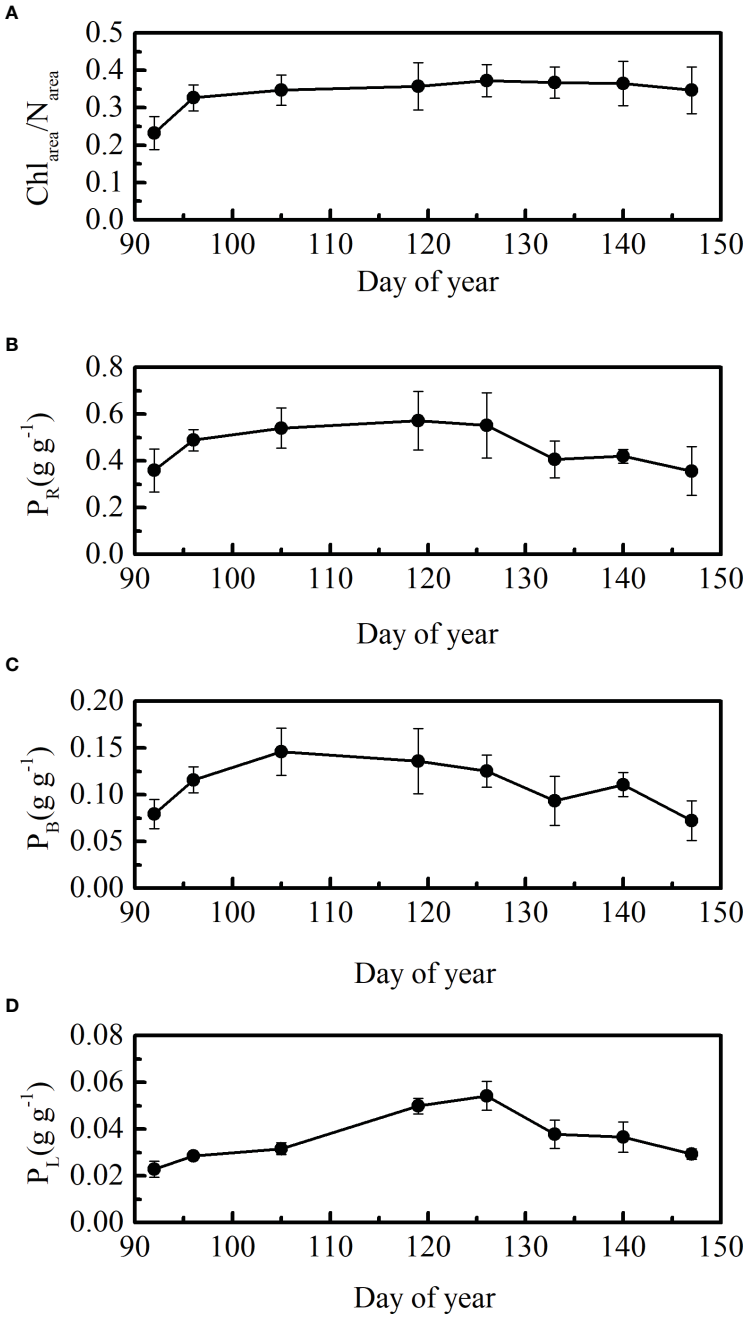

FIGURE 3
Seasonal patterns in **(A)** leaf Chl_{area} to N_{area} ratios, **(B)** P_R, **(C)** P_B, and **(D)** P_L, ± SD, in 2021.

f(N_{area}, Car_{area})) were all significantly higher than those of the two simple linear regression models for f(N_{area}) and f(Car_{area}) (R^2 = 0.36 and 0.47, respectively) in our study (Tables 3, 4). However, the estimation accuracy of the simple linear regression models for f(Chl_{area}) (R^2 = 0.69) was not significantly different from that of the binary linear regression models (Tables 3, 4). The model based on leaf N_{area}, Chl_{area}, and Car_{area} had the highest accuracy in estimating V_{cmax25} (R^2 = 0.75, $p<0.001$), which was only 0.06 higher than that of the simple linear regression models for f(Chl_{area}) (R^2 = 0.69) (Tables 3, 4). Thus, leaf Chl_{area} was a better predictor for V_{cmax25} than leaf N_{area} in winter wheat at the YC site (Tables 3, 4). Incorporating leaf photosynthetic pigments (chlorophyll and carotenoid content) into photosynthetic models can significantly improve the estimation accuracy of V_{cmax25} model based on leaf nitrogen for winter wheat.

$$V_{cmax25} = 15.17N_{area} + 1.99Chl_{area} - 34.43 \quad (6)$$

$$V_{cmax25} = 1.99Chl_{area} + 3.13Car_{area} - 43.51 \quad (7)$$

10.3389/fpls.2023.1225295

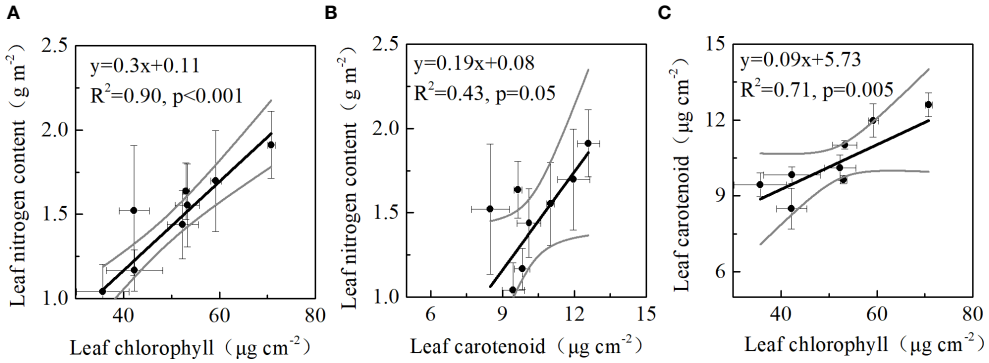

FIGURE 4
Relationships between **(A)** leaf nitrogen and chlorophyll contents, **(B)** leaf nitrogen and carotenoid contents, **(C)** leaf carotenoid and chlorophyll contents in 2021. Horizontal error bars denote standard deviation of leaf chlorophyll and leaf carotenoid. Vertical error bars refer to standard deviation of leaf nitrogen and leaf carotenoid.

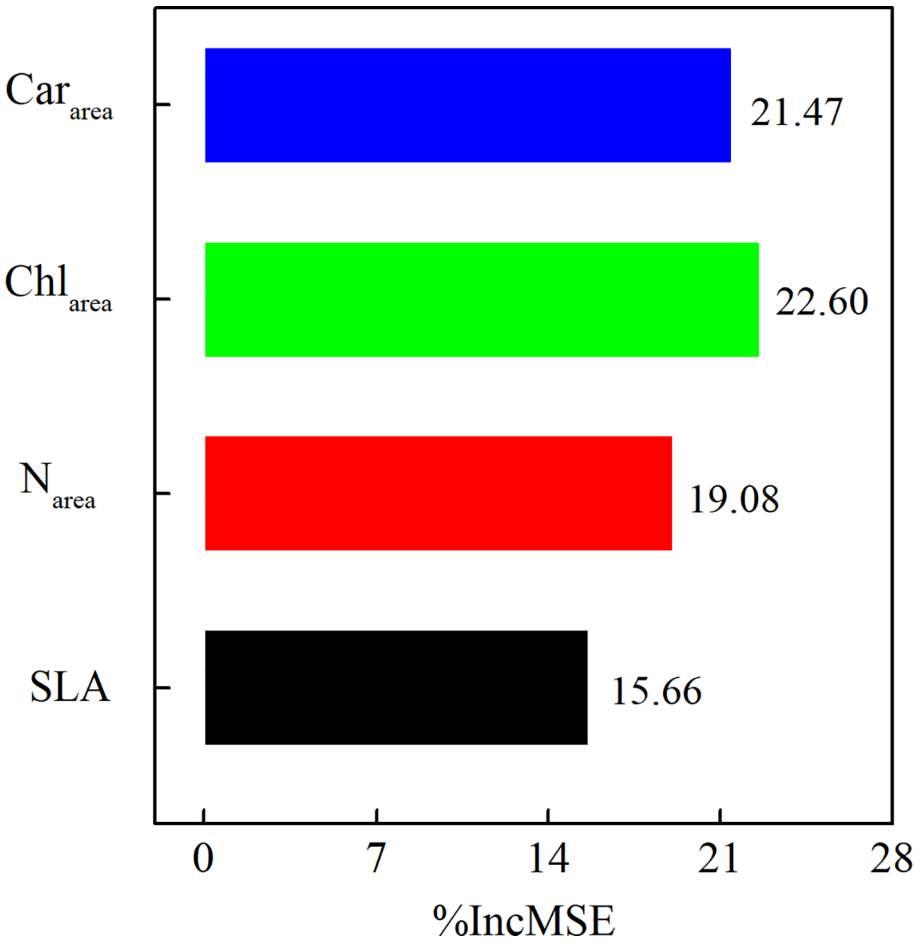

FIGURE 5
The importance of leaf Car_{area}, leaf Chl_{area}, leaf N_{area}, and SLA to V_{cmax25} in 2021.

TABLE 4 Coefficient of determination (r^2) of V_{cmax25} models based on different leaf traits variables.

V_{cmax25} models	R^2	p-value
$f(N_{area}, Chl_{area})$	0.72	<0.001
$f(Chl_{area}, Car_{area})$	0.70	<0.001
$f(N_{area}, Car_{area})$	0.69	<0.001
$f(N_{area}, Chl_{area}, Car_{area})$	0.75	<0.001

$$V_{cmax25} = 37.48N_{area} + 12.68Car_{area} - 98.92 \quad (8)$$

$$V_{cmax25} = 22.30N_{area} + 1.26Chl_{area} + 6.18Car_{area} - 71.99 \quad (9)$$

4 Discussion

4.1 Differences in seasonal trends of photosynthetic parameters

In our study, leaf A_{sat} and photosynthetic parameters appeared to follow trends in leaf chlorophyll content. However, there were some differences in the seasonal patterns of leaf chlorophyll, nitrogen, and carotenoid contents. Leaf N_{area} was relatively high at the elongation stage relative to leaf Chl_{area} (Figures 1A, B), which may be attributed to the inorganic nitrogen present in buds before leaf flushing. The different trends in leaf nitrogen and leaf chlorophyll maybe attributed to dynamic changes in leaf nitrogen partitioning among photosynthetic pools (Croft et al., 2017; Liu et al., 2023a). Fertilization management can also maintain high leaf nitrogen content at the start of season (Lu et al., 2020). Leaf Car_{area} showed smaller seasonal variations compared to leaf Chl_{area} in winter wheat, particularly after the flowering stage (Figure 1B). As there is massive loss of leaf chlorophyll in winter wheat during senescence in the filling stage, carotenoids are retained in the leaves for a much longer time (Wong et al., 2019). In the early growth stage, the leaf Chl_{area} is higher than the leaf Car_{area}. The leaves appear green because green light is almost completely reflected. In the late stage, leaf chlorophyll is heavily damaged, but leaf carotenoids are only slightly affected, causing the leaves to turn yellow (Stylinski et al., 2002; Garrity et al., 2011). Flowering stage is an important physiological stage for winter wheat, since all the photosynthetic parameters have inflection point in this period. The results are consistent with Lu et al. (2020). The temperature rises gradually after the greening period. At this period, plant root is vigorous, enzyme activity and plant photosynthetic capacity increases. Thus, leaf photosynthetic parameters increase gradually and reach the maximum point at the flowering stage. The reproductive growth of winter wheat is dominant after flowering stage. Leaf and other vegetative organs gradually stop growing and aging. Therefore, leaf photosynthetic parameters decrease gradually (Yang et al., 2020).

4.2 Relationships among leaf V_{cmax25}, nitrogen and photosynthetic pigments

Leaf nitrogen was closely correlated with leaf chlorophyll in previous studies, with a fixed value of leaf Chl_{area}/N_{area} ratio (Sage et al., 1987; Evans, 1989; Houborg et al., 2013). Our results also showed a strong linear relationship between leaf Chl_{area} and N_{area} (R^2 = 0.90; p< 0.001) (Figure 3A). The robustness of the linear correlation between leaf nitrogen and chlorophyll contents was influenced by changes in leaf nitrogen allocation to chlorophyll (Lu et al., 2020). A relatively stable allocation of leaf nitrogen to leaf chlorophyll (Chl_{area}/N_{area} ratio of approximately 0.36) was found in our study for winter wheat (Figure 4A), which contributed to a good linear relationship between leaf Chl_{area} and N_{area} (Figure 3A).

V_{cmax25} was closely related to leaf N_{area}, leaf Chl_{area}, and SLA in previous studies (Houborg et al., 2013; Houborg et al., 2015; Croft et al., 2017; Watanabe et al., 2018; Miner and Bauerle, 2019; Qian et al., 2021; Lu et al., 2022). However, the results are inconsistent in different studies, indicating that these relationships vary among species and are difficult to apply at large scales. Qian et al. (2021) showed a stronger linear relationship between V_{cmax25} and Chl_{area} than between leaf V_{cmax25} and N_{area} across 13 species. In other ecosystems, a strong relationship exists between leaf V_{cmax25} and N_{area} and the slopes vary among species (Walker et al., 2014; Quebbeman and Ramirez, 2016). However, the slopes of the relationship in N_{area}-V_{cmax25} varies greatly with environmental conditions and PFTs (Walker et al., 2014; Rogers et al., 2017). A weaker correlation between leaf V_{cmax25} and leaf N_{area} than between leaf V_{cmax25} and Chl_{area} were showed in our study (Figure 2; Table 3), which is in agreement with Qian et al. (2021). Rubisco-N allocation (P_R), rather than the total leaf nitrogen content, was more related to V_{cmax} based on the meta-analysis (Ali et al., 2015). P_R showed significant seasonal variation during the growing season in our study (Figure 4B). The weak correlation between leaf N_{area} and V_{cmax25} may also be attributed to variations in P_R (Figures 2, 4B; Table 3). Therefore, leaf N_{area} is not an ideal predictor for V_{cmax25} in the present study. The temporal variations in leaf P_L coordinated with changes in P_R, which indicated that the allocation of leaf nitrogen to leaf carotenoids was dynamic. Consequently, A weak correlation between the leaf N_{area} and leaf Car_{area} for winter wheat area was showed in our study (Figure 3B).

4.3 Physiological mechanism for the relationships between leaf photosynthetic pigments and V_{cmax25}

Our results showed a stronger correlation between V_{cmax25} with both leaf Chl_{area} (R^2 = 0.69) and Car_{area} (R^2 = 0.47) than with leaf N_{area} (R^2 = 0.36) (Figure 2; Table 3). Leaf photosynthetic pigments are a better predictor for V_{cmax25} in winter wheat. The underlying mechanism of this phenomenon is the driving role of leaf pigment in light harvesting of photosynthesis (Zhang et al., 2009; Gitelson et al.,

2014; Li et al., 2018b). The random forest regression analysis also showed leaf chlorophyll and carotenoid contents were more important than leaf nitrogen content for V_{cmax25} (Figure 5). Compared with other leaf traits, V_{cmax25} can be accurately retrieved based on leaf chlorophyll content from remote sensing data (Gitelson et al., 2006; Croft et al., 2013). Moreover, leaf chlorophyll can effectively eliminate the influence of nonphotosynthetic nitrogen since it only reflects the changes of photosynthetic active N pool (Alton, 2017; Croft et al., 2017). Carotenoid, which is important component of plant photosynthesis, participate in the collection of sunlight, especially at wavelengths where leaf chlorophyll molecules are not absorbed strongly (Ritz et al., 2000). Leaf carotenoid also protect chlorophyll molecules from photo-oxidation. Carotenoid is commonly referred to as "auxiliary pigments" in light harvesting center, promoting the transfer of excitation energy to the reaction center (Niyogi et al., 1997). Leaf chlorophyll and carotenoid molecules are usually arranged in clusters to maximize the capture of light energy (Croft and Chen, 2018).

Leaf chlorophyll and carotenoid contents are the most important factors determining photosynthetic rate, owing to their important roles in light capture and absorption of photosynthetic effective radiation (Zhang et al., 2009; Zhang et al., 2011; Kooistra and Clevers, 2016). Therefore, leaf photosynthetic pigments play an important role in simulating vegetation productivity processes (Croft et al., 2017; Luo et al., 2018). The construction of a V_{cmax25} model based on photosynthetic pigments can improve the accuracy of ecological process model simulations (Luo et al., 2019; Liu et al., 2023b). The multiple linear regression models established in our study showed that f ((N_{area}, Chl_{area}, Car_{area}) had the highest optimization accuracy for the V_{cmax25} model (R^2 = 0.75), which represents different information expressed by the leaf N_{area} and leaf photosynthetic pigment. The estimation accuracy of the V_{cmax25} model based on N_{area}, Chl_{area}, and Car_{area} (R^2 = 0.75) was only 0.05 higher than that of the V_{cmax25} model based on Chl_{area} and Car_{area} (R^2 = 0.70). However, the estimation accuracy of the V_{cmax25} model based on Chl_{area} and Car_{area} (R^2 = 0.70) was 0.34 higher than that of the V_{cmax25} model based on N_{area} (R^2 = 0.36). Leaf photosynthetic pigments can significantly improve the estimation accuracy of V_{cmax25} based on leaf nitrogen in winter wheat.

Data availability statement

The raw data supporting the conclusions of this article will be made available by the authors, without undue reservation.

Author contributions

YL analysed date and wrote the manuscript. The experiments were designed by TQ. QW and TF performed the experiments. YQ and LH revised the manuscript. All authors contributed to the article and approved the submitted version.

Funding

This work was co-supported by the National Natural Science Foundation of China (32001130) and Natural Science Foundation of Hebei Province, China (Grant No. C2021402011, C2020402022, E2021402031).

Conflict of interest

The authors declare that the research was conducted in the absence of any commercial or financial relationships that could be construed as a potential conflict of interest.

Publisher's note

All claims expressed in this article are solely those of the authors and do not necessarily represent those of their affiliated organizations, or those of the publisher, the editors and the reviewers. Any product that may be evaluated in this article, or claim that may be made by its manufacturer, is not guaranteed or endorsed by the publisher.

References

Ali, A. A., Xu, C. G., Rogers, A., McDowell, N. G., Medlyn, B. E., Fisher, R. A., et al. (2015). Global-scale environmental control of plant photosynthetic capacity. *Ecol. Appl.* 25 (8), 2349–2365. doi: 10.1890/14-2111.1.sm

Alton, P. B. (2017). Retrieval of seasonal rubisco-limited photosynthetic capacity at global FLUXNET sites from hyperspectral satellite remote sensing: impact on carbon modelling. *Agric.For. Meteorol.* 232, 74–88. doi: 10.1016/j.agrformet.2016.08.001

Anav, A., Friedlingstein, P., Beer, C., Ciais, P., and Harper, A. (2015). Spatiotemporal patterns of terrestrial gross primary production: a review. *Rev. Geophysics* 53 (3), 785–818. doi: 10.1002/2015RG000483

Bonan, G. B., and Doney, S. C. (2018). Climate, ecosystems, and planetary futures: the challenge to predict life in earth system models. *Science* 359 (6375), 533–533. doi: 10.1126/science.aam8328

Bondeau, A., Smith, P. C, Zaehle, S., Schaphoff, S., Lucht, W., Cramer, W., et al. (2007). Modelling the role of agriculture for the 20th century global terrestrial carbon balance. *Global Change Biol.* 13(3), 679–706. doi: 10.1111/j.1365-2486.2006.01305.x

Breiman, L. (2001). Random forests. *Mach. Learn.* 45 (1), 5–32. doi: 10.1023/A:1010933404324

Croft, H., and Chen, J. M. (2018). Leaf pigment content - sciencedirect. *Comprehensive Remote Sens* 3, 117–142. doi: 10.1016/b978-0-12-409548-9.10547-0

Croft, H., Chen, J. M., Luo, X., Bartlett, P., Chen, B., and Staebler, R. M. (2017). Leaf chlorophyll content as a proxy for leaf photosynthetic capacity. *Global Change Biol.* 23 (9), 3513–3524. doi: 10.1111/gcb.13599

Croft, H., Chen, J. M., Wang, R., Mo, G., Luo, S., Luo, X., et al. (2020). The global distribution of leaf chlorophyll content. *Remote Sens. Environ.* 236, 111479. doi: 10.1016/j.rse.2019.111479

Croft, H., Chen, J. M., Zhang, Y., and Simic, A. (2013). Modelling leaf chlorophyll content in broadleaf and needle leaf canopies from ground, CASI, landsat TM 5 and MERIS reflectance data. *Remote Sens. Environ.* 133, 128–140. doi: 10.1016/j.rse.2013.02.006

Delgado-Baquerizo, M., Eldridge, D. J., Maestre, F. T., Karunaratne, S. B., Trivedi, P., Reich, P. B., et al. (2017). Climate legacies drive global soil carbon stocks in terrestrial ecosystems. *Sci. Adv.* 3 (4), e1602008. doi: 10.1126/sciadv.1602008

Dietze, M. C. (2014). Gaps in knowledge and data driving uncertainty in models of photosynthesis. *Photosynth Res.* 119 (1-2), 3–14. doi: 10.1007/s11120-013-9836-z

Dillen, S. Y., Op de Beeck, M., Hufkens, K., Buonanduci, M., and Phillips, N. G. (2012). Seasonal patterns of foliar reflectance in relation to photosynthetic capacity and color index in two co-occurring tree species, quercus rubra and betula papyrifera. *Agric.For. Meteorol.* 160, 60–68. doi: 10.1016/j.agrformet.2012.03.001

Effah, Z., Li, L., Xie, J., Karikari, B., Xu, A., Wang, L., et al. (2023). Widely untargeted metabolomic profiling unearths metabolites and pathways involved in leaf senescence and n remobilization in spring-cultivated wheat under different n regimes. *Front. Plant Sci.* 14. doi: 10.3389/fpls.2023.1166933

Ethier, G. J., and Livingston, N. J. (2004). On the need to incorporate sensitivity to CO2 transfer conductance into the farquhar–von caemmerer–berry leaf photosynthesis model. *Plant Cell Environ.* 27 (2), 137–153. doi: 10.1111/j.1365-3040.2004.01140.x

Evans, J. R. (1989). Photosynthesis and nitrogen relationships in leaves of c-3 plants. *Oecologia* 78 (1), 9–19. doi: 10.1007/Bf00377192

Fargasova, A., and Molnarova, M. (2010). Assessment of cr and Ni phytotoxicity from cutlery-washing waste-waters using biomass and chlorophyll production tests on mustard sinapis alba l. seedlings. *Environ. Sci. pollut. Res.* 17 (1), 187–194. doi: 10.1007/s11356-009-0136-2

Farquhar, G. D., Caemmerer, S. V., and Berry, J. A. (1980). A biochemical-model of photosynthetic Co2 assimilation in leaves of c-3 species. *Planta* 149 (1), 78–90. doi: 10.1007/Bf00386231

Garrity, S., Eitel, J., and Vierling, L. (2011). Disentangling the relationships between plant pigments and the photochemical reflectance index reveals a new approach for remote estimation of carotenoid content RID a-8929-2011. *Remote SENS Environ.* 115 (2), 628–635. doi: 10.1016/j.rse.2010.10.007

Gitelson, A. A., Keydan, G. P., and Merzlyak, M. N. (2006). Three-band model for noninvasive estimation of chlorophyll, carotenoids, and anthocyanin contents in higher plant leaves. *Geophys. Res. Lett.* 33 (11), 431–433. doi: 10.1029/2006gl026457

Gitelson, A. A., Peng, Y., Arkebauer, T. J., and Schepers, J. (2014). Relationships between gross primary production, green LAI, and canopy chlorophyll content in maize: implications for remote sensing of primary production. *Remote Sens. Environ.* 144 (Complete), 65–72. doi: 10.1016/j.rse.2014.01.004

Grassi, G., Vicinelli, E., Ponti, F., Cantoni, L., and Magnani, F. (2005). Seasonal and interannual variability of photosynthetic capacity in relation to leaf nitrogen in a deciduous forest plantation in northern Italy. *Tree Physiol.* 25 (3), 349–360. doi: 10.1093/treephys/25.3.349

Hga, B., Jing, L. A., Msa, C., Xxa, C., and Zhu, O. (2020). Lowering carbon footprint of wheat-maize cropping system in north China plain: through microbial fertilizer application with adaptive tillage. *J. Cleaner Production* 268, 122255. doi: 10.1016/j.jclepro.2020.122255

Houborg, R., Cescatti, A., Migliavacca, M., and Kustas, W. P. (2013). Satellite retrievals of leaf chlorophyll and photosynthetic capacity for improved modeling of GPP. *Agric.For. Meteorol.* 177, 10–23. doi: 10.1016/j.agrformet.2013.04.006

Houborg, R., McCabe, M. F., Cescatti, A., and Gitelson, A. A. (2015). Leaf chlorophyll constraint on model simulated gross primary productivity in agricultural systems. *Int. J. Appl. Earth. Obs.* 43, 160–176. doi: 10.1016/j.jag.2015.03.016

Huang, Z., Zhou, L., and Chi, Y. G. (2023). Spring phenology rather than climate dominates the trends in peak of growing season in the northern hemisphere. *Glob. Chang. Biol.* 00, 1–13. doi: 10.1111/gcb.16758

Jin, J., Liu, Y., Hou, W., Cai, Y., Zhang, F., Wang, Y., et al. (2023). Improvement of transpiration estimation based on a two-leaf conductance-photosynthesis model with seasonal parameters for temperate deciduous forests. *Front. Plant Sci.* 14. doi: 10.3389/fpls.2023.1164078

Kattge, J., Knorr, W., Raddatz, T., and Wirth, C. (2009). Quantifying photosynthetic capacity and its relationship to leaf nitrogen content for global-scale terrestrial biosphere models. *Global Change Biol.* 15 (4), 976–991. doi: 10.1111/j.1365-2486.2008.01744.x

Kenzo, T., Ichie, T., Watanabe, Y., Yoneda, R., Ninomiya, I., and Koike, T. (2006). Changes in photosynthesis and leaf characteristics with tree height in five dipterocarp species in a tropical rain forest. *Tree Physiol.* 26 (7), 865–873. doi: 10.1093/treephys/26.7.865

Knyazikhin, Y., Schull, M. A., Stenberg, P., Mottus, M., Rautiainen, M., Yang, Y., et al. (2013). Hyperspectral remote sensing of foliar nitrogen content. *Proc. Natl. Acad. Sci.* 110 (3), E185–E192. doi: 10.1073/pnas.1210196109

Kooistra, L., and Clevers, J. G. P. W. (2016). Estimating potato leaf chlorophyll content using ratio vegetation indices. *Remote Sens Lett.* 7 (6), 611–620. doi: 10.1080/2150704x.2016.1171925

Lal, R. (2001). World cropland soils as a source or sink for atmospheric carbon. *Adv Agron.* 71, 145–191. doi: 10.1016/S0065-2113(01)71014-0

Lebauer, D. S., Wang, D., Richter, K. T., Davidson, C. C., and Dietze, M. C. (2013). Facilitating feedbacks between field measurements and ecosystem models. *Ecol. Monogr.* 83 (2), 133–154. doi: 10.1890/12-0137.1

Li, W., Ciais, P., Wang, Y., Yin, Y., Peng, S., and Zhu, Z. (2018a). Recent changes in global photosynthesis and terrestrial ecosystem respiration constrained from multiple observations. *Geophys. Res. Lett.* 45 (2), 1058–1068. doi: 10.1002/2017GL076622

Li, Y., Liu, C. C., Zhang, J. H., Yang, H., Xu, L., Wang, Q. F., et al. (2018b). Variation in leaf chlorophyll concentration from tropical to cold-temperate forests: association with gross primary productivity. *Ecol. Indic.* 85, 383–389. doi: 10.1016/j.ecolind.2017.10.025

Liu, Y., Chen, J. M., He, L., Wang, R., Smith, N. G., Keenan, T. F., et al. (2023b). Global photosynthetic capacity of C3 biomes retrieved from solar-induced chlorophyll fluorescence and leaf chlorophyll content. *Remote Sens. Environ.* 287, 113457. doi: 10.1016/j.rse.2023.113457

Liu, J., Zhang, K., Bi, J., Yu, X., Luo, L., and Hu, L. (2023a). Mesophyll conductance and n allocation co-explained the variation in photosynthesis in two canola genotypes under contrasting nitrogen supply. *Front. Plant Sci.* 14. doi: 10.3389/fpls.2023.1171331

Lu, X., Croft, H., Chen, J. M., Luo, Y., and Ju, W. (2022). Estimating photosynthetic capacity from optimized rubisco–chlorophyll relationships among vegetation types and under global change. *Environ. Res. Lett.* 17 (1), 014028. doi: 10.1088/1748-9326/ac444d

Lu, X., Ju, W., Li, J., Croft, H., Chen, J. M., Luo, Y., et al. (2020). Maximum carboxylation rate estimation with chlorophyll content as a proxy of rubisco content. *J. Geophysical Research: Biogeosciences* 125 (8). doi: 10.1029/2020jg005748

Luo, X. Z., Croft, H., Chen, J. M., Bartlett, P., Staebler, R., and Froelich, N. (2018). Incorporating leaf chlorophyll content into a two-leaf terrestrial biosphere model for estimating carbon and water fluxes at a forest site. *Agric.For. Meteorol.* 248, 156–168. doi: 10.1016/j.agrformet.2017.09.012

Luo, X., Croft, H., Chen, J. M., He, L., and Keenan, T. F. (2019). Improved estimates of global terrestrial photosynthesis using information on leaf chlorophyll content. *Glob Chang Biol.* 25 (7), 2499–2514. doi: 10.1111/gcb.14624

Medvigy, D., Jeong, S. J., Clark, K. L., Skowronski, N. S., and Schafer, K. V. R. (2013). Effects of seasonal variation of photosynthetic capacity on the carbon fluxes of a temperate deciduous forest. *J. Geophys Res-Biogeo* 118 (4), 1703–1714. doi: 10.1002/2013jg002421

Miner, G. L., and Bauerle, W. L. (2019). Seasonal responses of photosynthetic parameters in maize and sunflower and their relationship with leaf functional traits. *Plant Cell Environ.* 42 (5), 1561–1574. doi: 10.1111/pce.13511

Niinemets, U., Bilger, W., Kull, O., and Tenhunen, J. D. (1998). Acclimation to high irradiance in temperate deciduous trees in the field: changes in xanthophyll cycle pool size and in photosynthetic capacity along a canopy light gradient. *Plant Cell Environ.* 21 (12), 1205–1218. doi: 10.1046/j.1365-3040.1998.00364.x

Niinemets, U., and Tenhunen, J. D. (1997). A model separating leaf structural and physiological effects on carbon gain along light gradients for the shade-tolerant species acer saccharum. *Plant Cell Environ.* 20 (7), 845–866. doi: 10.1046/j.1365-3040.1997.d01-133.x

Niyogi, K. K., Bjorkman, O., and Grossman, A. R. (1997). The roles of specific xanthophylls in photoprotection. *Proc. Natl. Acad. Sci.* 94 (25), 14162–14167. doi: 10.1073/pnas.94.25.14162

Onoda, Y., Wright, I. J., Evans, J. R., Hikosaka, K., Kitajima, K., Niinemets, U., et al. (2017). Physiological and structural tradeoffs underlying the leaf economics spectrum. *New Phytol.* 214 (4), 1447–1463. doi: 10.1111/nph.14496

Qian, X., Liu, L., Croft, H., and Chen, J. (2019). C3 plants converge on a universal relationship between leaf maximum carboxylation rate and chlorophyll content. *Biogeosci. Discuss.*, 1–18. doi: 10.5194/bg-2019-228

Qian, X., Liu, L., Croft, H., and Chen, J. (2021). Relationship between leaf maximum carboxylation rate and chlorophyll content preserved across 13 species. *J. Geophysical Research: Biogeosciences* 126 (2). doi: 10.1029/2020jg006076

Quebbeman, J. A., and Ramirez, J. A. (2016). Optimal allocation of leaf-level nitrogen: implications for covariation of vcmax and jmax and photosynthetic downregulation. *J. Geophys Res-Biogeo* 121 (9), 2464–2475. doi: 10.1002/2016jg003473

Ritz, T., Damjanović, A., Schulten, K., Zhang, J.-P., and Koyama, Y. (2000). Efficient light harvesting through carotenoids. *Photosynth Res.* 66 (1-2), 125–144. doi: 10.1023/A:1010750332320

Robertson, G. P., Paul, E. A., and Harwood, R. R. (2000). Greenhouse gases in intensive agriculture: Contributions of individual gases to the radiative forcing of the atmosphere. *Science.* 289(5486), 1922–1925. doi: 10.1126/science.289.5486.1922

Rogers, A., Medlyn, B. E., Dukes, J. S., Bonan, G., von Caemmerer, S., Dietze, M. C., et al. (2017). A roadmap for improving the representation of photosynthesis in earth system models. *New Phytol.* 213, 22–42. doi: 10.1111/nph.14283

Sage, R. F., Pearcy, R. W., and Seemann, J. R. (1987). The nitrogen use efficiency of c-3 and c-4 plants .3. leaf nitrogen effects on the activity of carboxylating enzymes in chenopodium-album (L) and amaranthus-retroflexus (L). *Plant Physiol.* 85 (2), 355–359. doi: 10.1104/pp.85.2.355

Sharkey, T. D. (2016). What gas exchange data can tell us about photosynthesis. *Plant Cell Environ.* 39 (6), 1161–1163. doi: 10.1111/pce.12641

Sharkey, T. D., Bernacchi, C. J., Farquhar, G. D., and Singsaas, E. L. (2007). Fitting photosynthetic carbon dioxide response curves for c-3 leaves. *Plant Cell Environ.* 30 (9), 1035–1040. doi: 10.1111/j.1365-3040.2007.01710.x

Smith, N. G., and Dukes, J. S. (2012). Plant respiration and photosynthesis in global-scale models: incorporating acclimation to temperature and CO2. *Global Change Biol.* 19 (1), 45–63. doi: 10.1111/j.1365-2486.2012.02797.x

Stylinski, C., Gamon, J., and Oechel, W. (2002). Seasonal patterns of reflectance indices, carotenoid pigments and photosynthesis of evergreen chaparral species. *Oecologia* 131 (3), 366–374. doi: 10.1007/s00442-002-0905-9

Taylor, A. M., Amiro, B. D., and Fraser, T. J. (2013). Net CO2 exchange and carbon budgets of a three-year crop rotation following conversion of perennial lands to annual cropping in Manitoba, Canada. *Agric.For. Meteorol.* 182, 67–75. doi: 10.1016/j.agrformet.2013.07.008

Voncaemmerer, S., and Farquhar, G. D. (1981). Some relationships between the biochemistry of photosynthesis and the gas-exchange of leaves. *Planta* 153 (4), 376–387. doi: 10.1007/Bf00384257

Walker, A. P., Beckerman, A. P., Gu, L. H., Kattge, J., Cernusak, L. A., Domingues, T. F., et al. (2014). The relationship of leaf photosynthetic traits - V-cmax and j(max) - to leaf nitrogen, leaf phosphorus, and specific leaf area: a meta-analysis and modeling study. *Ecol. Evol.* 4 (16), 3218–3235. doi: 10.1002/ece3.1173

Wang, S. Q., Li, Y., and Ju, W. (2020). Estimation of leaf photosynthetic capacity from leaf chlorophyll content and leaf age in a subtropical evergreen coniferous plantation. *J. Geophysical Research: Biogeosciences* 125 (3). doi: 10.1029/2019JG005020

Watanabe, M., Hoshika, Y., Inada, N., and Koike, T. (2018). Photosynthetic activity in relation to a gradient of leaf nitrogen content within a canopy of siebold's beech and Japanese oak saplings under elevated ozone. *Sci. Total Environ.* 636, 1455–1462. doi: 10.1016/j.scitotenv.2018.04.423

Wong, C. Y. S., D'Odorico, P., Bhathena, Y., Arain, M. A., and Ensminger, I. (2019). Carotenoid based vegetation indices for accurate monitoring of the phenology of photosynthesis at the leaf-scale in deciduous and evergreen trees. *Remote Sens. Environ.* 233, 111407. doi: 10.1016/j.rse.2019.111407

Yang, P., Liu, Z., Zhao, Y., Cheng, Y., and Huang, J. (2020). Comparative study of vegetative and reproductive growth of different tea varieties response to different fluoride concentrations stress. *Plant Physiol. Bioch.* 154, 419–428. doi: 10.1016/j.plaphy.2020.05.038

Yang, X., Tang, J. W., and Mustard, J. F. (2014). Beyond leaf color: comparing camera-based phenological metrics with leaf biochemical, biophysical, and spectral properties throughout the growing season of a temperate deciduous forest. *J. Geophys Res-Biogeo* 119 (3), 181–191. doi: 10.1002/2013jg002460

Zhang, Y. G., Guanter, L., Berry, J. A., Joiner, J., van der Tol, C., Huete, A., et al. (2014). Estimation of vegetation photosynthetic capacity from space-based measurements of chlorophyll fluorescence for terrestrial biosphere models. *Global Change Biol.* 20 (12), 3727–3742. doi: 10.1111/gcb.12664

Zhang, Q. Y., Middleton, E. M., Margolis, H. A., Drolet, G. G., Barr, A. A., and Black, T. A. (2009). Can a satellite-derived estimate of the fraction of PAR absorbed by chlorophyll (FAPAR(chl)) improve predictions of light-use efficiency and ecosystem photosynthesis for a boreal aspen forest? *Remote Sens. Environ.* 113 (4), 880–888. doi: 10.1016/j.rse.2009.01.002

Zhang, Y. J., Xie, Z. K., Wang, Y. J., Su, P. X., An, L. P., and Gao, H. (2011). Effect of water stress on leaf photosynthesis, chlorophyll content, and growth of oriental lily. *Russ. J. Plant Physl.* 58 (5), 844–850. doi: 10.1134/S1021443711050268

Zhu, K., Sun, Z., Zhao, F., Yang, T., and Li, S. (2020). Remotely sensed canopy resistance model for analyzing the stomatal behavior of environmentally-stressed winter wheat. *ISPRS J. Photogrammetry Remote Sens.* 168, 197–207. doi: 10.1016/j.isprsjprs.2020.08.012

Zhu, X. J., Yu, G. R., Wang, Q. F., Gao, Y. N., He, H. L., Zheng, H., et al. (2016). Approaches of climate factors affecting the spatial variation of annual gross primary productivity among terrestrial ecosystems in China. *Ecol. Indic.* 62, 174–181. doi: 10.1016/j.ecolind.2015.11.028

frontiers | Frontiers in Plant Science

TYPE Original Research
PUBLISHED 05 July 2023
DOI 10.3389/fpls.2023.1200155

OPEN ACCESS

EDITED BY
Qingpeng Yang,
Institute of Applied Ecology, Chinese Academy of Sciences (CAS), China

REVIEWED BY
Guofang Liu,
Institute of Botany, Chinese Academy of Sciences (CAS), China
Qing-Wei Wang,
Institute of Applied Ecology, Chinese Academy of Sciences (CAS), China

*CORRESPONDENCE
Xiangyi Li
lixy@ms.xjb.ac.cn

RECEIVED 04 April 2023
ACCEPTED 31 May 2023
PUBLISHED 05 July 2023

CITATION
Liu Y, Li L, Wang S and Li X (2023) Precipitation modulates the net effect of solar radiation on litter decomposition and CO_2 emission - a meta-analysis. *Front. Plant Sci.* 14:1200155. doi: 10.3389/fpls.2023.1200155

Precipitation modulates the net effect of solar radiation on litter decomposition and CO_2 emission - a meta-analysis

YaLan Liu[1,2,3,4], Lei Li[1,2,3,4], ShiQi Wang[4] and Xiangyi Li[1,2,3,4]*

[1]State Key Laboratory of Desert and Oasis Ecology, Xinjiang Institute of Ecology and Geography, Chinese Academy of Sciences, Urumqi, China, [2]Xinjiang Key Laboratory of Desert Plant Roots Ecology and Vegetation Restoration, Xinjiang Institute of Ecology and Geography, Chinese Academy of Sciences, Urumqi, China, [3]Cele National Station of Observation and Research for Desert-Grassland Ecosystems, Cele, China, [4]University of Chinese Academy of Sciences, Beijing, China

Introduction: Solar radiation plays a crucial role in the decomposition of litter and the cycling of nutrients. Previous studies have investigated that the net effect of solar radiation on litter decomposition depends on the balance of its facilitative and inhibitory effects on microbial activity; however, a gap in understanding the mechanism by which precipitation affects the net effect of solar radiation and the mechanism of litter decomposition on a global scale was observed.

Methods: In addressing this gap, a comprehensive meta-analysis of 351 data points from 37 published studies was conducted to estimate the sole radiation effect and interactive effect of solar radiation and precipitation on a global scale, as well as how they vary at different precipitation levels. In addition, the importance of influential factors regulating the net effect of solar radiation on litter decomposition was assessed to identify the key drivers of the response of mass loss to solar radiation at different precipitation levels.

Results: Our findings indicated that solar radiation largely regulates litter decomposition, and the direction and magnitude are potentially dependent on the precipitation regime. In addition, solar radiation significantly increased mass loss and decreased the nutrient remaining. Furthermore, the effects of solar radiation on mass loss, C remaining, and N remaining were found to be similar among areas with precipitation levels below 200 and above 800 mm and greater than in areas with precipitation levels between 200-400 mm and 400-800 mm. The effect of solar radiation on CO_2 emissions varied from 13.97% when precipitation was below 200 mm to –0.707% when precipitation was between 200 and 400 mm.

Conclusion: Climatic factors determine the response ratio of mass loss to solar radiation in arid lands, whereas the initial litter characteristics have a great influence on the response of mass loss to solar radiation in ecosystems that are not moisture limited. The effect of precipitation on the photodegradation mechanism of litter was primarily achieved by influencing the decomposition of lignin, and the main effect of solar radiation on litter decomposition will shift from the positive effect of "photopriming" to the negative effect of "microbial

inhibition" with the increase of precipitation. Our findings can provide a comprehensive understanding of litter decomposition patterns on a global scale, and our results showed that CO_2 emissions from photodegradation will be lessened by precipitation, which is important in predicting CO_2 emission and separating sources of CO_2 under future increasing precipitation scenarios, particularly in arid lands.

KEYWORDS

meta-analysis, precipitation, litter, photodegradation, microbial decomposition

1 Introduction

Litter decomposition is a crucial biogeochemical process that plays a vital role in the cycling of carbon and other nutrients in ecosystems (Swift et al., 1979; Wang et al., 2021). Various factors, such as microorganisms, local climate, and litter quality, are considered as primary determinants of litter decomposition (Coûteaux et al., 1995). Empirical models that incorporate these three factors have been developed to estimate litter decomposition in diverse ecosystems (Bonan et al., 2013). However, these models often underestimate the decomposition rate in semiarid and arid lands, and they cannot fully account for the variation of decomposition among different terrestrial ecosystems (Bonan et al., 2013). These findings indicate that additional factors may influence litter decomposition. Therefore, exploring more comprehensive mechanisms that affect litter decomposition and carbon cycling is essential to predict changes in carbon and nutrient dynamics in the face of climate change.

In the past few decades, scientists have increasingly recognized the impact of solar radiation on litter decomposition, particularly in arid lands where photodegradation can account for approximately 26% of mass loss (Adair et al., 2017). On the one hand, solar radiation can directly affect recalcitrant organic matter such as lignin, breaking it down into smaller, more easily decomposable organic materials and directly producing greenhouse gases such as CO_2 (Pancotto et al., 2003; Austin and Vivanco, 2006; Gallo et al., 2006; King et al., 2012; Austin et al., 2016). In addition, these smaller organic materials can indirectly enhance microbial decomposition by promoting microbial and enzymatic activities (King et al., 2012; Austin et al., 2016; Berenstecher et al., 2020). On the other hand, solar radiation can also inhibit microbial decomposition because microbes can absorb photons, which caused DNA damage (Johnson, 2003; Pancotto et al., 2003). Therefore, the net effect of solar radiation on litter decomposition depends on the balance between its facilitative and inhibitory effects on microbial activity (Johnson, 2003; Robson et al., 2005; Huang and Li, 2017; Lin et al., 2017; Wang et al., 2021).

Precipitation is a significant factor regulating the response of litter decomposition to solar radiation (Smith et al., 2010; Huang and Li, 2017). In semi-arid and arid regions, the positive effect of solar radiation on litter decomposition can offset the negative effect on microbes, and the net effect of solar radiation on litter decomposition is generally positively related to the amount of precipitation (Wang et al., 2015; Gliksman et al., 2017; Huang and Li, 2017; Pieristè et al., 2020). An increase in precipitation directly enhances litter leaching, facilitates nutrient dissolution, and produces more dissolved organic carbon (DOC), which can be easily degraded by solar radiation (Pancotto et al., 2003; Smith et al., 2010). However, the relative importance of photodegradation in the decomposition of litter remains unclear as some field studies have shown that precipitation can simultaneously increase photodegradation and microbial decomposition, and no assessment has been made of whether the improvement in photodegradation exceeds that of microbial decomposition (Smith et al., 2010; Huang and Li, 2017).

Similarly, the net effect of solar radiation on litter decay in relatively humid ecosystems and the mechanism by which it changes with increasing precipitation remain unclear with conflicting findings reported in various studies (Smith et al., 2010; Evans et al., 2020). These conflicts may be due to variations in litter traits, with some plants developing more protective structures, such as lignin, which make them more sensitive to solar radiation (Gehrke et al., 1995; Moody et al., 2001; Austin and Vivanco, 2006; Lin et al., 2017; Wang et al., 2021). Other factors that can reduce the contribution of litter photodegradation include periodic snow cover and a dense plant canopy, which can decrease cumulative irradiance (Egidi et al., 2023; Smith et al., 2010; Evans et al., 2020). In addition, experiments in relatively humid conditions have shown that the net effect of radiation shifts from "photopriming" to biological suppression with increasing precipitation (Moody et al., 2001; Pancotto et al., 2003; Smith et al., 2010). As future extreme precipitation is expected to increase, particularly in 40% of the global land area that is dryland (Reynolds et al., 2007; Yao et al., 2020), the mechanism of litter decomposition in global drylands will undergo fundamental changes. Therefore, understanding the mechanism of nutrient loss in the litter, particularly in arid ecosystems, is crucial for effectively predicting and managing global carbon and nutrient cycles.

In investigating our research questions, a comprehensive meta-analysis of photodegradation studies was conducted to examine the interactive effects of solar radiation and precipitation on litter decomposition on a global scale. Moreover, the impact of solar

radiation on litter decomposition was evaluated across various mean annual precipitation (MAP). The following specific questions were addressed: (1) How does the effect of radiation on litter decomposition vary with different precipitation levels? (2) Whether do the key drivers of the response of mass loss to solar radiation in different precipitation levels change? (3) Whether and how does the mechanism of photodegradation vary with different precipitation levels?

2 Materials and methods

2.1 Meta-analysis

Our dataset for meta-analysis was obtained by extracting 351 data points from 37 articles found in the "Web of Science" database (Figure 1; Table S1). These articles were published between 1995 and 2022, which contained keywords such as "UV", "Ultraviolet radiation", "radiation", "light", "irradiance", "solar", "photodegradation", "decomposition", "decay", and "degradation". We ensured that the selection process was systematic to avoid publication bias and that the data met the following criteria: (1) experiments involving litter collections were conducted on a soil surface in natural terrestrial systems, excluding studies in lab and aquatic systems; (2) the overall litter decomposition characteristics (i.e., K value and mass loss), litter quality traits (i.e., C, N, C:N, lignin, or dissolved organic carbon (DOC)), or microbial growth characteristics (i.e., microbial biomass carbon (MBC) and CO_2 emission) were analyzed during the experiment; (3) control and treatment experiments were consistently maintained under the same abiotic and biotic conditions; (4) the litters were exposed to a minimum of two levels of UV radiation, with the treatment group being exposed to ambient UV and the control group being subjected to conditions in which UV was blocked or reduced; (5) only the latest results were collected for experimental observations spanning multiple years; (6) if an article included multiple sites and species, each species and site were treated as an independent study.

In estimating the interactive effect of precipitation and radiation on litter decomposition, the observation was divided into two types, namely, "Radiation" and "Combine". "Radiation" studies included photodegradation experiments that did not receive extra water addition and included 351 data points. Meanwhile, "Combine" studies included photodegradation experiments that received extra water addition artificially and included 15 data points. The interactive effect of radiation and precipitation was obtained by comparing it to the treatment without radiation and water addition. However, given the insufficient data, the interactive effect between radiation and precipitation was not explored in depth. Therefore, the studies were categorized into the following four groups based on precipitation amounts, characteristics of precipitation distribution in the data, and precipitation characteristics of Koppen's climatic province (Beck et al., 2018): precipitation< 200 mm, 200–400 mm, 400–800 mm, and >800 mm, corresponding to arid, semiarid, subhumid, and humid lands. This technique allowed us to accurately estimate the interactive effect of precipitation and solar radiation on litter decomposition.

We extracted local site information, including latitude, longitude, mean annual temperature (MAT), MAP, experimental duration, and litter traits such as initial C, N, lignin, hemicellulose, cellulose, and DOC concentration, from the articles. Graphical data were obtained using Web Plot Digitizer 4.2. In evaluating the relationship between soil respiration and photodegradation, soil respiration data were retrieved from the Soil Respiration Database (SRDB V5) (Jian et al., 2021), which roughly corresponded to the geographic coordinates of the data points in the meta-analysis.

2.2 Data analysis

The meta-analysis was conducted using Metawin software. The impact of solar radiation alone and the interactive effect

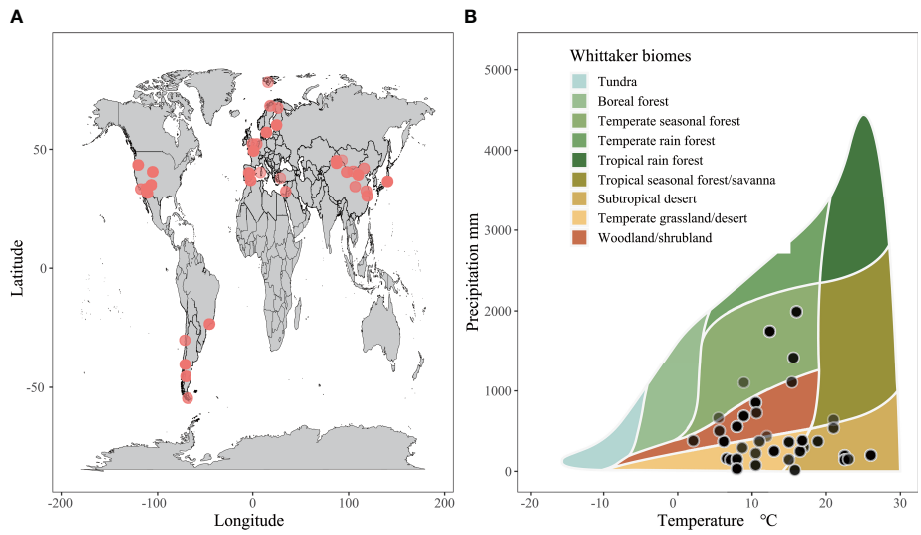

FIGURE 1
Global map of the study sites distribution **(A)**, and local climate and biomes **(B)** in this meta-analysis.

between solar radiation and precipitation on litter decomposition were evaluated through log response ratio (LnRR) as Hedges et al. (1999):

$$\mathrm{LnRR} = \mathrm{Ln}\left(\frac{Xt}{Xc}\right) = \mathrm{Ln}(Xt) - \mathrm{Ln}(Xc)$$

and a variance:

$$v = \frac{(St)^2}{Nt(Xt)^2} + \frac{(Sc)^2}{Nc(Xc)^2}$$

where Xt and Xc are the mean values of each variable in treatment and in the control, St and Sc are the standard deviations, and Nt and Nc are sample size. The variance in mean LnRR was computed by 95% confidence intervals.

$$W = (Nt * Nc)/(Nt + Nc)$$

where W is the weighting factor for each LnRR datapoint. To assess the overall weighted response ratio (LnRR++) of litter decomposition to precipitation, we employed a random model to computed it.

$$\mathrm{LnRR} + + = (\sum_i \mathrm{LnRR_i} * W_i)/(\sum_i W_i)$$

The variance in mean lnRR++ was computed by 95% confidence intervals (CIs), which were produced by bootstrapping function. Mean lnRR++ and its 95% confidence intervals (CIs) were used to calculate effect sizes:

$$\mathrm{Effect\ size}(\%) = (e^{\mathrm{LnRR++}} - 1) * 100\,\%$$

The Q test was performed to evaluate between-group heterogeneity and the subcategories, including precipitation levels (<200 mm, 200–400 mm, 400–800 mm, and >800 mm), ecosystem types (forest, shrubland, and grassland), species (tree, shrub, and herb), and experimental duration (<1 year, 1–3 years, and >3 years). Linear regression analysis was utilized to investigate the relationship between the LnRR of mass loss, carbon remaining, nitrogen remaining, lignin remaining, and geographic characteristics and initial litter traits, including latitude, longitude, MAT, MAP, soil respiration, initial carbon, nitrogen, lignin, and experimental duration. In addition, random-forest analysis was used to rank the importance of factors influencing the response of litter mass loss, which was determined using the percent increase in mean square error (%IncMSE) metric. Negative %IncMSE values indicate the lack of importance of predictors (Liaw and Wiener, 2002).

3 Results

3.1 Responses of litter decomposition to solar radiation in a global scale

Solar radiation played a significant role in litter decomposition (Figure 2). The results of the sole solar radiation treatment revealed that solar radiation increased mass loss by 17.89%;

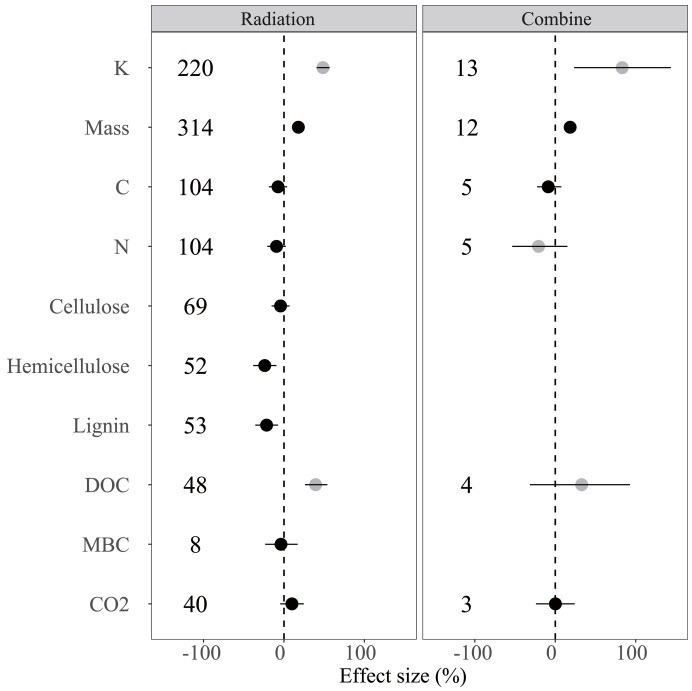

FIGURE 2
Responses of litter decomposition variables to solar radiation were examined through sole radiation treatment (Radiation) and the combination of water addition and radiation treatment (Combine). The results are presented as LnRR++ with 95%CI. The numbers indicate the number of data observations. Black points indicate a significant effect, whereas grey points indicate an insignificant effect. The indexes used are as follows: K = K value, Mass = mass loss, C = carbon remaining, N = nitrogen remaining, DOC = dissolved organic carbon concentration, Lignin = lignin remaining, MBC = microbial biomass carbon, and CO_2 = CO_2 emission from litter decomposition. Numbers indicate the number of data observations.

reduced C remaining by 7.41%, N remaining by 9.28%, cellulose remaining by 4.24%, hemicellulose remaining by 23.92%, lignin remaining by 21.62%, and MBC by 3.70%; and increased CO_2 emission by 9.99%. In the combined treatment, mass loss was increased by 18.05%, and C remaining was decreased by 8.73%, whereas CO_2 emission was increased slightly by 0.20%. No significant difference in mass loss and C remaining was observed between the "Radiation" and "Combined" treatments. In addition, mass loss, C remaining, and N remaining had no significant difference among different experimental durations but had remarkable differences in different ecosystems and species, which closely correlated with precipitation in our database (Figure S1).

In assessing the influence of precipitation on the net effect of solar radiation, we verify whether the response of litter decomposition to solar radiation varies with precipitation amount. Significant variations in the effect of solar radiation on litter decomposition and CO_2 emission were observed across different precipitation levels (Figure 3). Mass loss was significantly increased by 25.33% and 17.46% at precipitation levels below 200 mm and above 800 mm, whereas the increase was only 4.90% and 13.13% at precipitation levels of 200–400 mm and 400–800 mm, respectively. Similarly, the C remaining was reduced by 9.67% and 9.85% at precipitation levels below 200 mm and above 800 mm, respectively, and by 1.99% at a precipitation level of 200–400 mm. The N remaining was reduced by 15.17% and 16.30% at precipitation levels below 200 mm and above 800 mm but only 1.07% and 3.55% at precipitation levels of 200–400 mm and 400–800 mm, respectively. The reduction of the hemicellulose and lignin remaining was also greater at precipitation levels below 200 mm than that at other levels. Solar radiation significantly increased CO_2 emission by 13.97%, but it only showed a slight effect at precipitation levels of 200–400 mm and 400–800 mm.

3.2 The relationships between the response ratio of mass loss and various factors

The results showed that the response of mass loss to solar radiation was only negatively related to soil respiration, initial lignin concentration, and ln(MAP) on a global scale (Figure 4). The response of C remaining showed a positive relationship with latitude, longitude, and initial lignin concentration and a negative relationship with MAT and experimental duration (Figure S2). The response of N remaining was positively related to latitude, ln(MAP), soil respiration, initial C, and initial lignin concentration and negatively related to MAT (Figure S3). The response of lignin remaining was positively related to ln(MAP), initial C, and initial lignin concentration and negatively related to initial N and experimental duration (Figure S4).

3.3 Dominant factors regulating the responses of mass loss to radiation

On a global scale, random-forest analysis revealed that several factors were significantly associated with the effects of solar radiation on mass loss, including latitude, initial lignin concentration, experimental duration, MAT, MAP, longitude, and soil respiration (Figure 5). When precipitation was less than 200 mm, MAP plays an important role in regulating the response of mass loss to radiation. However, as precipitation increased, the relative importance of MAP in regulating mass loss decreased with MAP exerting no significant effect on the response ratio when the precipitation level was between 400–800 mm and >800 mm. At a precipitation level of 400–800 mm, soil respiration plays an important role in regulating the ratio, and the initial litter trait such as initial N and lignin concentration became increasingly important in driving the response of mass loss to radiation when the precipitation level was >800 mm.

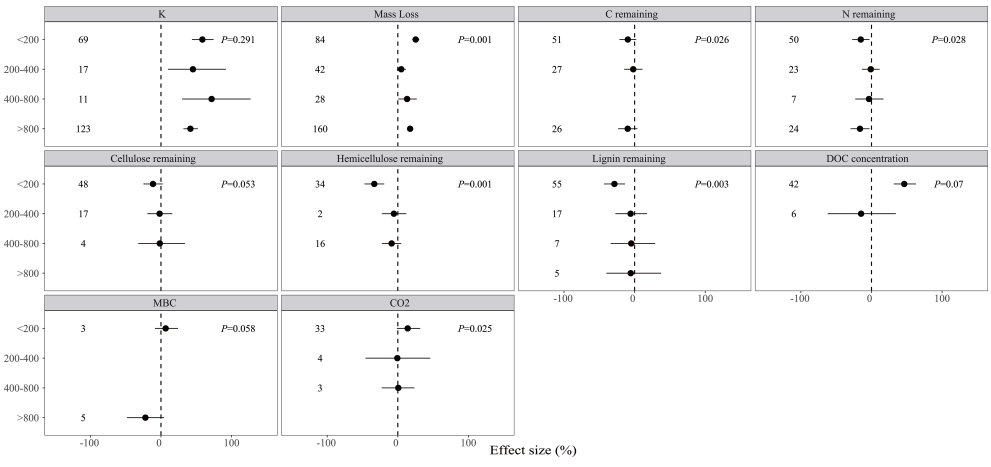

FIGURE 3
Effects of solar radiation on litter decomposition variables at different precipitation levels: <200mm, 200–400 mm, 400–800 mm, and >800 mm. Results were presented as LnRR++ with 95% confidence intervals. Numbers indicate the number of data observations. P indicates the result of the between-group heterogeneity test (QB) at different precipitation levels.

4 Discussion

4.1 Effects of the interactive effect on litter decomposition

Solar radiation is a critical factor in the regulation of litter decomposition. Our findings are consistent with previous research, demonstrating that solar radiation significantly increases mass loss in sole radiation and combined treatment. Moreover, the response of litter decomposition to solar radiation is closely related to MAP (Figure 4). In addition, no significant difference in the effect of solar radiation on mass loss is found among lands with precipitation levels below 200 mm and above 800 mm, which was higher than in other areas (Figure 3). In general, radiation plays a significant role in litter decomposition in extremely arid lands, (King et al., 2012; Austin et al., 2016; Berenstecher et al., 2020), whereas the contribution of photodegradation decreases in relatively humid ecosystems because of the increased microbes and plant canopy (Egidi et al., 2023; Smith et al., 2010; Evans et al., 2020). Contrary to previous studies indicating that radiation generally has a negligible effect on litter decomposition in wet ecosystems (Newsham et al., 1997; Moody et al., 2001), our results suggested that litter decomposition has a greater response to radiation at a precipitation level of >800 mm than those at 200–400 mm and 400–800 mm. These results answered questions (1) and (3), that is, the effect of radiation initially decreases and then increases with different precipitation levels, indicating that precipitation can change the litter decomposition mechanism. This result might be

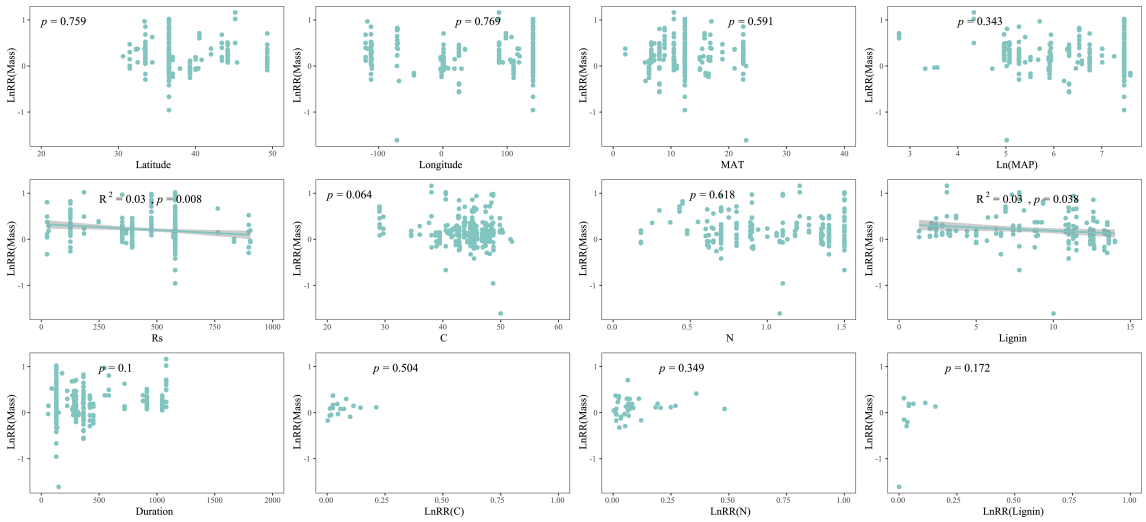

FIGURE 4
Relationships between the log response ratio (LnRR) of mass loss (Mass Loss) and various factors, including latitude, longitude, MAT, ln(MAP), soil respiration, initial litter C, N, lignin concentration, and experimental duration, as well as the log response ratios (LnRR) of the litter C and N remaining to solar radiation.

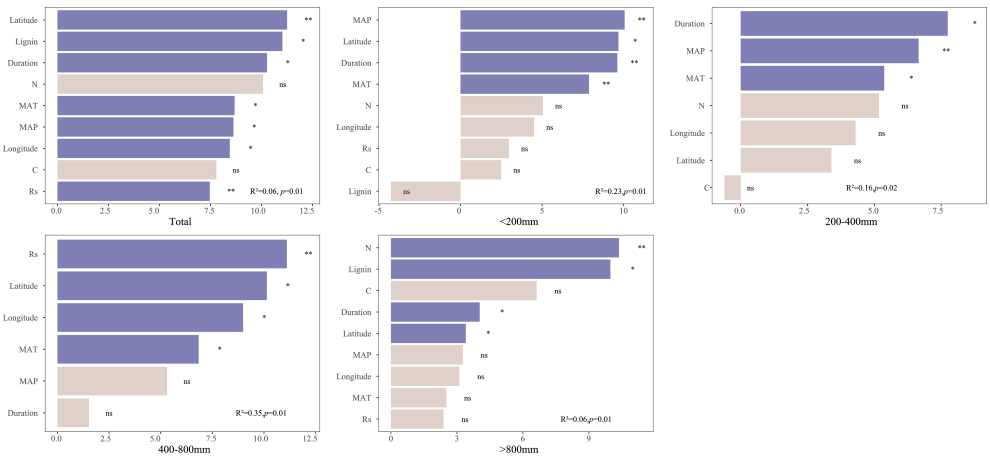

FIGURE 5
Random forest analysis was used to assess the importance of predictors of the log response ratio of mass loss to solar radiation on the global scale at precipitation levels of<200 mm, 200–400 mm, 400–800 mm, and >800 mm. The purple bar indicates the predictors that significantly influence mass loss, and the white bar indicates the predictors that exerted no significant influence on mass loss.

due to the condition of microbes in humid ecosystems where microbial biomass and diversity are significantly higher than in other areas, and previous research has shown that several soluble materials are produced by microbes, which exerted a positive effect on litter photodegradation (Gallo et al., 2006; Austin et al., 2009; Smith et al., 2010).

Classical models of global carbon turnover often fail to consider the impact of photodegradation on C loss during litter decomposition as previous studies have consistently neglected this factor. Our study suggests that sole radiation treatment and combined treatment had a significant but relatively minor effect on C remaining; however, a significant difference in precipitation amounts was observed (Figure 3). The response of C remaining to solar radiation was higher in areas with a precipitation level of<200 mm compared with other regions (except for a precipitation level of >800 mm). Similarly, the proportion of C, including cellulose, hemicellulose, and lignin, showed significant changes at a precipitation level of<200 mm, which supports our previous conclusion, that is, solar radiation has a greater impact in arid regions (Smith et al., 2010; Huang and Li, 2017). Solar radiation only decreased the lignin remaining at a precipitation level of<200 mm, and the mass loss and C, N, and lignin remaining had significant relationships with the initial litter lignin concentration (Figures 4, S2–S4), which is consistent with previous studies that have shown that lignin is the main target of photodegradation (Austin and Vivanco, 2006; King et al., 2012). Furthermore, solar radiation had a minor impact on lignin in other regions, particularly in areas where precipitation was greater than 800 mm, exhibiting similar mass loss and responses of C and N remaining to solar radiation in regions with a precipitation level of less than 200 mm (Figure 3). This finding indicated that lignin is more susceptible to solar radiation than to microbial decomposition (Vanderbilt et al., 2008; Bontti et al., 2009; Wang et al., 2015), which can directly absorb ultraviolet and short-wave visible light and produce smaller organic compounds (Austin and Vivanco, 2006; King et al., 2012). The relationship between the response of the lignin remaining and MAP also supports our view as the extent of the lignin remaining decreases with the increase of MAP (Figure S4). Therefore, increasing precipitation in the future will influence the mechanism driving lignin decomposition by altering the dominance of photodegradation and microbial decomposition. In addition, solar radiation increased litter DOC concentration at a precipitation level of<200 mm, although the effect was not significant. We can partly predict that the DOC concentration will increase with the increase in precipitation because of the breakdown and leaching effects (Smith et al., 2010; Austin, 2011; Huang and Li, 2017). This phenomenon will generate a positive feedback loop that improves litter decomposition decay because of its susceptibility to radiation and the provision of high-quality labile carbon to microbes.

Microbial activity primarily regulates the dynamics of litter N, with initial N continuously increasing because of microbial immobilization for growth, followed by a decrease as microbes mineralize N in later stages of decomposition (Brandt et al., 2007; Smith et al., 2010; Wang et al., 2015). In sole solar radiation treatment, N immobilization decreased (Figure 2), with a greater decline at a precipitation level of<200 mm (Figure 3). This trend is consistent with solar radiation exposure reducing microbial activity because biotic processes are inhibited (McLeod et al., 2008; Gliksman et al., 2017; Huang and Li, 2017; Marinho et al., 2020). However, the response of N remaining to solar radiation was not significant when precipitation was between 200-400 mm and 400-800 mm. These neutral results indicated that microbes are more resilient to the negative effects of radiation when moisture is not limited, and models of litter N dynamics should consider the mitigating effects of precipitation on microbial activity (King et al., 2012; Austin et al., 2016; Berenstecher et al., 2020). Compared with the moderately negative effect in areas with precipitation between 200–400 mm and 400–800 mm, the negative effect of radiation on N immobilization is stronger in humid ecosystems (precipitation >800 mm) where microbial decomposition dominantly regulates the process. In wet ecosystems, solar radiation can speed up nitrogen mineralization by microorganisms, thereby reducing the nitrogen remaining (Smith et al., 2010; Wei et al., 2022). Therefore, microbial decomposition is typically faster in areas with higher moisture content and more likely to progress to later stages of degradation (Austin and Vivanco, 2006; Smith et al., 2010; Gliksman et al., 2017). Thus, conducting long-term and short-term interactive N dynamic studies in different ecosystems is necessary to provide a comprehensive understanding of the interactive effects of multiple factors on N dynamics.

4.2 Effects of the interactive effect on microbial activity and CO_2 emission

The inhibition of microorganisms by radiation may occur through several distinct mechanisms, such as DNA damage and decreased spore germination (Moody et al., 2001; Johnson, 2003; Austin and Vivanco, 2006; Parton et al., 2007; Austin, 2011), and modifications to the structure of microbial communities (Pancotto et al., 2003; Smith et al., 2010; Sala et al., 2015; Marinho et al., 2020). Although the precise role of water in this process remains unclear, microorganisms are more resilient to harm when not experiencing water stress. However, our meta-analysis found that solar radiation had a negative impact on MBC, particularly in ecosystems with high precipitation (>800 mm), whereas MBC increased in ecosystems with low precipitation (<200 mm) probably because the positive effect of photodegradation on microbial activity offsets the negative effect in arid lands. As the moisture level increases, the primary effect of radiation on litter decomposition may transition from “photopriming” to the suppression of microorganisms. However, given the restricted availability of MBC data, further experiments must be conducted to confirm this conclusion. Therefore, conducting experiments in the future is necessary to examine the interaction between water and radiation on MBC and elucidate the changes in the mechanism of litter decomposition under increasing precipitation. In addition, although the change in MBC was unclear, CO_2 emission increased across all treatments and precipitation levels (except 200-400 mm). This increase was due to the emission of C-based trace gases produced by the photochemical mineralization of recalcitrant compounds (McLeod et al., 2008; Rutledge et al., 2010). However, the response of CO_2 emission to solar radiation decreased with the increase of precipitation

compared with the response when the precipitation level was<200 mm. This finding provides a new insight into the influence of precipitation on CO_2 emission, where CO_2 emission may significantly change with the increase of precipitation in photodegradation ways, particularly in xeric lands. However, given the data limitations, CO_2 obtained from global photomineralized sources cannot be quantified. Thus, future research projects are necessary to gain a more integrated understanding of the effects of radiation on CO_2 emission.

4.3 Dominant factors regulating the responses of the mass loss to solar radiation

The impact of solar radiation on litter decomposition is complex, and it varies depending on its magnitude and other factors. On a global scale, latitude and initial lignin concentration play crucial roles in regulating the response ratio of mass loss to solar radiation. This finding supports earlier studies that consider lignin as the primary target for photodegradation (Austin and Vivanco, 2006; Brandt et al., 2007; Wang et al., 2022). Similarly, initial litter traits, such as N and lignin concentration, play important roles in regulating the response ratio of mass loss to solar radiation at a precipitation level of >800 mm, which might be due to no moisture limitation in this region; moreover, intense microbial activity was observed, and the photodegradation activity was not limited by other factors (Coûteaux et al., 1995). However, climatic factors appear to have a greater influence on litter decomposition than initial litter traits in ecosystems that are moisture limited, which answers our second question (2) and presents challenges in predicting global litter decomposition. With the expected increase in precipitation in the future, MAP may become more significant and affect CO_2 emission through leaching and microbial growth. Therefore, long-term experiments that consider biotic and abiotic factors, including MAP, are essential for predicting litter decomposition and CO_2 emission in a changing climate.

5 Conclusion and prospects

We conducted a meta-analysis and found that the effect of radiation on litter decomposition depends on the magnitude of MAP. In particular, a similar effect of radiation on litter mass loss was observed in arid lands and humid ecosystems, and precipitation can increase resilience to the negative effects of radiation on microbes. Furthermore, the mechanism of litter decomposition and the regulatory factors of photodegradation would change with increasing precipitation. Moreover, radiation increased the CO_2 emission rate for all precipitation amounts, particularly in arid lands. As precipitation continues to increase in the future, litter decomposition, carbon cycling, and CO_2 emission caused by photodegradation may change significantly.

We also found that the heterogeneity of radiation's impact on litter decomposition can be explained by climatic factors and initial litter traits. This knowledge may help us comprehensively understand the mechanism by which radiation affects litter decomposition and CO_2 emission in different ecosystems. Future studies should focus on investigating the interactive effect of precipitation and solar radiation on litter decomposition and microbial activity in relatively humid ecosystems to obtain a comprehensive understanding of how climate change will affect litter decomposition. Furthermore, more research must be conducted to accurately assess the effect of radiation on CO_2 emission caused by photodegradation. A comprehensive understanding of the contribution of biodegradation and photodegradation to litter decomposition will help us in predicting how litter decomposition will respond to climate change.

Data availability statement

The original contributions presented in the study are included in the article/Supplementary Material. Further inquiries can be directed to the corresponding author.

Author contributions

YL analyzed data and wrote the manuscript. LL and XL conceived the work and supervised the research. SW contributed to analyze the manuscript. All authors contributed to the article and approved the submitted version.

Funding

This research was supported by the National Natural Science Foundation of China (42171066; 41877420); West Light Foundation of The Chinese Academy of Sciences (2019-FPGGRC).

Conflict of interest

The authors declare that the research was conducted in the absence of any commercial or financial relationships that could be construed as a potential conflict of interest.

Publisher's note

Supplementary material

The Supplementary Material for this article can be found online at: https://www.frontiersin.org/articles/10.3389/fpls.2023.1200155/full#supplementary-material

References

Adair, E. C., Parton, W. J., King, J. Y., Brandt, L. A., and Lin, Y. (2017). Accounting for photodegradation dramatically improves prediction of carbon losses in dryland systems. *Ecosphere* 8 (7), e01892. doi: 10.1002/ecs2.1892

Austin, A. T. (2011). Has water limited our imagination for aridland biogeochemistry? *Trends Ecol. Evol.* 26 (5), 229–235. doi: 10.1016/j.tree.2011.02.003

Austin, A. T., Araujo, P. I., and Leva, P. E. (2009). Interaction of position, litter type, and water pulses on decomposition of grasses from the semiarid Patagonian steppe. *Ecology* 90, 2642–2647. doi: 10.1890/08-1804.1

Austin, A. T., Méndez, M. S., and Ballaré, C. L. (2016). Photodegradation alleviates the lignin bottleneck for carbon turnover in terrestrial ecosystems. *PNAS.* 113 (16), 4392–4397. doi: 10.1073/pnas.1516157113

Austin, A. T., and Vivanco, L. (2006). Plant litter decomposition in a semi-arid ecosystem controlled by photodegradation. *Nature* 442, 555–558. doi: 10.1038/nature05038

Beck, H. E., Zimmermann, N. E., McVicar, T. R., Vergopolan, N., Berg, A., and Wood, E. F. (2018). Present and future köppen-Geiger climate classification maps at 1-km resolution. *Sci. Data* 5, 180214. doi: 10.1038/sdata.2018.214

Berenstecher, P., Vivanco, L., Perez, L. I., Ballare, C. L., and Austin, A. (2020). Sunlight doubles aboveground carbon loss in a seasonally dry woodland in Patagonia. *Curr. Biol.* 30 (16), 3243–3251. doi: 10.1016/j.cub.2020.06.005

Bonan, G. B., Hartman, M. D., Parton, W. J., and Wieder, W. R. (2013). Evaluating litter decomposition in earth system models with long-term litterbag experiments: an example using the community land model version 4 (CLM4). *Global Change Biol.* 19, 957–974. doi: 10.1111/gcb.12031

Bontti, E. E., Decant, J. P., Munson, S. M., Gathany, M. A., Przeszlowska, A., Haddix, M. L., et al. (2009). Litter decomposition in grasslands of central north America (US great plains). *Global Change Biol.* 15, 1356–1363. doi: 10.1111/j.1365-2486.2008.01815.x

Brandt, L. A., King, J. Y., and Milchunas, D. G. (2007). Effects of ultraviolet radiation on litter decomposition depend on precipitation and litter chemistry in a shortgrass steppe ecosystem. *Global Change Biol.* 13, 2193–2205. doi: 10.1111/j.1365-2486.2007.01428.x

Coûteaux, M. M., Bottner, P., and Berg, B. (1995). Litter decomposition, climate and liter quality. *Trends Ecol. Evol.* 10 (2), 63–66. doi: 10.1016/S0169-5347(00)88978-8

Egidi, E., Delgado-Baquerizo, M., Berdugo, M., Guirado, E., Albanese, D., Singh, B. K., et al. (2023). UV Index and climate seasonality explain fungal community turnover in global drylands. *Global Ecol. Biogeogr.* 32, 132–144. doi: 10.1111/geb.13607

Evans, S., Todd-Brown, K. E. O., Jacobson, K., and Jacobson, P. (2020). Non-rainfall moisture: a key driver of microbial respiration from standing litter in arid, semiarid, and mesic grasslands. *Ecosystems* 23, 1154–1169. doi: 10.1007/s10021-019-00461-y

Gallo, M. E., Sinsabaugh, R. L., and Cabaniss, S. E. (2006). The role of ultraviolet radiation in litter decomposition in arid ecosystems. *Appl. Soil Ecol.* 34, 82–91. doi: 10.1016/j.apsoil.2005.12.006

Gehrke, C., Johanson, U., Callaghan, T. V., Chadwick, D., and Robinson, C. H. (1995). The impact of enhanced UV-b radiation on litter quality and decomposition processes in vaccinum leaves from the subarctic. *Oikos* 72, 213–222. doi: 10.2307/3546223

Gliksman, D., Rey, A., Seligmann, R., Dumbur, R., Sperling, O., Navon, Y., et al. (2017). Biotic degradation at night, abiotic degradation at day: positive feedbacks on litter decomposition in drylands. *Global Change Biol.* 23, 1564–1574. doi: 10.1111/gcb.13465

Hedges, L. V., Gurevitch, J., and Curtis, P. S. (1999). The meta-analysis of response ratios in experimental ecology. *Ecology* 80, 1150–1156. doi: 10.1890/0012-9658(1999)080[1150:TMAORR]2.0.CO;2

Huang, G., and Li, Y. (2017). Photodegradation effects are related to precipitation amount, precipitation frequency and litter traits in a desert ecosystem. *Soil Biol. Biochem.* 115, 383–392. doi: 10.1016/j.soilbio.2017.08.034

Jian, J., R.Vargas, K. J., Anderson-Teixeira, E., Stell, V., Herrmann, M., Horn, N., et al. (2021). *A global database of soil respiration data, version 5.0* (Oak Ridge, Tennessee, USA: ORNL DAAC). doi: 10.3334/ORNLDAAC/1827

Johnson, D. (2003). Response of terrestrial microorganisms to ultraviolet-b radiation in ecosystems. *Res. Microbiol.* 154, 315–320. doi: 10.1016/S0923-2508(03)00078-0

King, J. Y., Brandt, L. A., and Adair, E. C. (2012). Shedding light on plant litter decomposition: advances, implications and new directions in understanding the role of photodegradation. *Biogeochemistry* 111, 57–81. doi: 10.1007/s10533-012-9737-9

Liaw, A., and Wiener, M. (2002). Classification and regression by random forest. *R. News* 2, 18–22.

Lin, Y., Karlen, S. D., Ralph, J., and King, J. Y. (2017). Short-term facilitation of microbial litter decomposition by ultraviolet radiation. *Sci. Total Environ.* 615, 838–848. doi: 10.1016/j.scitotenv.2017.09.239

Marinho, O. A., Martinelli, L. A., Duarte-Neto, P. J., Mazzi, E. A., and King, J. Y. (2020). Photodegradation influences litter decomposition rate in a humid tropical ecosystem, Brazil. *Sci. Total Environ.* 715, 136601. doi: 10.1016/j.scitotenv.2020.136601

McLeod, A. R., Fry, S. C., Loake, G. J., Messenger, D. J., Reay, D. S., Smith, K. A., et al. (2008). Ultraviolet radiation drives methane emissions from terrestrial plant pectins. *New Phytol.* 180, 124–132. doi: 10.1111/j.1469-8137.2008.02571.x

Moody, S. A., Stoddard, M. T., Chappell, E. A., Harmon, M. E., and Jackson, R. B. (2001). The direct effects of UV-b radiation on betula pubescens litter decomposing at four European field sites. *Plant Ecol.* 154, 29–36. doi: 10.1023/A:1012965610170

Newsham, K. K., McLeod, A., Roberts, J. D., Greenslade, P. D., and Emmett, B. A. (1997). Direct effects of elevated UV-B radiation on the decomposition of Quercus robur leaf litter. *Oikos* 79 (3), 592–602.

Pancotto, V. A., Sala, O. E., Cabello, M., and López, R. P. (2003). Solar UV-b decreases decomposition in herbaceous plant litter in tierra del fuego, Argentina: potential role of an altered decomposer community. *Global Change Biol.* 9, 1465–1474. doi: 10.1046/j.1365-2486.2003.00667.x

Parton, W., Silver, W. L., Burke, I. C., Grassens, L., Harmon, M. E., Currie, W. S., et al. (2007). Global-scale similarities in nitrogen release patterns during long-term decomposition. *Science* 315, 361–364. doi: 10.1126/science.1134853

Pieristè, M., Neimane, S., Solanki, T., Nybakken, L., Jones, A. G., Forey, E., et al. (2020). Ultraviolet radiation accelerates photodegradation under controlled conditions but slows the decomposition of senescent leaves from forest stands in southern Finland. *Plant Physiol. Bioch.* 146, 42–54. doi: 10.1016/j.plaphy.2019.11.005

Reynolds, J. F., Smith, D. M. S., Lambin, E. F., Turner, I. I. B. L., Mortimore, M., Batterbury, S. P. J., et al. (2007). Global desertification: building a science for dryland development. *Science* 316, 847–851. doi: 10.1126/science.1131634

Robson, T., Pancotto, V., Scopel, A., Flint, S., and Caldwell, M. (2005). Solar UV-b influences microfaunal community composition in a tierra del fuego peatland. *Soil Biol.Bioch.* 37, 2205–2215. doi: 10.1016/j.soilbio.2005.04.002

Rutledge, S., Campbell, D. I., Baldocchi, D., and Schipper, L. A. (2010). Photodegradation leads to increased carbon dioxide losses from terrestrial organic matter. *Global Change Biol.* 16, 3065–3074. doi: 10.1111/j.1365-2486.2009.02189.x

Sala, O. E., Gherardi, L. A., and Peters, D. P. (2015). Enhanced precipitation variability effects on water losses and ecosystem functioning: differential response of arid and mesic regions. *Climatic Change* 131 (2), 213–227. doi: 10.1007/s10584-015-1389-z

Smith, W. K., Gao, W., Steltzer, H., Wallenstein, M. D., and Tree, R. (2010). Moisture availability influences the effect of ultraviolet-b radiation on leaf litter decomposition. *Global Change Biol.* 16, 484–495. doi: 10.1111/j.1365-2486.2009.01973.x

Swift, M. J., Heal, O. W., and Anderson, J. (1979). *Decomposition in terrestrial ecosystems* (Oakland, CA, USA: University of California Press).

Vanderbilt, K., Schmitz, O. J., and Gebauer, R. L. E. (2008). Aboveground decomposition in arid environments: results of a long-term study in central new Mexico. *J. Arid. Environ.* 72, 696–709. doi: 10.1016/j.jaridenv.2007.10.010

Wang, J., Liu, L., Wang, X., and Chen, Y. (2015). The interaction between abiotic photodegradation and microbial decomposition under ultraviolet radiation. *Global Change Biol.* 21 (5), 2095–2104. doi: 10.1111/gcb.12812

Wang, Q. W., Pieristè, M., Kotilainen, T. K., Forey, E., Chauvat, M., Robson, T. M., et al. (2022). The crucial role of blue light as a driver of litter photodegradation in terrestrial ecosystems. *Plant Soil*, 1–16. doi: 10.1007/s11104-022-05596-x

Wang, Q.-W., Pieristè, M., Liu, C., Kenta, T., Robson, T. M., and Kurokawa, H. (2021). The contribution of photodegradation to litter decomposition in a temperate forest gap and understorey. *New Phytol.* 229, 2625–2636. doi: 10.1111/nph.17022

Wei, B., Zhang, D., Kou, D., Yang, G., Liu, F., Peng, Y., et al. (2022). Decreased ultraviolet radiation and decomposer biodiversity inhibit litter decomposition under continuous nitrogen inputs. *Funct.Ecol.* 36, 998–1009. doi: 10.1111/1365-2435.14015

Yao, J. Y., Liu, H. P., Huang, J. P., Gao, Z. M., Wang, G. Y., Li, D., et al. (2020). Accelerated dryland expansion regulates future variability in dryland gross primary production. *Nat. Commun.* 11, 1665. doi: 10.1038/s41467-020-15515-2

frontiers | Frontiers in Plant Science

TYPE Original Research
PUBLISHED 06 July 2023
DOI 10.3389/fpls.2023.1212406

OPEN ACCESS

EDITED BY
Qingpeng Yang,
Chinese Academy of Sciences (CAS), China

REVIEWED BY
Jun Ma,
Fudan University, China
Dandan Yu,
Ministry of Ecology and Environment, China

*CORRESPONDENCE
Jiangtao Xiao
jiangtao.xiao@sicnu.edu.cn

RECEIVED 26 April 2023
ACCEPTED 14 June 2023
PUBLISHED 06 July 2023

CITATION
Lin Y, Cong N, Xiao J, Kou Y, Li Y, Yu X, Qi G, Gou C, Bai Y and Ren P (2023) Projecting future aboveground carbon sequestration rate of alpine forest on the eastern Tibetan Plateau in response to climate change.
Front. Plant Sci. 14:1212406.
doi: 10.3389/fpls.2023.1212406

Projecting future aboveground carbon sequestration rate of alpine forest on the eastern Tibetan Plateau in response to climate change

Yang Lin[1,2], Nan Cong[3], Jiangtao Xiao[1,2]*, Yongping Kou[4], Yuanyuan Li[1,2], Xinran Yu[1,2], Gang Qi[1,2], Chaolong Gou[5], Yongping Bai[5] and Ping Ren[2]

[1]Key Lab of Land Resources Evaluation and Monitoring in Southwest China, Ministry of Education, Sichuan Normal University, Chengdu, China, [2]The Faculty of Geography and Resources Sciences, Sichuan Normal University, Chengdu, China, [3]Key Laboratory of Ecosystem Network Observation and Modeling, Lhasa Plateau Ecosystem Research Station, Institute of Geographic Sciences and Natural Resources Research, Chinese Academy of Sciences, Beijing, China, [4]Key Laboratory of Mountain Ecological Restoration and Bioresource Utilization & Ecological Restoration and Biodiversity Conservation Key Laboratory of Sichuan Province, Chengdu Institute of Biology, Chinese Academy of Sciences, Chengdu, China, [5]Forestry and Grassland Bureau in Mao Country, Aba Tibetan and Qiang Autonomous Prefecture, China

The aboveground carbon sequestration rate (ACSR) of forests serves as an indicator of their carbon sequestration capacity over time, providing insights into the potential carbon sequestration capacity of forest ecosystems. To explore the long-term Spatiotemporal variation of ACSR in the transitional ecotone of the eastern Tibetan Plateau under climate change scenarios, we utilized a forest landscape model that was parameterized with forest inventory data from the eastern Tibetan Plateau to simulate this ecological function changes. The study found that climate warming had significant effect on forests ACSR in different types of forests. ACSR was significantly reduced ($p<0.05$) in cold temperate coniferous and temperate coniferous forests, whereas it was significantly increased in deciduous broad-leaved forests. However, the impact of climate warming on evergreen broad-leaved forests was found to be negligible. At the species level, climate warming has mostly suppressed the ACSR of coniferous trees, except for Chinese hemlock. The main dominant species, spruce and fir, have been particularly affected. Conversely, the ACSR of most broad-leaved trees has increased due to climate warming. In addition, at the landscape scale, the ACSR within this region is expected to experience a steady decline after 2031s-2036s. Despite the effects of climate warming, this trend is projected to persist. In conclusion, the forests ACSR in this region will be significantly affected by future climate warming. Our research indicates that climate warming will have a noticeable suppressive effect on conifers. It is imperative that this factor be taken into account when devising forest management plans for the future in this region.

KEYWORDS

aboveground carbon sequestration rate, climate change, ecological process model, species and community, Tibetan Plateau, carbon stock

1 Introduction

Numerous studies have shown that human activities have caused noticeable global warming for decades, which have direct effects on the growth, maturation, and interspecific competition of tree species, changing the productivity, carbon sequestration capacity, and other ecological functions of forests (Lindner et al., 2010; Bachelot et al., 2020; Liu et al., 2021; Liang et al., 2023). The response of forests to future climate remains highly uncertain (Liu et al., 2013; Frank et al., 2015; Schurman et al., 2019). On one hand, high levels of CO_2 emissions can benefit the growth and productivity of tree species (Franks et al., 2013; Gustafson et al., 2018). However, different tree species exhibit varying responses to elevated CO_2 concentrations (Kallarackal and Roby, 2012). On the other hand, moderate temperature increases can prolong the growing season and enhance productivity of tree species (Duveneck and Thompson, 2017), but excessive temperature increases can induce heat stress in tree species, resulting in decreased productivity and reduced carbon sequestration capacity (Teskey et al., 2015). This complex process highlights the need for a flexible and suitable indicator to reflect changes in forest carbon sequestration capacity under climate disturbance, the aboveground carbon sequestration rate (ACSR) could reflect the dynamic changes of forest carbon sequestration capacity timely and determine the potential carbon sequestration capacity of forest ecosystems (Chapin et al., 2002; Chen et al., 2013).

Several studies have revealed that climate change will significantly influence the carbon sequestration capacity of forests on a large scale (Ma et al., 2014; Zhou et al., 2022). Yao et al. (2018) introduced a semi-empirical model that demonstrates the positive relationship between rising CO_2 concentration due to climate change and the increase in total forest biomass and forest carbon sequestration in China. Specifically, transition zone forests have been identified as highly susceptible to the impacts of climate change (Dai et al., 2016; Wu et al., 2020). To fully understand the impact of climate change on forest carbon sequestration capacity, it is crucial to investigate the response of transition zone forests to these changes.

The alpine forests of western Sichuan are the transition zone from the Sichuan Basin to the Tibetan Plateau and are an important ecological barrier in the upper reaches of the Yangtze River, transition from broadleaf-dominated forests of southeast low mountain region to conifers-dominated forest of the northwest alpine region. The transitional ecotone between biomes represents areas where abrupt changes exist in response to climate change (Frelich and Reich, 2010), making this ecotone forest a sensitive region to climate change (Wei and Fang, 2013). In addition, this area has experienced severe harvesting and artificial regeneration (Miao et al., 2014), the forest structure and composition of this region have experienced substantial changes under the interaction of natural restoration and climate change, forest carbon sequestration has also been affected (Huo et al., 2010; Zhang et al., 2023). Therefore, it is necessary to explore the long-term spatial and temporal variation of ACSR in the alpine forests of western Sichuan in the context of climate warming, to develop appropriate forest management strategies for the characteristics of the region.

Assessing the long-term impact of climate change on the carbon sequestration capacity of forests is a challenge, which usually requires a large spatial and temporal scale to be represented, and the long-term complexity of climate change impacts on forest carbon stocks makes changes in forest vegetation carbon with a significant lag (Nevins et al., 2021). Most recent studies on carbon sinks in forest ecosystems on the Tibetan Plateau in response to long-term climate change have been based on model simulations and remote sensing monitoring (Dong and Ni, 2011; Zhao et al., 2014; Sun et al., 2022). However, these models only consider climate change as the main driving force and directly or indirectly ignore forest landscape processes. Whereas forest landscape models provide a favorable tool for studying changes in forest carbon sequestration capacity under climate change at the integrated scale of tree species, community, and landscape over long periods of time, which can not only reflect natural forest succession dynamics, but also set up different disturbance scenarios to help understand the dynamics of forest carbon pools in the context of climate warming through repeated simulation experiments (Shifley et al., 2008; Gustafson et al., 2010).

In this study, we conducted simulation experiments using the LANDIS-II forest landscape model (Scheller et al., 2007), to quantitatively evaluate the temporal and spatial variation characteristics of the ACSR in western Sichuan transitional forests in the next 100 years (2016-2116) under three climate warming scenarios. The aims of this research were to (1) explore the temporal and spatial variation characteristics of the ACSR in alpine forests in western Sichuan under different climate scenarios at various levels, (2) analyze the differences in the impact of different climate scenarios on ACSR using statistical methods, (3) provide scientific insight for selecting appropriate forest management schemes for alpine forests in western Sichuan under the climate warming scenarios. We want to answer these questions to provide useful scientific information for achieving the goals of sustainable forest management to improve the carbon sequestration capacity of the western Sichuan alpine mountains under future climate change.

2 Materials and methods

2.1 Study area

We conducted our simulation experiment within Mao Country (102°56′~104°10′E, 31°25′~32°16′N)), located in the Western Sichuan Province of Southwestern China (Figure 1). The study area encompasses 3903.28 km^2, with approximately 67.5% of the area covered in forests. The elevation of the region varies greatly, ranging from 890 m to 5230 m, resulting in a diverse vertical and regional climate. The climate in the region is characterized as a highland monsoon, with an average annual temperature of 11.0°C and an annual precipitation of 486.3 mm. The forest landscape of the region is predominantly a mixed forest comprised of both coniferous and broad-leaved forests. The main dominant species in the subalpine region at elevations between 1900 m-3000 m are spruce (*Picea asperata*) and fir (*Abies fabri*). And birch (*Betula* spp.), maple (*Acer* spp.) and ring-cupped oak (*Cyclobalanopsis glauca*) are the

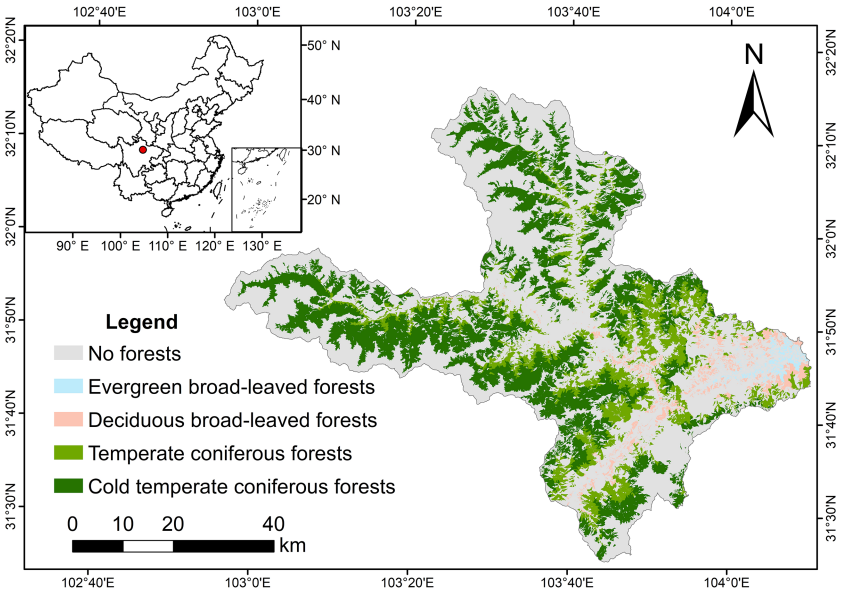

FIGURE 1
Location and forest landscape types of our simulation.

main broad-leaved tree species, which are distributed at lower elevations.

The region experienced a large-scale forest harvesting event before 1998, which led to serious damage to its forest ecosystem, and since the implementation of the Natural Forest Protection Project, the forest cover in the region has been restored through afforestation, but due to the homogeneous composition and age structure of planted forests, causing significant changes in forest structure and composition (Zhao and Shao, 2002). At present, the forests in the region are mainly for ecological protection, and forest management is based on natural succession, with no harvesting and afforestation, it can be expected that carbon sequestration capacity will be affected (Piao et al., 2019).

2.2 Climate data

To investigate the impact of future climate change on forests ACSR, we considered the current climate and three emission scenarios (RCP2.6, RCP4.5 and RCP8.5) in the experiment (Supplementary Figure 1). In the current climate, the monthly mean temperature and precipitation for the study area were obtained from data from 12 surrounding meteorological stations for the period 1980s-2020s and interpolated by regression kriging, and we assumed that the current climate conditions will not change in the next 100 years. In the future climate scenarios, climate datasets that were derived from the Coupled Model Intercomparison Project Phase 5 (CMIP5) framework of the World Climate Research Programme (IPCC, 2013), it is compiled by averaging projections from multiple climate models, which are then reduced and interpolated to a 30-inch grid by the MarkSimGCM weather generator (http://gisweb.ciat.cgiar.org/MarkSimGCM/). CO_2 concentrations data were from the RCP database (http://tntcat.iiasa), and the photosynthetically active radiation (PAR) data was from the Chinese Ecosystem Research Network Data Center (http://www.nesdc.org.cn/), due to the low changeable rate of PAR (Zhu et al., 2010), we assumed that PAR remains constant in the future scenarios of our study area.

2.3 Simulation model

We used a spatially explicit landscape model LANDIS-II v6.0 and an ecological process-based model PnET-II to conduct our research. The LANDIS-II is a stochastic, process-based model that simulates forest development (seed dispersal, tree establishment, growth, competition, mortality) on large spatiotemporal scales (Scheller et al., 2007). Within LANDIS-II model, landscapes are represented as a grid of spatially interacting cells, and each cell is aggregated into different ecological land types according to its site conditions (e.g., climate, soil), forest composition is formed through the use of age cohorts of one or more tree species on each cell, these tree species compete with each other through a variety of vital attributes, ultimately driving successional pathways through competition. And PnET-II is a process-based model that could stimulate the growth of forest trees under specific soil, climate and hydrological conditions (Aber and Federer, 1992), so we used it to calculate the aboveground net primary production (ANPP) and tree species establishment probability (SEP) needed for the LANDIS-II model by simulating the carbon, nitrogen and water cycle processes in the forest.

The key input parameters for the LANDIS-II model include tree species life history parameters, ANPP, SEP and stand spatial parameters (initial tree species distribution raster and ecoregion raster). Life history parameters for 16 dominant tree species were obtained from previous studies and consultation with local forestry experts (Liu et al., 2021) (Table 1). The initial distribution raster map of

tree species was synthesized by using the forestry survey data of Mao County in 2016. And we divided the study region into five ecoregions based on elevation, land type and soil, including an inactive ecoregion and four active ecoregions, the inactive ecoregion was no-forested and shrubs, the four ecoregions were classified mainly based on elevation, with ecoregion 1 being above 1500 m, ecoregion 2 ranging from 1500 to 2000 m, ecoregion 3 ranging from 2000 to 2800 m, and ecoregion 4 being above 2800 m (Supplementary Figure 2). We uniformly set the resolution of the spatial data to 100 m×100 m.

The parameters selected for the PnET-II include climate data (monthly temperature, monthly mean precipitation, PAR and CO_2 concentration), species physiological parameters (Supplementary Table 1), and site conditions parameters. The species physiological parameters reflect the differentiation in the response of different tree species to climate and environmental changes, and the physiological parameters of each tree species are mainly from the relevant literature review and site survey (Duan et al., 2014; Wang et al., 2017; Cai et al., 2019). Latitude and water holding capacity (WHC) are the main parameters in the site conditions, water holding capacity was calculated by rock fragment, clay and sand content obtained from a national soil database (http://gis.soil.csdb.cn/).

The applicability of the LANDIS-II model has been well demonstrated in previous studies (Xu et al., 2009; Gustafson et al., 2010), but the lack of long-term observations on large spatial and temporal scales makes it difficult to visually validate the spatial model. In this study, we compared the initial forest simulation data of LANDIS-II with actual observations (Supplementary Figure 3). The comparison results show that the model can better simulate the forest dynamics in Mao County.

2.4 Data analysis

To compare the differences in forest carbon sequestration capacity over the next 100 years under different climate scenarios, we calculated aboveground carbon sequestration rates from 2016 to 2116 at the tree species-, community-, and landscape-scales (Fang et al., 2001). ACSR was calculated using the following equation:

$$CSR_i = (C_{i,t1} - C_{i,t2})/(t_2 - t_1)$$

where CSR_i is the ACSR at a certain period, $C_{i,t1}$ is the biomass at the time t_1 and $C_{i,t2}$is the biomass at the time t_2.

To visualize the spatial and temporal variation of forest carbon sequestration capacity, we produced spatial maps of aboveground carbon stocks for each cell in the study region. Five iterations of each climate scenario were simulated to reduce the stochasticity of the models. We tested differences in ACSR across climate scenarios by one-way ANOVA with multiple comparisons using LSD, and different letters representing significant differences ($P<0.05$).

3 Results

3.1 ACSR at landscape level

ACSR of forests under different climate scenarios varied noticeably in the next 100 years (Figure 2). The overall trend in ACSR was consistent over the simulation period under different climate scenarios, with a continuous increase in ACSR from 2016s to 2036s, followed by a persistent decrease in ACSR over the next 50

TABLE 1 Life-history attributes of the main tree species in the study area.

Species	Common name	LONG	MTR	ST	ESD	MSD	VSR
Picea asperata	Spruce	300	60	4	50	150	0
Abies *fabri*	Fir	300	60	4	50	150	0
Tsuga chinensis	Chinese hemlock	400	80	4	100	150	0
Pinus armandii	Huashan pine	200	35	2	30	100	0
Pinus tabuliformis	Chinese pine	150	35	2	30	100	0
Quercus wutaishanica	Liaodong oak	300	40	2	50	200	1
Quercus semicarpifolia	Brown oak	250	40	2	50	200	1
Quercus variabilis	Cork oak	200	20	3	50	300	0.8
Cyclobalanopsis glauca	Ring-cupped oak	250	20	2	50	200	0.9
Cupressus chengiana	Minjiang cypress	300	30	3	200	500	0
Sophora japonica	Locust	150	15	1	300	1500	0.9
Toona sinensis	Chinese toon	120	15	1	300	1000	0.9
Acer spp.	Maple	200	20	3	50	200	0.5
Betula spp.	Birch	150	15	1	200	1500	0.8
Populus spp.	Aspen	150	15	1	300	1500	0.9
Alnus cremastogyne	Alder	150	15	2	200	1000	0.8

LONG, longevity (years); MTR, age of maturity; ST, shade tolerance (1-5), 1 represents minimal shade tolerance, and 5 represents maximum shade tolerance; ESD, effective seeding distance; MSD, maximum seeding distance; VSR, vegetative reproduction probability (0-1).

years, with a short period of fluctuation by the end of the simulation. The overall ACSR was maximum under the RCP8.5 scenario with a mean value of 0.36 t ha^{-1} a^{-1}, the mean ACSR under the current climate scenario was 0.27 t ha^{-1} a^{-1}, which was slightly lower than the RCP8.5 scenario. The ACSR was minimum in the RCP2.6 and RCP4.5 scenarios, and the difference between them was minor, with mean values of 0.18 t ha^{-1} a^{-1} and 0.17 t ha^{-1} a^{-1}, respectively.

3.2 ACSR at community level

Four forest communities with varying ACSR were simulated under different climate scenarios (Figure 3). The ACSR exhibited an overall decreasing trend in all climate scenarios in cold temperate coniferous forests. Furthermore, the forest ACSR was suppressed in the climate warming scenario, particularly in the late simulation period, with negative ACSR observed in all climate warming scenarios. The ACSR of temperate coniferous forests continued to decline under all climate scenarios during the simulation period, and warming also harmed the ACSR of temperate coniferous forests, with the ACSR under all warming scenarios was always lower that than current climate. The ACSR of deciduous broad-leaved forests showed a "v" shape for all climate scenarios during the simulation period, with the minimum values occurring in the 2081s-2086s. And climate warming had a positive effect on the ACSR of deciduous broad-leaved forests, as temperatures increased, this effect became more pronounced, with the highest ACSR observed under the RCP8.5 scenario. The impact of climate warming on the ACSR of evergreen broad-leaved forests was found to be negligible. The ACSR of evergreen broad-leaved forests showed a noticeable increase from 2016s-2036s, regardless of the climate scenario, during this period, the ACSR values shifted from negative to almost 0, eventually stabilizing at around 0.

3.3 ACSR at species level

The simulated response of coniferous species ACSR to climate change in the next 100 years was roughly the similar excluding Chinese hemlock (Figure 4). Our study found that climate warming had a negative impact on ACSR in the majority of coniferous forests in the study area. However, it did not alter the overall trend of ACSR in tree species. Like the spruce (Figure 4A), the ACSR generally displayed a consistent downward trend throughout the simulation across all climate scenarios, furthermore, its ACSR became negative towards the end of the simulation, with this trend being further amplified by warming. The impact of climate warming on fir was significant, as shown in Figure 4B, the ACSR experienced a fluctuating decline under the current climate scenario, although the decline was relatively minor, during the simulation period, the ACSR changed from 0.17 t ha^{-1} a^{-1} to 0.05 t ha^{-1} a^{-1}, and this change was exacerbated by climate warming. According to the RCP8.5 scenario, the ACSR decreased from 0.16 t ha^{-1} a^{-1} to -0.19 t ha^{-1} a^{-1}, similarly, under the RCP4.5 scenario, it decreased from 0.085 t ha^{-1} a^{-1} to -0.16 t ha^{-1} a^{-1}, and under the RCP2.6 scenario, it decreased from 0.066 t ha^{-1} a^{-1} to -0.15 t ha^{-1} a^{-1}. Warming had a positive effect on the ACSR of Chinese

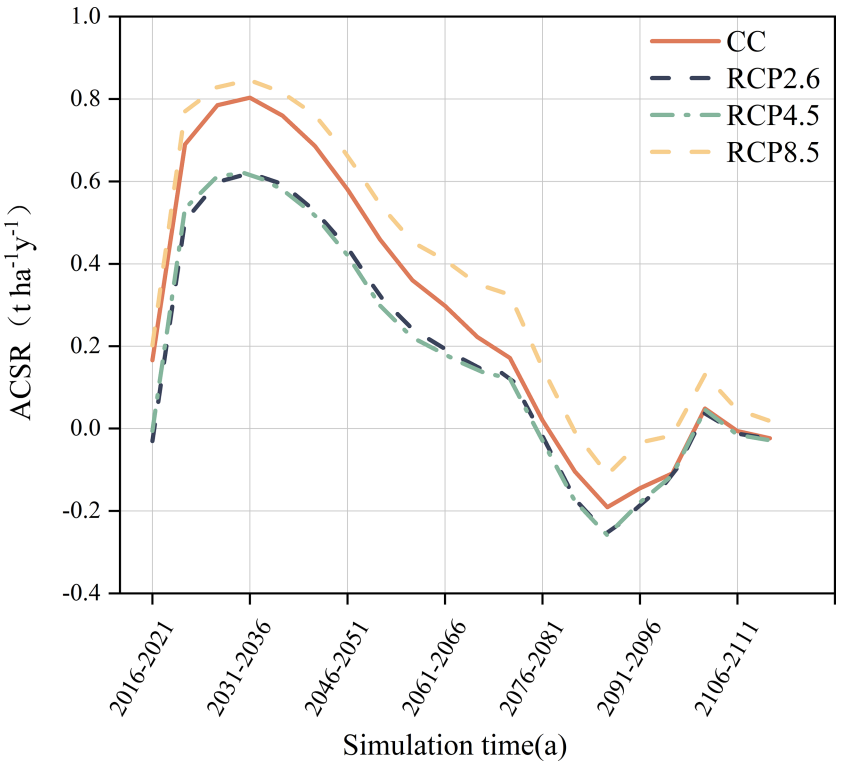

FIGURE 2
Forest aboveground carbon sequestration rate in landscape level.

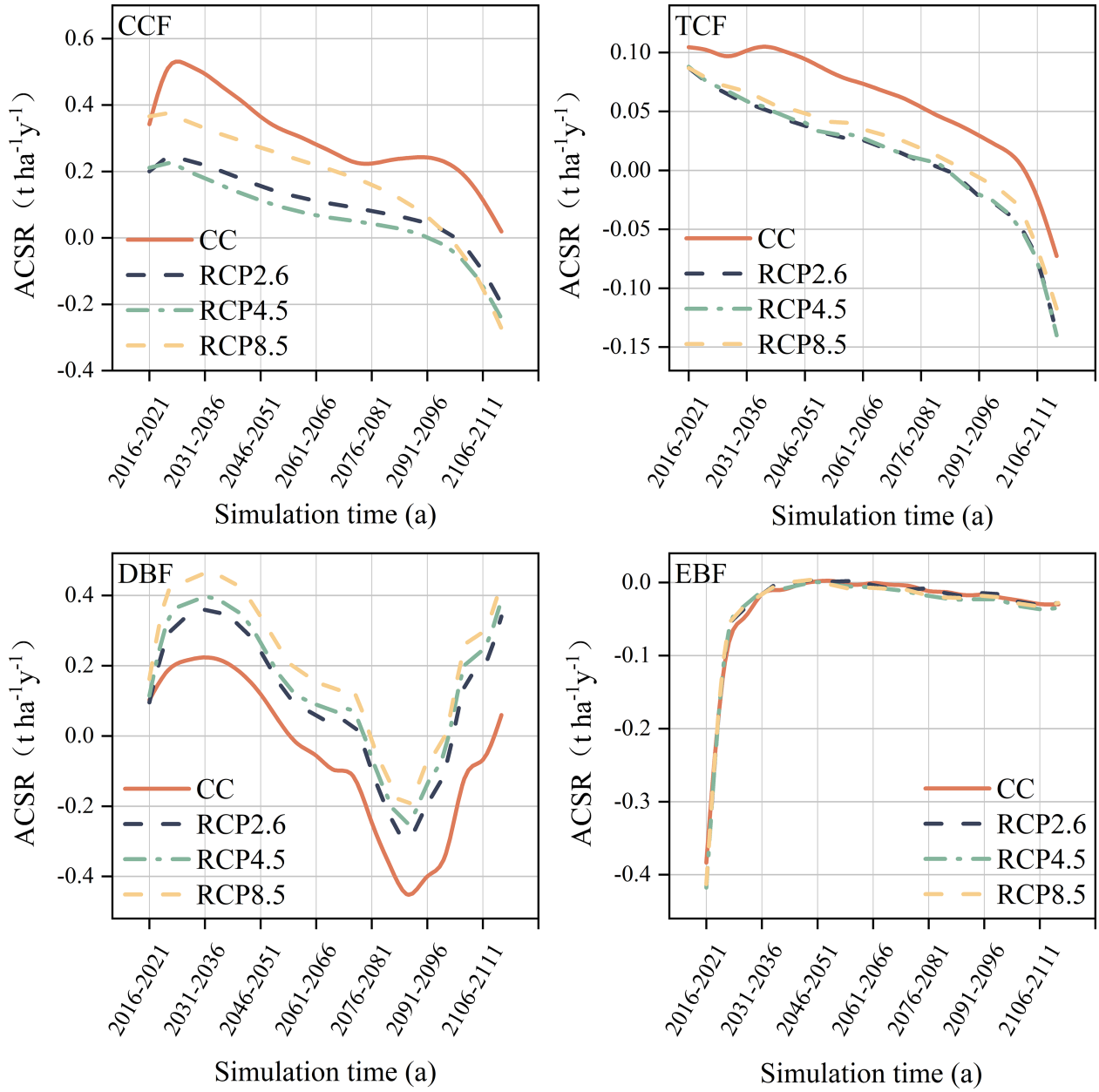

FIGURE 3
Forest aboveground carbon sequestration rate of different communities. CCF, Cold temperate coniferous forest; TCF, Temperate coniferous forests; DBF, Deciduous broad-leaved forest; EBF, Evergreen broad-leaved forest.

hemlock (Figure 4C), and increased its ACSR substantially throughout the simulation period, with the most pronounced promotion by RCP8.5. ACSR of Huashan pine, Chinese pine and Minjiang cypress has been negatively affected by climate warming, which has exacerbated the decline of their ACSR (Figures 4D–F).

The simulation showed that broad-leaved trees had complex dynamics, as depicted in Figure 5. Additionally, the study found that climate warming had a positive impact on the ACSR of the majority of broad-leaved tree species. The ACSR of Liaodong oak exhibited an initial increase followed by a subsequent decrease, specifically, between 2016s and 2036s, the ACSR demonstrated a rapid increase before gradually declining, climate warming does not alter this trend, but enhances the ACSR to some extent when compared to current climate scenario. Throughout the simulation period, warming shifted the mean ACSR of Liaodong oak from a negative value under the current climate to a positive value. The impact of climate warming on brown oak and ring-cupped oak was relatively minor, and the effect of warming on their ACSR was not noticeable. During the simulation period, the ACSR of cork oak exhibited a trend of increasing and then decreasing. The impact of warming on the ACSR was considerable, particularly between 2021s and 2026s, resulting in a substantial increase in the peak ACSR of cork oak. The effect of warming on maple was similar to that on Liaodong oak. The variation of birch's ACSR resulted in a "v" shape, with a decrease followed by an increase, and the minimum value was observed between 2081s and 2086s. The ACSR of birch was pronouncedly increased due to climate warming, and the most evident

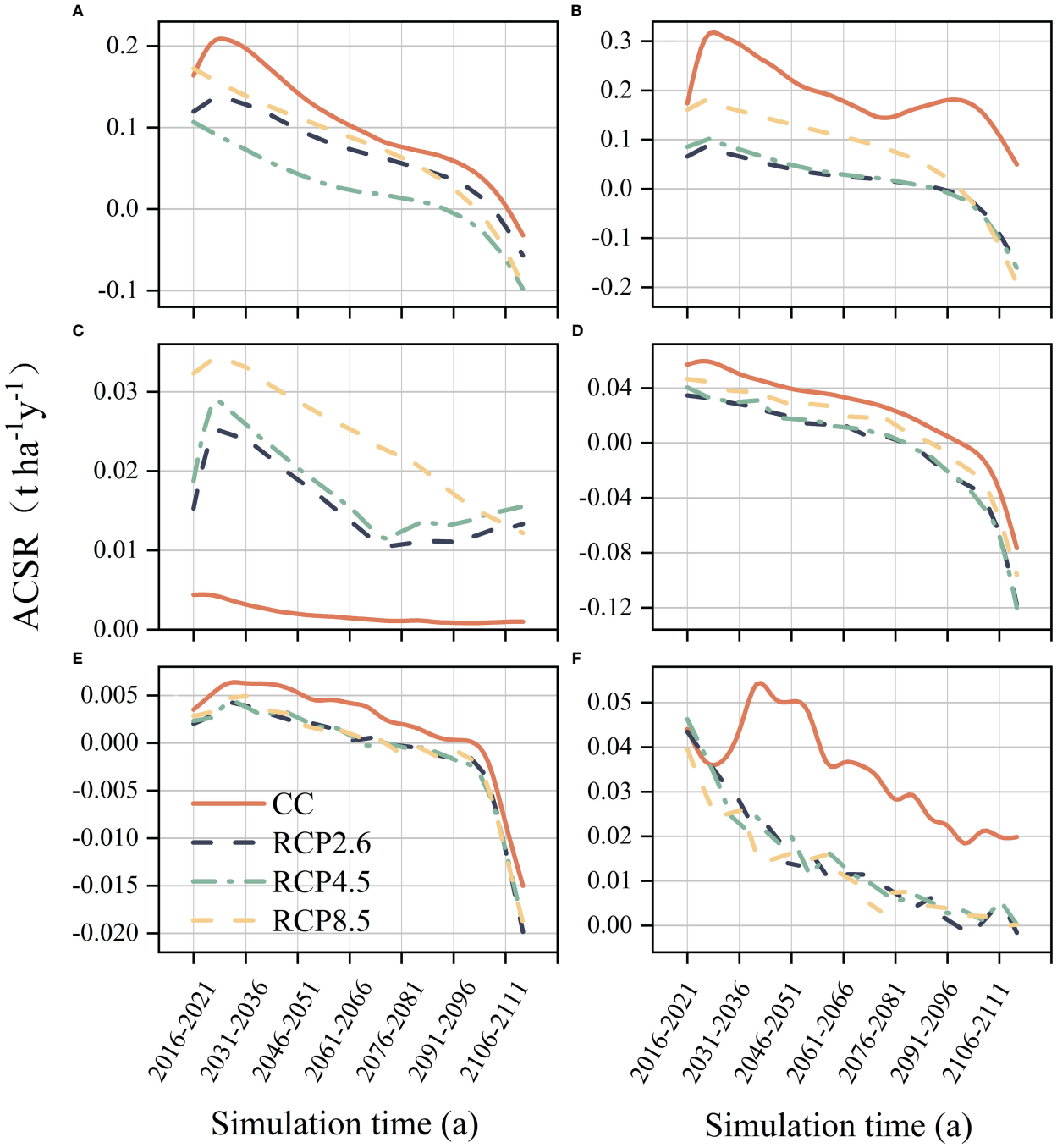

FIGURE 4
Forest aboveground carbon sequestration rate of coniferous species trees. **(A)** Spruce, **(B)** Fir, **(C)** Chinese hemlock, **(D)** Huashan pine, **(E)** Chinese pine, **(F)** Minjiang cypress.

positive effect was observed in the RCP8.5 scenario, the simulation revealed that the maximum ACSR can reach 0.43 t ha^{-1} a^{-1}.

3.4 Differences of ACSR among climate scenarios

The results of ANOVA indicated significant differences in ACSR between cold temperate coniferous forests, temperate coniferous forests and deciduous broad-leafed forests under different climate scenarios ($p<0.05$) (Figure 6), and there was no significant effect of climate change on ACSR in evergreen broad-leaved forests. The ACSR of cold temperate coniferous forests has been significantly reduced due to climate warming, with the RCP4.5 scenario showing a significant difference from the other two warming scenarios (Figure 6A). Climate warming had a significant negative impact on ACSR in temperate coniferous forests (Figure 6B). In deciduous broad-leaved forests, the increase in climate warming led to a significant rise in their ACSR, this resulted in a shift from negative to positive mean values as per simulations (Figure 6C).

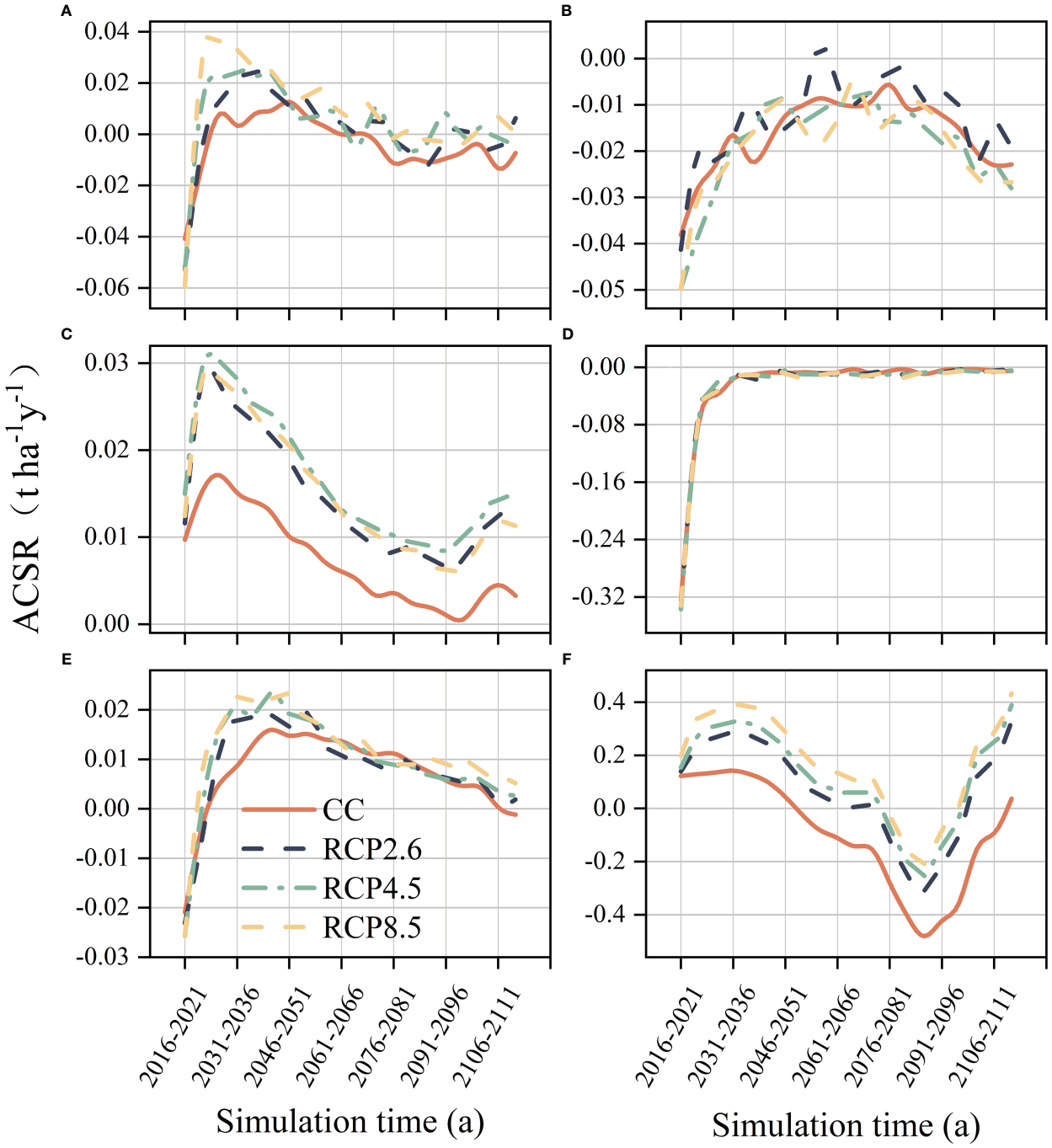

FIGURE 5
Forest aboveground carbon sequestration rate of broad-leaved species trees. **(A)** Liaodong oak, **(B)** Brown oak, **(C)** Cork oak, **(D)** Ring-cupped oak, **(E)** Maple, **(F)** Birch.

Climate change only significantly affected the ACSR of some tree species (Supplementary Table 2). Specifically, the ACSR of spruce was significantly reduced by climate warming, with no discernible difference observed across various warming scenarios (Figure 7A). The ACSR of fir was negatively impacted by climate warming, however, it was observed that the effects of RCP8.5 were significantly different from the other two warming scenarios (Figure 7B). The Chinese hemlock exhibited a significantly higher ACSR for all warming scenarios compared to the current climate, among the three warming scenarios, the ACSR for RCP8.5 was significantly higher than the other two (Figure 7C). The impact of climate warming on Minjiang cypress was found to be similar to that of spruce, the study revealed that warming had significant negative effect on the ACSR of Minjiang cypress (Figure 7D). The ACSR of cork oak and birch was significantly increased by climate warming, especially RCP8.5 produced a significant increase in the ACSR of birch (Figures 7E, H). ACSR of locust and Chinese toon had significant decreases under warming scenarios (Figures 7F, G).

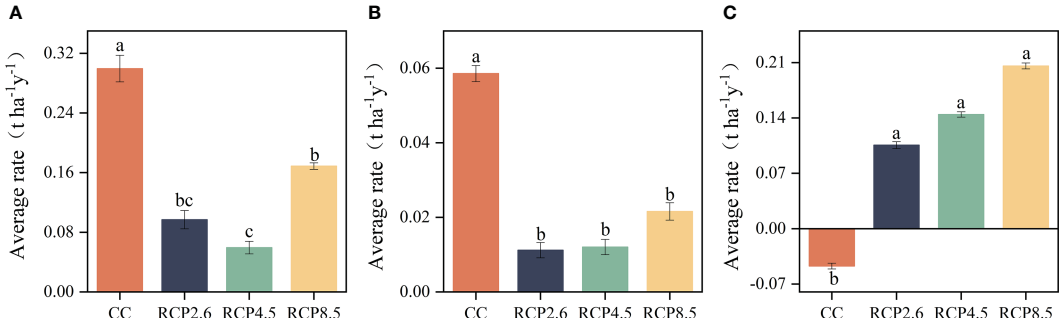

FIGURE 6
Results of multiple comparisons of the influences on the aboveground carbon sequestration rates of the communities. **(A)** Cold temperate coniferous forests, **(B)** Temperate coniferous forests, **(C)** Deciduous broad-leaved forests. Significant differences between different climate scenarios are indicated with different lowercase letters ($P < 0.05$).

3.5 Spatial distribution of carbon stocks

Forest carbon stocks showed a large variation in different stages under different climate scenarios (Figure 8). Our study found that climate warming had a mixed impact on forest carbon stocks in the area. In the RCP2.6 scenario, there was a positive effect on forest carbon stocks until the 2060s, followed by a slight suppression. Similarly, in the RCP4.5 scenario, there was a positive effect until the 2040s. However, in the RCP8.5 scenario, there was a dramatic warming that noticeably reduced forest carbon stocks. Our study also found that appropriate climate warming promoted carbon stock in the southeastern part of the area, whereas drastic warming had a suppression effect in the high-altitude areas of the western and northeastern regions.

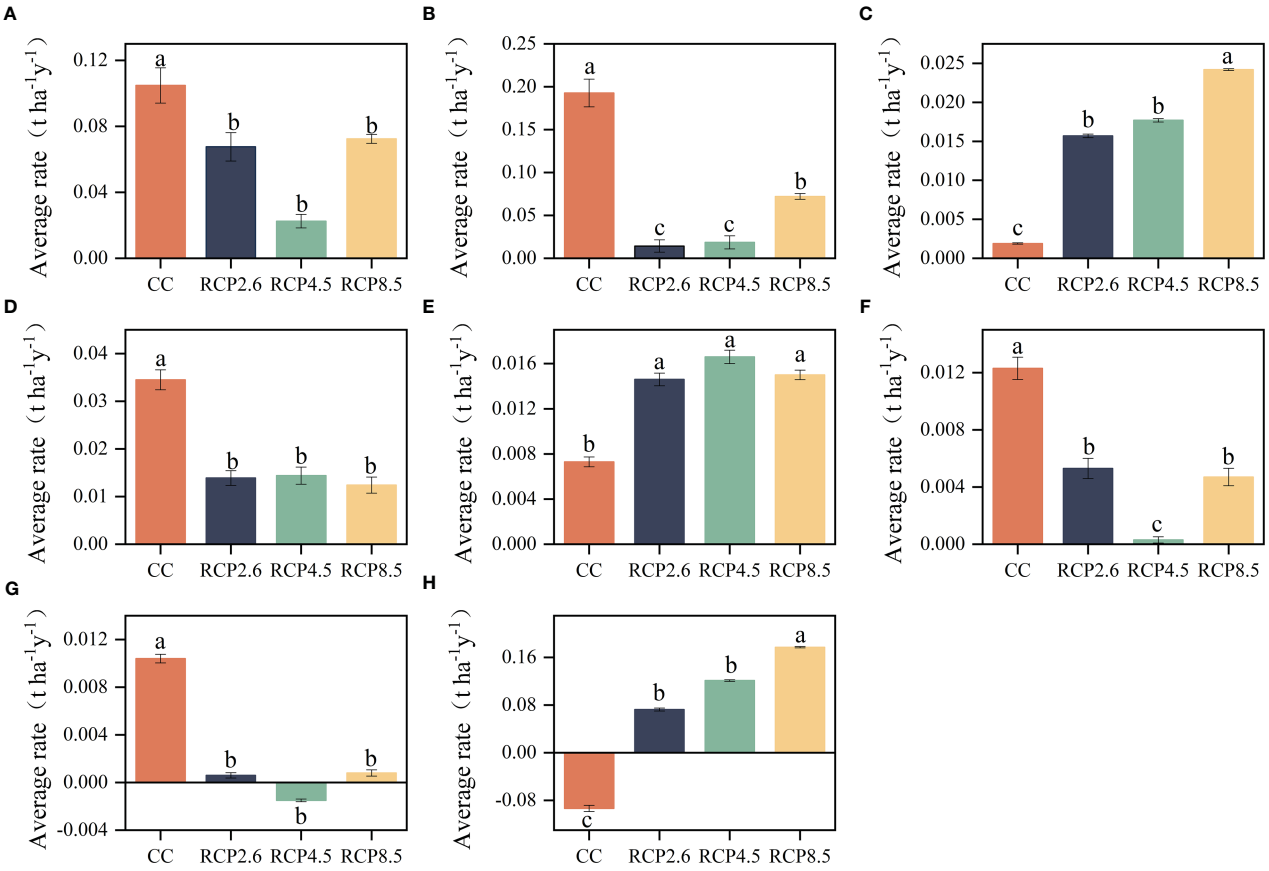

FIGURE 7
Results of multiple comparisons of the influences on the aboveground carbon sequestration rates major tree species. **(A)** Spruce, **(B)** Fir, **(C)** Chinese hemlock, **(D)** Minjiang cypress, **(E)** Cork oak, **(F)** Locust, **(G)** Chinese toon, **(H)** Birch. Significant differences between different climate scenarios are indicated with different lowercase letters ($P < 0.05$).

4 Discussion

Our study found that climate warming has a significant impact on the ACSR of forests in this transitional ecotone. More specifically, we found that forest ACSR was influenced by various climate change scenarios, forest types, species, and successional stages. The findings of our study suggest that warming has a significant impact on different tree species. In particular, it was observed that warming led to a decrease in the ACSR of coniferous trees, whereas it had a positive effect on the ACSR in broad-leaved trees. These results are consistent with previous research conducted in this field (Ma et al., 2014). The study revealed that warming had a negative impact on the ACSR of spruce and fir, and this negative trend was observed in the later stages of the simulation. We suggest that this may be attributed to the species' adaptation to current temperature conditions and the inhibitory effect of increased temperature on their photosynthesis. Consequently, warming is expected to exert a stronger negative impact on the ACSR of spruce and fir compared to CO_2 fertilization, and further warming could continue to inhibit their growth (Coops and Waring, 2011). Consistent with our findings, Liao et al. demonstrated that future warming scenarios would result in a contraction of the habitat range of spruce and fir on the eastern Tibetan Plateau, highlighting their vulnerability to climate warming (Liao et al., 2020). The warming has positively influenced the ACSR of Chinese hemlock, with the RCP8.5 scenario having the most pronounced enhancing effect. This may be attributed to the higher maximum photosynthetic temperature tolerance of Chinese hemlock, the current warming not yet surpassing its threshold, and the temperature increase promoting its photosynthesis, consequently increasing its ACSR. Other coniferous trees, such as Minjiang cypress and Huashan pine, exhibit a similar response to climate warming as spruce and fir. Broad-leaved tree species generally exhibit a positive response in terms of ACSR to climate warming (Cheng and Yan, 2008; Zhang et al., 2023). Research indicates that climate warming is more favorable for broad-leaved trees as compared to subalpine conifers, the latter is experiencing a decline in growth due to standing encroachment (Cao et al., 2021). Climate warming can greatly enhance the ACSR of birch, resulting in a distinct "v" shape in the ACSR change. This is due to the fact that birch, as a pioneer tree species, reaches its natural lifespan and experiences mortality after a short period of increased ACSR, leading to a subsequent decline in ACSR. At the community level, climate warming negatively affected the ACSR of cold temperate coniferous and temperate coniferous forests. In contrast, deciduous broad-leaved forests exhibited a significant increase in ACSR as a result of climate warming. The impact of climate warming on evergreen broad-leaved forests was relatively smaller, which could be attributed to their lower proportion in the region, resulting in a less significant effect.

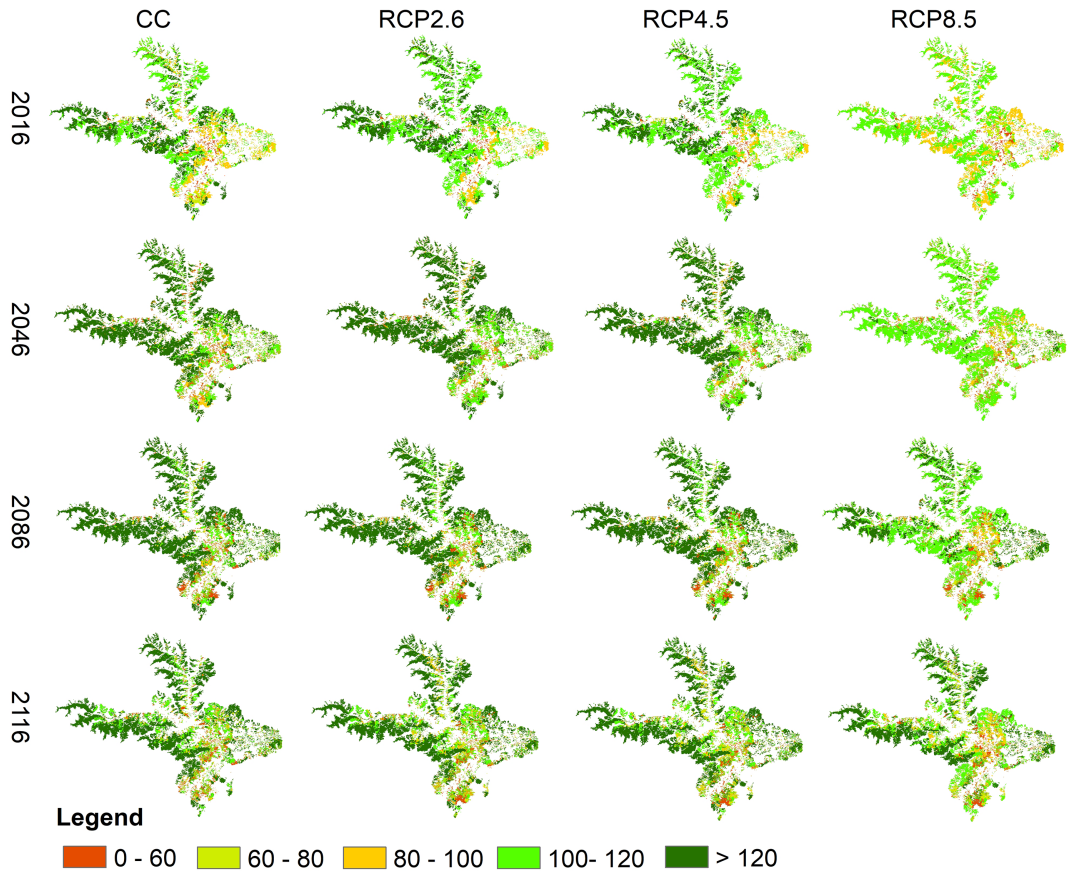

FIGURE 8
Spatial distribution of forest carbon stocks under different climate scenarios.

Our study revealed that climate warming does not alter the trend of ACSR at the landscape scale. After a brief increase, the ACSR continues to decline. This decline may be attributed to artificial plantations established after harvesting in this ecotone. The current forest is in a young state and capable of ongoing carbon sequestration. However, the natural mortality of uniformly planted plantations leads to a significant reduction in ACSR (Wang et al., 2016; Urbano and Keeton, 2017). At the landscape scale, the RCP8.5 scenario has exhibited certain positive effects on ACSR in this ecotone. However, the RCP4.5 and RCP2.6 scenarios have resulted in a decrease in ACSR compared to the current climate. This can be attributed to a notable increase in ACSR of broad-leaved trees resulting from the RCP8.5 scenario. The ACSR of broad-leaved trees has experienced a significant rise due to climate warming. However, under severe climate warming scenarios in the future, the forest carbon stock in the area will be significantly diminished. This is because spruce and fir forests, which represent the dominant communities in our study region, cover the largest area and possess the highest forest carbon sequestration capacity in this ecoregion (Zhang et al., 2013). However, the climate warming scenario has significantly suppressed the ACSR of spruce and fir, leading to a decrease in forest carbon stock.

Our results do not aim to accurately predict the ACSR of this transition ecotone under climate warming scenarios. Instead, the experimental design and model results aim to uncover general patterns of warming effects on carbon sequestration capacity across different ecological scales through controlled experiments. However, the experimental design does not consider certain factors that undoubtedly influence species succession and carbon sequestration capacity, such as increased frequency of fires in warming scenarios, land use changes, and pests and diseases. These limitations indicate a direction for future research. Previous studies have examined the sensitivity and uncertainty of the LANDIS-II model (Gustafson et al., 2010; Thompson et al., 2011; Xiao et al., 2017), revealing that the model input is highly stable. To minimize stochastic error, we conducted repeated simulations and found minimal variability between these repetitions. Our study yields reliable results that highlight the variations in forest ACSR across different scales within the transitional ecotone of the eastern Tibetan Plateau, under different warming scenarios. These findings offer valuable insights for enhancing the forest carbon sequestration capacity in the region.

5 Conclusion

In this study, the forest landscape model LANDIS-II was utilized to simulate the effects of climate warming on the ACSR of the eastern Tibetan Plateau Forest transition ecotone. Our results demonstrated that climate warming significantly affects the ACSR in this region. At the landscape scale, it was found that climate warming did not have a significant impact on ACSR, however, the RCP8.5 scenario led to an increase in forest ACSR, whereas the RCP2.6 and RCP4.5 scenarios resulted in a decrease in forest ACSR. The impact of climate warming on ACSR varied in different forest types. In cold temperate coniferous forests and temperate coniferous forests, ACSR was significantly reduced. However, in deciduous broad-leaved forests, ACSR increased significantly due to climate warming. Evergreen broad-leaved forests in the study area were found to be less responsive to climate change. At the scale of tree species, the top communities in our research region, namely spruce and fir, exhibited a significant decrease in ACSR as a result of climate warming. Additionally, climate warming led to a decrease in ACSR of other coniferous trees, with the exception of Chinese hemlock. The response of broad-leaved species' ACSR to climate warming was mostly positive, particularly in the case of birch, where there was a significant increase in ACSR due to climate warming. In addition, the study found that a moderate increase in temperature had a positive effect on the increase of forest carbon stock in the area, however, a drastic increase in temperature had a significant negative impact on the forest carbon stock in the study area. The findings of this study provide valuable insights into the connection between forest carbon sequestration capacity and climate warming in the eastern Tibetan Plateau. Additionally, these results have practical applications for promoting sustainable forest management in the region in the coming years.

Data availability statement

The original contributions presented in the study are included in the article/Supplementary Material. Further inquiries can be directed to the corresponding author.

Author contributions

YL: formal analysis, investigation, and writing - original draft. NC: conceptualization, resources, writing – review & editing. JX: conceptualization, methodology, resources, writing – review & editing, and funding acquisition. YK: conceptualization, writing – review & editing, and funding acquisition. YYL, XY, and GQ: formal analysis and validation. CG and YB: investigation and data acquisition. PR: writing – review & editing, and funding acquisition. All authors contributed intellectual input and assistance to this study and manuscript preparation.

Funding

This research was supported by the National Natural Science Foundation of China (41801185, 32171550), and the Sichuan Science and Technology Program (2023NSFSC0191, 2023NSFSC1979), and the Youth Innovation Promotion Association of Chinese Academy of Sciences (2021371).

Acknowledgments

We would like to express our sincere gratitude to the editors and reviewers, who have put considerable time and effort into their comments on this paper.

Conflict of interest

The authors declare that the research was conducted in the absence of any commercial or financial relationships that could be construed as a potential conflict of interest.

Publisher's note

All claims expressed in this article are solely those of the authors and do not necessarily represent those of their affiliated organizations, or those of the publisher, the editors and the reviewers. Any product that may be evaluated in this article, or claim that may be made by its manufacturer, is not guaranteed or endorsed by the publisher.

Supplementary material

The Supplementary Material for this article can be found online at: https://www.frontiersin.org/articles/10.3389/fpls.2023.1212406/full#supplementary-material

References

Aber, J. D., and Federer, C. A. (1992). A generalized, lumped-parameter model of photosynthesis, evapotranspiration and net primary production in temperate and boreal forest ecosystems. *Oecologia* 92, 463–474. doi: 10.1007/BF00317837

Bachelot, B., Alonso-Rodríguez, A. M., Aldrich-Wolfe, L., Cavaleri, M. A., Reed, S. C., and Wood, T. E. (2020). Altered climate leads to positive density-dependent feedbacks in a tropical wet forest. *Global Change Biol.* 26, 3417–3428. doi: 10.1111/gcb.15087

Cai, Q., Ding, J., Zhang, Z., Hu, J., Wang, Q., Yin, M., et al. (2019). Distribution patterns and driving factors of leaf c, n and p stoichiometry of coniferous species on the eastern qinghai-xizang plateau, China. *Chin. J. Plant Ecol.* 43, 1048–1060. doi: 10.17521/cjpe.2019.0221

Cao, J., Liu, H., Zhao, B., Li, Z., Liang, B., Shi, L., et al. (2021). High forest stand density exacerbates growth decline of conifers driven by warming but not broad-leaved trees in temperate mixed forest in northeast Asia. *Sci. Tot. Environ.* 795, 148875. doi: 10.1016/j.scitotenv.2021.148875

Chapin, F. S., Matson, P. A., Mooney, H. A., and Vitousek, P. M. (2002). *Principles of terrestrial ecosystem ecology* New York: Springer New York. 285–287.

Chen, Q., Xu, W., Li, S., Fu, S., and Yan, J. (2013). Aboveground biomass and corresponding carbon sequestration ability of four major forest types in south China. *Chin. Sci. Bull.* 58, 1551–1557. doi: 10.1007/s11434-012-5100-8

Cheng, X., and Yan, X. (2008). Effects of climate change on typical forest in the northeast of China. *Acta Ecol. Sin.* 28, 534–543. doi: 10.3321/j.issn:1000-0933.2008.02.011

Coops, N. C., and Waring, R. H. (2011). Estimating the vulnerability of fifteen tree species under changing climate in Northwest north America. *Ecol. Model.* 222, 2119–2129. doi: 10.1016/j.ecolmodel.2011.03.033

Dai, E. F., Wu, Z., Ge, Q., Xi, W., and Wang, X. (2016). Predicting the responses of forest distribution and aboveground biomass to climate change under RCP scenarios in southern China. *Global Change Biol.* 22, 3642–3661. doi: 10.1111/gcb.13307

Dong, D., and Ni, J. (2011). Modeling changes of net primary productivity of karst vegetation in southwestern China using the CASA model. *Acta Ecol. Sin.* 31, 1855–1866. doi: CNKI:SUN:STXB.0.2011-07-014

Duan, B., Dong, T., Zhang, X., Zhang, Y., and Chen, J. (2014). Ecophysiological responses of two dominant subalpine tree species betula albo-sinensis and abies faxoniana to intra-and interspecific competition under elevated temperature. *For. Ecol. Manage.* 323, 20–27. doi: 10.1016/j.foreco.2014.03.036

Duveneck, M. J., and Thompson, J. R. (2017). Climate change imposes phenological trade-offs on forest net primary productivity. *J. Geophys. Res.: Biogeoscie.* 122, 2298–2313. doi: 10.1002/2017JG004025

Fang, J., Chen, A., Peng, C., Zhao, S., and Ci, L. (2001). Changes in forest biomass carbon storage in China between 1949 and 1998. *Science* 292, 2320–2322. doi: 10.1126/science.1058629

Frank, D., Reichstein, M., Bahn, M., Thonicke, K., Frank, D., Mahecha, M. D., et al. (2015). Effects of climate extremes on the terrestrial carbon cycle: concepts, processes and potential future impacts. *Global Change Biol.* 21, 2861–2880. doi: 10.1111/gcb.12916

Franks, P. J., Adams, M. A., Amthor, J. S., Barbour, M. M., Berry, J. A., Ellsworth, D. S., et al. (2013). Sensitivity of plants to changing atmospheric CO 2 concentration: from the geological past to the next century. *New Phytol.* 197, 1077–1094. doi: 10.1111/nph.12104

Frelich, L. E., and Reich, P. B. (2010). Will environmental changes reinforce the impact of global warming on the prairie–forest border of central north America? *Front. Ecol. Environ.* 8, 371–378. doi: 10.1890/080191

Gustafson, E. J., Miranda, B. R., and Sturtevant, B. R. (2018). Can future CO_2 concentrations mitigate the negative effects of high temperature and longer droughts on forest growth? *Forests* 9 (11), 664. doi: 10.3390/f9110664

Gustafson, E. J., Shvidenko, A. Z., Sturtevant, B. R., and Scheller, R. M. (2010). Predicting global change effects on forest biomass and composition in south-central Siberia. *Ecol. Appl.* 20, 700–715. doi: 10.1890/08-1693.1

Huo, C., Cheng, G., Lu, X., and Fan, J. (2010). Simulating the effects of climate change on forest dynamics on gongga mountain, southwest China. *J. For. Res.* 15, 176–185. doi: 10.1007/s10310-009-0173-1

IPCC (2013). *Climate change 2013: the physical science basis. contribution of working group I to the fifth assessment report of the intergovernmental panel on climate change. climate change* Vol. 2013 (New York: Cambridge University Press).

Kallarackal, J., and Roby, T. (2012). Responses of trees to elevated carbon dioxide and climate change. *Biodiversity Conserv.* 21, 1327–1342. doi: 10.1007/s10531-012-0254-x

Liang, Y., Gustafson, E. J., He, H. S., Serra-Diaz, J. M., Duveneck, M. J., and Thompson, J. R. (2023). What is the role of disturbance in catalyzing spatial shifts in forest composition and tree species biomass under climate change? *Global Change Biol.* 29, 1160–1177. doi: 10.1111/gcb.16517

Liao, Z., Zhang, L., Nobis, M. P., Wu, X., Pan, K., Wang, K., et al. (2020). Climate change jointly with migration ability affect future range shifts of dominant fir species in southwest China. *Diversity Distribut.* 26, 352–367. doi: 10.1111/ddi.13018

Lindner, M., Maroschek, M., Netherer, S., Kremer, A., Barbati, A., Garcia-Gonzalo, J., et al. (2010). Climate change impacts, adaptive capacity, and vulnerability of European forest ecosystems. *For. Ecol. Manage.* 259, 698–709. doi: 10.1016/j.foreco.2009.09.023

Liu, H., Park Williams, A., Allen, C. D., Guo, D., Wu, X., Anenkhonov, O. A., et al. (2013). Rapid warming accelerates tree growth decline in semi-arid forests of inner Asia. *Global Change Biol.* 19, 2500–2510. doi: 10.1111/gcb.12217

Liu, J., Zou, H. X., Bachelot, B., Dong, T., Zhu, Z., Liao, Y., et al. (2021). Predicting the responses of subalpine forest landscape dynamics to climate change on the eastern Tibetan plateau. *Global Change Biol.* 27, 4352–4366. doi: 10.1111/gcb.15727

Ma, J., Hu, Y., Bu, R., Chang, Y., Deng, H., and Qin, Q. (2014). Predicting impacts of climate change on the aboveground carbon sequestration rate of a temperate forest in northeastern China. *PloS One* 9, e96157. doi: 10.1371/journal.pone.0096157

Miao, N., Zhou, Z., Shi, Z., and Feng, Q. (2014). Successional dynamics of community structure and species diversity after clear-cutting of faxon fir (Abies faxoniana) forest stands. *Acta Ecol. Sin.* 34, 3661–3671. doi: 10.5846/stxb201211151605

Nevins, M. T., D'Amato, A. W., and Foster, J. R. (2021). Future forest composition under a changing climate and adaptive forest management in southeastern Vermont, USA. *For. Ecol. Manage.* 479, 118527. doi: 10.1016/j.foreco.2020.118527

Piao, S.-l., Zhang, X., Wang, T., Liang, E., Wang, S., Zhu, J., et al. (2019). Responses and feedback of the Tibetan plateau's alpine ecosystem to climate change. *Chin. Sci. Bull.* 64, 2842–2855. doi: 10.1360/TB-2019-0074

Scheller, R. M., Domingo, J. B., Sturtevant, B. R., Williams, J. S., Rudy, A., Gustafson, E. J., et al. (2007). Design, development, and application of LANDIS-II, a spatial landscape simulation model with flexible temporal and spatial resolution. *Ecol. Model.* 201, 409–419. doi: 10.1016/j.ecolmodel.2006.10.009

Schurman, J. S., Babst, F., Björklund, J., Rydval, M., Bače, R., Čada, V., et al. (2019). The climatic drivers of primary picea forest growth along the Carpathian arc are changing under rising temperatures. *Global Change Biol.* 25, 3136–3150. doi: 10.1111/gcb.14721

Shifley, S. R., Thompson, F. R.III, Dijak, W. D., and Fan, Z. (2008). Forecasting landscape-scale, cumulative effects of forest management on vegetation and wildlife habitat: a case study of issues, limitations, and opportunities. *For. Ecol. Manage.* 254, 474–483. doi: 10.1016/j.foreco.2007.08.030

Sun, J., Ye, C. C., Liu, M., Wang, Y., Chen, J., Wang, S., et al. (2022). Response of net reduction rate in vegetation carbon uptake to climate change across a unique gradient

zone on the Tibetan plateau. *Environ. Res.* 203, 111894. doi: 10.1016/j.envres.2021.111894

Teskey, R., Wertin, T., Bauweraerts, I., Ameye, M., McGuire, M. A., and Steppe, K. (2015). Responses of tree species to heat waves and extreme heat events. *Plant Cell Environ.* 38, 1699–1712. doi: 10.1111/pce.12417

Thompson, J. R., Foster, D. R., Scheller, R., and Kittredge, D. (2011). The influence of land use and climate change on forest biomass and composition in Massachusetts, USA. *Ecol. Appl.* 21, 2425–2444. doi: 10.1890/10-2383.1

Urbano, A. R., and Keeton, W. S. (2017). Carbon dynamics and structural development in recovering secondary forests of the northeastern US. *For. Ecol. Manage.* 392, 21–35. doi: 10.1016/j.foreco.2017.02.037

Wang, J., Wang, G.-X., Wang, C.-T., Ran, F., and Chang, R.-Y. (2016). Carbon storage and potentials of the broad-leaved forest in alpine region of the qinghai-xizang plateau, China. *Chin. J. Plant Ecol.* 40, 374–384. doi: 10.17521/cjpe.2015.0152

Wang, B., Zeng, Q., An, S., Zhang, H., and Bai, X. (2017). C: N: P stoichiometry characteristics of plants-litter-soils in two kind types of natural secondary forest on the ziwuling region of the loess plateau. *Acta Ecol. Sin.* 37, 5461–5473. doi: 10.5846/stxb201605150936

Wei, Y., and Fang, Y. (2013). Spatio-temporal characteristics of global warming in the Tibetan plateau during the last 50 years based on a generalised temperature zone-elevation model. *PloS One* 8, e60044. doi: 10.1371/journal.pone.0060044

Wu, Z., Dai, E. F., Wu, Z. W., and Lin, M. Z. (2020). Assessing differences in the response of forest aboveground biomass and composition under climate change in subtropical forest transition zone. *Sci. Tot. Environ.* 706, 135746. doi: 10.1016/j.scitotenv.2019.135746

Xiao, J. T., Liang, Y., He, H. S., Thompson, J. R., Wang, W. J., Fraser, J. S., et al. (2017). The formulations of site-scale processes affect landscape-scale forest change predictions: a comparison between LANDIS PRO and LANDIS-II forest landscape models. *Landscape Ecol.* 32, 1347–1363. doi: 10.1007/s10980-016-0442-2

Xu, C., Gertner, G. Z., and Scheller, R. M. (2009). Uncertainties in the response of a forest landscape to global climatic change. *Global Change Biol.* 15, 116–131. doi: 10.1111/j.1365-2486.2008.01705.x

Yao, Y. T., Piao, S. L., and Wang, T. (2018). Future biomass carbon sequestration capacity of Chinese forests. *Sci. Bull.* 63, 1108–1117. doi: 10.1016/j.scib.2018.07.015

Zhang, Y., Gu, F., Liu, S., Liu, Y., and Li, C. (2013). Variations of carbon stock with forest types in subalpine region of southwestern China. *For. Ecol. Manage.* 300, 88–95. doi: 10.1016/j.foreco.2012.06.010

Zhang, L., Lu, X.-M., Zhu, H.-Z., Gao, S., Sun, J., Zhu, H.-F., et al. (2023). A rapid transition from spruce-fir to pine-broadleaf forests in response to disturbances and climate warming on the southeastern qinghai-Tibet plateau. *Plant Diversity*. doi: 10.1016/j.pld.2023.03.002

Zhao, G., and Shao, G. (2002). Logging restrictions in China: a turning point for forest sustainability. *J. Forestry* 100, 34–37. doi: 10.1093/jof/100.4.34

Zhao, M. W., Yue, T. X., Zhao, N., Sun, X. F., and Zhang, X. Y. (2014). Combining LPJ-GUESS and HASM to simulate the spatial distribution of forest vegetation carbon stock in China. *J. Geograph. Sci.* 24, 249–268. doi: 10.1007/s11442-014-1086-2

Zhou, R. W., Zhang, Y. P., Peng, M. C., Jin, Y. Q., and Song, Q. H. (2022). Effects of climate change on the carbon sequestration potential of forest vegetation in yunnan province, southwest China. *Forests* 13, 306. doi: 10.3390/f13020306

Zhu, X., He, H., Liu, M., Yu, G., Sun, X., and Gao, Y. (2010). Spatio-temporal variation of photosynthetically active radiation in China in recent 50 years. *J. Geograph. Sci.* 20, 803–817. doi: 10.1007/s11442-010-0812-7

frontiers | Frontiers in Plant Science

TYPE Original Research
PUBLISHED 04 August 2023
DOI 10.3389/fpls.2023.1227286

OPEN ACCESS

EDITED BY
Ming Xu,
Beijing Normal University, Zhuhai, China

REVIEWED BY
Zhaosheng Wang,
Chinese Academy of Sciences (CAS), China
Ruichang Shen,
Nanchang University, China

*CORRESPONDENCE
Lihua Hao
haolihua_000@sina.com
Yinshuai Tian
tyinshuai@163.com

RECEIVED 23 May 2023
ACCEPTED 13 July 2023
PUBLISHED 04 August 2023

CITATION
Chang Z, Hao L, Lu Y, Liu L, Chen C, Shi W, Li Y, Wang Y and Tian Y (2023) Effects of elevated CO_2 concentration and experimental warming on morphological, physiological, and biochemical responses of winter wheat under soil water deficiency. *Front. Plant Sci.* 14:1227286. doi: 10.3389/fpls.2023.1227286

Effects of elevated CO_2 concentration and experimental warming on morphological, physiological, and biochemical responses of winter wheat under soil water deficiency

Zhijie Chang[1], Lihua Hao[1*], Yunze Lu[2], Liang Liu[1], Changhua Chen[1], Wei Shi[1], Yue Li[3], Yanrui Wang[1] and Yinshuai Tian[2*]

[1]School of Water Conservancy and Hydropower, Hebei University of Engineering, Handan, Hebei, China, [2]School of Landscape and Ecological Engineering, Hebei University of Engineering, Handan, Hebei, China, [3]School of Earth Science and Engineering, Hebei University of Engineering, Handan, Hebei, China

Global climate change and freshwater scarcity have become two major environmental issues that constrain the sustainable development of the world economy. Climate warming caused by increasing atmospheric CO_2 concentration can change global/regional rainfall patterns, leading to uneven global seasonal precipitation distribution and frequent regional extreme drought events, resulting in a drastic reduction of available water resources during the critical crop reproduction period, thus causing many important food-producing regions to face severe water deficiency problems. Understanding the potential processes and mechanisms of crops in response to elevated CO_2 concentration and temperature under soil water deficiency may further shed lights on the potential risks of climate change on the primary productivity and grain yield of agriculture. We examined the effects of elevated CO_2 concentration ($e[CO_2]$) and temperature (experimental warming) on plant biomass and leaf area, stomatal morphology and distribution, leaf gas exchange and mesophyll anatomy, rubisco activity and gene expression level of winter wheat grown at soil water deficiency with environmental growth chambers. We found that $e[CO_2]$ × water × warming sharply reduced plant biomass by 57% and leaf photosynthesis (P_n) 50%, although elevated $[CO_2]$ could alleviated the stress from water × warming at the amount of gene expression in *RbcL3* (128%) and *RbcS2* (215%). At ambient $[CO_2]$, the combined stress of warming and water deficiency resulted in a significant decrease in biomass (52%), leaf area (50%), P_n (71%), and G_s (90%) of winter wheat. Furthermore, the total nonstructural carbohydrates were accumulated 10% and 27% and increased R_d by 127% and 99% when subjected to water × warming and $e[CO_2]$ × water × warming. These results suggest that water × warming may cause irreversible damage in winter wheat and thus the effect of "CO_2 fertilization effect" may be overestimated by the current process-based ecological model.

KEYWORDS

water deficiency, CO_2, warming, biomass, photosynthesis, gene expression

Introduction

Atmospheric CO_2 concentration ($[CO_2]$) has currently exceeded 420 μmol mol^{-1} with an increase rate of 2 μmol mol^{-1} from 280 μmol mol^{-1} at the beginning of the industrialization era and will continually be over 800 μmol mol^{-1} by the end of 21st century (IPCC, 2021). As a result, the increased atmospheric $[CO_2]$ has resulted in a rapid rise in global surface temperature over the past decades (Barlow et al., 2015; Jin et al., 2017), even the average global temperature is predicted to rise 2 to 6 °C depending on the concentrations of greenhouse gases such as CO_2 in the atmosphere (IPCC, 2021). It has been estimated that global precipitation may decline under future climatic warming, and meanwhile the spatial and temporal patterns of global/regional precipitation distribution may also become uneven (Chun et al., 2011; Zhang et al., 2020), thus drought and elevated temperature may constrain plant growth and crop yield alone or in combination (Yu et al., 2012), although elevated $[CO_2]$ generally facilitates plant growth and promotes plant adaptation to climate change (Kirkham, 2011; Xu, 2015; Li et al., 2021). Unfortunately, simultaneous drought stress, elevated $[CO_2]$ and elevated temperature has already occurred in summer in many regions throughout the world, which is even more detrimental to plant growth than either stress alone. Nevertheless, the underlying response mechanisms of elevated $[CO_2]$ and elevated temperature on crops such as winter wheat at different soil water status are still unclear (Abebe et al., 2016; Fan et al., 2020; Zheng et al., 2020), and thus these uncertainties not only restrict the capacity to accurately predict agricultural carbon sequestration, but also limit understanding of the potential impacts of climate change on agricultural productivity (Ainsworth and Long, 2020; Muluneh, 2020).

It has been well demonstrated that various physiological, biochemical, and molecular processes of plants are sensitive to water deficiency, elevated $[CO_2]$, and elevated temperature alone or the combination (Mirwais et al., 2006; Yu et al., 2012; Bencze et al., 2014; Xu, 2015; Zheng et al., 2018; Duan et al., 2019a; Zheng et al., 2020; Li et al., 2021). Elevated $[CO_2]$ generally promotes leaf photosynthesis, plant growth, and crop yield through the "CO_2 fertilization" effect with enhancing the ribulose-1,5-bisphosphate carboxylase oxygenase (Rubisco) carboxylation efficiency (Arndal et al., 2014; Niaz et al., 2020) and inhibiting leaf respiration rates (Yu et al., 2012; Xu, 2015). For example, Duan et al. (2019a) found that elevated $[CO_2]$ from 400 μmol mol^{-1} to 640 μmol mol^{-1} increased plant biomass, leaf area, and leaf number of *Eucalyptus tereticornis*, which attributed to the enhanced net photosynthetic rate and the reduced dark respiration. However, several recent studies have reported that soil water status could modify the CO_2 fertilization effect on crops such as winter wheat (Zheng et al., 2020) and green pepper (Fan et al., 2020) with changing leaf photosynthesis, stomatal traits, and non-structural carbohydrates, which are generally regulated by soil water availability and plant water status (Yu et al., 2012; Duan et al., 2019a). On the other hand, water deficiency often results in obvious reduction in leaf photosynthesis and plant biomass, and elevated $[CO_2]$ may mitigate the negative effects of water deficiency with regulating leaf photosynthesis, stomatal conductance, and leaf transpiration (Fan et al., 2020), which are coupled with stomatal traits such as stomatal density, stomatal openness, and the distribution pattern of stomata (Xu, 2015; Zheng et al., 2020). Nevertheless, the underlying mechanisms and processes of elevated $[CO_2]$ alleviates the effect of water stress on crops is remain unknown, thus studies focus on these topics will help to fill the knowledge gap, and meanwhile allow us to fully understand the impacts of water stress on global agriculture productivity in a higher atmospheric $[CO_2]$ world.

Due to the elevated atmospheric $[CO_2]$, climate models have also projected that water deficiency may also be accompanied by elevated temperature, namely climate warming. It is well demonstrated that many physiological processes of plants such as leaf photosynthesis and respiration are strongly dependent on growth temperature and soil/plant water status (Hatfield et al., 2011; Zhang et al., 2015). As a result, elevated temperature and drought stress usually decrease leaf photosynthesis and increase leaf respiration (Parry et al., 2003; Kurek et al., 2007; Bencze et al., 2014; Duan et al., 2019b), and limit plant growth and reduce crop yields when growth temperature and soil water content exceed the optimum for plant growth (Salvucci and Crafts-Brandner, 2004; Zhao et al., 2017; Hao et al., 2019). In addition, the negative effects of water deficiency and heat stress on plant growth and crop yield can be mitigated with elevated $[CO_2]$ (Mirwais et al., 2006; Wei et al., 2018). Mirwais et al. (2006) show that higher temperatures or drought inhibited many processes, while elevated $[CO_2]$ partially mitigated some of the adverse effects, such as total dry matter mass, net photosynthetic rate, and abscisic acid. Many previous studies have investigated the mitigating effects of elevated $[CO_2]$ on crop drought or warming, but the effect of high $[CO_2]$ on crop leaf structure, physiological processes, and biochemical synergistic responses to water deficiency and warming has rarely been reported (Mirwais et al., 2006; Yu et al., 2012).

Winter wheat (*Triticum aestivum* L.) in the North China Plain accounts for about 40% of the total arable land area and is one of the most important foodstuffs for humans (Wang et al., 2016). However, previous work predicted that the global climate has warmed in recent years and that groundwater resources are scarce (Tao et al., 2006), so not only warming and water deficiency may directly affect winter wheat growth and development by altering physiological and biochemical processes (Farooq et al., 2011; Zheng et al., 2020), but water deficiency and warming may also indirectly and synergistically affect grain yield of winter wheat as crop phenology and growth stages change (Hatfield et al., 2011). Wall et al. (2006) has shown that elevated $[CO_2]$ can increase the net photosynthetic rate in winter wheat, alleviate warming or water deficiency by reducing stomatal conductance and transpiration rate, and improve crop water use efficiency (Keshav et al., 2014). Meanwhile, elevated $[CO_2]$ can also inhibit the respiration process and Rubisco oxygenation reaction in winter wheat, which in turn increases the net photosynthetic rate (Li et al., 2004; Xu, 2015). Understanding the impact of elevated $[CO_2]$ on the physiology of winter wheat in response to water deficiency and/or warming alone or simultaneously has great potential for the development of stress-tolerant germplasm and new practices. Therefore, the objectives of this study were to observe (1) the interactive effect of elevated $[CO_2]$, experimental warming, and water deficiency on morphological traits and physiological processes; (2) the relationships between gas exchange, stomatal characteristics, leaf anatomical characteristics, non-structural carbohydrates, and Rubisco gene expression under $e[CO_2]$ ×

water × warming; and (3) to investigate whether elevated [CO_2] could mitigate the negative effects of water deficiency or warming on winter wheat.

Materials and methods

Plant materials and experimental design

In the current study, a commonly cultivated variety (Shimai 15) of winter wheat (*Triticum aestivum*) in the North China Plain was selected as the research material. We firstly sowed six wheat seeds in each plastic pot, where the height was 27 cm and the top and bottom areas were 531 cm^2 and 380 cm^2, respectively. This large volume at the bottom of pot was enough for root growth of winter wheat plants. The soil in pots for sustaining plant growth was the mixtures of yellow loam and nutrient soil with a volume ratio of 2:1. In addition, the field capacity was 24.5% and the bulk density was 1.28 g cm^{-3} of soil. Then, four pots were set up to each of eight environmental growth chambers (Model BDP-2000, Ningbo Prandt Instrument Co., Ltd, China) to sustain plant growth with a temperature regime of 21/16°C (day/night) and 1000 μmol m^{-2} s^{-1} photosynthetic active radiation, and 60%-70% relative humidity for 30 days for establishing plant canopy and roots. The space inside these environmental growth chambers (1.83 m high × 1.79 m long × 0.68 m wide) was large enough for the growth of winter wheat.

Wheat plants were treated with a split plot design consisting of three environmental factors (water, CO_2 concentration, and temperature), where watering was treated as the main plot, and temperature and CO_2 concentration were treated as subplots. Therefore, wheat plants in the eight environmental growth chambers were subjected to two water conditions, namely plants in four environmental growth chambers were well-watered with 75%-80% field capacity as full irrigation, and plants in the other four environmental growth chambers were treated as water deficiency with 45%-50% field capacity. The soil water content in all pots were measured with a Time Domain Reflectometry (TDR). The CO_2 concentrations were controlled at two levels of 400 μmol mol^{-1} (ambient CO_2 concentration, a[CO_2]) and 800 μmol mol^{-1} (elevated CO_2 concentration, e[CO_2]), and growth temperature treatments were 21/16°C (day/night, optimal growth temperature) and 26/21°C (day/night, elevated growth temperature). Therefore, the four environmental growth chambers subjected to full irrigation or water deficiency were randomly allocated to four treatments including Control (growth temperature is 21/16°C and CO_2 concentration is 400 μmol mol^{-1}), e[CO_2] (growth temperature is 21/16°C and CO_2 concentration is 800 μmol mol^{-1}), Warming (growth temperature is 26/21°C and CO_2 concentration is 400 μmol mol^{-1}), and e[CO_2] × warming (growth temperature is 26/21°C and CO_2 concentration is 800 μmol mol^{-1}). In the current study, the four pots planted with winter wheats in each environmental growth chamber were treated as the biological replicates (n=4). The photosynthetic active radiation was 1000 μmol m^{-2} s^{-1} with a 12-h photoperiod from 8:00 to 20:00, and relative humidity was controlled at 60%-70% in the eight environmental growth chambers. Wheat plants were fertilized once a week with half-strength Hoagland solution during the 90-day treatment period. Additionally, in the current study, we randomly changed the [CO_2] of each growth chamber to reduce the confounding effects from the various environmental growth chambers while concurrently shifting the treated winter wheat to the environmental growth chambers with appropriate [CO_2] monthly.

Measurement on leaf area, plant biomass, and leaf anatomy

All leaves of the winter wheat from each pot were sampled and leaf area was measured with a leaf area meter (LI-3100, LICOR, USA). Then, all the winter wheat tissues (leaves, stems and roots) from each pot were collected separately into paper bags, and dried at 80°C to constant weight. The dry weight of wheat plants was weighed using a high-precision electronic balance to finally obtain total biomass.

We obtained leaf cross-sections of the middle part of leaves on winter wheat with the paraffin section method of Sage et al (1995). The anatomical features of the leaves were observed and photographed under a microscopy and measured using Image J software (NIH, USA). We measured the thickness of the leaf mesophyll layer between the epidermal layers at five points in each cross-section. Twenty well-defined cells of the palisade layer and 20 cells of the spongy layer were randomly selected from each leaf cross-sectional image to measure cell length, cell width, cell area, and cell perimeter using the Auto CAD software.

Measuring stomatal traits

Leaves of three winter wheat plants were randomly selected in each pot and stomatal imprints were collected by applying colorless and transparent nail varnish to the middle of the adaxial and abaxial for measuring the morphological traits of individual stoma during 10:00-12:00 am after 90-day treatments in the environmental growth chambers. The slides of stomatal imprints were placed under a photographic microscope for observation and photograph three microscopic fields were randomly selected and then four microscope photographs were taken from each field. We counted the number of stomata in each photograph and then calculated stomatal density on leaves of winter wheat, stomatal length, stomatal width, stomatal perimeter, stomatal area, and stomatal shape index were also measured and calculated with the AutoCAD 2010 software.

In this study, the center of stomatal openings on the surface of winter wheat leaves was used as the focal point to further determine the spatial distribution pattern of stomata on the leaves of winter wheat. The micrographs characterizing the distribution of stomata on the leaves were digitized in the same coordinate system by Arc GIS 10.0 software to obtain the spatial coordinate values of each stoma. Next, the point pattern analysis was estimated with Ripley's K-function, a cumulative density function using the second moment of all point-to-point distances to evaluate two-dimensional distribution patterns at different scales (Xu, 2015; Zheng et al., 2020; Li et al., 2021). The results were plotted as

Lhat(d) values, calculated as:

$$Lhat(d) = \sqrt{\frac{K(d)}{\pi}} - d \quad (1)$$

where K(d), which represents the surface area of a circle with radius d, is the Ripley's exponential function. When the pattern is Poisson random, the Lhat(d) is an expectation of zero for any value of d (Li et al., 2021). By executing a random distribution 100 times, we used the Monte Carlo simulation to estimate the 95% boundary. At a given scale of d, the Lhat(d) value for stomata randomly distributed on the leaf surface should be within the 95% boundary. If the Lhat(d) value is greater than the upper 95% boundary, the stomata follow a cluster distribution, otherwise, the stomata follow a regular distribution at the scale (Xu, 2015).

Measuring leaf gas exchange

Five individual mature leaves (second fully expanded leaf from the top) were randomly selected from each treatment for measuring leaf gas exchange with a portable photosynthesis measurement system (LI-6400XT; LI-COR, USA) during 9:00-11:00 am after 90-day treatments. Leaves were firstly placed into the leaf chamber to determine the net photosynthetic rates (P_n), stomatal conductance (G_s), and transpiration rates (T_r) at the light level of 1000 μmol photon m^{-2} s^{-1} from a red-blue light source, which is the light saturation point for leaves of winter wheat. The temperature in the leaf chamber was set to 21°C (Control) or 26°C(warming) and the CO_2 concentration was controlled at 400 μmol mol^{-1} ($a[CO_2]$) or 800 μmol mol^{-1} ($e[CO_2]$) during the leaf gas exchange measurements on winter wheat. We also calculated the leaf-level instantaneous water use efficiency (*WUEI*) with the ratio of leaf P_n and T_r (Zheng et al., 2020). Then, leaf dark respiration rate (R_d) was also determined from the same leaves for measuring P_n. After leaf P_n measurements, we turned off the red-blue light source in the leaf chamber of LI-6400XT, and then measured leaf R_d at the same temperature and CO_2 concentration as the P_n measurements in the leaf chamber.

Analyzing biochemical compositions

The dried leaves of winter wheat were ground to powders using a ball mill, and then analyzed the contents of glucose, fructose, sucrose, and starch according to the method of Hedrix et al. (1994). In addition to nonstructural carbohydrates, leaf total carbon (C) and nitrogen (N) were also determined with an elemental analyzer (VarioMax CN, Elementary Corp. Germany).

Measuring enzyme activity and genes expression of Rubisco

The enzyme activity of Rubisco was measured by the method of Jiang et al. (2012). Moreover, we also analyzed the expression of Rubisco coding gene *RbcL3* and *RbcS2* according to the method of Livak et al. (2001). Specifically, total RNA was extracted using an RNA purification kit (Shanghai Shenggong Bioengineering Technology Service Co., Ltd.), and first-strand cDNA was synthesized according to the instructions of AMV first-strand cDNA synthesis kit (Shanghai Shenggong Bioengineering Technology Service Co., Ltd.). The primers for *RbcL3*, *RbcS2*, and *actin* were designed separately for amplification using Primer Premier 5.0 according to the sequences in the Genebank database. Specifically, the primer sequences for Rubisco key coding gene *RbcL3* were 5'-TAAATCACAGGCCGAAAC-3' and 5'-GGCAA TAATGAGCCAAAGT-3'. The primer sequence of *RbcS2* is 5'-AGCA ACGGCGGAAGGAT-3' and 5'-GCTCACGGAAGACGAAACC-3'. Subsequently, the expression of Rubisco coding gene was determined using a fluorescent quantitative PCR instrument.

Statistical analysis

In the current study, we used a split-plot experimental design with three factors: water deficiency, $[CO_2]$ and warming. The split-plot three-way ANOVA was used to test the main effects of water deficiency, $[CO_2]$ and warming on plant biomass, stomatal traits, leaf gas exchanges, and biochemical compositions of winter wheat. The homogeneity and normal distribution of variances assumptions were evaluated before we ran the ANOVA analysis, and all of our data passed the assumptions. Results were considered significant if $P \leq 0.05$. All statistical analyses were used SPSS 13.0 software (SPSS Inc., Chicago, IL, USA), with all graphs produced in sigmaplot 10.

Results

The main effects of water deficiency, $e[CO_2]$, and warming

We found negative impacts of soil water deficiency on winter wheat, where the plant biomass and leaf area were decreased by net photosynthetic rate. Furthermore, water deficiency treatment (D) had negative effects on some morphological traits, such as total biomass and leaf areas, stomatal parameters, and spatial distribution pattern of winter wheat, more specifically

TABLE 1 Interactive effects of elevated $[CO_2]$ and experimental warming on the biomass and leaf area parameters at different water conditions of winter wheat.

Treatments	Total biomass	Leaf area
$[CO_2]$	p=0.940	p=0.347
Water	**p<0.001**	**p<0.001**
Warming	**p<0.001**	**p=0.030**
$[CO_2]$ × water	p=0.272	**p=0.004**
$[CO_2]$ × warming	p=0.055	**p=0.028**
Water × warming	**p=0.027**	**p<0.001**
$[CO_2]$ × water × warming	p=0.674	p=0.260

Note that the bold values indicate a significant effect on the indicators.

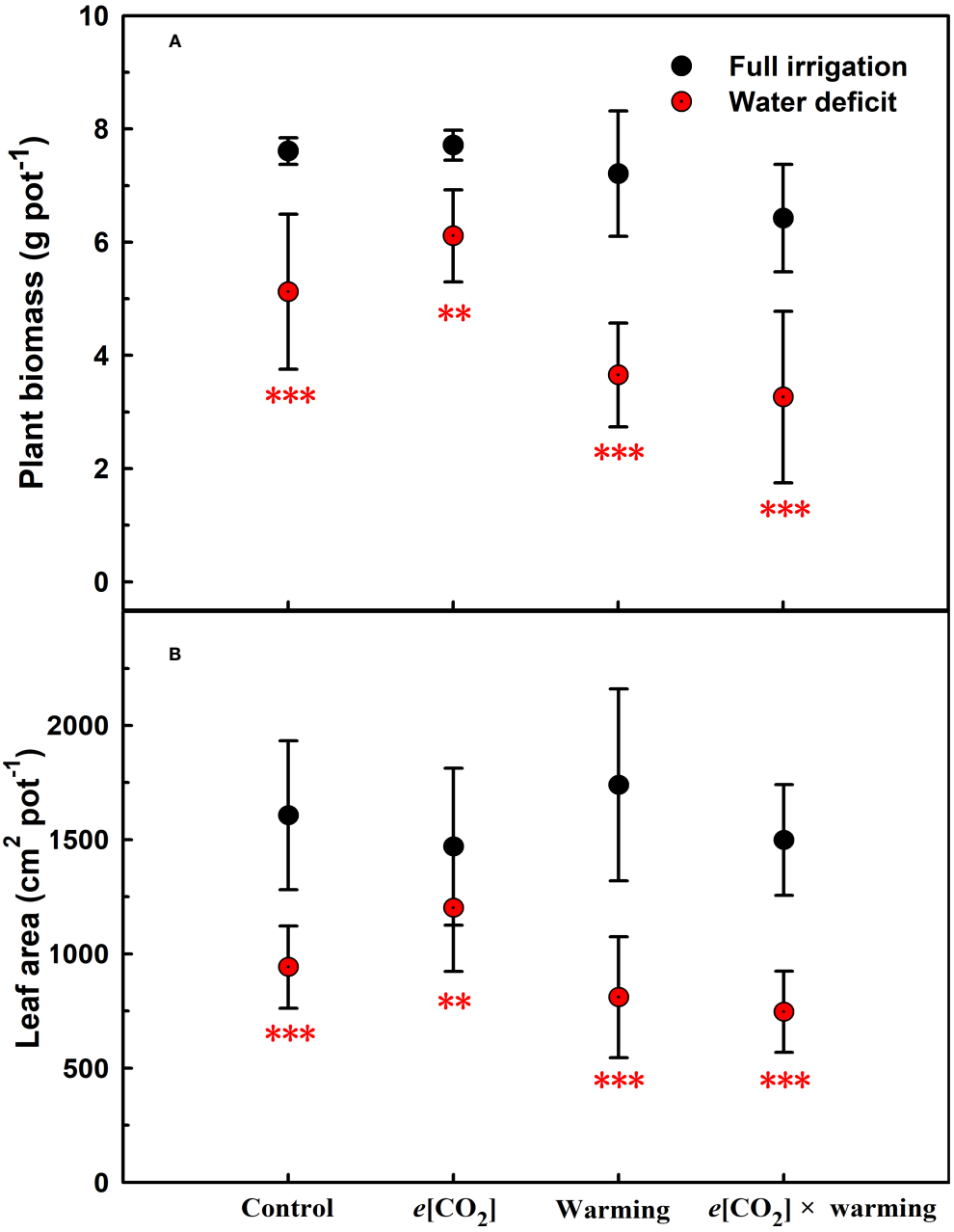

FIGURE 1
Effects of elevated [CO_2] and experimental warming on the biomass **(A)** and leaf area **(B)** at different water conditions of winter wheat. Note that the black circle represents full irrigation, and the red circle represents water deficit. Values are means ± SD (n = 4). The symbol ** and *** indicate that the significant difference between full irrigation and water deficit under *e*[CO_2], warming, and *e*[CO_2] × warming are p<0.01 and p<0.001, respectively.

D decreased total biomass and leaf areas (all p<0.001) and stomatal regular patterns on abaxial of winter wheat (Table 1; Figures 1, 2B). By contrast, water deficiency significantly increased the stomatal width (p<0.001), stomatal area (p<0.001), and stomatal shape index (SSI) (p<0.001) on the adaxial leaf surface (Tables 2, 3). Moreover, water deficiency substantially decreased the net photosynthetic rates (P_n), transpiration rates (T_r), stomatal conductance (G_s) (all p<0.001), and intercellular CO_2 concentration (C_i) (p=0.046), while drastically increased the leaf dark respiration rates (R_d) of winter wheat (p<0.001; Figure 3; Table 4). Water deficiency significantly reduced the total soluble sugar content of winter wheat (p<0.05), which was mainly due to a significant decline in sucrose content (p<0.05; Figure 4). Furthermore, water deficiency enhanced the Rubisco activation state and soluble protein content (Figure 5), but the initial Rubisco activity and total Rubisco activity were markedly decreased by water deficiency. In addition, water deficiency significantly increased the mesophyll cell perimeter (p=0.002), mesophyll cell area (p=0.006), mesophyll cell length (p=0.002), and leaf thickness (p<0.001; Table 7).

Elevated CO_2 concentration (*e*[CO_2]) increased stomatal density on both leaf surfaces (all p<0.001) as well as enhanced the stomatal area on the abaxial leaf surface (p=0.003) and the

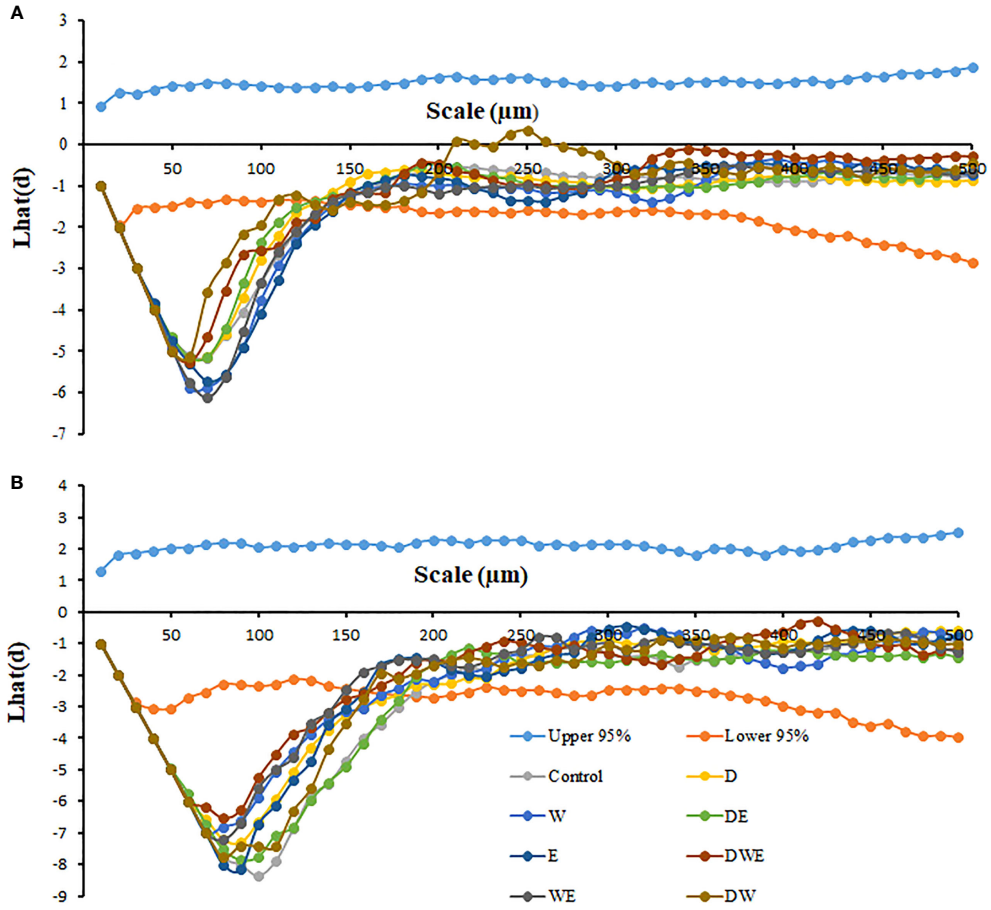

FIGURE 2
Effects of elevated [CO_2] and experimental warming on the leaf spatial distribution pattern of stomata on the adaxial **(A)** and abaxial **(B)** surfaces at different water conditions of winter wheat. (The upper 95% means the upper boundary of the 95% confidence envelope, the lower 95% means the lower boundary of the 95% confidence envelope. The Lhat(d) value is the nearest neighbor distance, and stomata follow a regular distribution at the scale when the Lhat(d) value is lower than the 95% boundary with the smaller the minimum Lhat(d) value, the more regular spatial distribution pattern of stomata).

TABLE 2 Effects of elevated [CO_2] and experimental warming on the stomatal density and morphological traits of individual stomata at different water conditions of winter wheat.

Parameters	Leaf surfaces	Full irrigation				Water deficiency				*p*-values
		Control	*e*[CO_2]	Warming	*e*[CO_2] × warming	Drought	*e*[CO_2]	Warming	*e*[CO_2] × warming	
Stomatal density (SD No. mm^{-2})	adaxial	29.2 ± 3.5	40.3 ± 8.1	38.5 ± 9.1	45.0 ± 10.1	32.5 ± 3.3	34.7 ± 3.4	38.5 ± 6.0	42.8 ± 4.5	***p*<0.001**
	abaxial	51.1 ± 5.4	64.8 ± 9.3	55.7 ± 6.1	60.4 ± 7.9	61.2 ± 5.4	60.1 ± 8.9	56.4 ± 7.6	47.6 ± 10.6	***p*<0.001**
Stomatal length (SL μm)	adaxial	40.4 ± 4.0	38.0 ± 1.8	40.7 ± 3.1	38.9 ± 4.2	38.9 ± 5.2	40.3 ± 4.2	32.9 ± 4.7	38.1 ± 1.8	***p*=0.001**
	abaxial	37.0 ± 3.5	39.2 ± 6.0	39.1 ± 2.2	34.8 ± 1.8	38.9 ± 3.2	42.5 ± 2.6	34.9 ± 3.6	37.3 ± 2.4	***p*=0.001**
Stomatal width (SW μm)	adaxial	4.1 ± 0.7	3.6 ± 0.5	5.1 ± 0.5	4.3 ± 0.4	4.7 ± 0.4	3.5 ± 0.1	3.4 ± 0.5	3.7 ± 0.9	***p*<0.001**
	abaxial	4.0 ± 1.3	4.1 ± 1.0	4.4 ± 0.3	3.9 ± 0.2	4.3 ± 0.5	3.5 ± 0.3	3.1 ± 0.6	3.4 ± 0.8	*p*=0.070

(Continued)

TABLE 2 Continued

Parameters	Leaf surfaces	Full irrigation				Water deficiency				*p*-values
		Control	$e[CO_2]$	Warming	$e[CO_2]$ × warming	Drought	$e[CO_2]$	Warming	$e[CO_2]$ × warming	
Stomatal perimeter (SP μm)	adaxial	85.2 ± 8.7	79.3 ± 4.0	86.6 ± 6.4	81.8 ± 8.5	82.5 ± 10.1	83.9 ± 8.4	69.9 ± 8.6	79.4 ± 6.4	***p*=0.001**
	abaxial	78.3 ± 8.3	83.1 ± 13.6	82.7 ± 4.3	73.4 ± 4.2	82.3 ± 6.6	88.8 ± 4.9	72.8 ± 8.4	78.6 ± 4.9	***p*=0.011**
Stomatal area (SA μm^2)	adaxial	167.4 ± 54.0	129.5 ± 21.1	211.1 ± 29.2	162.8 ± 22.3	191.4 ± 34.3	129.1 ± 18.7	102.4 ± 30.3	122.9 ± 37.9	***p*<0.001**
	abaxial	146.4 ± 66.5	171.2 ± 68.2	174.1 ± 17.0	138.6 ± 16.1	167.9 ± 26.7	146.9 ± 10.2	111.5 ± 36.4	121.7 ± 26.2	*p*=0.123
Stomatal shape Index (SSI)	adaxial	0.15 ± 0.01	0.14 ± 0.01	0.17 ± 0.01	0.16 ± 0.01	0.17 ± 0.01	0.14 ± 0.01	0.14 ± 0.01	0.14 ± 0.01	***p*<0.001**
	abaxial	0.15 ± 0.02	0.15 ± 0.01	0.16 ± 0.01	0.16 ± 0.01	0.16 ± 0.01	0.14 ± 0.01	0.14 ± 0.01	0.14 ± 0.01	***p*=0.008**

Note that the bold values indicate a significant effect on the indicators.

regularity of stomatal distribution on the adaxial leaf surface (Figure 2A), whereas decreased the stomatal width (p<0.001), stomatal area (p=0.003) and stomatal shape index (p<0.001) on the adaxial surface of leaves (Tables 2, 3). Furthermore, $e[CO_2]$ substantially decreased leaf G_s (p=0.008) and T_r (p=0.014) mainly due to the declines of stomatal area. As a result, the leaf-level instantaneous water use efficiency (*WUEI*) was enhanced by $e[CO_2]$ (p<0.001; Figure 3; Table 4), although P_n was barely affected under $e[CO_2]$ (p>0.05; Figure 3; Table 4). Moreover, the soluble sugar content was significantly reduced (p=0.015) under $e[CO_2]$, mainly attributed to the decrease in fructose content (p=0.005), but $e[CO_2]$ marginally increased the leaf carbon content (p=0.017; Figures 4, 7; Tables 5, 8). Meanwhile, Rubisco activation state and soluble protein content of winter wheat under $e[CO_2]$ was obviously higher than control (all p<0.05; Figure 5) due to the increase of the amount of gene expression in *RbcL3* and *RbcS2* (all p<0.001; Figure 6; Table 6). In terms of the anatomical traits, $e[CO_2]$ also increased mesophyll cell length, but drastically decreased the leaf thickness (all p<0.001; Table 7).

Our results also showed that experimental warming increased the leaf area (p=0.030), stomatal length (p<0.001), stomatal perimeter (p<0.001), and stomatal area (p=0.030), but decreased the total plant

TABLE 3 Interactive effects of elevated $[CO_2]$ and experimental warming on stomatal parameters at different water conditions of winter wheat.

Stomatal traits	SD	SL	SW	SP	SA	SSI
$[CO_2]$	***p*<0.001**	*p*=0.180	***p*<0.001**	*p*=0.402	***p*=0.003**	***p*<0.001**
Water	*p*=0.138	*p*=0.337	***p*<0.001**	*p*=0.209	***p*<0.001**	***p*<0.001**
Warming	*p*=0.142	***p*<0.001**	*p*=0.120	***p*<0.001**	***p*=0.030**	*p*=0.313
Leaf surface	***p*<0.001**	*p*=0.360	*p*=0.156	*p*=0.404	*p*=0.462	*p*=0.881
$[CO_2]$ × water	***p*<0.001**	***p*<0.001**	*p*=0.940	***p*<0.001**	*p*=0.394	***p*<0.001**
$[CO_2]$ × warming	***p*=0.011**	*p*=0.479	*p*=0.167	*p*=0.553	*p*=0.405	*p*=0.011
$[CO_2]$ × leaf surface	***p*=0.042**	*p*=0.724	***p*=0.026**	*p*=0.427	***p*=0.027**	***p*=0.006**
Water × warming	***p*=0.025**	***P*=0.001**	***p*<0.001**	***p*=0.001**	***p*<0.001**	***p*<0.001**
Water × leaf surface	*p*=0.777	***p*=0.018**	*p*=0.845	***p*=0.029**	*p*=0.414	*p*=0.244
Warming × leaf surface	***p*<0.001**	*p*=0.343	*p*=0.221	*p*=0.227	*p*=0.148	*p*=0.824
$[CO_2]$ × water × warming	*p*=0.297	*P*=0.069	***p*<0.001**	***p*=0.040**	***p*<0.001**	***p*<0.001**
$[CO_2]$ × water × leaf surface	***p*=0.022**	*p*=0.544	*p*=0.740	*p*=0.608	*p*=0.336	*p*=0.579
$[CO_2]$ × warming × leaf surface	*p*=0.059	***p*=0.009**	*p*=0.433	***p*=0.016**	***p*=0.034**	*p*=0.622
Water × warming × leaf surface	***p*=0.019**	*p*=0.565	***p*=0.020**	*p*=0.483	***p*=0.046**	*p*=0.051
$[CO_2]$ × water × warming × leaf surface	*p*=0.450	*p*=0.605	*p*=0.837	*p*=0.505	*p*=0.984	*p*=0.557

Note that the bold values indicate a significant effect on the indicators.

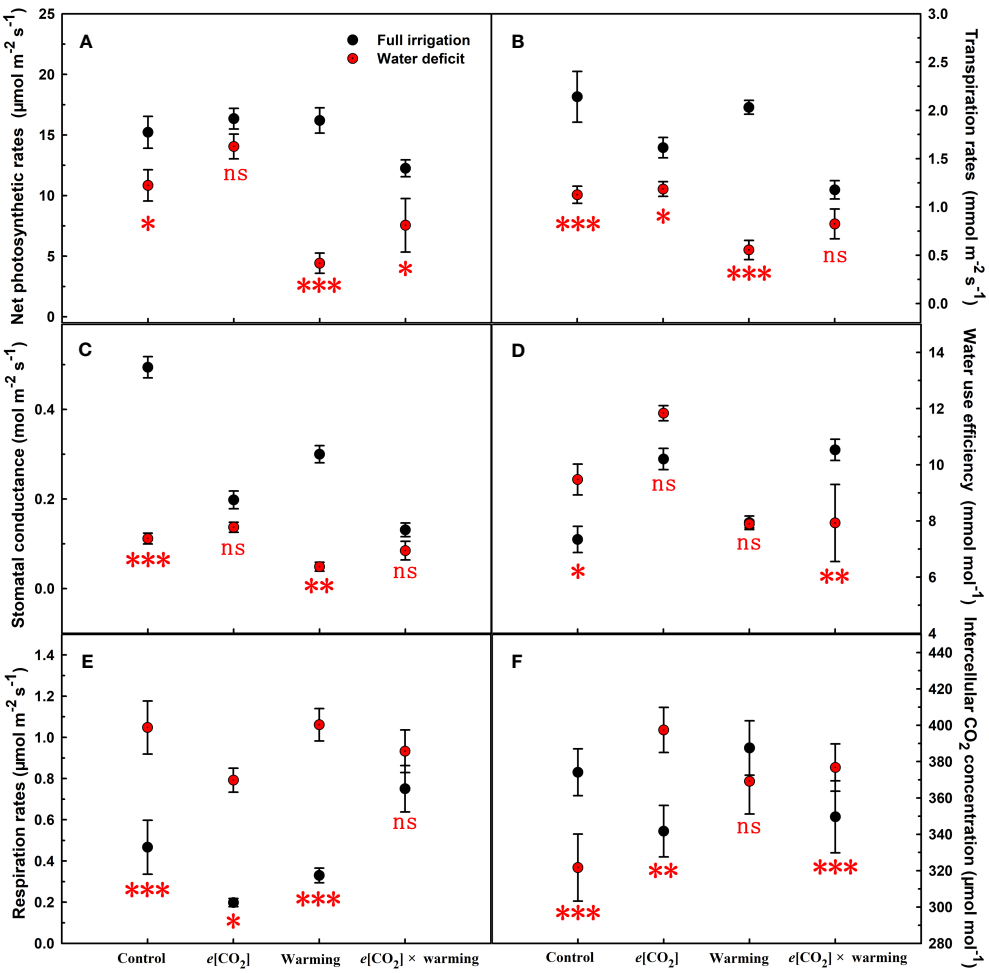

FIGURE 3
Responses of leaf net photosynthetic rates **(A)**, transpiration rates **(B)**, stomatal conductance **(C)**, water use efficiency **(D)**, respiration rates **(E)**, and intercellular CO_2 concentration **(F)** to elevated [CO_2] and experimental warming at different water conditions of winter wheat. Note that the black circle represents full irrigation, and the red circle represents water deficit. Values are means ± SD (n = 4). The symbol *, **, and *** indicate that the significant difference between full irrigation and water deficit under e[CO_2], warming, and e[CO_2] × warming are p<0.05, p<0.01, and p<0.001, respectively; ns denote no significant differences in full irrigation and water deficit at 0.05 level.

biomass of winter wheat (p<0.001; Figure 1; Tables 1–3). Moreover, the stomatal distribution regularity on the adaxial surface was enhanced by experimental warming (Figure 2). Similarly, experimental warming increased the Pn (p<0.001), WUE (p=0.018), and Ci (p<0.001), while decreased the Tr (p<0.001), Gs (p=0.013), and glucose content (p=0.042; Figures 3, 4; Tables 4, 5). The mesophyll cell length, cell width, cell perimeter, cell area, and leaf thickness were also magically reduced under experimental warming (all p<0.001; Table 7).

TABLE 4 Interactive effects of elevated [CO_2] and experimental warming on photosynthesis parameters at different water conditions of winter wheat.

Treatments	P_n	T_r	G_s	*WUE*	R_d	C_i
[CO_2]	p=0.361	***p*=0.014**	***p*=0.008**	***p*<0.001**	p=0.946	p=0.917
Water	***p*<0.001**	***p*<0.001**	***p*<0.001**	p=0.551	***p*<0.001**	***p*=0.046**
Warming	***p*<0.001**	***p*=0.001**	***p*=0.013**	***p*=0.018**	p=0.257	***p*<0.001**
[CO_2] × water	***p*=0.021**	***p*<0.001**	***p*=0.001**	p=0.108	***p*=0.007**	***p*<0.001**
[CO_2] × warming	p=0.185	p=0.774	p=0.343	p=0.170	***p*=0.049**	p=0.091
Water × warming	***p*=0.014**	p=0.347	p=0.317	***p*=0.001**	p=0.967	***p*<0.001**
[CO_2] × water ×warming	p=0.197	p=0.195	p=0.423	p=0.274	p=0.268	p=0.081

Note that the bold values indicate a significant effect on the indicators.

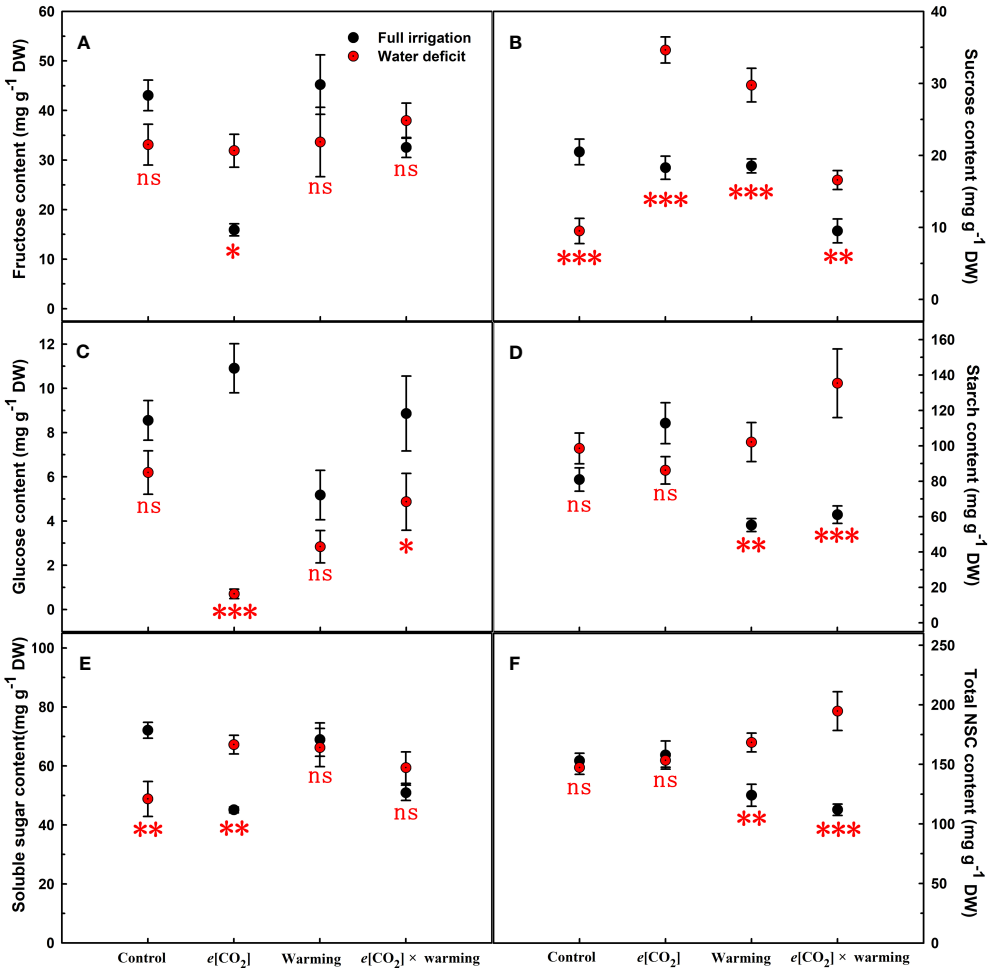

FIGURE 4
Effects of elevated [CO_2] and experimental warming on fructose **(A)**, sucrose **(B)**, glucose **(C)**, starch **(D)**, soluble sugar **(E)**, and total NSC **(F)** at different water conditions of winter wheat. Note that the black circle represents full irrigation, and the red circle represents water deficit. Values are means ± SD (n = 4). The symbol *, **, and *** indicate that the significant difference between full irrigation and water deficit under e[CO_2], warming, and e[CO_2] × warming are p<0.05, p<0.01, and p<0.001, respectively; ns denote no significant differences in full irrigation and water deficit at 0.05 level.

The interactive effects of water deficiency and experimental warming

Experimental warming had a negative impact on plant biomass (p=0.027), leaf area under water deficiency (all p<0.001; Figure 1; Table 1). Meanwhile, the stomatal density (p=0.025), stomatal length (p=0.001), stomatal width (p<0.001), stomatal perimeter (p=0.001), stomatal area (p<0.001), and stomatal shape index (p<0.001) as well as the regularity of abaxial stomatal spatial distribution pattern were also reduced under

TABLE 5 Interactive effects of elevated [CO_2] and experimental warming on nonstructural carbohydrates at different water conditions of winter wheat.

Treatments	Fructose	Sucrose	Glucose	Soluble sugar	Starch	TNC
[CO_2]	***p*=0.005**	*p*=0.871	*p*=0.406	***p*=0.015**	*p*=0.056	*p*=0.345
Water	*p*=0.992	***p*<0.001**	***p*<0.001**	*p*=0.719	***p*=0.001**	***p*<0.001**
Warming	***p*=0.042**	*p*=0.067	*p*=0.114	*p*=0.346	*p*=0.405	*p*=0.639
[CO_2] × water	***p*=0.001**	***p*<0.001**	***p*=0.005**	***p*<0.001**	*p*=0.566	*p*=0.142
[CO_2] × warming	*p*=0.105	***p*<0.001**	***p*=0.008**	*p*=0.214	*p*=0.507	*p*=0.900
Water × warming	*p*=0.314	***p*=0.008**	*p*=0.053	*p*=0.590	***p*<0.001**	***p*<0.001**
[CO_2] × water ×warming	*p*=0.459	***p*<0.001**	*p*=0.054	***p*=0.013**	***p*=0.021**	*p*=0.165

Note that the bold values indicate a significant effect on the indicators.

10.3389/fpls.2023.1227286

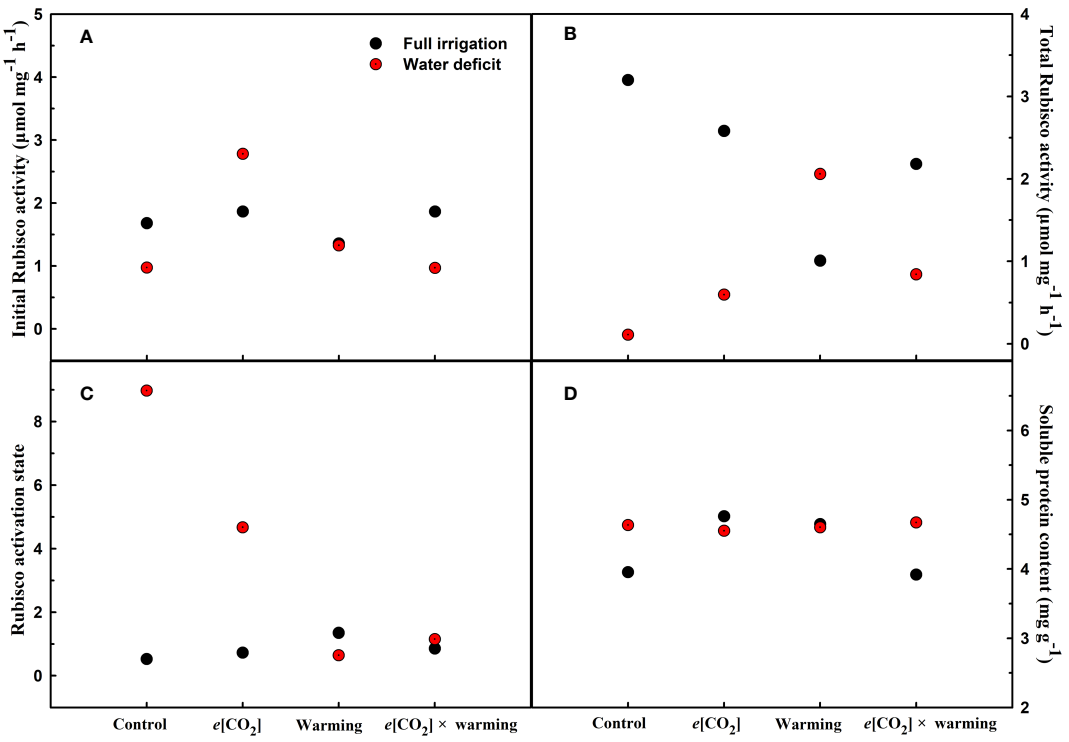

FIGURE 5
Effects of elevated [CO_2] and experimental warming on initial Rubisco activity **(A)**, total Rubisco activity **(B)**, Rubisco activity state **(C)**, and soluble protein **(D)** at different water conditions of winter wheat. Note that the black circle represents full irrigation, and the red circle represents water deficit.

experimental warming and water deficiency (Figure 2; Tables 2, 3). Similarly, we also found negatively interactive effects of experimental warming and water deficiency on leaf P_n (p=0.014), *WUE* (p=0.001), and Rubisco activation state (Figure 5) of wheat plants, although positive effects were observed on leaf sucrose (p=0.008), starch (p<0.001), TNC (p<0.001), and the amount of gene expression in *RbcL3* (p<0.001) and *RbcS2* (p<0.001) under experimental warming and water deficiency condition. Moreover, experimental warming significantly decreased the mesophyll cell length (p=0.012), cell perimeter (p<0.001), cell area (p<0.001), and leaf thickness (p<0.001) under water deficiency (Table 7).

The interactive effects of soil water deficiency and elevated CO_2 concentration

Our three-way ANOVA results showed interactive effects of $e[CO_2]$ and water deficiency on the morphological traits of leaves and stomata (all p<0.05). We found that $e[CO_2]$ significantly increased the leaf area of winter wheat under water deficiency (p=0.004; Figure 1; Table 1). Meanwhile, $e[CO_2]$ also increased the stomatal density on the adaxial leaf surface, and the stomatal length and perimeter on both leaf surfaces of winter wheat at water deficiency condition (all p<0.001; Tables 2, 3). Moreover, $e[CO_2]$ substantially enhanced leaf P_n, T_r, and G_s by *c.* 30% (p=0.021), 50% (p<0.001), and 20% (p=0.001) under water deficiency, indicating the negative impacts of water deficiency on winter wheat might be partially mitigated by $e[CO_2]$, which could also be supported by the significantly interactive effects of $e[CO_2]$ and water deficiency on leaf P_n (p=0.021), T_r (p<0.001), and G_s (p=0.001) of winter wheat (Table 4). Furthermore, $e[CO_2]$ and water deficiency also interactively affected leaf carbon (p=0.007) and soluble sugar (p<0.001) with increasing leaf fructose (p=0.001) and sucrose (p<0.001). In addition, the expression amount of Rubisco coding genes were also significantly affected by the interactions of $e[CO_2]$ and water deficiency through enhancing the amount of gene expression in *RubcL3* (p<0.001; Figure 6; Table 6). Additionally, our ANOVA results also showed significantly interactive effects on the mesophyll cell width (p=0.017), cell perimeter (p<0.001), cell area (p<0.001), and leaf thickness under [CO_2] × water (p<0.001; Table 7).

The interactive effects of elevated CO_2 concentration and experimental warming

Our results showed that $e[CO_2]$ significantly decreased the leaf area of winter wheat grown at experimental warming (p=0.028).

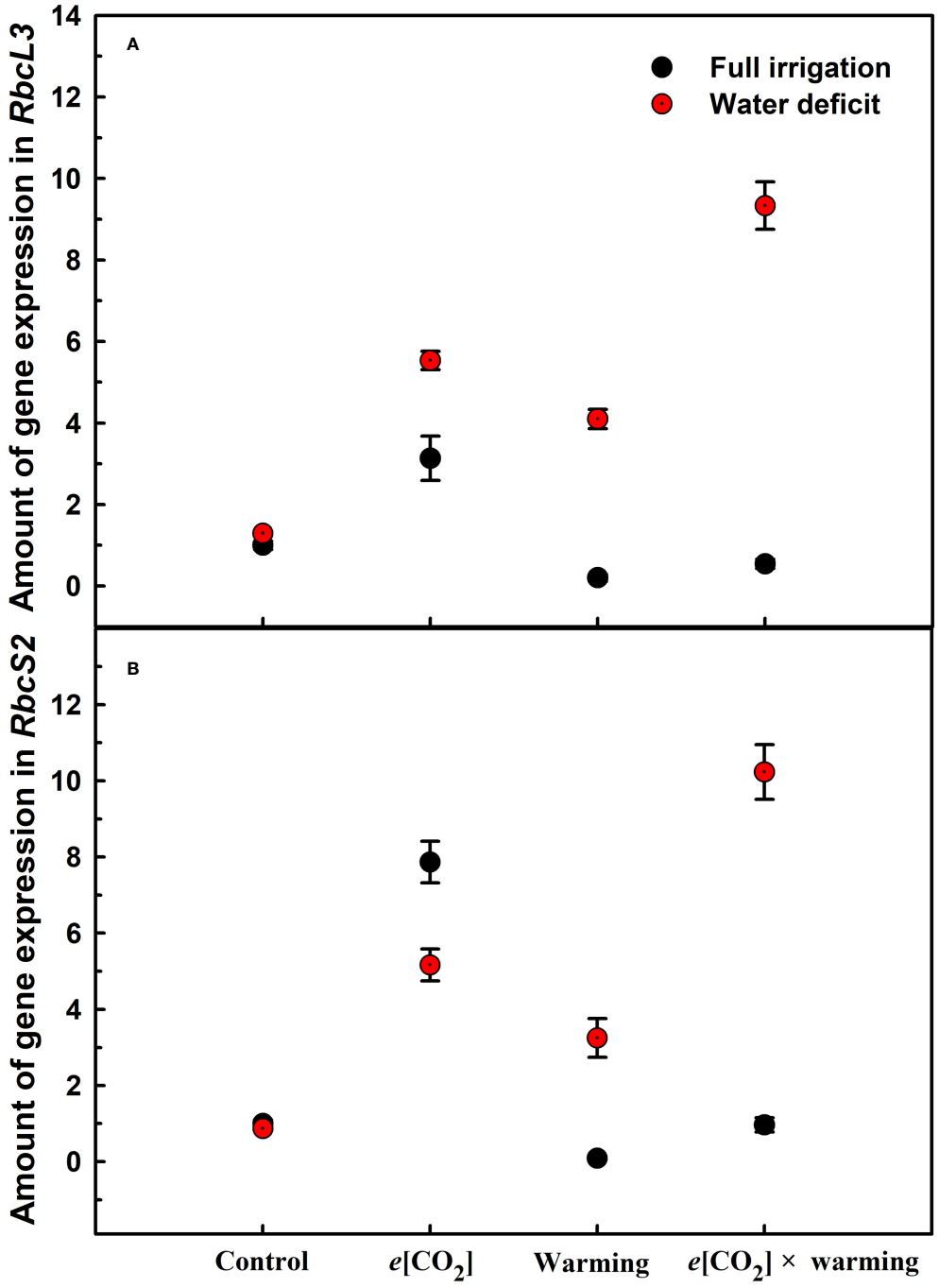

FIGURE 6
Effects of elevated [CO_2] and experimental warming on the amount of gene expression in RbcL3 **(A)** and RbcS2 **(B)** of Rubisco at different water conditions in winter wheat leaves. Note that the black circle represents full irrigation, and the red circle represents water deficit.

However, the stomatal density and regularity of stomatal distribution pattern on the adaxial leaf surface was increased under $e[CO_2]$ and experimental warming conditions (Figures 1, 2; Tables 2, 3). Moreover, $e[CO_2]$ × warming reduced leaf sucrose content ($p<0.001$; Figure 4; Table 5), but dramatically increased leaf carbon ($p=0.014$; Figure 7; Table 8). Additionally, $e[CO_2]$ decreased total Rubisco activity, mesophyll cell width ($p=0.025$) and leaf thickness ($p<0.001$) under experimental warming (Figure 5; Table 7).

The interactive effects of elevated CO_2 concentration, water deficiency and experimental warming

We found significantly interactive effects of water deficiency, $e[CO_2]$, and experimental warming on the morphological traits of stomata such as stomatal width ($p<0.001$), stomatal perimeter ($p=0.04$), stomatal area ($p<0.001$), and stomatal shape index ($p<0.001$; Table 3). Meanwhile, the biochemical compositions in wheat leaves

TABLE 6 Interactive effects of elevated [CO_2] and experimental warming on the amount of gene expression of Rubisco at different water conditions of winter wheat.

Treatments	*RbcL3*	*RbcS2*
[CO_2]	***p*<0.001**	***p*<0.001**
Water	***p*<0.001**	***p*<0.001**
Warming	***p*<0.001**	*p*=0.624
[CO_2]×water	***p*<0.001**	***p*<0.001**
[CO_2]×warming	*p*=0.178	***p*<0.001**
Water×warming	***p*<0.001**	***p*<0.001**
[CO_2]×water×warming	***p*<0.001**	***p*<0.001**

Note that the bold values indicate a significant effect on the indicators.

were also obviously changed under water deficiency, *e*[CO_2], and experimental warming as shown by their interactions on leaf sucrose ($p<0.001$), starch ($p=0.021$), and soluble sugars ($p=0.013$; Figure 4; Table 5) as well as leaf carbon ($p<0.001$; Figure 7; Table 8). In addition to stomata and biochemical compositions, the expression amount of Rubisco coding gene *RbcL3* and *RbcS2* as well as leaf thickness were also interactively affected by water deficiency, *e*[CO_2], and experimental warming (all $p<0.001$).

Discussion

The interactive effects of water deficiency and elevated [CO_2]

The reduction in biomass and photosynthetic rate under water deficiency may be due to stomatal limitation or non-stomatal limitation (Yu et al., 2012; Wang et al., 2017). The former is typically caused by stomatal number, stomatal distribution pattern, and stomatal opening (Fan et al., 2020; Zheng et al., 2020), while the latter is attributed to metabolic disorders such as imbalance of carbon sink and source or reduced carboxylation efficiency due to reduced Rubisco activity (Parry et al., 2003; Aranjuelo et al., 2011). In the current study, we found a *c.*29% decrease in photosynthesis under water deficiency, mainly due to a significant *c.*77% decrease in stomatal conductance, and the increase in starch that inhibited the reduction phase of the Calvin cycle (Figures 3, 4; Tables 4, 5) (Sheen, 1990). Significantly lower G_s and C_i under water stress suggest that carboxylation efficiency may be severely restricted by water deficiency, as reported by others (Flexas et al., 2004; Yu et al., 2012).

Previous studies found that elevated [CO_2] had a strong "fertilization effect" on C_3 plants because the current environment did not reach the optimal CO_2 concentration for photosynthetic rates (Xu, 2015; Zheng et al., 2018), while Högy et al. (2013) showed that increasing CO_2 concentration by 150 μmol mol^{-1} barely affects the growth and development of winter wheat. In the present study, we found elevated [CO_2] from 400 μmol mol^{-1} to 800 μmol mol^{-1} also did not affect biomass and P_n of winter wheat may be due to the decrease of G_s. Nevertheless, elevated [CO_2] did not interact with water deficiency on plant biomass, elevated [CO_2] alleviated P_n in winter wheat under drought treatment, which was related to Gs, metabolic activity, and anatomical structure. Results showed that under *e*[CO_2] × water, the reduction of T_r could suppress water loss in winter wheat to ensure normal metabolism. Additionally, the study found that elevated [CO_2] allowed more photosynthetic products to be stored in the form of soluble sugars when winter wheat plants were subjected to water deficiency (Figure 3; Table 4),

TABLE 7 Effects of elevated CO_2 concentration and experimental warming on leaf mesophyll cells at different water conditions of winter wheat.

Parameters		Cell length	Cell width	Cell perimeter	Cell area	Leaf thickness
Full irrigation	Control	22.45 ± 2.10	17.47 ± 1.68	66.97 ± 6.65	332.16 ± 65.1	132.04 ± 9.00
	e[CO_2]	24.06 ± 2.54	15.94 ± 2.41	62.41 ± 8.97	286.88 ± 80.10	121.04 ± 5.83
	Warming	20.78 ± 0.99	14.94 ± 1.28	64.13 ± 4.54	294.31 ± 37.78	102.10 ± 4.51
	e[CO_2]×Warming	22.23 ± 2.24	15.53 ± 1.22	63.01 ± 6.10	290.31 ± 61.50	125.67 ± 10.21
Water deficiency	Drought	24.18 ± 1.73	17.14 ± 1.7	71.51 ± 6.21	360.21 ± 54.40	157.60 ± 9.96
	e[CO_2]	26.66 ± 2.50	17.84 ± 1.94	77.16 ± 7.46	418.73 ± 75.31	130.62 ± 11.29
	Warming	20.60 ± 1.15	14.54 ± 1.05	57.20 ± 3.55	236.72 ± 29.88	148.83 ± 9.70
	e[CO_2]×Warming	22.83 ± 2.37	15.92 ± 1.61	66.02 ± 5.30	313.16 ± 46.93	138.06 ± 8.98
[CO_2]		***p*<0.001**	*p*=0.358	*p*=0.066	*p*=0.056	***p*<0.001**
Water		***p*=0.002**	*p*=0.214	***p*=0.002**	***p*=0.006**	***p*<0.001**
Warming		***p*<0.001**	***p*<0.001**	***p*<0.001**	***p*<0.001**	***p*<0.001**
[CO_2]×water		*p*=0.281	***p*=0.017**	***p*<0.001**	***p*<0.001**	***p*<0.001**
[CO_2]×warming		*p*=0.788	***p*=0.025**	*p*=0.166	*p*=0.185	***p*<0.001**
Water×warming		***p*=0.012**	*p*=0.207	***p*<0.001**	***p*<0.001**	***p*<0.001**
[CO_2]×water×warming		*p*=0.955	*p*=0.245	*p*=0.956	*p*=0.599	***p*<0.001**

Note that the bold values indicate a significant effect on the indicators.

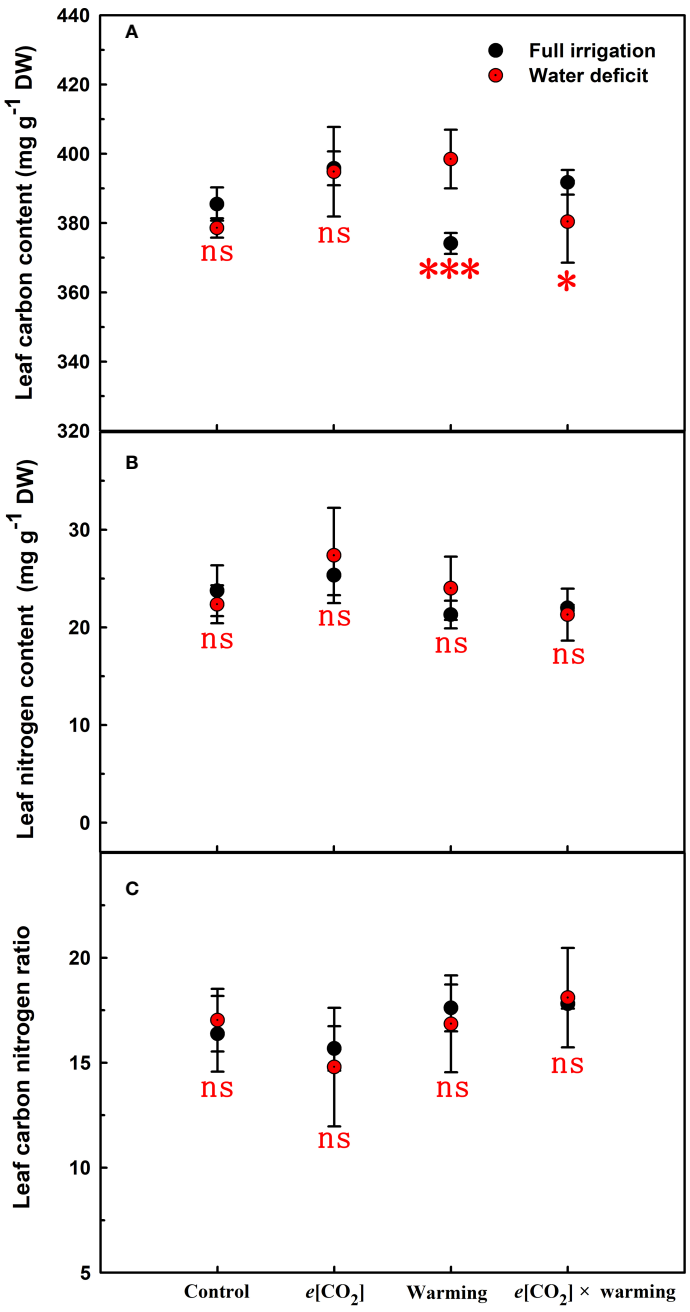

FIGURE 7
Effects of elevated [CO_2] and experimental warming on leaf carbon **(A)**, nitrogen **(B)**, and carbon nitrogen ratio **(C)** at different water conditions of winter wheat. Note that the black circle represents full irrigation, and the red circle represents water deficit. Values are means ± SD (n = 4). The symbol * and *** indicate that the significant difference between full irrigation and water deficit under *e*[CO_2], warming, and *e*[CO_2] × warming are $p<0.05$, and $p<0.001$, respectively; ns denote no significant differences in full irrigation and water deficit at 0.05 level.

which may indicate that elevated CO_2 concentrations from 400 µmol mol^{-1} to 800 µmol mol^{-1} favored Rubisco carboxylation rather than RuBP regeneration (Xu, 2015) may also partially explain that the biomass was barely affected (Wong, 1990; Zheng et al., 2018). Meanwhile, the nitrogen content in the leaves was not limited by elevated [CO_2] and water deficiency, which ensured photosynthesis (Zong and Shangguan, 2016). Furthermore, we also found elevated [CO_2] concentrations alleviated photosynthesis probably associated with elevated Rubisco activity as well as the amount of gene expression in *RbcL3* and *RbcS2* when plant under water deficiency (Parry et al., 2003; Hou et al., 2021). In addition to physiological factors, under water deficiency conditions, elevated [CO_2] significantly enlarged the mesophyll cell area, which largely determined photosynthesis, as more chloroplasts could be accommodated (Zheng et al., 2018).

Previous results showed that drought significantly increased plant R_d *c.*24%, which may result in greater carbohydrate consumption (Yu et al., 2012), while R_d decreased by 20% by doubling ambient [CO_2]

TABLE 8 Interactive effects of elevated [CO_2] and experimental warming on leaf carbon (C) and nitrogen (N).

Treatments	Carbon	Nitrogen	C/N ratio
[CO_2]	***p*=0.017**	*p*=0.205	*p*=0.552
Water	*p*=0.627	*p*=0.461	*p*=0.776
Warming	*p*=0.343	***p*=0.007**	***p*=0.013**
[CO_2] × water	***p*=0.007**	*p*=0.994	*p*=0.845
[CO_2] × warming	***p*=0.014**	***p*=0.021**	*p*=0.087
Water × warming	*p*=0.051	*p*=0.702	*p*=0.924
[CO_2] × water × warming	***p*<0.001**	*p*=0.064	*p*=0.306

Note that the bold values indicate a significant effect on the indicators.

(Drake et al., 1997). Our study found that under water deficiency, the respiration rate was downregulated by 24.4% at elevated [CO_2], which facilitated the development of drought tolerance in winter wheat and thus stored more carbohydrates.

The interactive effect of experimental warming and elevated [CO_2]

Several studies have shown that experimental warming may promote plant growth by increasing photosynthesis in leaves while inhibiting plant growth at high temperatures (Hatfield et al., 2011). For example, Liu et al. (2020) showed that maize significantly increased P_n, but decreased total biomass at 31°C, mainly because its growth temperature was still at its optimal temperature and the increase in Rubisco activity due to warming while P_n and total biomass decreased at 37°C, probably due to the accumulation of potent reactive oxygen species (ROS) at high temperature (Chen et al., 2022). The interactive effects of temperature and elevated [CO_2] on plant growth are complex and tend to be multivariate (Liu et al., 2020; Yu et al., 2012; Duan et al., 2019a). For instance, Yu et al. (2012) found that elevated [CO_2] mitigated the negative effects of experimental warming (30°C) on tall fescue by reducing Gs (20%), Rd (7%). However, Liu et al. (2020) concluded that elevated [CO_2] could not alleviate P_n and total biomass of maize under experimental warming (31°C), while significantly enhanced plants P_n under high temperature stress (37°C). In the present study, the growth temperature of winter wheat was raised from 21 to 26°C, and plant biomass was barely affected by the experimental warming, which was directly supported by the slight variation in leaf photosynthesis. Interestingly, the significant decline in plant biomass of winter wheat due to *e*[CO_2] × warming implies that wheat may be more affected under future climate change with warming and elevated [CO_2] (Yu et al., 2012; Duan et al., 2019a; Wang et al., 2021). Our results showed that the decrease in plant photosynthesis (19.5%) was associated with the decrease in G_s (73%) and mesophyll cell area (12.6%) and the increase in C/N (10%), although the increase in WUE was due to a decrease in transpiration. Many studies found that elevated [CO_2] reduced soluble protein content and increased C/N of winter wheat, which is consistent with our results (Wang et al., 2013; Xu, 2015). And we observed that *e*[CO_2] × warming significantly increased R_d in winter wheat, which was mainly from TNC depletion. Overall, these results suggest that CO_2 fertilization effects can be reduced by warming, and therefore the risk of climate change to global wheat yields may be underestimated.

The interactive effect of water deficiency experimental warming and elevated [CO_2]

The interactive effect of drought and warming under ambient [CO_2] is more detrimental for plant growth than stress alone, which is consistent with the study of Yu et al. (2012). Previous studies have shown that elevated [CO_2] can alleviate water stress or heat stress (Jagadish et al., 2014; Xu, 2015; Duan et al., 2019a; Zheng et al., 2020), but our results show that the biomass and P_n of winter wheat further decreased and C/N increased under the combined effect of elevated [CO_2], experimental warming and water deficiency, implying that the combination of long-term water deficiency and experimental warming resulted in irreversible physiological damage in winter wheat. Yu et al. (2012) concluded that elevated [CO_2] further reduced tall fescue F_v : F_m (33%), V_{cmax} (8%), and J_{max} (13%) under the combined effect of experimental warming and water deficiency, suggesting that elevated [CO_2] may have played an additional negative effect under water × warming. Furthermore, in the current study, we observed that osmoregulation is reduced when plants are subjected to stress and nonstructural carbohydrates are not properly converted into structural carbohydrates for plant growth. (Zheng et al., 2014). However, elevated [CO_2] significantly increased amount of gene expression in *RbcL3* and *Rbcs2* under water × warming deficiency but slightly affected Rubisco activity of winter wheat, which may be due to the plants were subjected to irreversible combined stress caused by experimental warming and drought (Aranjuelo et al., 2005; Yu et al., 2012). Overall, plants adapt to stress by adjusting their growth, physiology, cellular and molecular activities (Ahuja et al., 2010). Since winter wheat lacks vernalization in the environmental growth chamber, we did not conduct further studies on the effect of *e*[CO_2] × water × warming on crop yield. It is worth noting that the combined effects of *e*[CO_2] × water × warming deficiency on growth, physiology, and molecular mechanisms of winter wheat may also be confounded with other factors such as nitrogen deposition, phosphorus deficiency and, ozone concentration. Therefore, to better predict the effects of climate change on wheat

production, further multifactorial experimental studies are necessary to fully understand the mechanisms and processes between plant growth and environmental changes.

Conclusions

We found that water deficiency and experimental warming decreased the leaf P_n and G_s, but increased the nonstructural carbohydrates, and thus reduced the biomass of winter wheat. In addition, elevated [CO_2] partially alleviated the stress in winter wheat at the molecular level but could not alleviate the irreversible damage to the plant caused by water deficiency × warming. Overall, our results suggest that the synergistic effects of elevated [CO_2], warming, and water deficiency may reduce plant biomass and leaf photosynthesis, thereby the global grain yield of winter wheat may be reduced under future climate change.

Data availability statement

The original contributions presented in the study are included in the article/supplementary material. Further inquiries can be directed to the corresponding authors.

Author contributions

ZC, LH, YZL, and YT designed the study. ZC, YL, LL, CC, and YW performed the experiment. ZC, YL, LL, CC, and WS analyzed the data. ZC, LH, YZL and YT wrote the initial manuscript. All authors contributed to the article and submitted and approved the submitted section.

Funding

This research was partially supported by the National Natural Science Foundation of China (32071608, 32001130), the Natural Science Foundation of Hebei Province (E2021402031, C2021402011, D2021402044), and the Central Guidance on Local Science and Technology Development Funding of Hebei Province (226Z6401G).

Conflict of interest

The authors declare that the research was conducted in the absence of any commercial or financial relationships that could be construed as a potential conflict of interest.

Publisher's note

References

Abebe, A., Pathak, H., Singth, S. D., Bhatia, R. C., and Kumar, V. (2016). Growth, yield and quality of maize with elevated atmospheric carbon dioxide and temperature in north–west India. *Agr. Ecosyst. Environ.* 218, 66–72. doi: 10.1016/j.agee.2015.11.014

Ahuja, I., de Vos, R. C., Bones, A. M., and Hall, R. D. (2010). Plant molecular stress responses face climate change. *Trends Plant Sci.* 15, 664–674. doi: 10.1016/j.tplants.2010.08.002

Ainsworth, E. A., and Long, S. P. (2020). 30 years of free-air carbon dioxide enrichment (FACE): What have we learned about future crop productivity and its potential for adaptation? *Glob. Change Biol.* 27, 27–49. doi: 10.1111/gcb.15375

Aranjuelo, I., Cabrera-Bosquet, L., Morcuende, R., Avice, J. C., Nogués, S., Araus, J. L., et al. (2011). Does ear C sink strength contribute to overcoming photosynthetic acclimation of wheat plants exposed to elevated CO_2? *J. Exp. Bot.* 62, 3957–3969. doi: 10.1093/jxb/err095

Aranjuelo, I., Perez, P., Hernandez, L., Irigoyen, J. J., Zita, G., Martinez-Carrasco, R., et al. (2005). The response of nodulated alfalfa to water supply, temperature and elevated CO_2: Photosynthetic downregulation. *Physiol. Plant* 123, 348–358. doi: 10.1111/j.1399-3054.2005.00459.x

Arndal, M. F., Schmidt, I. K., Kongstad, J., Beier, C., and Michelsen, A. (2014). Root growth and N dynamics in response to multi-year experimental warming, summer drought and elevated CO_2 in a mixed heath land-grass ecosystem. *Funct. Plant Biol.* 41, 1–10. doi: 10.1071/FP13117

Barlow, K. M., Christy, B. P., O'Leary, G. J., Riffkin, P. A., and Nuttall, J. G. (2015). Simulating the impact of extreme heat and frost events on wheat crop production: a review. *Field Crops Res.* 171, 109–119. doi: 10.1016/j.fcr.2014.11.010

Bencze, S., Bamberger, Z., Janda, T., Balla, K., Varga, B., Bedő, Z., et al. (2014). Physiological response of wheat varieties to elevated atmospheric CO_2 and low water supply levels. *Photosynthetica* 52, 71–82. doi: 10.1007/s11099-014-0008-y

Chen, J. H., Tang, M., Jin, X. Q., Li, H., Chen, L. S., Wang, Q. L., et al. (2022). Regulation of Calvin–Benson cycle enzymes under high temperature stress. *aBIOTECH* 3 (1), 1–13. doi: 10.1007/s42994-022-00068-3

Chun, J. A., Wang, Q. G., Timlin, D., Fleisher, D., and Reddy, V. R. (2011). Effect of elevated carbon dioxide and water stress on gas exchange and water use efficiency in corn. *Agric. For. Meteorol.* 151, 378–384. doi: 10.1016/j.agrformet.2010.11.015

Drake, B. G., Gonzàlez-Meler, M. A., and Long, S. P. (1997). More efficient plants: A consequence of rising atmospheric CO_2? *Annu. Rev. Plant Biol.* 48, 609–639. doi: 10.1146/annurev.arplant.48.1.609

Duan, H. L., Li, Y. Y., Xu, Y., Zhou, S. X., Liu, J., Tissue, D., et al. (2019b). Contrasting drought sensitivity and post-drought resilience among three co-occurring tree species in subtropical China. *Agric. For. Meteorol.* 272-273, 55–68. doi: 10.1016/j.agrformet.2019.03.024

Duan, H. L., Ontedhu, J., Milham, P., Lewis, J. D., and Tissue, D. T. (2019a). Effects of elevated carbon dioxide and elevated temperature on morphological, physiological and anatomical responses of Eucalyptus tereticornis along a soil phosphorus gradient. *Three Physiol.* 39 (11), 1821–1837. doi: 10.1093/treephys/tpz094

Fan, X. D., Cao, X., Zhou, H. R., Dong, W., He, C. L., Xu, M., et al. (2020). Carbon dioxide fertilization effect on plant growth under soil water stress associates with changes in stomatal traits, leaf photosynthesis, and foliar nitrogen of bell pepper (*Capsicum annuum* L.). *Environ. Exp. Bot.* 179, 104203. doi: 10.1016/j.envexpbot.2020.104203

Farooq, M., Bramley, H., Palta, J. A., and Siddique, K. H. M. (2011). Heat stress in wheat during reproductive and grain–filling phases. *Crit. Rev. Plant Sci.* 30 (6), 491–507. doi: 10.1080/07352689.2011.615687

Flexas, J., Bota, J., Loreto, F., Cornic, G., and Sharkey, T. D. (2004). Diffusive and metabolic limitations to photosynthesis under drought and salinity in C_3 plants. *Plant Biol.* 6 (3), 269–279. doi: 10.1055/s-2004-820867

Hao, L. H., Guo, L. L., Li, R. Q., Cheng, Y., Huang, L., Zhou, H. R., et al (2019). Responses of photosynthesis to high temperature stress associated with changes in leaf structure and biochemistry of blueberry (Vaccinium corymbosum L.). *Sci. Hortic -AMSTERDAM* 246, 251–264. doi: 10.1016/j.scienta.2018.11.007

Hatfield, J. L., Boote, K. J., Kimball, B. A., Ziska, L. H., Izaurralde, R. C., Ort, D., et al. (2011). Climate impacts on agriculture: Implications for crop production. *Agron. J.* 103 (2), 371–381. doi: 10.2134/agronj2010.0304

Hedrix, D. L., Mauney, J. R., and Kimball, B. A. (1994). Influence of elevated CO_2 and mild water stress on nonstructural carbohydrates in field-grown cotton tissues. *Agric. For. Meteor.* 70, 153–162. doi: 10.1016/0168-1923(94)90054-X

Högy, P., Brunnbauer, M., Koehler, P., Schwadorf, K., Breuer, J., Franzaring, J., et al. (2013). Grain quality characteristics of spring wheat (Triticum aestivum) as affected by free-air CO_2 enrichment. *Environ. Exp. Bot.* 88, 11–18. doi: 10.1016/j.envexpbot.2011.12.007

Hou, L. P., Shang, M. Y., Chen, Y., Zhang, J., Xu, X. Y., Song, H. X., et al. (2021). Physiological and molecular mechanisms of elevated CO_2 in promoting the growth of pak choi (*Brassica rapa ssp. chinensis*). *Sci. Hortic.* 288, 110318. doi: 10.1016/J.SCIENTA.2021.110318

IPCC (2021). "Summary for policymakers," in *Climate Change 2021: The Physical Science Basis. Contribution of Working Group I to the Sixth Assessment Report of the Intergovernmental Panel on Climate Change*. Eds. V. Masson-Delmotte, P. Zhai, A. Pirani, S. L. Connors, C. Péan, S. Berger, N. Caud, Y. Chen, L. Goldfarb, M. I. Gomis, M. Huang, K. Leitzell, E. Lonnoy, J. B. R. Matthews, T. K. Maycock, T. Waterfield, O. Yelekçi, R. Yu and B. Zhou (Cambridge, United Kingdom and New York, NY, USA: Cambridge University Press), 1–30.

Jagadish, K. S. V., Kadam, N. N., Xiao, G., Melgar, R. J., Bahuguna, R. N., Quinones, C., et al. (2014). Agronomic and physiological responses to high temperature, drought, and elevated CO_2 interactions in cereals. *Adv. Agron.* 127, 111–156. doi: 10.1016/B978-0-12-800131-8.00003-0

Jiang, Y. P., Cheng, F., Zhou, Y. H., Xia, X. J., Mao, W. H., Shi, K., et al. (2012). Cellular glutathione redox homeostasis plays an important role in the brassinosteroid-induced increase in CO_2 assimilation in Cucumis sativus. *New Phytol.* 194, 932–943. doi: 10.1111/j.1469-8137.2012.04111.x

Jin, Z., Zhuang, Q., Wang, J., Archontoulis, S. V., Zobel, Z., and Kotamarthi, V. R. (2017). The combined and separate impacts of climate extremes on the current and future US rainfed maize and soybean production under elevated CO_2. *Glob. Chang. Biol.* 23, 2687–2704. doi: 10.1111/gcb.13617

Keshav, D., Vicki, L. K., William, C. P., and Norman, P. A. H. (2014). Enhancement of photosynthetic performance, water use efficiency and grain yield during long-term growth under elevated CO_2 in wheat and rye is growth temperature and cultivar dependent. *Environ. Exp. Bot.* 106, 207–220. doi: 10.1016/j.envexpbot.2013.11.015

Kirkham, M. B. (2011). Elevated carbon dioxide: Impact on soil and plant water relations. *Exp. Agr.* 48 (1), 151–151. doi: 10.1017/S0014479711000986

Kurek, I., Chang, T. K., Bertain, S. M., Madrigal, A., Liu, L., Lassner, M. W., et al. (2007). Enhanced thermostability of Arabidopsis Rubisco activase improves photosynthesis and growth rates under moderate heat stress. *Plant Cell.* 19, 3230–3241. doi: 10.1105/TPC.107.054171

Li, F., Guo, D., Gao, X., and Zhao, X. (2021). Water deficiency modulates the CO_2 fertilization effect on plant gas exchange and leaf-level water use efficiency: A meta-analysis. *Front. Plant Sci.* 12. doi: 10.3389/fpls.2021.775477

Li, F. S., Kang, S. Z., and Zhang, J. H. (2004). Interactive effects of elevated CO_2, nitrogen and drought on leaf area, stomatal conductance, and evapotranspiration of wheat. *Agric. Water Manage.* 67 (3), 221–233. doi: 10.1016/j.agwat.2004.01.005

Liu, L., Hao, L. H., Li, F., Guo, L. L., Zhang, X. X., He, C. L., et al (2004). Effects of CO2 concentration and temperature on leaf photosynthesis and water use efficiency in maize. *Transactions of the CSAE.* 2020, 36 (5), 122–129. doi: 10.11975/j.issn.1002-6819.2020.05.014

Livak, K. J., and Schmittgen, T. D. (2001). Analysis of relative gene expression data using real-time quantitative PCR and the 2(-Dwlta Delta C (T)) method. *Methods* 25 (4), 402–408. doi: 10.1006/meth.2001.1262

Muluneh, A. (2020). Impact of climate change on soil water balance, maize production, and potential adaptation measures in the Rift Valley drylands of Ethiopia. *J. Arid. Environ.* 179, 104195. doi: 10.1016/j.jaridenv.2020.104195

Niaz, A., Syed, S. Z., and Shahid, M. (2020). Alternative routes to improving photosynthesis in field crops. *Trends Plant Sci.* 25 (10), 958–960. doi: 10.1016/j.tplants.2020.07.003

Parry, M. A. J., Andralojc, P. J., Mitchell, R. A. C., Madgwick, P. J., and Keys, A. J. (2003). Manipulation of Rubisco: the amount, activity, function and regulation. *J. Exp. Bot.* 54 (386), 1321–1333. doi: 10.1093/JXB/ERG141

Mirwais, M. Q., Leonid, V. K., and and David, M. R. (2006). Growth and physiological responses of canola (*Brassica napus*) to three components of global climate change: Temperature, carbon dioxide and drought. *Physiol. Plant* 128 (4), 710–721. doi: 10.1111/j.1399-3054.2006.00804.x

Sage, T. L., and Williams, E. G. (1995). Structure, ultrastructure, and histochemistry of the pollen tube pathway in the milkweed Asclepias exaltata L. *Sex Plant Reprod.* 8 (5), 257–265. doi: 10.1007/BF00229381

Salvucci, M. E., and Crafts-Brandner, S. J. (2004). Inhibition of photosynthesis by heat stress: The activation state of Rubisco as a limiting factor in photosynthesis. *Physiol. Plant* 120 (2), 179–186. doi: 10.1111/j.0031-9317.2004.0175.x

Sheen, J. (1990). Metabolic repression of transcription in higher plants. *Plant Cell.* 2 (10), 1027–1038. doi: 10.2307/3869242

Tao, F. L., Yokozawa, M., Xu, Y. L., Hayashi, Y., and Zhang, Z. (2006). Climate changes and trends in phenology and yields of field crops in China 1981–2000. *Agric. For. Meteorol.* 138 (1), 82–92. doi: 10.1016/j.agrformet.2006.03.014

Wall, G. W., Garcia, R. L., Kimball, B. A., Hunsaker, D. J., Pinter, J. P. J., Long, S. P., et al. (2006). Interactive effects of elevated carbon dioxide and drought on wheat. *Agron. J.* 98 (2), 354–381. doi: 10.2134/agronj2004.0089

Wang, L., Feng, Z. Z., and Schjoerring, J. K. (2013). Effects of elevated atmospheric CO_2 on physiology and yield of wheat (*Triticum aestivum* L.): a meta-analytic test of current hypotheses. *Agric. Ecosyst. Environ.* 178, 57–63. doi: 10.1016/j.agee.2013.06.013

Wang, F., Guo, B. B., Sun, Z. G., Yin, F., Liu, L., Jiao, N. Y., et al. (2021). Effects of elevated temperature and CO_2 concentration on growth and yield of maize under intercropping with peanut. *Acta Agronomica Sinica.* 47 (11), 2220–2231. doi: 10.3724/SP.J.1006.2021.03018

Wang, C. Y., Zhang, Y. J., and Zhang, J. Q. (2016). Risk assessment of main meteorological disasters of winter wheat in North China. *Trans. Chin. Soc. Agric. Engineering.* 32 (s1), 203–213. doi: 10.11975/j.issn.1002-6819.2016.z1.029

Wang, H., Zhou, G. S., Jiang, Y. L., Shi, Y. H., and Xu, Z. Z. (2017). Photosynthetic acclimation and leaf traits of Stipa bungeana in response to elevated CO_2 under five different water conditions. *Photosynthetica* 55, 164–175. doi: 10.1007/s11099-016-0239-1

Wei, Z., Du, T., Li, X., Fang, L., and Liu, F. (2018). Interactive effects of CO_2 concentration elevation and nitrogen fertilization on water and nitrogen use efficiency of tomato grown under reduced irrigation regimes. *Agric. Water Manage.* 202, 174–182. doi: 10.1016/j.agwat.2018.02.027

Wong, S. C. (1990). Elevated atmospheric partial pressure of CO_2 and plant growth: II. Non-structural carbohydrate content in cotton plants and its effect on growth parameters. *Photosynth. Res.* 23 (2), 171–180. doi: 10.1007/BF00035008

Xu, M. (2015). The optimal atmospheric CO_2 concentration for the growth of winter wheat (*Triticum aestivum*). *Plant Physiol.* 184, 89–97. doi: 10.1016/j.jplph.2015.07.003

Yu, J. J., Chen, L. H., Xu, M., and Huang, B. R. (2012). Effects of elevated CO_2 on physiological responses of tall fescue to elevated temperature drought stress, and the combined stresses. *Crop Sci.* 52, 1848–1858. doi: 10.2135/cropsci2012.01.0030

Zhang, T., Cao, Y., Chen, Y. M., and Liu, G. B. (2015). Non-structural carbohydrate dynamics in Robinia pseudoacacia saplings under three levels of continuous drought stress. *Trees* 29 (6), 1837–1849. doi: 10.1007/s00468-015-1265-5

Zhang, D. S., Li, A., Lam, S. K., Li, P., Zong, Y. Z., Gao, Z. Q., et al. (2020). Increased carbon uptake under elevated CO_2 concentration enhances water-use efficiency of C_4 broomcorn millet under drought. *Agr. Water Manage.* 245, 106631. doi: 10.1016/j.agwat.2020.106631

Zhao, C., Liu, B., Piao, S. L., Wang, X. H., Lobell, D. B., Huang, Y., et al. (2017). Temperature increase reduces global yields of major crops in four independent estimates. *Proc. Natl. Acad. Sci. U.S.A.* 114 (35), 9326–9331. doi: 10.1073/pnas.1701762114

Zheng, Y. P., He, C. L., Guo, L. L., Hao, L. H., Cheng, D. J., Li, F., et al. (2020). Soil water status triggers CO_2 fertilization effect on the growth of winter wheat (*Triticum aestivum*). *Agric. For. Meteorol.* 291, 108097. doi: 10.1016/j.agrformet.2020.108097

Zheng, Y. P., Li, F., Hao, L. H., Shedayi, A. A., Guo, L. L., Ma, C., et al. (2018). The optimal CO_2 concentrations for the growth of three perennial grass species. *BMC Plant Biol.* 18 (1), 27. doi: 10.1186/s12870-018-1243-3

Zheng, Y. P., Wang, H. X., Lou, X., Yang, Q. P., and Xu, M. (2014). Changes of non-structural carbohydrates and its impact factors in trees: A review. *Chin. J. Appl. Ecology.* 25 (4), 1188–1196. doi: 10.13287/j.1001-9332.2014.0110

Zong, Y., and Shangguan, Z. (2016). Increased sink capacity enhances C and N assimilation under drought and elevated CO_2 conditions in maize. *J. Integr. Agr.* 15 (12), 2775–2785. doi: 10.1016/S2095-3119(16)61428-4

frontiers | Frontiers in Forests and Global Change

TYPE Original Research
PUBLISHED 01 September 2023
DOI 10.3389/ffgc.2023.1218005

OPEN ACCESS

EDITED BY
Heidi Renninger,
Mississippi State University, United States

REVIEWED BY
Xiaodong Niu,
Chinese Academy of Forestry, China
Ben Wang,
Huazhong Agricultural University, China

*CORRESPONDENCE
Peng Liu
✉ pengliu0312@bjfu.edu.cn

RECEIVED 06 May 2023
ACCEPTED 08 August 2023
PUBLISHED 01 September 2023

CITATION
Yang R, Liu P, Tian Y, Ma J, Bai Y, Li C, Huang S, Mu Y, Hayat M, Iqbal S, Yu H, Zhang F and Ma H (2023) Interannual variation in evapotranspiration in an urban forest reserve with respect to drought.
Front. For. Glob. Change 6:1218005.
doi: 10.3389/ffgc.2023.1218005

Interannual variation in evapotranspiration in an urban forest reserve with respect to drought

Ruizhi Yang[1,2], Peng Liu[1,2]*, Yun Tian[1,2], Jingyong Ma[1,2], Yujie Bai[1,2], Cheng Li[1,2], Songyu Huang[1,2], Yanmei Mu[1,2], Muhammad Hayat[1,2], Sundas Iqbal[1,2], Haiqun Yu[3], Feng Zhang[3] and Hong Ma[3]

[1]School of Soil and Water Conservation, Beijing Forestry University, Beijing, China, [2]Beijing Engineering Research Center of Soil and Water Conservation, Beijing Forestry University, Beijing, China, [3]Beijing Forestry Carbon Administration, Beijing, China

Introduction: A warming global climate is expected to perturb the hydrological cycle, resulting in deviations in both frequency and duration of drought and thus being hypothesized to lead to interannual variation in evapotranspiration (ET). Interannual variation in ET in urban forest ecosystems in response to drought remains poorly understood.

Methods: Here, ET in an urban forest reserve in the megalopolis of Beijing was investigated using eddy-covariance measurements collected over six consecutive years (2012–2017).

Results: The mean annual cumulative ET was 462 ± 83mm (±first standard deviation), with a coefficient of variation of 18%. Interannual variation in both annual and monthly ET was shown to be largely controlled by canopy conductance *(gs)*, affected by environmental factors. The main factors affecting interannual variation in monthly ET varied seasonally, namely, soil volumetric water content (VWC) and normalized difference vegetation index (NDVI) in spring, precipitation and soil temperature in summer, and VWC and net radiation (Rn) in autumn. Interannual variation in annual ET was driven largely by spring and mid-summer droughts induced by insufficient precipitation during the non-growing and mid-growing seasons, respectively. Spring drought reduced annual ET by restricting leafing out, shortening growing season length (GSL), and reducing the normalized difference vegetation index (NDVI). The summer drought reduced annual ET by reducing stomatal conductance.

Discussion and conclusion: Results from this study point to the importance of precipitation timing and volume and the soil moisture carry-over effect in controlling interannual variation in ecosystem ET. Irrigation during the early spring and mid-summer is viewed as a practical management measure for sustaining growth and better ecosystem services in urban forests in Northern China.

KEYWORDS

drought, evapotranspiration, interannual variability, precipitation, urban forests

1. Introduction

Global climate models project an increase in climatic variability, including more frequent extreme events in future (e.g., drought, convective and synoptic storms, and heat waves; IPCC, 2014). The devastating effect of climate change is becoming increasingly apparent in Northeastern China (Zhai et al., 2010). An increase in both the severity and frequency of drought is expected to affect the hydrological cycle at regional-to-local scales. These

changes may lead to disruptions in the energy balance and ecosystem structure and functioning by, in part, influencing the plant-mediated component of evapotranspiration (ET; Liu et al., 2018). Evapotranspiration, as the second largest constituent of the global hydrological cycle (Liu et al., 1998), shares in the energy and nutrient exchange in ecosystems as well as other important ecological processes (Miao et al., 2009). As a phase change of water, the transformation of liquid water to water vapor consumes energy. This process on large spatial scales can benefit cities by restricting the level of warming attained (Jacobs et al., 2015). Urban forest ecosystems in China, distinguished by their distinct vegetation composition and structures (i.e., from near natural or plantation), have been expanding during the past decades because of the rapid expansion of urban spaces (Jim and Chen, 2009; Chen et al., 2019). Through their reuse, the amount of land use change from agricultural land or forest to urbanized land can be reduced, and the cooling effect of urban forest ET has been becoming critical (Ordónez and Duinker, 2014; Fan et al., 2019). However, many elements of water vapor dynamics in urban forest plantations remain inadequate as they concern the quantitative understanding of interannual variation (IAV) in forest plantations, especially in relation to urban forests. Therefore, understanding the role of environmental drivers in ET is essential to characterize the ecosystem processes and services (Hallegatte and Corfee-Morlot, 2011) as well as for the proper assessment of regional and global water budgets in a changing climate.

Evapotranspiration is still arguably the most uncertain eco-hydrological variable in (i) the development of ecosystem water budgets (Sun et al., 2016) and (ii) the understanding of ecological impacts attributed to extreme climatic events (Vose et al., 2016) as well as the effects of urbanization (Hao et al., 2015). Evapotranspiration is controlled by numerous abiotic and biotic factors, including solar radiation, air and soil temperatures, soil water content, water vapor pressure deficit, leaf area index (LAI), and leaf-level stomatal conductance, which are all predicted to vary over a range of spatiotemporal scales. Earlier studies have reported that ET in forest ecosystems has considerable seasonal IAV. Intra-annual variation in ET and its controlling mechanisms have been documented for many ecosystems around the world (Chen et al., 2018). However, the comprehension of IAV in ET and its controlling mechanisms is currently inadequate (Xu et al., 2014), particularly in urban forests. Generally, very little is known about how the ecosystem-level ET of forest plantations responds annually to climate-induced drought.

Some studies have found that IAV in ET was mostly small relative to the year-to-year variation in annual rainfall. Furthermore, IAV failed to be explained by any single hydrometeorological parameter neither over the summer (May–August) nor annually (Gielen et al., 2010; Launiainen, 2010; Kume et al., 2011; Tsuruta et al., 2016). Others have found that IAV in ET is significant, which could not be ignored. Several climatic factors have been identified as drivers of ET, such as solar energy, temperature, and precipitation, through their effect on plant phenology, growing season length, or canopy structure (Tang et al., 2021; Xiang et al., 2023). Drought-induced soil moisture deficits have been reported to be the most important controlling factor of IAV in the ET of water-limited ecosystems (Wilson and Baldocchi, 2000; Barr et al., 2007; Thomas et al., 2009; Zha et al., 2010; Xue et al., 2012; Saitoh et al., 2013; Vadeboncoeur et al., 2018) largely because it triggers stomatal closure, suppression in leaf development, and changes in phenology in drought-affected plants. Given more extreme changes in the climate system, attaining a mechanistic understanding of the long-term dynamics of ecosystem ET is fundamental to acquiring an accurate prognostication of future water cycling in urban plantations and addressing the consequences of management decisions on the fate of large urban forests.

It is hypothesized that precipitation amount and seasonal distribution coincidental with drought are the most important drivers of IAV in ET. To test this hypothesis, we analyzed a 6-year record (2012–2017) of continuous ET data collected over an urban forest reserve in Beijing, China. The measurement period covered events of extremely low-to-high levels of precipitation as compared to the past 50 years from 1961 to 2010. The specific objectives of the research were to detect the major environmental variables affecting ET annually and to examine the impacts of drought on IAV in ET.

2. Materials and methods

2.1. Site description

The study site is located in Beijing Olympic Forest Park (40.02°N, 116.38°E), Megalopolis of Beijing, China. It is the largest urban forest park in Asia, with an area of 680 ha and vegetation cover of ∼96%. The forest reserve is located in the middle of the northeastern section of the park, an area committed to ecological conservation and reclamation, with no open water or roads in the area. Tourists are restricted from entering our research plot in order to minimize human disturbance. The terrain is flat and uniform. The soil is mainly of the fluvo-aquic type, with soil porosity of 40.3%, pH of 7.8, and an estimated field capacity and permanent wilting point of 26 and 10%, respectively. The site is characterized by a temperate continental monsoon climate. The 50-year annual mean temperature and annual precipitation are 12.5°C and 592 mm, respectively. The seasonal distribution of precipitation is highly uneven, with 80% of annual rainfall falling from June to August. The plant species in the forest reserve are endemic to the North China Plain. Tree species present include *Sophora japonica* L., *Fraxinus chinensis*, *Pinus tabuliformis*, and *Platycladus orientalis*. The understory consists mainly of *Iris tectorum* and *Dianthus chinensis*. The tree stand density in 2015 is recorded to be ∼210 stems ha^{-1}, with a mean tree height of 7.7 m and a mean diameter at breast height of 20 cm. The cover ratio of trees-to-shrubs is ∼7:3. Shrubs include *Prunus davidiana*, *Amygdalus triloba*, *Swida alba*, and *Syzygium aromaticum*, with a mean height of 2.8 m. All trees in the reserve have shallow roots with a depth of ∼0.08–0.4 m.

2.2. Flux, meteorological, and vegetation measurements

Water vapor fluxes were measured at 12 m above the ground surface with an eddy-covariance (EC) system, consisting of a three-dimensional sonic anemometer [CSAT3A; Campbell Scientific, Inc., Logan, UT, USA (CSI)] and a closed-path infrared gas analyzer (model EC155; CSI), which was calibrated once a month. The EC flux measurements began in April 2011. Continuous high-frequency data (at 10 Hz) were collected and processed in the calculation of 30 min fluxes. Fluxes were subsequently recorded on a datalogger (CR3000; CSI).

Hydrometeorological variables, including air and soil temperatures (T_a and T_s, °C), relative humidity (RH, %), net radiation (R_n, W m^{-2}), precipitation (P, mm), and soil volumetric water content (VWC, %) were measured simultaneously. Air temperatures, relative humidity, and net radiation were measured at 12 m above the ground surface. Precipitation was measured within an opening (unvegetated) area near the EC tower. Soil volumetric water content and T_s were measured at a 10 cm depth at five locations around the tower. Data for all hydrometeorological variables were stored on a datalogger (CR3000; CSI). Further details on instrumentation and sampling procedures can be found in Xie et al. (2016) study.

To characterize land cover and temporal changes in the canopy structure in response to climate variations, we used time series processed images (i.e., image-pixel containing the EC tower) of normalized difference vegetation index (NDVI; MOD13Q1 products) at 250 m resolution downloaded from the Earth Observing System Data Gateway. The images were downloaded as 16-day composites covering the entire flux-measurement period from 2012 to 2017.

2.3. Data processing and analysis

Post-processing was performed using the EddyPro 4.0.0 software (LI-COR Inc., USA), including spike removal, double coordinate rotation, time delay corrections, frequency response corrections, detrending (block averaging), and flux computation (Burba, 2013). Half-hourly turbulent fluxes and meteorological data were carefully controlled for quality and spurious data points. Outliers were removed following the approach described by Papale et al. (2006). Data gaps were filled using the standard method used by the Fluxnet Canada Research Network (Amiro et al., 2006). Three diagnostic variables, including the surface conductance (g_s), the Priestley–Taylor coefficient (α), and the decoupling coefficient (Ω), were used to interpret the relative importance of biophysical control on ET.

Variable g_s of a dry surface mostly reflect the stomatal control of plants on ET. The α-coefficient in the Priestley–Taylor model can be viewed as a normalization of ET (Blanken et al., 1997), which provides a comparison of measured ET to climatological expectations. Usually, $\alpha \geq 1$ occurs in mesic ecosystems, indicating sufficient water supply so that latent heat fluxes are limited by available energy. In contrast, $\alpha < 1$ occurs in semiarid and arid ecosystems, where latent heat fluxes are limited by the availability of soil water (Jia et al., 2016). Ω indicates the degree of canopy decoupling from the bulk air, with Ω varying from 0 (completely coupling) to 1 (decoupling), as the biological control on ET becomes weaker as Ω approaches 1.

We estimated g_s (mm s^{-1}) by inverting the Penman–Monteith equation (Monteith and Unsworth, 2007), such that

$$g_s = \frac{\gamma \lambda E g_a}{\Delta (R_n - G) + \rho C_p VPD g_a - \lambda E (\Delta + \gamma)} \quad (1)$$

where γ is the psychrometric constant (kPa K^{-1}), Δ is the rate of change of saturation water vapor pressure as a function of T_a (kPa K^{-1}), R_n is the net radiation (W m^{-2}), λE is the latent heat flux (W m^{-2}), G is the soil heat flux (W m^{-2}), ρ is the air density (kg m^{-3}), C_p is the specific heat of air (J kg^{-1} K^{-1}), and VPD is the water vapor pressure deficit (kPa).

The aerodynamic conductance (g_a, in mm s^{-1}; Monteith and Unsworth, 2007) was calculated as

$$g_a = \left(\frac{u}{u_*^2} + 6.2 u_*^{-0.67}\right)^{-1} \quad (2)$$

where u_* and u are the friction velocity and wind speed, respectively, both given in m s^{-1}. The Priestley–Taylor coefficient (α; Priestley and Taylor, 1972) was calculated from

$$\alpha = \frac{\Delta + \gamma}{\Delta} \frac{\lambda E}{(R_n - G)}. \quad (3)$$

Ω is calculated as (Jarvis and McNaughton, 1986)

$$\Omega = \frac{\Delta + \gamma}{\Delta + \gamma \left(1 + \frac{g_a}{g_s}\right)} \quad (4)$$

α, Ω, and g_s were calculated based on non-gap-filled 30 min data from daytime hours (when PAR > 5 μmol m^{-2} s^{-1}), during periods when the soils were unfrozen, i.e., when $T_s > 0.5$°C and for days with no rain. The α, Ω, and g_s values were aggregated to daily means and longer periods.

2.4. Growing season and statistical analysis

Growing season length (GSL) was determined from the daily mean gross ecosystem production time series, following procedures reported by Zha et al. (2009). Growing seasons spanned DOY (day of the year) 96–303, 104–298, 98–302, 108–302, 97–302, and 94–297 for 2012–2017, respectively. Normally, tree leaf expansion and coloration stages commence in April and October, respectively. According to the seasonal variation in NDVI, we defined March to June as the leaf expansion period, July to September as the leaf-expanded period, and October to November as the leaf coloration period. We defined the period from the previous November to March of the following year as the non-growing season. Following Xie et al. (2016), we defined drought as the occurrence of days when VWC was <12.5% from March to November, March through May

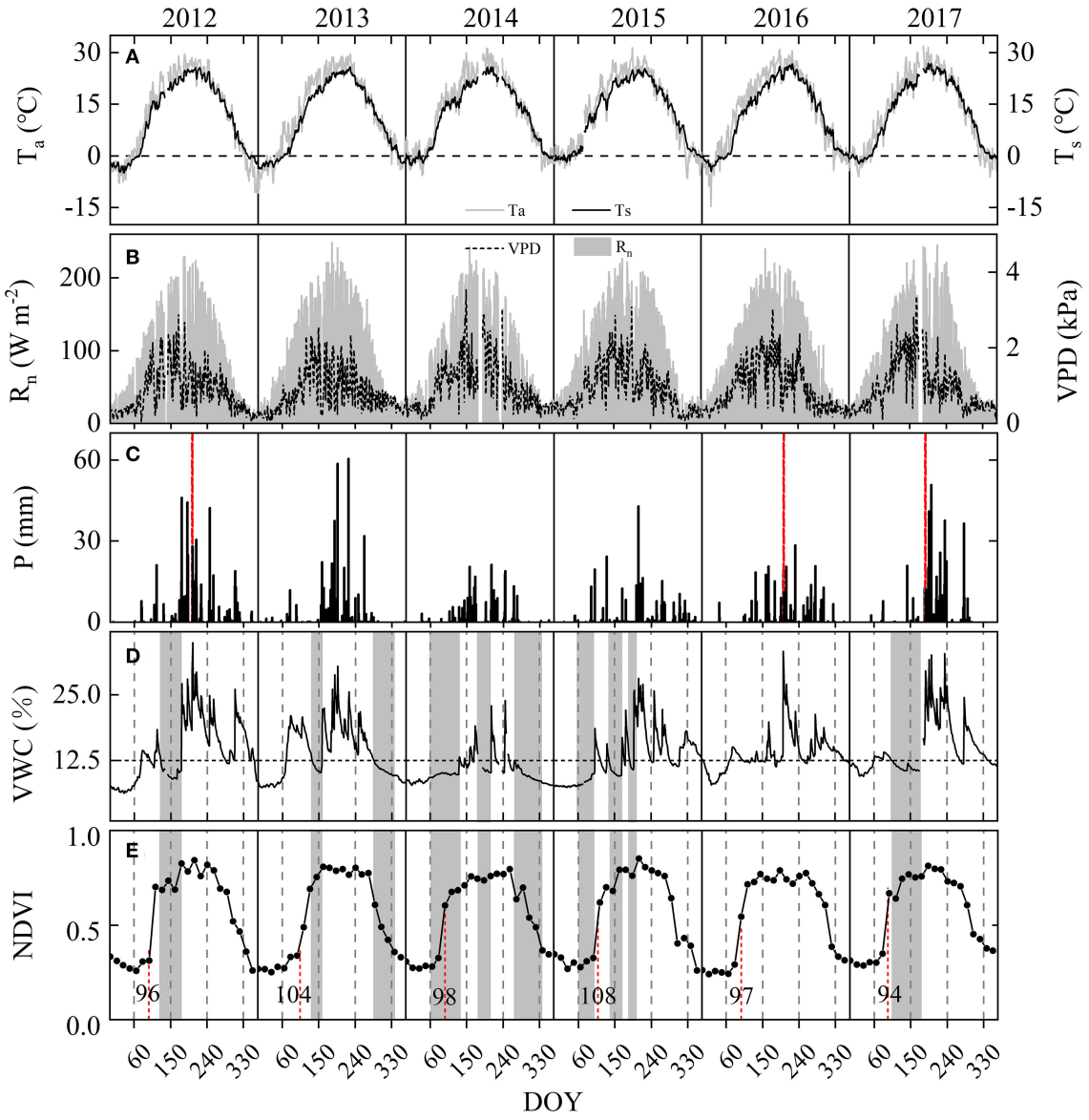

FIGURE 1
Daily mean. **(A)** Air temperature (T_a) and soil temperature (T_s), **(B)** net radiation (R_n) and vapor pressure deficit (VPD), **(C)** daily precipitation (P), **(D)** soil volumetric water content (VWC), and **(E)** normalized difference vegetation index (NDVI) from 2012 to 2017. All data are non-gap-filled data. The red dashed vertical line in plot **(C)** indicates intensive rainfall events and in plot **(E)** indicates the onset of the growing season. Gray-shaded bands in plots **(D, E)** indicate periods of drought (i.e., VWC < 12.5% during spring to autumn).

as spring, June through August as summer, and September through November as autumn.

Linear regression was used to examine the relationships between ET and the target biophysical variables (i.e., R_n, T_s, VWC, P, NDVI, and g_s) at various timescales. To evaluate the contribution of different phenological phases to the variability in annual ET, the difference between the standard deviation of cumulative ET from a given month or season and its preceding one (DstDev) was calculated to quantify the contribution of each month or season to the observed interannual variability of the ET. All statistical analyses were performed in Matlab (The MathWorks, Natick, MA, USA).

3. Result

3.1. Environmental factors

Variation in major environmental factors during the 6 years is shown in Figures 1–3. Compared to the annual analysis, some factors (i.e., monthly R_n, monthly VPD, monthly T_a, monthly T_s, and monthly NDVI) were much more variable during the years 2012–2017 (Figure 2; Tables 1, 2). Interannual variation of monthly mean $R_n$and monthly mean VPD were highest in June; monthly mean T_s and NDVI were non-negligible in April (Figure 2). By contrast, interannual variation of annual mean T_a, T_s, R_n, VPD,

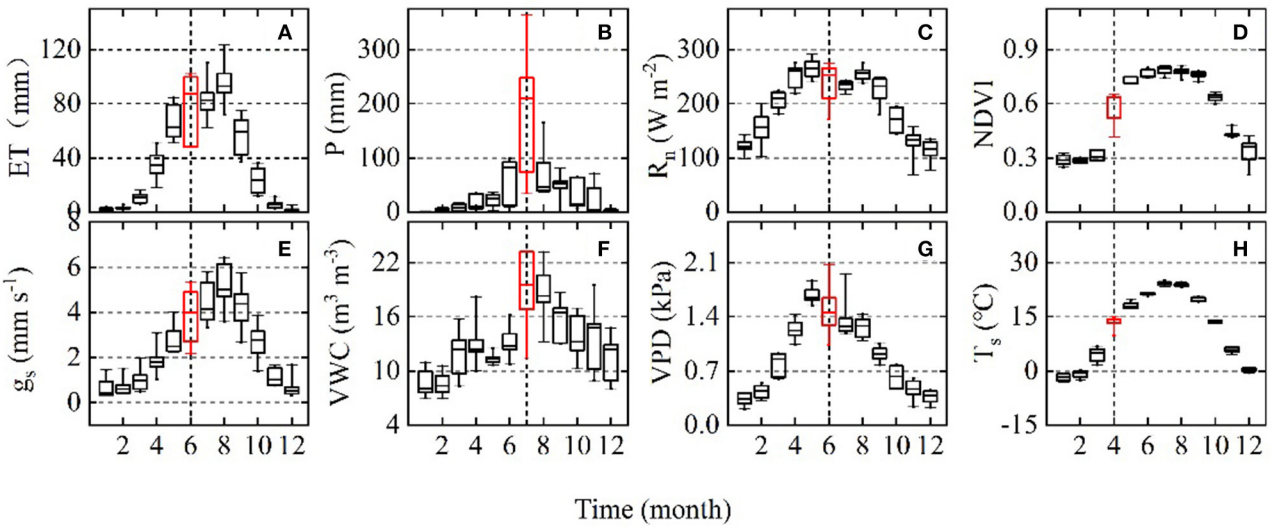

FIGURE 2
Box plot showing the interannual variation in **(A)** monthly evapotranspiration (ET), **(B)** main explanatory variables precipitation *(P)*, **(C)** net radiation *(Rn)*, **(D)** normalized difference vegetation index (NDVI), **(E)** mean daytime surface conductance *(gs)*, **(F)** soil volumetric water content (VWC), **(G)** vapor pressure deficit (VPD), and **(H)** soil temperature *(T_s)* over the 6-year period (2012-2017). The red marks the part with the most variation.

and NDVI were imperceptible (Table 1). Annual mean T_a above the canopy increased from 2012 to 2015 and then decreased slightly over the remaining 3 years (2015–2017). The years after 2014 were all warmer than the 50-year mean of 12.5°C (1961–2010; Table 1), showing a warming climate.

Precipitation regime and soil volumetric water content (VWC) varied significantly both seasonally and annually at the site (Figures 1C, D, 2B, F; Table 1). The VWC at 10 cm depth varied with soil thaw in early spring and *P* amount (Figures 1C, D), increasing abruptly in March or June with the start of the rainy season and peaking in the middle of the growing season. Interannual variation in monthly *P* and monthly mean VWC were highest in July (Figures 2B, F). The mean annual total *P* was 473.52 ± 168.54 mm, with a CV of 35.6% (Table 1), and the lowest and highest annual mean were 270.9 and 738.3 mm in 2014 and 2012, respectively. The wet year 2012 had many irregular and intensive precipitation events, with 24% of the annual total *P* falling during a single summer rainfall event (i.e., 176 mm on DOY 203, dashed vertical line in Figure 1C). The year 2016 had one intensive rainfall event with 172.3 mm on DOY 202 (dashed vertical line in Figure 1C), which accounted for approximately 31% of the annual total *P*. In contrast, annual *P* in other years was all below the 50-year mean, especially the dry years 2014 and 2015 with 311 and 268 mm (Table 1). The dry year 2014 had the lowest mean annual VWC of 10.4% among the 6 years (Table 1). High spring VWC in 2013 was mainly caused by high non-growing season *P* (~99 mm) during the preceding year (i.e., 2012; Figures 1C, D).

Soils in late spring to early summer were generally dry over the 6 years (Figure 1D). According to the number of consecutive low VWC days during the growing season, 2012 had one extremely dry soil period (DOY 125–176) in spring, with a mean VWC of 10.0%. The year 2013 had two extremely dry soil periods, one in spring and one during the leaf coloration phase (i.e., DOY 134–157 and 286–334), with a mean VWC of 10.9 and 10.8%, respectively. The dry year 2014 had three extremely dry soil periods, one during each of the leaf expansion, leaf-expanded, and leaf coloration phases (DOY 60–131, 190–210, and 270–330), with a mean VWC of 9.9, 10.5, and 10.1%, respectively. The dry year 2015 had three extremely dry soil periods, two during the leaf-expansion phase and one during the leaf-expanded phase (DOY 60–101, 137–167, and 187–199), with a mean VWC of 8.8, 10.2, and 11.5, respectively. The year 2017 had one dry soil period during the leaf expansion phase (DOY 105–172), with a mean VWC of 11.1%. There was no dry soil period in the year 2016.

3.2. The interannual variation in ET

Both monthly and annual ET varied significantly among years at the site (Figures 2A, 3A). Interannual variation of monthly ET was highest in June (Figure 2A). Over the 6 years, annual ET was highest in 2016 and lowest in 2015. The mean annual ET was 462.17 ± 83.58 mm, with a CV of 18% (Table 1).

Over the 6 years, monthly ET was positively correlated to *P* in July (Figure 4A), to T_s in August (Figure 4F), to R_n in September (Figure 4C), and to g_s in all months during the leaf-expanded period (with *p*'s < 0.05; Figure 4H). Total ET over the spring and autumn were both positively correlated to mean VWC over the corresponding period (*p*'s < 0.05; Figure 5), with a higher sensitivity in spring than autumn. Over the 6 years, annual ET values were positively correlated to annual total *P*, especially *P* in July (Figure 6) and the non-growing season (November through March; $n = 5$, $p < 0.05$, $R^2 = 0.98$; Figure 7A).

10.3389/ffgc.2023.1218005

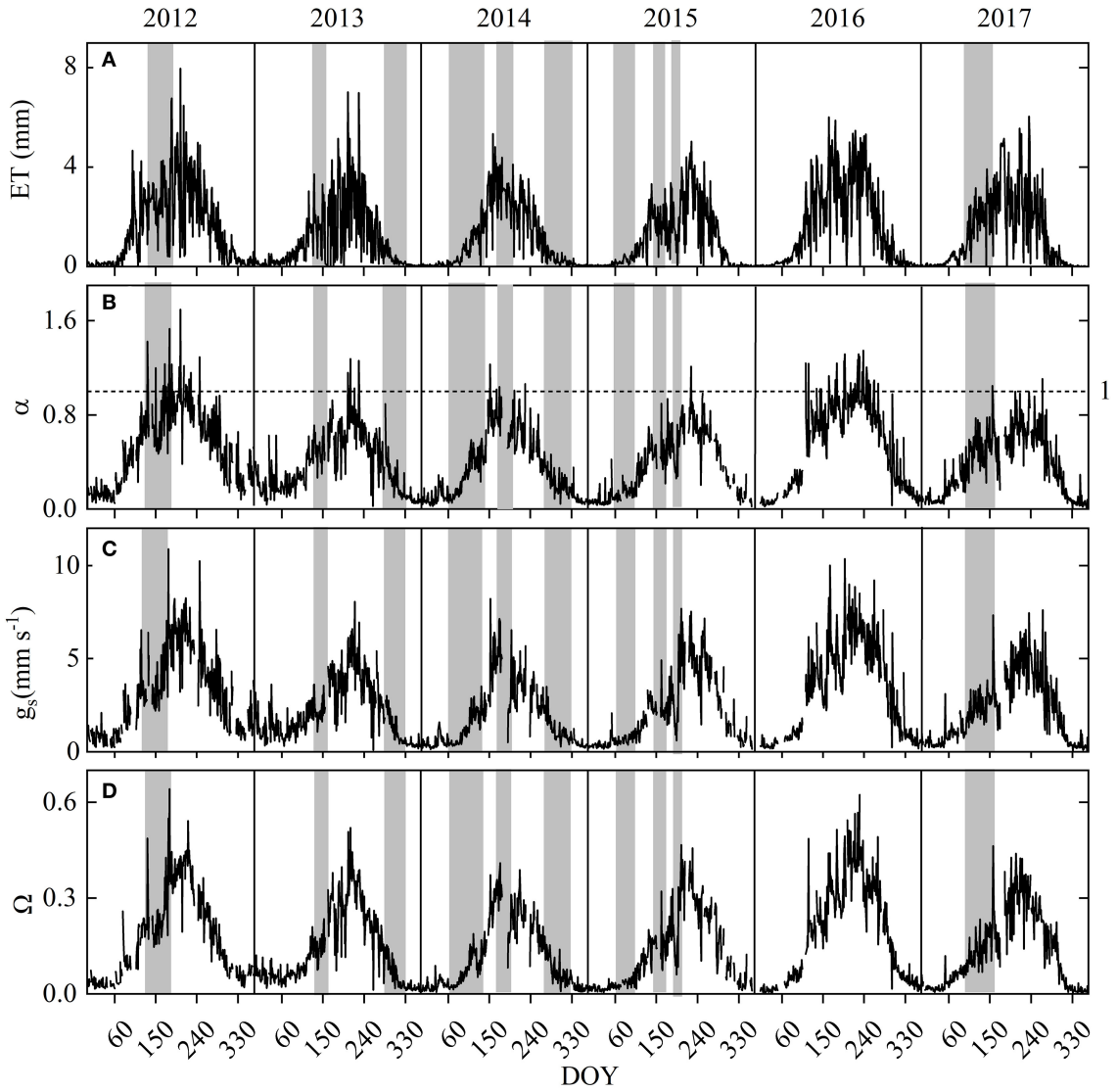

FIGURE 3
Seasonal variations in site **(A)** daily evapotranspiration (ET), **(B)** mean daily daytime Priestley-Taylor coefficient (α), **(C)** mean daytime surface conductance *(gs)*, and **(D)** mean daily decoupling coefficient (Ω) for years 2012-2017. Gray-shaded bands indicate periods of drought (i.e., when VWC < 12.5%).

3.3. Water balance

Cumulative ET showed a seasonal trend similar to cumulative *P* (Figure 8). Cumulative *P* exceeded cumulative ET on DOY 203 in 2012 and DOY 182 in 2013, remaining greater than the cumulative ET until the end of the year (Figures 8A, B), yielding annual cumulative difference between *P* and ET (i.e., *P* and ET) of 176 and 85 mm, respectively. In contrast, 2014 and 2015 provided cumulative ET greater than cumulative *P* after DOY 146, yielding annual cumulative *P* and ET of −135 and −72 mm, respectively (Figures 8C, D). During 2016 and 2017, annual cumulative ET approximately equaled that of *P*, with most rainfall refilling the soils in mid-summer (Figures 8E, F).

3.4. Impacts of drought on evapotranspiration

Daily ET decreased during dry periods (Figure 3). Daily α, Ω, and g_s displayed a trend similar to that demonstrated by ET. The extended dry spell in 2014–2015 led to an analogous reduction in annual ET, α, Ω, and g_s (Table 1), causing a substantial decline in the cumulative difference between *P* and ET (Figure 8). Mean annual ET for the dry year 2014 and 2015 (∼292 mm yr^{-1}) was 30% lower than the non-drought year in 2016 (∼565 mm yr^{-1}). Accordingly, the derived parameters α and g_s also showed large wet-dry contrasts, with dry vs. wet year reductions of 29% (α), 35% (Ω), and 35% (g_s). The shorter duration of spring drought led to annual ET being higher (Figure 9).

TABLE 1 Annual mean air temperature (Ta, °C), soil temperature (Ts, °C), net radiation (Rn, W m^{-2}), vapor pressure deficit (VPD, kPa), and soil volumetric water content (VWC, %), annual total precipitation (P, mm), evapotranspiration (ET, mm) and growing-season (from May to October) normalized difference vegetation index (NDVI), midday (10:00–14:00 h, LST = GMT + 8) surface bulk parameters (gs, mm s^{-1} and α) and growing-season length (GSL, days).

Year	ET	NDVI	T_a	T_s	R_n	P	VPD	VWC	g_s	α	Ω	gso	gse	GSL
2012	562.13	0.75	11.97	11.18	84.28	738.3	0.83	14.25	4.66	0.76	0.19	96	303	207
2013	390.6	0.75	12.41	11.01	81.75	475.6	0.81	13.93	3.42	0.58	0.15	104	298	194
2014	404.6	0.73	12.8	11.48	79.82	270.9	0.95	10.42	3.04	0.56	0.12	98	302	204
2015	386.17	0.75	13.28	12.31	91.63	314.4	0.92	13.06	3.53	0.57	0.14	108	302	194
2016	565.72	0.74	13.09	11.93	88.62	543.8	0.94	13.45	5.04	0.80	0.20	97	302	205
2017	463.79	0.73	13.05	12.26	89.03	498.1	0.95	14.72	3.51	0.58	0.15	94	297	203
Mean	462.17	0.74	12.76	11.69	83.23	473.52	0.9	13.31	3.87	0.64	0.16	99.5	300	201
SD	83.58	0.01	0.49	0.55	4.7	168.54	0.06	1.53	0.79	0.11	0.03	5.36	2.50	5
CV	0.18	0.01	0.04	0.05	0.06	0.36	0.07	0.11	0.20	0.17	0.17	0.05	0.01	0.02

4. Discussion

4.1. Interannual variation of annual ET

Our study demonstrated that the annual P, especially P in the non-growing season and July controlled the IAV of ET (Figures 6, 7A). This result supports the hypothesis that long-term, local-scale ET is generally sensitive to the IAV of P in water-limited environments (Fatichi and Ivanov, 2014). It was also consistent with previous findings that soil water replenishment through P during the non-growing period of the previous year and mid-growing season significantly affected current-year ET and was largely responsible for the interannual variation observed in ET in temperate forest ecosystems (Ma et al., 2018). Precipitation in different periods may affect annual ET through different mechanisms. Since the water availability in pre- and early-growing seasons was confirmed to be essential for the growth of forests in water-limited regions of temperate China (Wu et al., 2009, 2016), P in the non-growing season and leaf expansion period could primarily affect annual ET by its regulation on canopy development. At our site, we found that P in the non-growing season could provide higher spring soil moisture content that can benefit spring canopy formation (Supplementary Figure S1) and make a higher spring ET (Figure 5A). The result is comparable to the results obtained by previous research, which showed a lag effect of P on ET in temperate China (Xu et al., 2014). Notably, too much P during the non-growing season might lead to a decrease in spring ET. According to some reports, a wet winter can delay the growing season start and affect vegetation growth due to its effect on absorbed radiation energy and growing degree days of boreal forests at high latitudes (>40°N) (Piao et al., 2011; Fu et al., 2014; Yun et al., 2018), it is reasonable to assume that P (99 mm) during the non-growing season of 2012 caused the highest spring VWC but lower T_s, R_n (Table 2), leading to a delayed growing season start and restricted canopy development in early spring (Figures 1E, 5A), reducing days with abundant light and active vegetation, thus a lower spring ET (Figure 5A) of 2013.

After the canopy completed construction (July to September), our result showed that ET was positively related to P in July ($ET_{July\ to\ Sep} = 0.27P_{Jul} + 184.5$, $R^2 = 0.69$, $p < 0.05$) but not to P during July to September ($ET_{July\ to\ Sep} = 0.21P_{Jul\ to\ Sep} + 172.1$, $R^2 = 0.50$, $p = 0.12 > 0.05$), indicating that the effect of P in July played a more important role than P in later months in regular ET during the leaf expanded period. This may have occurred for the following reasons. First, as the cumulative P–ET was always negative before July (Figure 8), P in July contains 45% of annual P in mid-summer non-drought years (Figure 5B; Table 2), and it is very important to supply soil water during the leaf expanded period. Our result also showed that P in July could explain 50% of the variation in VWC during the leaf expanded period ($n = 6$, $R^2 = 0.5$). Second, in instances of a more favorable water supply, ET becomes more constrained by atmospheric demand (Liu et al., 2018), and rainfall may offset the positive effects of available energy on increasing ET (Ryu et al., 2008; Kume et al., 2011). August and September had the highest mean monthly α, and Ω and relatively higher VWC during the 6 years (Figures 1D, 3, 4E; Table 2); more mild, longer duration P might lead to lower R_n and soil temperature, resulting in an uncertain effect of P amount on ET. That is the reason why the forest showed a strong interannual response of monthly ET to P for July but not for other summer months (Figures 4A, 6). Thus, the large variability of P at the onset of the monsoon may lead to IAV in the ET during the whole leaf expanded period in forests of Northern China. The results suggest that ET in our forest may be affected by possible changes in the rainfall regime. These observations together suggested the importance of the amount, intensity, and timing of precipitation control on IAV of ET.

10.3389/ffgc.2023.1218005

TABLE 2 Seasonal variation in evapotranspiration (ET), daytime Priestley–Taylor coefficient (α), and main meteorological variables for years 2012–2017.

Variable	Year	Month							
		Mar	Apr	May	Jun	Jul	Aug	Sep	Oct
ET (mm)	2012	16.30	50.98	79.08	76.21	110.52	102.25	67.89	36.10
	2013	10.00	28.70	51.46	48.06	85.20	88.47	42.45	19.87
	2014	6.08	28.26	58.09	99.77	79.89	72.16	37.26	11.72
	2015	6.94	18.00	55.43	47.97	62.46	97.10	59.05	32.05
	2016	11.48	41.68	84.61	102.02	88.07	123.59	74.79	26.65
	2017	12.93	40.55	66.85	99.31	75.48	88.05	59.18	14.46
α	2012	0.30	0.59	0.70	0.78	0.95	0.90	0.69	0.70
	2013	0.21	0.32	0.50	0.62	0.69	0.74	0.54	0.50
	2014	0.12	0.36	0.51	0.80	0.67	0.65	0.47	0.51
	2015	0.13	0.24	0.47	0.47	0.58	0.76	0.68	0.47
	2016	0.19	0.40	0.74	0.82	0.87	0.99	0.84	0.74
	2017	0.25	0.41	0.54	0.54	0.64	0.71	0.64	0.54
T_s (°C)	2012	2.08	13.27	18.77	21.62	24.61	23.64	19.24	13.23
	2013	1.56	9.74	17.32	20.68	23.97	24.00	19.16	13.14
	2014	6.87	14.92	17.61	21.22	24.57	23.20	19.31	13.69
	2015	5.76	13.31	17.92	21.54	23.35	23.82	19.42	13.98
	2016	3.98	13.38	17.23	21.67	24.29	24.64	20.36	13.89
	2017	6.00	14.31	19.78	21.35	25.16	24.00	20.63	13.72
VPD (kPa)	2012	0.62	1.16	1.66	1.36	1.19	1.14	0.96	0.78
	2013	0.59	1.04	1.54	1.04	1.21	1.23	0.77	0.63
	2014	0.93	1.25	1.75	1.29	1.95	1.44	0.88	0.62
	2015	0.91	1.19	1.63	1.54	1.37	1.33	0.86	0.76
	2016	0.92	1.32	1.62	1.64	1.32	1.37	0.99	0.47
	2017	0.80	1.43	1.86	2.07	1.21	1.09	1.05	0.47
VWC (%)	2012	11.52	13.47	10.63	12.41	23.22	20.63	18.71	13.13
	2013	15.73	18.24	12.52	16.20	21.60	18.36	16.95	12.28
	2014	9.68	9.97	11.31	14.08	11.49	13.22	13.02	10.31
	2015	8.30	12.42	11.35	12.38	17.55	18.24	16.94	13.31
	2016	13.40	12.08	11.48	13.20	16.82	17.62	13.06	16.13
	2017	13.30	12.45	11.02	10.72	23.25	23.16	16.06	16.88
P (mm)	2012	14.30	33.60	12.00	99.30	364.00	40.10	80.80	16.40
	2013	17.20	8.60	2.50	92.20	200.70	90.10	52.20	7.70
	2014	1.2	12.40	28.40	82.80	34.70	36.60	57.00	11.50
	2015	0.9	35.20	31.60	9.50	74.20	44.90	53.10	12.50
	2016	0.00	6.60	35.50	81.60	248.20	47.20	44.10	64.10
	2017	12.40	0.30	21.50	12.00	218.40	165.10	1.10	64.70
R_n (W m^{-2})	2012	74.01	101.01	136.91	121.61	129.88	128.54	109.87	67.09
	2013	67.96	119.77	126.46	98.68	134.61	134.12	106.09	64.88
	2014	77.13	104.44	138.53	152.56	135.93	127.28	80.38	55.57
	2015	82.55	120.43	145.18	138.33	135.64	143.76	104.09	65.69
	2016	86.90	122.30	139.84	150.43	121.65	136.27	106.39	60.55
	2017	78.43	125.17	153.03	159.53	140.36	141.92	110.33	51.47

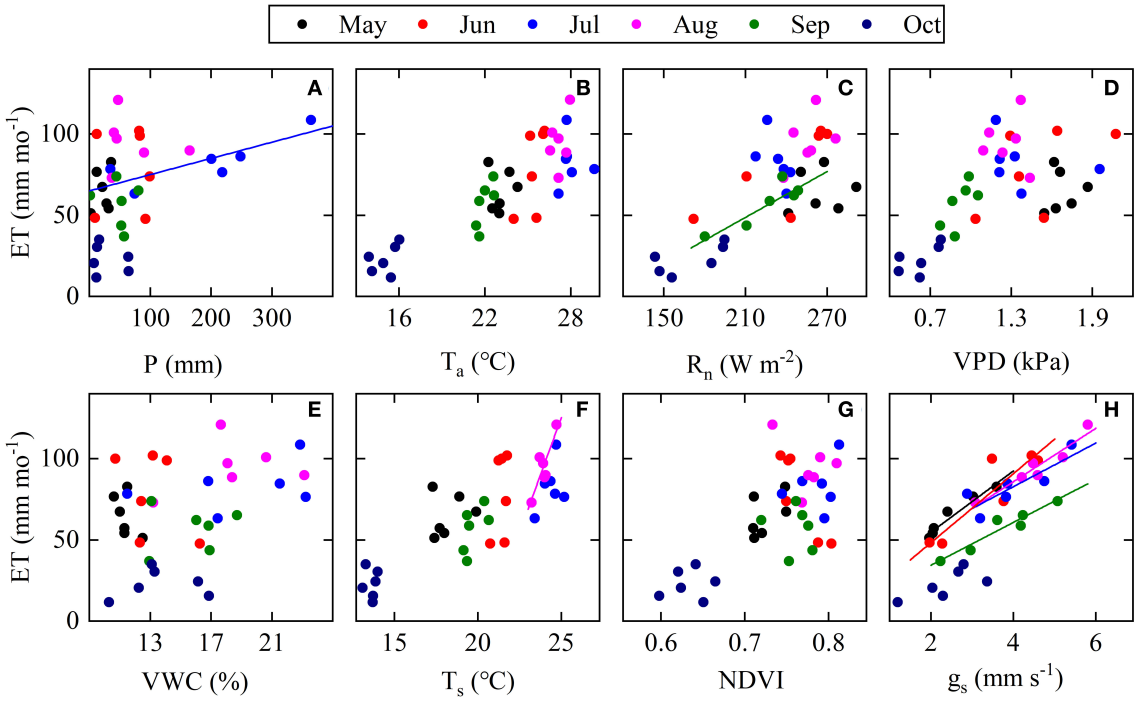

FIGURE 4
Interannual relationships between monthly ET (mm) and respective main explanatory variables **(A)** monthly P (mm), **(B)** monthly mean air temperature (T_a), **(C)** monthly mean net radiation (R_n), **(D)** monthly mean vapor pressure deficit (VPD), **(E)** monthly mean soil volumetric water content (VWC), **(F)** monthly mean soil temperature (T_s), **(G)** monthly mean NDVI and **(H)** monthly mean daytime surface conductance (g_s) from May to October across years (2012–2017; $n = 6$ for each month and $n = 36$ for each plot). Solid lines are fitted line ($p < 0.05$) and dash lines are fitted line ($p < 0.01$).

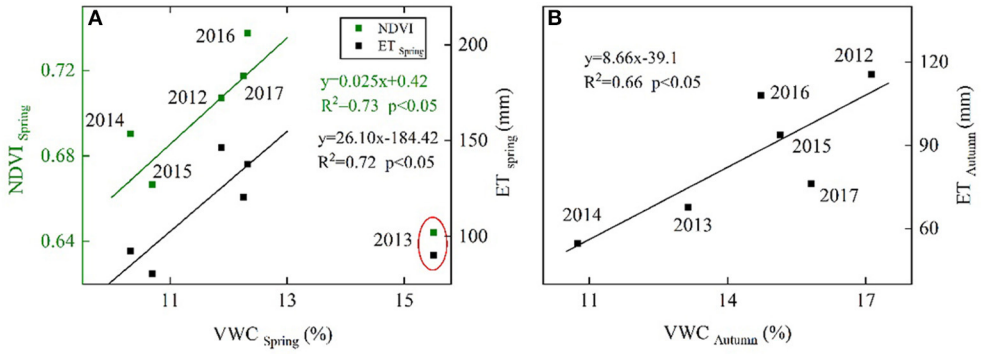

FIGURE 5
Interannual relationships between **(A)** ET (mm), NDVI, and VWC during spring (i.e., March to May) and **(B)** between ET (mm) and VWC (%) during autumn (i.e., September to November). The solid line is the fitted line ($p < 0.05$).

4.2. Interannual variation in ET in relation to drought

The 6-year study (2012–2017) provided an opportunity to study the interannual responses of ET to drought. Drought events at the site occurred randomly at any phenophases and decreased the ET (Figure 1) whenever they happened. However, the mechanism and extent to which drought-affected annual ET differed with the timing and duration of drought occurrence.

In previous temperate forest studies, soil drought due to seasonal and interannual variations in rainfall could be a determining factor for interannual variations in ET due to stomatal closure or leaf fall (Wilson and Baldocchi, 2000; Thomas et al., 2009). Spring drought has been reported to suppress canopy development in a deciduous temperate forest (Noormets et al., 2008). At our study site, we found that the values of spring NDVI in years with spring drought were lower than the year 2016 (Figures 1E, 5A), while ET during spring had a positive relationship

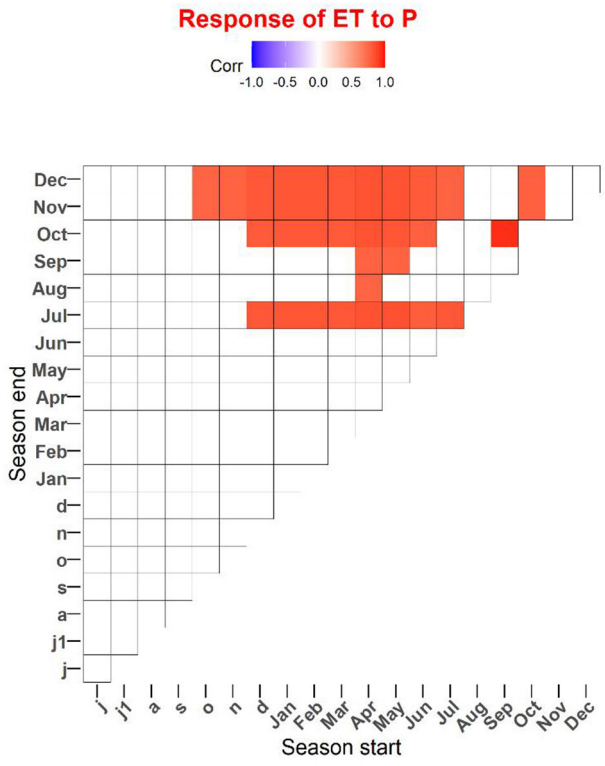

FIGURE 6
Responses of annual total evapotranspiration (ET) to precipitation (*P*) across 2012–2017. The figure presents significant correlations between *P* and ET. The correlations for individual months are shown as diagonal, whereas consecutive seasons starting in a given month extend upward. The blank square indicates correlations that were not significant ($p > 0.05$). Small and capital letters refer to the previous and current years.

with spring NDVI ($p = 0.06$, $R^2 = 0.65$) and IAV in annual ET ($p < 0.05$, $R^2 = 0.96$; Figure 7B). This might indicate that the drought in spring can hinder canopy development and might result in an overall reduction in annual ET. As the photosynthetic structure in the leaf is determined by conditions at the time of leaf development (Kull and Tulva, 2002), the spring drought might have a detrimental effect on the canopy development of the growing season. That appears to be why the mean value of NDVI during the leaf expanding period was positively related to spring NDVI ($y = 2.28\ x - 0.97$, $n = 6$, $R^2 = 0.71$, $p < 0.05$). As g_s depends on leaf area index (LAI) and leaf-level stomatal conductance, reduced NDVI can lead to suppressed g_s, and thus ET (Figure 7D). The drought in spring may also affect annual ET by regulating plant phenology. Some studies found that drought happening in spring or autumn can influence the lifespan of annual deciduous and grassland in temperate regions, thus affecting growing season length and regulating days with active vegetation and IAV in annual ET (Wilson and Baldocchi, 2000; Ryu et al., 2008; Thomas et al., 2009; Zha et al., 2010). Our study also showed that the GSL had a positive influence on annual ET (Figure 7C). The variability of the onset date exceeded that of the end (Figure 8; Table 1) and the variability in the NDVI during the onset of the growing season exceeded that during the end of the growing season (Figure 2D) due to soil water replenishment through *P* during the summer month and less soil moisture deficit during the autumn (Figures 1C, D). As a result, ET was shown to be more sensitive to the availability of soil moisture during the onset of the greenness period than the transition to the senescence period (Figures 2, 5). Consequently, due to the monsoon circulation features (soil water replenishment through *P* in summer), the variability in the intensity of drought in spring may play a more important role in regular GSL and annual ET than that in autumn in temperate forest ecosystems. The more intense spring drought may lead to lower annual ET. Our result is that the most severe early spring drought in 2015 came with the lowest VWC in March (Table 2), leading to the latest date of onset, the shortest GSL; adding days with inactive vegetation and the lowest annual ET over 6 years (Figures 1D, E, 7C) can further support this.

We found that low *P* in mid-summer coincided with extreme drought and low ET during July to September, which occupied 52% of annual ET on average, particularly in 2014 (Figure 1D; Table 2). During the mid-summer, T_a and R_n reached their maxima, and water supply was substantially limited (Figures 1D, 8). Drought during the mid-growing season has been reported to reduce both photosynthetic capacity and transpiration, resulting in inhibited plant growth, earlier canopy senescence, self-protection by stomatal regulation against water losses, and limited ET (Restrepo and Arain, 2005; Yang et al., 2016). At our site, the NDVI showed little variability (Figures 2D, 4G) and decreased slightly during the mid-growing season drought in 2014 and 2015 (Figure 1E). More importantly, we found that lower *P* coupled with higher T_a and VPD, which can induce higher stomatal closure (Barron-Gafford et al., 2007), lead to suppressed g_s and ET (Figures 4A, B, D; Table 2). This result is comparable to the results obtained by previous research, showing that the suppression of ET by summer drought was not related to early canopy senescence but resulted primarily from reductions in stomatal conductance in deciduous forests in temperate regions (Zha et al., 2010).

We conclude that the timing of drought can affect annual ET in different ways and that spring drought primarily affects ET by restricting leafing out and canopy development, while summer drought primarily reduces stomatal conductance in this region. However, to compare the effect of drought in different periods on annual ET, longer (decade scales) time series and a wider range of VWC and P conditions are needed. In fact, the data suggest that the variations of ET during spring appear to have had a smaller contribution to IAV in annual ET in this study (Supplementary Figure S2A) in part because of the smaller proportion of spring ET (<25%) in the annual total. However, the result that IAV in ET during spring and summer were both the primary factors determining the IAV in annual total ET (Supplementary Figure S2A) and IAV of annual ET being more sensitive to IAV of spring ET (Supplementary Figure S2B) may indicate that the variability in the intensity of drought in spring may have played a more important role in regular annual ET than summer drought. Moreover, the extended duration of the spring drought resulted in reduced annual ET (Figure 9), indicating that, in addition to its immediate negative impact on ET during spring, the spring drought may also have a more prolonged carryover effect

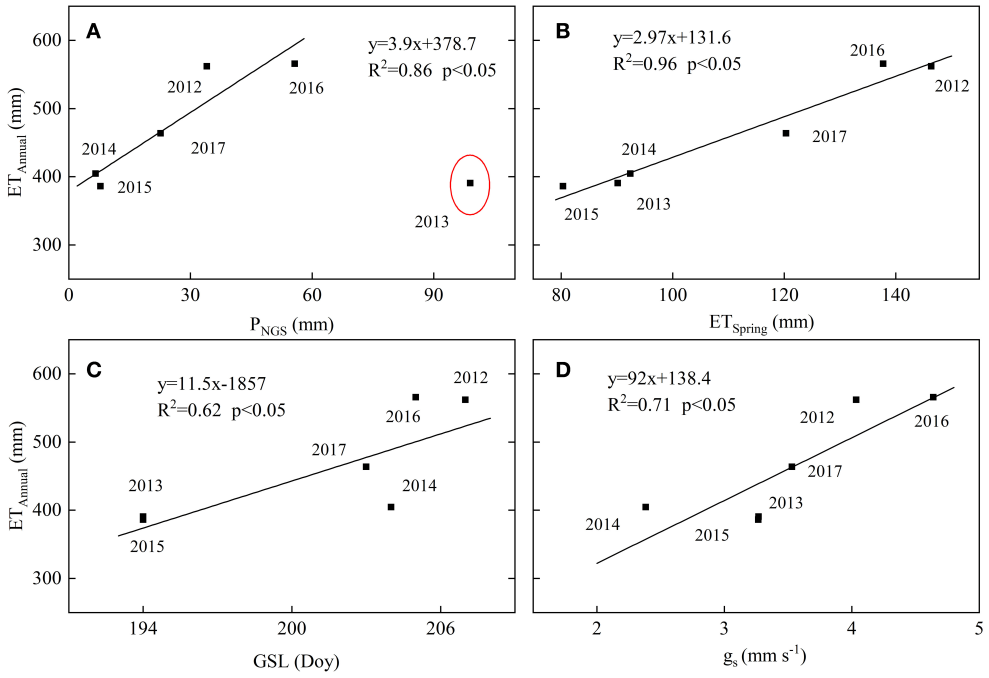

FIGURE 7
Annual total evapotranspiration (ET_{Annual}) as a function of **(A)** non-growing season precipitation (P_{NGS}), **(B)** spring ET (ET_{Spring}), **(C)** growing season length (GSL), and **(D)** growing season canopy conduction (g_s) over 2012–2017. The dashed line is the fitted line ($p < 0.05$).

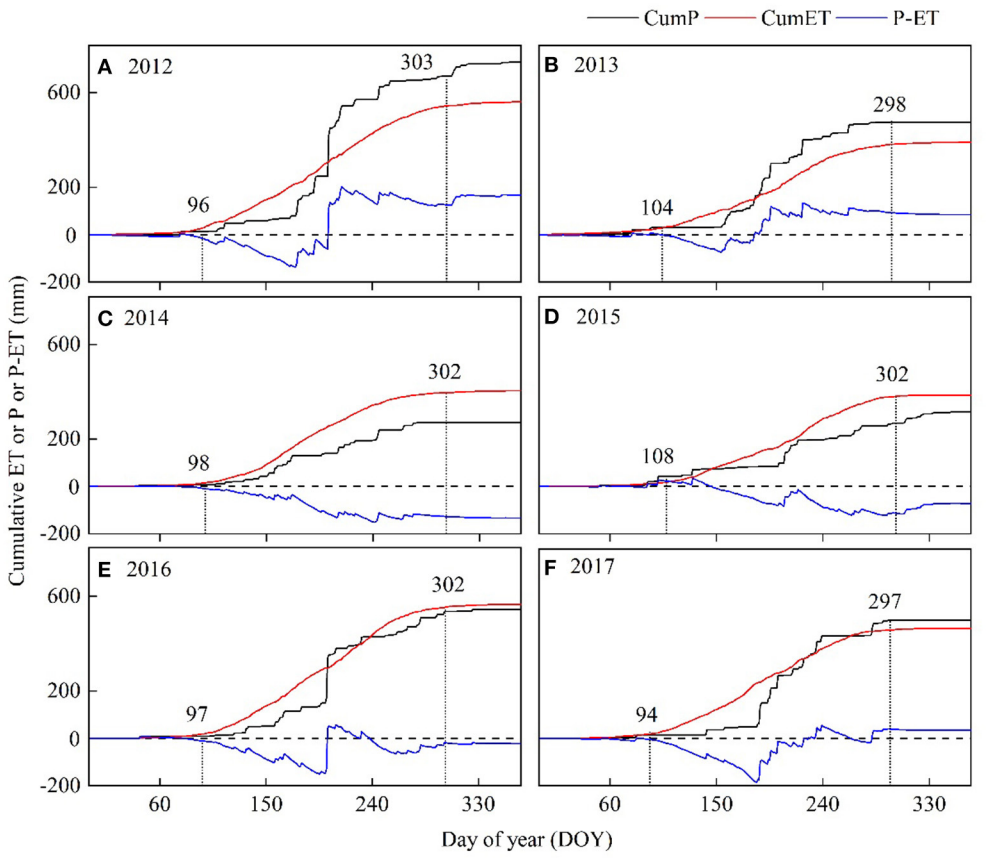

FIGURE 8
Annual cumulative evapotranspiration (ET, black solid lines), precipitation (*P* red line), and their differences (*P*-ET, blue dashed lines) for years 2012-2017. i.e., **(A)** year 2012, **(B)** year 2013, **(C)** year 2014, **(D)** year 2015, **(E)** year 2016, and **(F)** year 2017, respectively. Vertical dot line represents start and end of growing season.

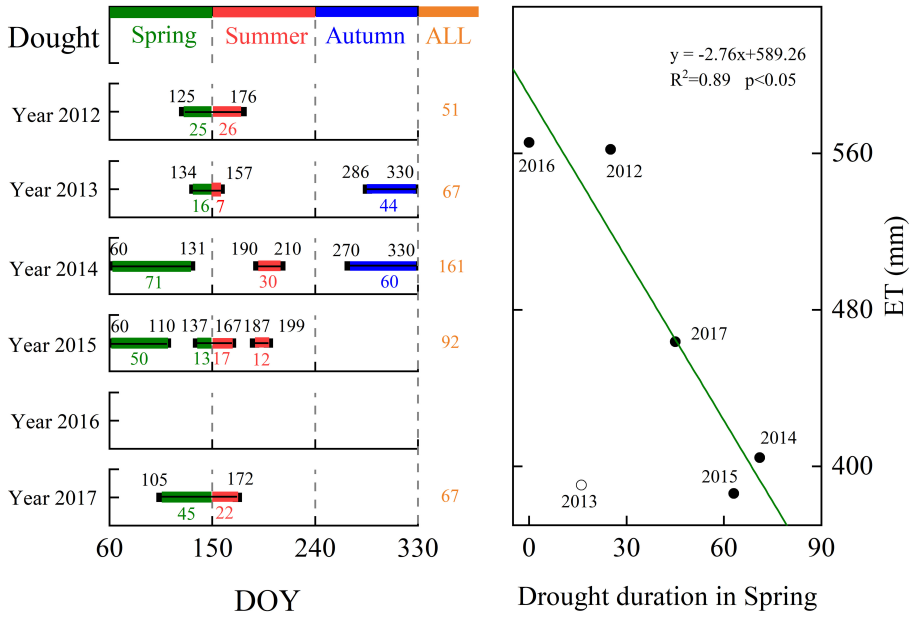

FIGURE 9
Drought period (seasons) and their duration in days and the interannual relationships between annual ET and the number of dry days in spring over 2012–2017. The dashed line is the fitted line ($p < 0.05$).

on annual ET compared to the summer drought. Some studies have reported that an earlier spring uses the soil water reservoir sooner, which leads to summer drought in the northern hemisphere (Angert et al., 2005). In the context of climate change that less precipitation occurs as winter snow in temperate regions, without enough water supply from winter snowfall and/or seasonally frozen soil (Wu et al., 2018), forests across temperate China might become more vulnerable to changing hydrological processes and intensified drought stress. Thus, irrigation during early spring is viewed as a practical and efficient management measure for sustaining tree growth and ecosystem services in urban forests of Northern China.

5. Conclusion

We arrived at the following conclusions with regard to our leading hypotheses based on 6 years of EC measurements in an urban forest in Northern China. First, the interannual variation of both annual ET and monthly ET was controlled by g_s modified by environmental factors. The interannual variation of annual ET was significantly influenced by non-growing season and mid-growing season precipitation. However, the main controlling factors on the interannual variation of ET differed seasonally, namely, VWC and NDVI in spring, precipitation and T_s in summer, and VWC and R_n in autumn. Second, our results emphasized the importance of the timing and duration of drought in controlling the interannual variation of ET in this urban forest. Drought during the leaf expansion period reduced annual ET by restricting leafing out and canopy development, while drought during the expanded period reduced ET by reducing stomatal conductance. We also found that although autumn droughts may reduce ET, their contribution to the interannual variability of ET is less important than spring and summer droughts. Overall, this study emphasized the importance of the seasonality of the precipitation pattern in controlling interannual variation in ET in urban forests. Irrigation support in early spring and mid-summer is an effective measure for sustaining tree growth and ecosystem services in urban forests of Northern China.

Data availability statement

The original contributions presented in the study are included in the article/Supplementary material, further inquiries can be directed to the corresponding author.

Author contributions

RY collected and analyzed data and wrote the manuscript. All authors contributed to the article and approved the submitted version.

Funding

This study was supported by the National Key Research and Development Program of China (2020YFA0608100) and grants from the National Natural Science Foundation of China (NSFC, Proj. Nos. 32101588 and 32071842). The U.S. China Carbon Consortium (USCCC) supported this study by providing an opportunity for instructive discussions and exchange' of ideas.

Acknowledgments

The authors are grateful to JM for his assistance with the field measurements and instrumentation maintenance. The authors would also like to thank the editors and reviewers for their constructive and detailed comments on earlier versions of the manuscript. This work was supported by the Fundamental Research Funds for the Central Universities (2021ZY49).

Conflict of interest

The authors declare that the research was conducted in the absence of any commercial or financial relationships that could be construed as a potential conflict of interest.

Publisher's note

All claims expressed in this article are solely those of the authors and do not necessarily represent those of their affiliated organizations, or those of the publisher, the editors and the reviewers. Any product that may be evaluated in this article, or claim that may be made by its manufacturer, is not guaranteed or endorsed by the publisher.

Supplementary material

The Supplementary Material for this article can be found online at: https://www.frontiersin.org/articles/10.3389/ffgc.2023.1218005/full#supplementary-material

References

Amiro, B. D., Barr, A. G., Black, T. A., Iwashitad, H., Kljun, N., McCaughey, J. H., et al. (2006). Carbon, energy and water fluxes at mature and disturbed forest sites, Saskatchewan, Canada. *Agric. For. Meteorol.* 136, 237–251. doi: 10.1016/j.agrformet.2004.11.012

Angert, A., Biraud, S., Bonfils, C., Henning, C. C., Buermann, W., Pinzon, J., et al. (2005). Drier summers cancel out the CO_2 uptake enhancement induced by warmer springs. *Proc. Natl. Acad. Sci.U. S. A.* 102, 10823–10827. doi: 10.1073/pnas.0501647102

Barr, A. G., Black, T. A., Hogg, E. H., Griffis, T. J., Morgenstern, K., Kljun, N., et al. (2007).. Climatic controls on the carbon and water balances of a boreal aspen forest, 1994–2003. *Glob. Change Biol.* 13, 561–576. doi: 10.1111/j.1365-2486.2006.01220.x

Barron-Gafford, G. A., Grieve, K. A., and Murthy, R. (2007). Leaf- and stand-level responses of forested mesocosm to independent manipulations of temperature and vapor pressure deficit. *New Phytol.* 174, 614–625. doi: 10.1111/j.1469-8137.2007.02035.x

Blanken, P. D., Black, T. A., Yang, P. C., Neumann, H. H., Nesic, Z., Staebler, R., et al. (1997). Energy balance and canopy conductance of a boreal aspen forest: partitioning overstory and understory components. *J. Geophys. Res. Atmos.* 102, 28915–28927. doi: 10.1029/97JD00193

Burba, G. (2013). *Eddy Covariance Method for Scientific, Industrial, Agricultural and Regulatory Applications*. Lincoln, OR: LI-COR Biosciences.

Chen, C., Park, T., Wang, X. H., Piao, S. L., Xu, B. D., Chaturvedi, R. K., et al. (2019). China and India lead in greening of the world through land-use management. *Nat. Sustain.* 2, 122–129. doi: 10.1038/s41893-019-0220-7

Chen, Y., Xue, Y., and Hu, Y. (2018). How multiple factors control evapotranspiration in North America evergreen needleleaf forests. *Sci. Total Environ.* 622–623, 1217–1224. doi: 10.1016/j.scitotenv.2017.12.038

Fan, H. Y., Yu, Z. W., Yang, G. Y., and Liu, Y. T. (2019). How to cool hot-humid (Asian) cities with urban trees? An optimal landscape size perspective. *Agric. For. Meteorol.* 265, 339–348. doi: 10.1016/j.agrformet.2018.11.027

Fatichi, S., and Ivanov, V. Y. (2014). Interannual variability of evapotranspiration and vegetation productivity. *Water Resour. Res.* 50, 3275–3294. doi: 10.1002/2013WR015044

Fu, Y. H., Piao, S., and Zhao, H. (2014). Unexpected role of winter precipitation in determining heat requirement for spring vegetation green-up at northern middle and high latitudes. *Glob. Change Biol.* 20, 3743–3755. doi: 10.1111/gcb.12610

Gielen, B., Verbeeck, H., Neirynck, J., Sampson, D. A., Vermeiren, F., and Janssens, I. A. (2010). Decadal water balance of a temperate Scots pine forest (*Pinus sylvestris* L.) based on measurements and modelling. *Biogeosciences* 7, 1247–1261. doi: 10.5194/bg-7-1247-2010

Hallegatte, S., and Corfee-Morlot, J. (2011). Understanding climate change impacts, vulnerability and adaptation at city scale: an introduction. *Clim. Change* 104, 1–12. doi: 10.1007/s10584-010-9981-8

Hao, L., Sun, G., Liu, Y., Wan, J., Qin, M., Qian, H., et al. (2015). Urbanization dramatically altered the water balances of a paddy fielddominated basin in southern China. *Hydrol. Earth Syst. Sci.* 19, 3319–3331. doi: 10.5194/hess-19-3319-2015

IPCC (2014). *Climate Change 2014–Impacts, Adaptation and Vulnerability: Regional Aspects*. Cambridge: Cambridge University Press.

Jacobs, C., Elbers, J., Brolsma, R., Hartogensis, O., and Moors, E. (2015). Assessment of evaporative water loss from Dutch cities. *Build. Environ.* 83, 27–38. doi: 10.1016/j.buildenv.2014.07.005

Jarvis, P. G., and McNaughton, K. G. (1986). Stomatal control of transpiration: scaling up from leaf to region. *Adv. Ecol. Res.* 15, 1–49. doi: 10.1016/S0065-2504(08)60119-1

Jia, X., Zha, T. S., Gong, J. N., Wu, B., Zhang, Y. Q., Qin, S. G., et al. (2016). Energy partitioning over a semi-arid shrubland in northern China. *Hydrol. Process.* 30, 972–985. doi: 10.1002/hyp.10685

Jim, C. Y., and Chen, W. Y. (2009). Ecosystem services and valuation of urban forests in China. *Cities* 26, 187–194. doi: 10.1016/j.cities.2009.03.003

Kull, O., and Tulva, I. (2002). Shoot structure and growth along a vertical profile within a Populus-Tilia canopy. *Tree Physiol.* 22, 1167–1175. doi: 10.1093/treephys/22.15-16.1167

Kume, T. N., Tanaka, K., Kuraji, H., Komatsu, N., Yoshifuji, T. M., and Saitoh, M., et al. (2011). Ten-year evapotranspiration estimates in a Bornean tropical rainforest. *Agric. For. Meteorol.* 151, 1183–1192. doi: 10.1016/j.agrformet.2011.04.005

Launiainen, S. (2010). Seasonal and inter-annual variability of energy exchange above a boreal Scots pine forest. *Biogeosciences* 7, 3921–3940. doi: 10.5194/bg-7-3921-2010

Liu, S. G., Riekerk, H., and Gholz, H. L. (1998). Simulation of evapotranspiration from Florida pine flatwoods. *Ecol. Modell.* 114, 19–34. doi: 10.1016/S0304-3800(98)00103-3

Liu, X. D., Sun, G., and Mitra, B. (2018). Drought and thinning have limited impacts on evapotranspiration in a managed pine plantation on the southeastern United States coastal plain. *Agric. For. Meteorol.* 262, 14–23. doi: 10.1016/j.agrformet.2018.06.025

Ma, J., Zha, T., Jia, X., and Tian, Y. (2018). Energy and water vapor exchange over a young plantation in northern China. *Agric. For. Meteorol.* 263, 334–345. doi: 10.1016/j.agrformet.2018.09.004

Miao, H., Chen, S., Chen, J., Zhang, W., and Zhang, P. (2009). Cultivation and grazing altered evapotranspiration and dynamics in Inner Mongolia steppes. *Agric. For. Meteorol.* 149, 1810–1819. doi: 10.1016/j.agrformet.2009.06.011

Monteith, J., and Unsworth, M. (2007). *Principles of Environmental Physics*. Cambridge, MA: Academic Press.

Noormets, A., McNulty, S. G., DeForest, J. L., Sun, G., Li, Q., and Chen, J. (2008). Drought during canopy development has lasting effect on annual carbon balance in a deciduous temperate forest. *New Phytol.* 179, 818–828. doi: 10.1111/j.1469-8137.2008.02501.x

Ordónez, C., and Duinker, P. N. (2014). Assessing the vulnerability of urban forests to climate change. *Environ. Rev.* 22, 311–321. doi: 10.1139/er-2013-0078

Papale, D., Reichstein, M., Aubinet, M., Canfora, E., Berhofer, C., Kutsch, W., et al. (2006). Towards a standardized processing of Net Ecosystem Exchange measured with

eddy covariance technique: algorithms and uncertainty estimation. *Biogeosciences* 3, 571–583. doi: 10.5194/bg-3-571-2006

Piao, S. L., Wang, X. H., Ciais, P., Zhu, B., Wang, T., and Liu, J. (2011). Changes in satellite-derived vegetation growth trend in temperate and boreal Eurasia from 1982 to 2006. *Glob. Change Biol*. 17, 3228–3239. doi: 10.1111/j.1365-2486.2011.02419.x

Priestley, C. H. B., and Taylor, R. J. (1972). On the assessment of surface heat flux and evaporation using large-scale parameters. *Monthly Weather Rev*. 100, 81–92. doi: 10.1175/1520-0493(1972)100<0081:OTAOSH>2.3.CO;2

Restrepo, N. C., and Arain, M. A. (2005). Energy and water exchanges from a temperate pine plantation forest. *Hydrol. Process*. 19, 27–49. doi: 10.1002/hyp.5758

Ryu, Y., Baldocchi, D. D., Ma, S., and Hehn, T. (2008). Interannual variability of evapotranspiration and energy exchange over an annual grassland in California. *J. Geophys. Res*. 113, D09104. doi: 10.1029/2007JD009263

Saitoh, T. M., Tamagawa, I., Muraoka, H., and Kondo, H. (2013). An analysis of summer evapotranspiration based on multi-year observations including extreme climatic conditions over a cool-temperate evergreen coniferous forest, Takayama, Japan. *Hydrol. Process*. 27, 3341–3349. doi: 10.1002/hyp.9834

Sun, G., Domec, J. C., and Amatya, D. M. (2016). "Forest evapotranspiration: measurement and modelling at multiple scales," in *Forest hydrology: Processes, management and assessment* (Wallingford: CABI). 32–50. doi: 10.1079/9781780646602.0032

Tang, Y. K., Jia, C., Wang, L. N., Wen, X. F., and Wang, H. M. (2021). Solar energy dominates and soil water modulates net ecosystem productivity and evapotranspiration across multiple timescales in a subtropical coniferous plantation. *Agric. For. Meteorol*. 300, 108310. doi: 10.1016/j.agrformet.2020.108310

Thomas, C., Law, B. E., Irvine, J., Martin, J. G., Pettijohn, J. C., and Davis, K. J. (2009). Seasonal hydrology explains interannual and seasonal variation in carbon and water exchange in a semiarid mature ponderosa pine forest in central Oregon. *J. Geophys. Res*. 114, G04006. doi: 10.1029/2009JG001010

Tsuruta, K., Kosugi, Y., Takanashi, S., and Tani, M. (2016). Inter-annual variations and factors controlling evapotranspiration in a temperate Japanese cypress forest. *Hydrol. Process*. 30, 5012–5026. doi: 10.1002/hyp.10977

Vadeboncoeur, M. A., Green, M. B., Asbjornsen, H., et al. (2018). Systematic variation in evapotranspiration trends and drivers across the Northeastern United States. *Hydrol. Process*. 32, 3547–3560. doi: 10.1002/hyp.13278

Vose, J. M., Miniat, C. F., Luce, C. H., Asbjornsen, H., Caldwell, P. V., Campbell, J. L., et al. (2016). Ecohydrological implications of drought for forests in the United States. *For. Ecol. Manage*. 380, 335–345. doi: 10.1016/j.foreco.2016.03.025

Wilson, K. B., and Baldocchi, D. D. (2000). Seasonal and interannual variability of energy fluxes over a broadleaved temperate deciduous forest in North America. *Agric. For. Meteorol*. 100, 1–18. doi: 10.1016/S0168-1923(99)00088-X

Wu, X., Li, X., and Liu, H. (2018). Uneven winter snow influence on tree growth across temperate China. *Glob. Change Biol*. 2019, 25. doi: 10.1111/gcb.14464

Wu, X., Liu, H., Li, X., Liang, E., Beck, P. S., and Huang, Y. (2016). Seasonal divergence in the interannual responses of Northern Hemisphere vegetation activity to variations in diurnal climate. *Sci. Rep*. 6, 19000. doi: 10.1038/srep19000

Wu, X., Liu, H., Ren, J., He, S., and Zhang, Y. (2009). Water-dominated vegetation activity across biomes in mid-latitudinal eastern China. *Geophys. Res. Lett*. 36, L04402. doi: 10.1029/2008GL036940

Xiang, J., Hayat, M., Qiu, G. Y., Xiao, W. Y., Xu, X. L., Mao, P., et al. (2023). Assessing the variations of evapotranspiration and its environmental controls over a subalpine wetland valley in China. *J. Hydrol*. 617, 129058. doi: 10.1016/j.jhydrol.2022.129058

Xie, J., Zha, T., Zhou, C., Jia, X., Yu, H., Yang, B., et al. (2016). Seasonal variation in ecosystem water use efficiency in an urban-forest reserve affected by periodic drought. *Agric. For. Meteorol*. 221, 142–151. doi: 10.1016/j.agrformet.2016.02.013

Xu, M., Wen, X., Wang, H., Zhang, W., Dai, X., Song, J., et al. (2014). Effects of climatic factors and ecosystem responses on the inter-annual variability of evapotranspiration in a coniferous plantation in subtropical china. *PLoS ONE* 9, E85593. doi: 10.1371/journal.pone.0085593

Xue, B.-L., Komatsu, H., Kumagai, T., Kotani, A., Otsuki, K., and Ohta, T. (2012). Interannual variation of evapotranspiration in an eastern Siberian larch forest. *Hydrol. Process*. 26, 2360–2368. doi: 10.1002/hyp.9195

Yang, Y. T., Guan, H. D., Batelaan, O., Mcvicar, T. R., Long, D., Piao, S. L., et al. (2016). Contrasting responses of water use efficiency to drought across global terrestrial ecosystems. *Sci. Rep*. 6, 23284. doi: 10.1038/srep23284

Yun, J., Jeong, S. J., Ho, C. H., Park, C. E., Park, H., and Kim, J. (2018). Influence of winter precipitation on spring phenology in boreal forests. *Glob. Change Biol*. 24, 5176–5187. doi: 10.1111/gcb.14414

Zha, T., Alang, B., Garth, V. D. K., Tandy, B., Jharry, M. C., and Lawrenceb, F. (2010). Interannual variation of evapotranspiration from forest and grassland ecosystems in western Canada in relation to drought. *Agric. For. Meteorol*. 150, 1476–1484. doi: 10.1016/j.agrformet.2010.08.003

Zha, T., Alang, B., Tandy, B., Jharry, M., Bhatti, J., Hawthorne, I., et al. (2009). Carbon sequestration in boreal jack pine stands following harvesting. *Glob. Change Biol*. 15, 1475–1487. doi: 10.1111/j.1365-2486.2008.01817.x

Zhai, J., Su, B., Krysanova, V., Vetter, T., Gao, C., and Jiang, T. (2010). Spatial variation and trends in PDSI and SPI indices and their relation to streamflow in 10 large regions of China. *J. Clim*. 23, 649–663. doi: 10.1175/2009JCLI2968.1

frontiers | Frontiers in Plant Science

TYPE Original Research
PUBLISHED 20 September 2023
DOI 10.3389/fpls.2023.1275464

OPEN ACCESS

EDITED BY
Yunpu Zheng,
Hebei University of Engineering, China

REVIEWED BY
Licong Dai,
Hainan University, China
Yaobin Niu,
Shanxi Agricultural University, China

*CORRESPONDENCE
Xuejie Zhang
zhangxuejie@sdnu.edu.cn
Shoujin Fan
fansj@sdnu.edu.cn

RECEIVED 10 August 2023
ACCEPTED 05 September 2023
PUBLISHED 20 September 2023

CITATION
Jiang P, Yan J, Liu R, Zhang X and Fan S (2023) Patterns of deep fine root and water utilization amongst trees, shrubs and herbs in subtropical pine plantations with seasonal droughts.
Front. Plant Sci. 14:1275464.
doi: 10.3389/fpls.2023.1275464

Patterns of deep fine root and water utilization amongst trees, shrubs and herbs in subtropical pine plantations with seasonal droughts

Peipei Jiang[1], Jinliang Yan[2], Rongxin Liu[1], Xuejie Zhang[1*] and Shoujin Fan[1*]

[1]Key Lab of Plant Stress Research, College of Life Sciences, Shandong Normal University, Ji'nan, Shandong, China, [2]Yangji Forest Farm (Yangtianshan Provincial Nature Reserve Protection Center) of Qingzhou, Weifang, Shandong, China

Introduction: Seasonal droughts will become more severe and frequent under the context of global climate change, this would result in significant variations in the root distribution and water utilization patterns of plants. However, research on the determining factors of deep fine root and water utilization is limited.

Methods: We measured the fine root biomass and water utilization of trees, shrubs and herbs, and soil properties, light transmission, and community structure parameters in subtropical pine plantations with seasonal droughts.

Results and Discussion: We found that the proportion of deep fine roots (below 1 m depth) is only 0.2-5.1%, but that of deep soil water utilization can reach 20.9-38.6% during the dry season. Trees improve deep soil water capture capacity by enhancing their dominance in occupying deep soil volume, and enhance their deep resource foraging by increasing their branching capacity of absorptive roots. Shrubs and herbs showed different strategies for deep water competition: shrubs tend to exhibit a "conservative" strategy and tend to increase individual competitiveness, while herbs exhibited an "opportunistic" strategy and tend to increase variety and quantity to adapt to competitions.

Conclusion: Our results improve our understanding of different deep fine root distribution and water use strategies between overstory trees and understory vegetations, and emphasize the importance of deep fine root in drought resistance as well as the roles of deep soil water utilization in shaping community assembly.

KEYWORDS

community structure, deep fine root, deep soil water utilization, light transmission, seasonal dynamics, soil property

1 Introduction

Under the context of global climate change, the intensity, frequency, and duration of drought are increasing, leading to changes in water utilization of plants as well as decreases in plant productivity and survival (Allen et al., 2010; Adams et al., 2017; Ripullone et al., 2020). To some extent, water uptake and utilization patterns of plants reflect the response of ecosystems to variations in environmental hydraulic status (Gulihanati et al., 2022). A better knowledge of plants' water use is necessary to enhance our understanding of plants adaptations to changes in the forest hydrologic cycle and our predictions on variations of the community composition and function in forest ecosystems with climate drying (Ding et al., 2018; Ripullone et al., 2020).

The distribution of roots is closely associated with the water access of plants. In forest ecosystems, trees usually distribute more fine roots in deeper layer than understory shrubs and herbs, and shrubs often distributed their fine root deeper than herbs (Achat et al., 2008; Sun et al., 2015). According to the two-layer model of woody and herbs coexistence (Walker and Noy-Meir, 1982), herbs with shallower roots are competitors of shallow soil moisture, and woody plants with deeper roots could monopolize the deep soil moisture. This model has been confirmed by many studies (Le Roux et al., 1995; Moreira et al., 2000; Eggemeyer et al., 2009). Previous studies also shown that deep soil water absorbed by trees with deeper roots can be utilized by shrubs and herbs with shallower roots through hydraulic lift (Yu and D'Odorico, 2015; Barron-Gafford et al., 2021). However, some studies shown that root depth is not directly associated with water uptake depth, since the water uptake of plants depended mainly on active roots (Ehleringer and Dawson, 1992; West et al., 2007). Therefore, it is very essential to determine the relationships between root distribution and water use of plants amongst life forms. In addition, intraspecific or interspecific competition also can affect the distribution of fine root and water utilization. Also, roots of trees that grown with understory vegetations was deeper than those without competition, while roots of herbs that grown with shrubs are mostly distributed in shallow soil (Rolo and Moreno, 2012; Cardinael et al., 2015). Similarly, sea-buckthorn in a mixed forest of trees and shrubs had higher deep soil water reliance than those in pure sea-buckthorn forest during the dry season (Wu et al., 2022). Moreover, *Robinia pseudoacacia* in the Loess Plateau was found to increase the reliance of shallow and middle soil water but decrease the reliance of deep soil water as thinning intensity increased (Liu et al., 2023). Current researches mainly focus on variations of root and soil water utilization at the upper 1 m depth of the soil profile, however, the distribution patterns of fine root and soil water utilization below the 1 m depth are still unclear.

Generally, plant water utilization is related to the distribution of soil moisture with time and soil depth (Eggemeyer et al., 2009; Chen et al., 2014; Yang et al., 2015). Plants with dimorphic root systems could transfer the main water source from shallow soil to deep soil with soil drying (Quesada et al., 2008; Eggemeyer et al., 2009; Chen et al., 2014). For example, Yang et al. (2015) discovered that three coniferous plants in subtropical region with a marked seasonal dry season transferred their main water source to deep soil layer in the dry season. Also, *Vitex negundo* in the Loess Plateau was found to primarily utilize top soil water of 0-40 cm layer and gradually transferred to soil water of deeper layers as the season progressed (Wang et al., 2017). Similarly, Zhu et al. (2021) found that *R. pseudoacacia* and *Jiziphus jujuba* in the Taihang Mountains mainly used soil water of the top soil layer (0-10 cm) in the wet season and that of the deeper soil layer (30-50 cm) in the dry season. However, plants' water use strategies can be variable due to the micro local changes in soil conditions, i.e. soil depth, stoniness, water holding capacity (Love et al., 2019; Carrière et al., 2020b). Because the water retention capacity of shallow soil was poor, plants growing on continuous dolostone outcrops and nearby thin soil layers mainly used deep soil moisture in both the wet and dry seasons (Nie et al., 2011). Similarly, woody plants with poor surface conditions (i.e. low water holding capacity) could allow their roots to utilize deep water reserves more intensively than those with better surface conditions (Carrière et al., 2020a).

Other abiotic factors (e.g. soil bulk density, rock fragment content, and light) can also affect the distribution patterns of fine roots and water use of plants. Generally, the development of root was severely restricted with the increase of soil bulk density since high mechanical could impede the elongation and proliferation of root (Pabin et al., 1998; McIvor et al., 2014). However, there are different opinions on whether the existence of rock fragment is beneficial for root growth of plant. Novák and Knava (2012) found that the existence of rock fragments can reduce soil hydraulic conductivity and water retention capacity and therefore affect the soil water availability for plants. In contrast, there are also studies showed that rock fragments can serve as reservoirs of plants and water conservation was found to be better in rocky soils under moderate water stress conditions (Danalatos et al., 1995; Tetegan et al., 2015). Moreover, light also had an important influence on the distribution of fine root, though this effect may be dependent on the availability of soil water and/or nutrients (Valladares and Pearcy, 2002; Schall et al., 2012). Generally, the amount of water that can be tapped and its transportation from roots to leaves is thought to be mainly related to transpiration without consuming metabolic energy (Ksenzhek and Volkov, 1998), which largely depends on the degree of opening and closing of stomata. However, the tension gradient caused by transpiration may be not sufficient to stimulate the transport systems of plants, and then plant would employ root pressure to pump water into xylem vessels at the cost of minimal metabolic energy consumption (Schwinning, 2010; Wu et al., 2021). Therefore, capturing and pumping from deep depth required more energy (through root pressure) than extracting shallow soil water. Therefore, low light transmittance could affect the transpiration and photosynthetic rates of plants and therefore affect the water utilization of plants (especially deep soil water utilization). However, studies on determining factors of deep soil water utilization across life forms still very lack.

In our study area, the understory vegetation species are rich and the soil heterogeneity is high, which can induce strong variations in soil conditions at very close distances (Jiang et al., 2023). In turn, this might affect the distribution of fine root and water utilization

for vegetations (Gargiulo et al., 2016; Love et al., 2019; Carrière et al., 2020a). This provides a suitable opportunity to research the distribution patterns of fine root and water utilization as well as their determining factors. Therefore, we measured the fine root distribution and water use of trees, shrubs, and herbs, community structure parameters (stem density of trees, and the dominance, richness and evenness of understory shrubs and herbs), light transmission, and soil properties (soil bulk density, pH, water content, rock fragment content, total carbon and nitrogen concentration) in subtropical pine plantations with seasonal droughts. The main aims of our study were: (i) to compare the deep fine root and water utilization allocation strategies amongst trees, shrubs and herbs; (ii) to determine the allocation of deep fine root and their determinants (including community structure parameters, soil properties, and light transmission) amongst trees, shrubs and herbs; (iii) to examine the deep soil water utilization strategy and their determinants (including fine root biomass, community structure parameters, soil properties, and light transmission) amongst life forms.

2 Materials and methods

2.1 Site description

This research was conducted at the Qianyanzhou Forest Ecosystem Research Station of the Chinese Academy of Sciences (QYZ for abbreviation; 26°44′39′′N, 115°03′33′′E), which is located in the Jiangxi Province of southeastern China (red circle in Figure 1A). Due to the uneven distribution of rainfall, seasonal droughts occur frequently in this region. The mean annual temperature and precipitation are 18.0°C and 1509.0 mm, respectively. The soil is an iron-rich red soil classified as Typic Dystrudept and Udept Inceptisols by the USDA soil taxonomic system. The vegetation mainly consists of *Pinus massoniana* and *P. elliottii* plantations which were planted in 1983, and the vegetation picture was shown in Figure 1C.

2.2 Experimental design and stand structures

A total of 29 plots (30 × 30 m) were established in the pine plantations, including 18 plots of *P. massoniana* and 11 plots of *P. elliottii*. The distribution of these plots was shown in Figure 1B. The dominant shrub species across 29 plots were *Loropetalum chinensis*, *Adinandra millettii*, *Camellia oleifera*, *Rhus chinensis*, *Eurya muricata* and *Rhaphiolepis indica*. The dominant herb species across 29 plots were *Dryopteris atrata*, *Woodwardia japonica*, *Dicranopteris dichotoma*, *Morinda umbellate*, and *Lophatherum gracile*.

The community structure was investigated in August 2015. Each plot was divided into nine quadrats (10 × 10 m) and then taken photos below the canopy. Light transmission was then determined by Side look and Gap Light Analyzer (Frazer et al., 1999). In each plot, the diameter at breast height (DBH) of each tree was measured. Three shrub subplots of 5 × 5 m were set along the diagonals within each tree plot. Then, the basal diameters, heights, and number of bushes of all shrubs in each subplot were measured. One herb quadrat of 1 × 1 m was set within each shrub subplot, and the heights and coverages of all herbs were then measured in each quadrat.

2.3 Soil properties and fine-root distributions

Soil cores of 10 cm diameter were sampled every 20 cm at the up-, mid-, and down slopes from soil surface to 200 cm depth in each plot. Living fine roots were carefully picked out and gently washed with running water. Living fine roots were then sorted to trees, shrubs, and herbs, according to their contrasting traits in terms of morphological structure, color, and mechanics (e.g. rigid or soft, rough or smooth). More details can be seen in Jiang et al. (2018a). The fine roots were classified using an order-based approach described by Pregitzer et al. (2002). Fine roots of woody species (trees and shrubs) were then divided into absorptive (1-3 order) and transport (4-5 order) categories, while those of herbs were not distinguish between the absorptive and transport categories.

After root extraction, rock fragments (> 2 mm) were picked up from the soil samples, and then air-dried and weighed. The rock fragment content of each soil sample was determined by using a stone density of 2.65 g cm^{-3} (Diochon et al., 2009). Due to the rocky properties of soil in our study area, the use of standard soil core method could not accurately determine the soil bulk density, and therefore the differences between volumes of soil cores and stones were applied to determine the soil bulk density (Klinka et al., 1981; Diochon et al., 2009). Soil pH was determined in a 1:2.5 mixture of air-dried soil/distilled water mixture by using an electrode pH meter (S40, Mettler Toledo, Switzerland). Total carbon and nitrogen contents of the surface layer (0-20 cm) were measured by an elemental analyser (vario MACRO cube, Germany).

2.4 Soil water utilization of plants

Plant samples for water isotope analysis was collected during mid-morning in both the dry season (August 2016) and the wet season (April 2017). For trees, stems from two to three sample trees of middle diameter were collected in each plot, and phloem tissue was peeled off to avoid potential contamination (Querejeta et al., 2007). For shrubs and herbs, ten shrub species and three fern species were sampled in each plot, with the average coverage of the collected species relative to the total coverage of all shrubs or herbs was 63.6 ± 3.3% and 75.3 ± 5.8% across 29 plots, respectively. The water use of these collected shrubs and herbs was used for representing the overall water use of the shrub and herb layers. For shrubs, green tissues were removed from the branches to avoid contamination (Ehleringer and Dawson, 1992). Meanwhile, the basal diameter of shrub individuals was controlled between 10 and 25 mm to avoid the potential effects of plant age on water

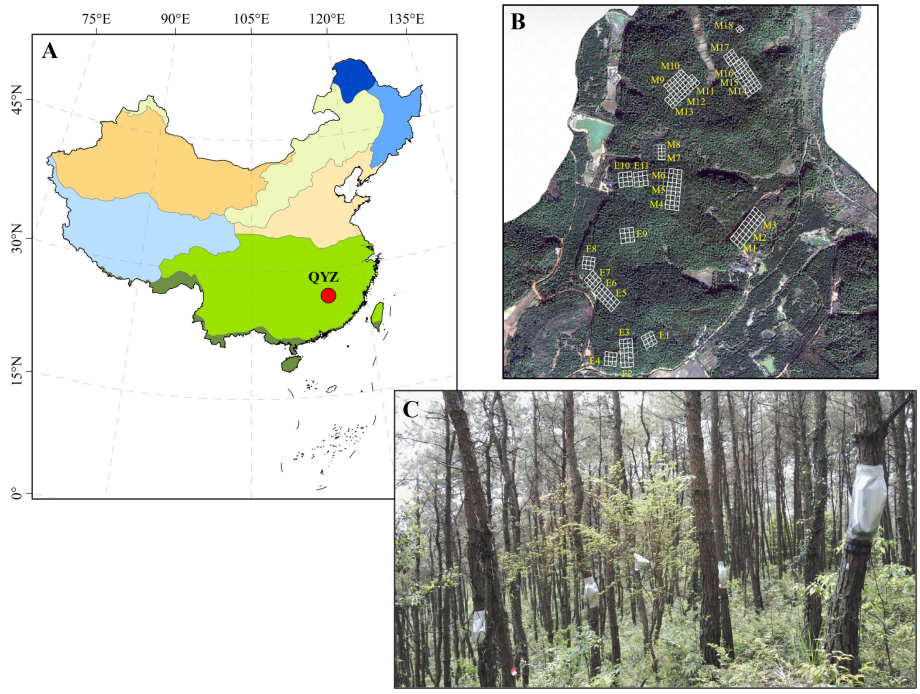

FIGURE 1
Location of study area (in red circle, **A**), and distribution **(B)** and vegetation picture **(C)** of the sampling plots. In **(B)** M1-M18 represent the 18 plots of *P. massoniana* plantations and E1-E11 represent the 11 plots of *P. elliottii* plantations.

absorption. For herbs, the thick and fleshy root crowns were collected, since this part had the most stable water isotopic ratios (Barnard et al., 2006). Soil samples were collected at depth of 0-20, 20-60, 60-100, 100-150, 150-200 cm in each plot. Then, each soil sample was separated into two subsamples: one subsample was used for water extraction, and the other subsample was used for measuring the soil water content. Soil water content was then measured by dividing fresh weight minus dry weight by dry weight.

We extracted water from plant and soil samples through an automatic low-temperature vacuum distilled water extraction system (Li-2100, Beijing, China). The extraction time for plant and soil sample was 3 h and 2.5 h, respectively. We analyzed the water isotope ratio of water samples using a liquid water isotope analyzer (912-0050, LGR, California, USA). The IsoSource model was applied to calculate the relative contribution of soil water at different depths to plant (Phillips et al., 2005). See Jiang et al. (2020b) for details. Because the accuracy in hydrogen isotopes analysis was relatively lower than that of oxygen stable isotopes when using the Isotopic Ratio Infrared Spectroscopy (IRIS) method (Wen et al., 2012), $\delta^{18}O$ was shown to be more sensitive than δD in evaluating water uptake of plant and therefore $\delta^{18}O$ was used to detect the water uptake depths of plants.

2.5 Data analysis

Due to the 0-100 cm soil depth accounts for over 90% of the total fine root biomass of the entire 0-200 cm soil profile in all life forms and the $\delta^{18}O$ value of the upper 100 cm soil was different from the below 100 cm depth (Figures S1, S2), the 100-200 cm depth was defined as the deep soil layer. Then, fine root biomass in the deep soil layer was determined by the sum of fine root biomass below the 100 cm depth of the entire 0-200 cm soil profile. The deep soil water utilization was determined by the sum of soil water proportions in 100-150 and 150-200 cm depth. Since the P. massoniana and P. elliottii plantations had the similar root distribution and water utilization allocation patterns (Yang et al., 2015, Yang et al., 2017; Jiang et al., 2020b), we combined the data from the two pine plantations. For trees, the seasonal plasticity of deep soil water utilization (DWP) was calculated as:

$$DWP = \frac{2 \times (DDW - WDW)}{DDW + WDW} \quad (1)$$

where DDW is the deep soil water utilization during the dry season and WDW is the deep soil water utilization during the wet season (Padilla et al., 2007; Jiang et al., 2020a; Jiang et al., 2020b). For shrubs and herbs, the community-weighted mean DDW in each plot was calculated. First, dividing the number of individuals of each species by the total number of shrub (or herb) species to determine the weight of each species in each subplot, and then calculate the weight of each species in each plot as the mean value of the three subplots. Second, the community-weighted mean DDW of each plot was calculated as the sum of the product of the average weight of each species and its DDW. Then, the community-weighted mean DDW of shrubs and herbs was used to calculate the DWP according to equation (1). The biodiversity index of each plot was determined by "Biodixcel.xlsx" in Microsoft Office Excel 2007 (Kong et al., 2012).

To test the differences of fine root biomass and water source in deep soil layer amongst life forms, a one-way analysis of variance

(ANOVA) was conducted in SPSS (2010, ver.19.0; SPSS Inc., USA). To test the differences between trees and shrubs (or between seasons), the independent sample T test was applied in SPSS. To analyse the relationships between the fine root biomass and water utilization in the deep soil layer and the abiotic and biotic factors, the RDA-ordination biplot was carried out in the CANOCO software (ver.5.0, Ithaca, NY, USA). Significance was defined at the 0.05 level.

3 Results

3.1 Deep fine root biomass and water utilization amongst life forms

In our study, trees and understory vegetations showed contrast deep fine allocation and water use strategies (Figures 2, 3). We found trees and shrubs distributed more fine roots than herbs in deep soil layer (Figure 2). The fine root biomass of trees was significantly higher than that of shrubs, however, the differences in deep fine root proportion between them was not significant. Trees tended to distribute more absorptive fine roots than shrubs in deep soil, however, the deep transport fine root biomass between trees and shrubs didn't show significant differences (Figure 3). Trees have a significant deep soil water reliance in both the wet and dry seasons, while shrubs and herbs had a lower deep soil water reliance during the wet season and a higher deep soil water reliance during the dry season (Figures 4, S3). Therefore, trees showed a smaller seasonal plasticity of deep soil water reliance than shrubs and herbs (Figure 4).

3.2 Determining factors of fine root and water utilization in the deep soil layer amongst life forms

The RDA ordination biplot displayed that the major determining abiotic and biotic factors of deep fine root and water utilization were different (Figures 5, 6). For the deep fine root biomass, the C%, N%, light transmission, and rock fragment content were the major abiotic factors (Figure 5A), which contributed 35.7%, 25.3%, 17.0%, and 11.3% variations in these factors; the dominance and richness of shrubs were the major biotic factors (Figure 5B), which contributed 33.8% and 23.9% variations in these factors, respectively. For details, C% and N% displayed a predominantly positive relationship with total and absorptive fine root biomass of shrubs and herbs, while light transmission showed a predominantly negative relationship with fine root biomass of trees; the dominance of shrubs displayed a positive relationship with fine root biomass of shrubs and herbs, while the richness of shrubs was negatively related to total and absorptive fine root biomass of trees. For the deep soil water utilization in the dry season and its plasticity between seasons, the soil bulk density and water content were the major abiotic factors (Figure 6A), which contributed 32.7% and 26.2% variations in these factors; the dominance and evenness of shrubs, and the richness of herbs were the major biotic factors (Figure 6B), which contributed 16.0%, 13.3% and 12.5% variations in these factors. For details, soil bulk density and water content were negatively correlated with deep soil water utilization in the dry season and its plasticity between seasons amongst life forms; dominance and evenness of shrubs was positively related to deep soil water utilization of trees and its seasonal plasticity, while the richness of herbs was positively associated with the deep soil water utilization of shrubs as well as its seasonal plasticity (Table S1).

4 Discussion

4.1 Deep fine root biomass and water utilization amongst life forms

We found trees and shrubs distributed more fine roots than herbs in deep soil. Though the proportion of total deep fine root biomass in trees and shrubs was not significant, trees had higher proportion of absorptive fine root biomass than shrubs in deep soil. Generally, absorptive roots can make more efficient use of soil resources due to the thinner diameter and thus occupying a dominant position in total length and surface area of root (Guo et al., 2004). That is, trees can effectively improve deep soil nutrient absorption efficiency by increasing root branching capacity

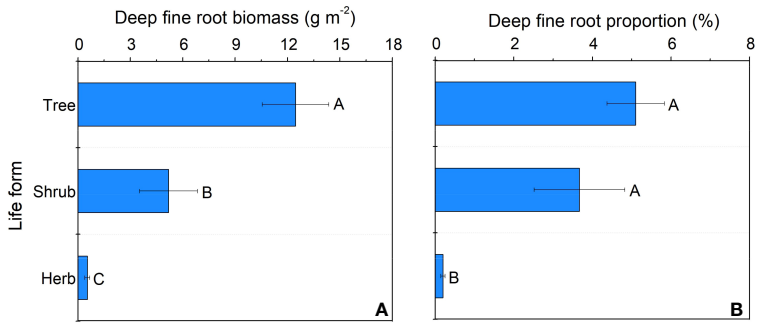

FIGURE 2
Deep fine root biomass **(A)** and proportion **(B)** for different life forms. Different letters represent significant differences in deep fine root biomass or proportion across life forms.

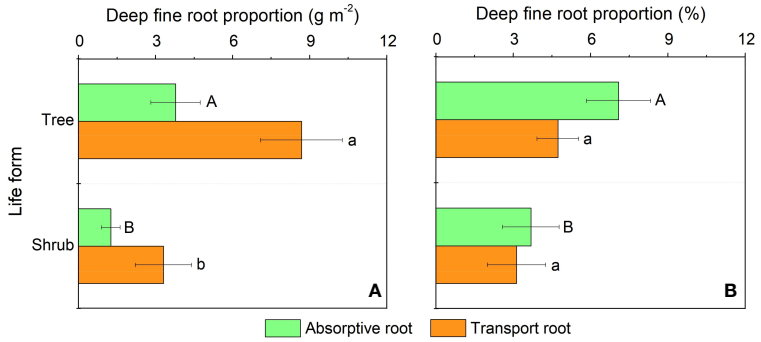

FIGURE 3
Biomass **(A)** and proportion **(B)** of the absorptive and transport fine root biomass for trees and shrubs in deep soil layer. Different uppercase and lowercase letters represent significant differences in deep fine root proportion for absorptive and transport fine root between trees and shrubs, respectively.

(increase the proportion of absorptive roots) and thus adapt to the limited soil conditions (Liu et al., 2015; Li et al., 2017). This might be a key strategy for overstory trees to avoid competing with understory vegetations for limited surface soil resources. Moreover, the proportion of deep fine root biomass (below 1 m depth) is only 0.2-5.1%, but their proportion of deep soil water utilization can reach 20.9-38.6% in the dry season, which highlight the importance of deep fine root in plant drought resistance.

In our study, we found that trees and understory vegetations had contrast deep water use strategies. For details, trees have a significant deep soil water reliance throughout the year (especially with the addition of water source from 60-100 cm soil layer; Figures 4, S3), and thus had low seasonal plasticity of deep soil water use. In contrast, shrubs and herbs are less dependent on deep soil moisture during the wet season but highly dependent on deep soil moisture during the dry season, and thus had high plasticity of deep soil water reliance. This might be because trees have more fine roots distributed in deep soil layer than understory vegetations, and fine roots in the deep soil would increase the diameter of stele and xylem conduits to and thereby minimizing flow resistance and maximizing water absorption efficiency (Pate et al., 1995; Pate et al., 1998; McElrone et al., 2004). Moreover, trees tend to have higher proportions of absorptive fine roots in deep soil layer than those of shrubs. Considering that the deep soil is less fertile than the shallow soil (Jobbagy and Jackson, 2001; Jobbagy and Jackson, 2004), trees can improve their deep soil nutrient absorption efficiency by increasing their branching capacity of absorptive fine roots in the deep soil. Compared with trees, understory vegetations had greater seasonal plasticity in deep soil water utilization. This may be due to the fact that the volume of trees was larger and therefore they are more resistant to droughts than understory vegetations. Since the water storage capacity in stems of trees was larger and thus could more efficiently buffer the daily fluctuation and decrease of leaf water potential with soil drying (Chapotin et al., 2006; Oliva Carrasco et al., 2015), and their large horizontal area for root foraging can to some extent compensate for the decrease in shallow soil moisture content (Meinzer et al., 1999). Second, the seasonal plasticity of shrubs and herbs was closely correlated with fine root biomass of trees and shrubs (Figure 6), which indicated that the important role of hydraulic lift. Also, the high deep water use plasticity of shrubs and herbs suggests that they are good at utilizing shallower soil moisture that is briefly replenished by dry season precipitation, while trees tend to rely on deeper soil moisture which is more stable over time (Cui et al., 2017).

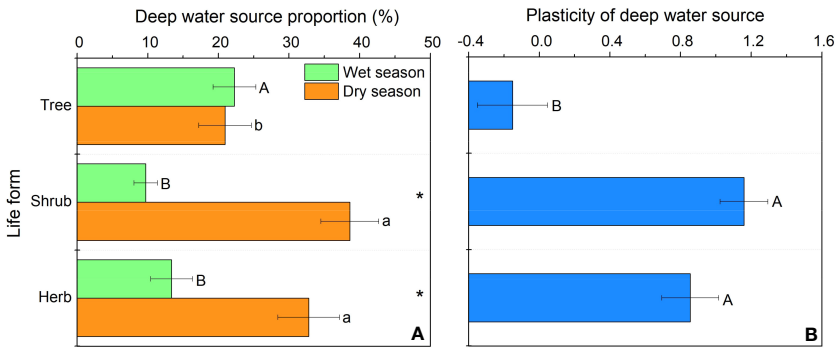

FIGURE 4
Deep soil water utilization in the wet and dry season **(A)** and its seasonal plasticity **(B)** for different life forms. In **(A)** different uppercase and lowercase letters represent significant differences in deep soil water utilization during the wet or dry season across life forms, respectively; in **(B)** different letters represent significant differences in seasonal plasticity of deep soil water use across life forms.

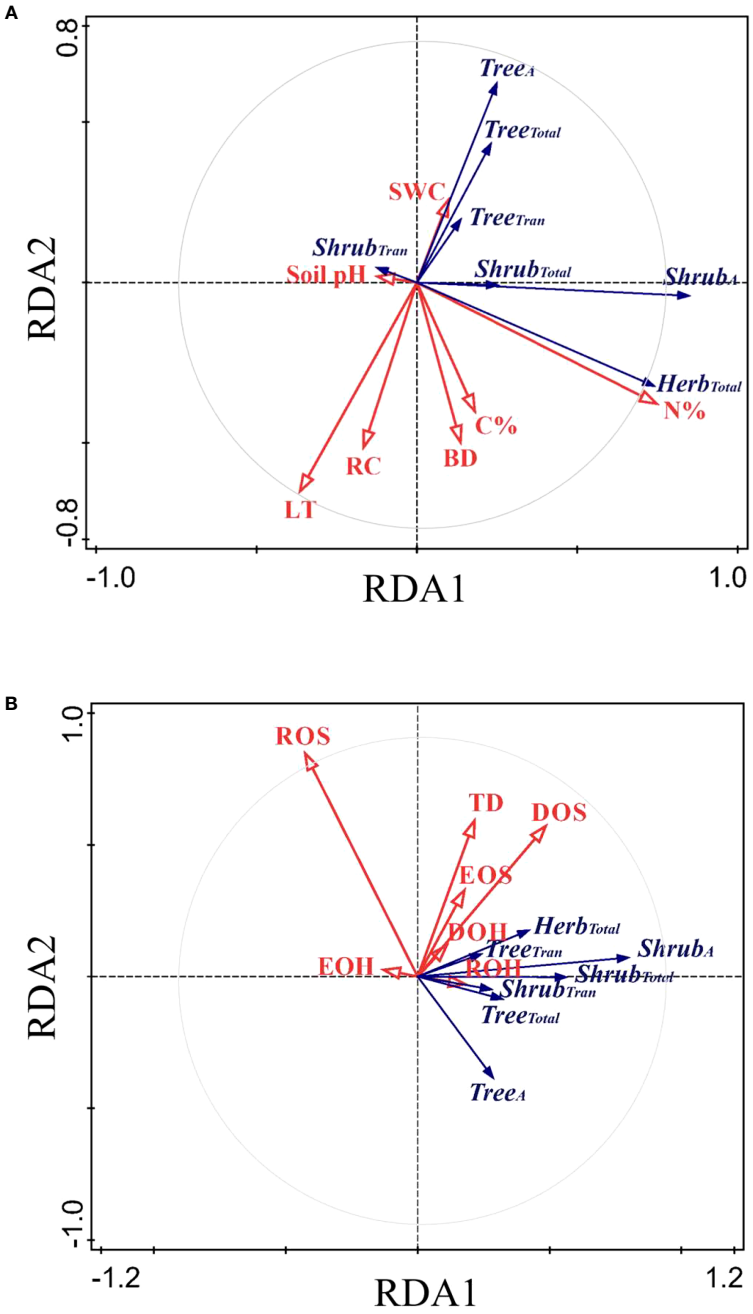

FIGURE 5
RDA-ordination biplot for the fine root biomass of deep soil layer amongst life forms and abiotic factors **(A)** and biotic factors **(B)**. $Tree_A$/$Shrub_A$, absorptive fine root biomass of trees/shrubs; $Tree_{Tran}$/$Shrub_{Tran}$, transport fine root biomass of trees/shrubs; $Tree_{Total}$/$Shrub_{Total}$/$Herb_{Total}$, total fine root biomass of trees/shrubs/herbs; LT, light transmission; C%, total soil carbon content in subsoil layer; N%, total nitrogen content in subsoil layer; RC, rock fragment content in deep soil layer; BD, soil bulk density in deep soil layer; SWC, soil water content in deep soil layer; pH, soil pH in deep soil layer. The same below.

4.2 Determining factors of fine root and water utilization in deep soil layer amongst life forms

We found that the distribution of deep fine root biomass was closely associated with soil nutrient content. This may be because when the availability of soil resources increases, the carbon allocated to the belowground part would increase, and fine roots can increase the absorption capacity of water and nutrients in soil by changing root morphological characteristics (Curt and Prévosto, 2003). Generally, the fine root biomass of understory vegetations (especially the shallow layer) increased with light transmission (Matjaž and Primož, 2010; Noguchi et al., 2021), and thus the competition between overstorey and understory vegetations would intensify. Therefore, we discovered that the fine root biomass of trees in deep soil layer was negatively related to the light

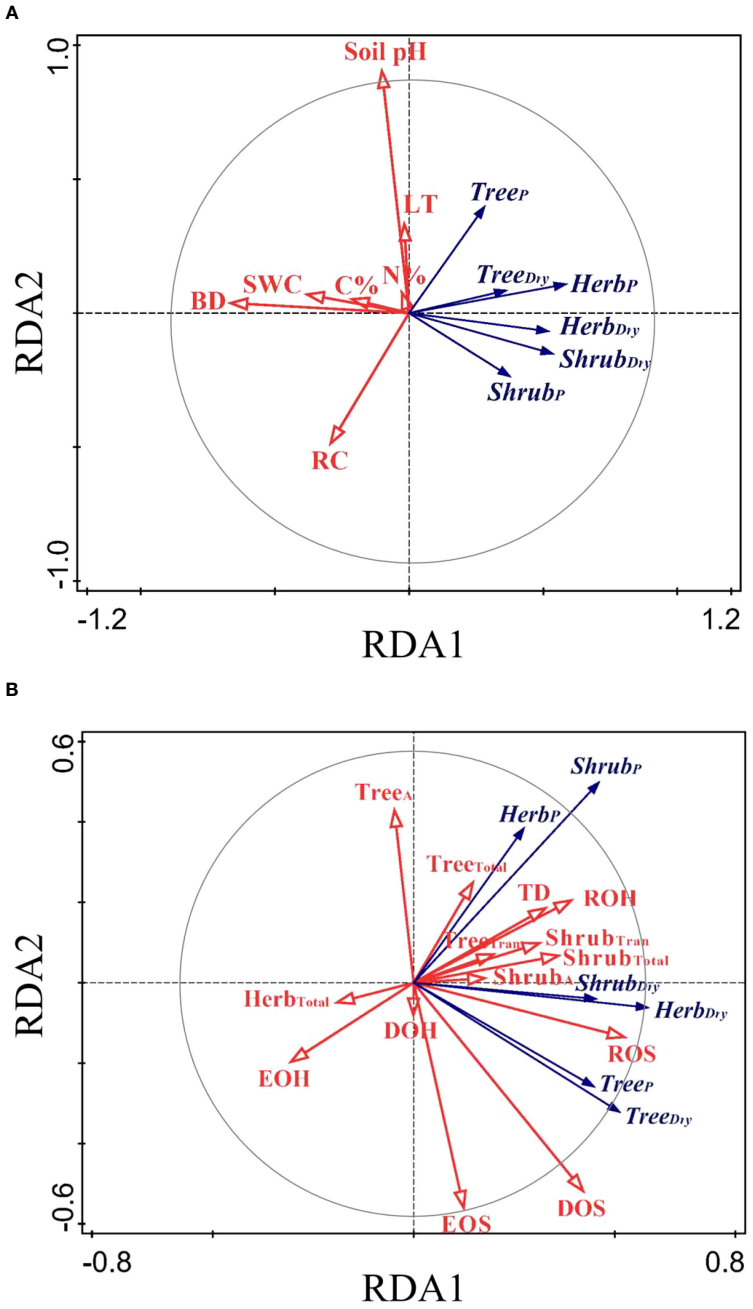

FIGURE 6
RDA-ordination biplot for deep soil water utilization and its seasonal plasticity amongst life forms and abiotic factors **(A)** and biotic factors **(B)**. $Tree_{Dry}$/$Shrub_{Dry}$/$Herb_{Dry}$, deep soil water utilization of trees/shrubs/herbs in the dry season; $Tree_P$/$Shrub_P$/$Herb_P$, seasonal plasticity in deep soil water utilization of trees/shrubs/herbs; TD, tree density; DOS/DOH, dominance of shrubs/herbs; ROS/ROH, richness of shrubs/herbs; EOS/EOH, evenness of shrubs/herbs.

transmission. We also found that the fine root biomass of trees displayed a negative correlation with rock fragment content, which may be explained by that the existence of rock fragments could reduce soil hydraulic conductivity and water retention capacity and therefore decrease the soil water availability for plants (Novák and Knava, 2012). However, previous studies also shown that rock fragments can serve as reservoirs for plants and water conservation was found to be better in rocky soils under moderate water stress conditions (Danalatos et al., 1995; Tetegan et al., 2015). The reason for these contrast results may be that rock fragments had a positive effect on plant growth and water consumption below a certain threshold, and therefore it is necessary to optimize the rock fragment content when evaluating water relations of plants in rocky ecosystems (Mi et al., 2016). In our study, the deep soil water utilization of plants increased with the decrease of deep soil water content. Similarly, the shallow soil water content was found to remain low and the deep soil moisture showed a downward trend in previous studies, which indicated that plants

increase the deep soil water utilization to ensure growth in the dry season (Jia and Shao, 2014; Cao et al., 2018; Li et al., 2021). Also, deep soil bulk density was negatively related to the deep soil water utilization of plants, which was mainly due to high mechanical could restrict the elongation and proliferation of root (Szota et al., 2007; McIvor et al., 2014; Miyatani et al., 2016).

Our results showed that the main biotic determining factors of the distribution of deep fine root biomass were the dominance and richness of shrubs (Figure 5B). In our study, the biomass of fine roots of shrubs displayed a positive correlation with shrub dominance. However, the absorptive and total fine root biomass of trees were negatively related to the richness of shrubs, indicating that deep fine root biomass of trees decreased due to intense competition with shrubs. Our results showed that the main biotic factors affecting the distribution of deep soil water utilization were the dominance and evenness of shrubs, and the richness of herbs (Figure 6B). Also, deep soil water utilization of trees could increase the dominance of shrubs, and that of shrubs could increase the richness of herbs in our study (Figure 6, Table S1). Similarly, previous studies showed that trees likely influence local resource availability (e.g. light, soil) and serve as a biotic filter in the understory community assembly (Jiang et al., 2018b; Luo et al., 2019). This might because the plots with higher deep soil water utilization of trees increased the probability of hydraulic uplift, and therefore the companion shrubs could obtain more water resource, thus increasing the dominance of shrubs. Similarly, the plots with higher deep soil water utilization of shrubs could also enhance the probability of the deep soil water being lifted and released into the surface soil, which could provide more water resources for shallow-rooted herb plants. This induced the enrichment of shallow-rooted herbs in the areas of hydraulic uplift to some extent, thus improving the richness of herbs in these regions (Maestre et al., 2003; Šenfeldr et al., 2016). Moreover, the plots with deep soil water utilization of trees (or shrubs) meant that shallow soil water consumption was more severe and the competition of water resource between different life forms was more intense. Therefore, the positive relationships between deep soil water utilization of trees and the dominance of shrubs and between deep soil water utilization of shrubs and the richness of herbs indicated that shrubs and herbs exhibited different "strategy" in response to competition. For details, shrubs exhibited a "conservative strategy" and tend to increase individual competitiveness and could maximize their resource acquisition in habitats with little disturbance. In contrast, herbs exhibited an "opportunistic strategy" and tend to increase variety and quantity to adapt to the competition and could survive in habitats with frequent disturbance. Our results highlighted the roles of deep soil water utilization in shaping community assembly as well as the necessary of linking biodiversity to ecosystem function (Schwartz et al., 2000; Dudgeon, 2010).

In our study, the explanation degree of RDA ordination biplot was only *c.* 30%, which was relatively low. This may be explained by that the traits we didn't measure (e.g. photosynthetic related properties, traits related to plant's water status), could further play important roles in determining the deep fine root and water utilization and thus the community assembly. Compared with shallow root, deep fine roots have larger diameters and higher tissue density and thus require more carbon investment (Prieto et al., 2015; Fort et al., 2017). Therefore, deep roots should be more closely related to physiological functions such as photosynthesis. Also, plant deep soil water utilization should be closely correlated with stomatal conductance and transpiration rate, since capturing and pumping from deeper soil required more energy (through root pressure) than extracting shallow soil water (Ksenzhek and Volkov, 1998; Wu et al., 2021). Similarly, plant water uptake was found to be closely associated with stomatal conductance, transpiration rate, and stomatal density (Romero-Aranda et al., 2001; Hepworth et al., 2016). This can also explain the positive correlation between light transmission and deep soil water utilization. Previous studies proposed that root hydraulics (instead of root length) could determine the water consumption of crops (Vadez, 2014; Cai et al., 2022), since root conductance synthesizes the effects of the architecture, length, and anatomy of root (Doussan et al., 2006; Strock et al., 2021). Similarly, our previous studies at the species level in the study area showed a positive correlation between deep water utilization and stem hydraulic conductance (Jiang et al., 2020a). Also, recent studies have showed that water uptake depth was coordinated with leaf economic spectrum in water-limited ecosystems (Pivovaroff et al., 2021; Illuminati et al., 2022). Therefore, future studies on plant water use should also focus on plant physiological properties (e.g photosynthetic related properties, hydraulic related properties) and economic spectrum traits.

5 Conclusion

Our results provide new insights into the different deep fine root distribution and water use strategies between trees and understory vegetations and improve our understandings of plants adaptations to variations in the forest hydrologic cycle and thus the community assembly processes. Although the proportion of deep fine roots (below 1 m depth) is only 0.2-5.1%, their proportion of deep soil utilization can reach 20.9-38.6% in the dry season, which highlight the roles of deep fine root in drought resistance. Compared with understory vegetations, trees had a significant deep soil water reliance throughout the year and distributed a higher proportion of absorptive roots in deep soil layer. This indicated that trees could improve deep soil water capture capacity by enhancing their dominance in occupying deep soil volume, and enhance their deep resource foraging by increasing their branching capacity of absorptive roots. Moreover, shrubs and herbs showed different strategies for deep water competition: shrubs and herbs exhibited different "strategy" in response to competition: shrubs exhibited a "conservative" strategy and tend to increase individual competitiveness, while herbs exhibited an "opportunistic" strategy and tend to increase variety and quantity to adapt to the competition. Due to the low interpretation rate of RDA ordination biplot, we assumed that traits we didn't measure might further play important roles in determining the deep fine root and water utilization and thus the community assembly. Future studies on deep fine root and water use patterns should also focus on plant

physiological properties (e.g photosynthetic related properties, hydraulic related properties) and economic spectrum traits.

Data availability statement

The original contributions presented in the study are included in the article/Supplementary Material. Further inquiries can be directed to the corresponding authors.

Author contributions

PJ: Funding acquisition, Investigation, Methodology, Software, Writing – original draft, Writing – review & editing. JY: Investigation, Writing – review & editing. RL: Investigation, Writing – review & editing. XZ: Methodology, Writing – review & editing. SF: Funding acquisition, Methodology, Writing – review & editing.

Funding

This work was funded by the National Natural Science Foundations of China (32201520), the Survey of Herbaceous Plant Germplasm Resources of Shandong Province Grant No. [[2021]01], and the Shandong Provincial Natural Science Foundation, China (ZR2021QC051).

Conflict of interest

The authors declare that the research was conducted in the absence of any commercial or financial relationships that could be construed as a potential conflict of interest.

Publisher's note

Supplementary material

The Supplementary Material for this article can be found online at: https://www.frontiersin.org/articles/10.3389/fpls.2023.1275464/full#supplementary-material

References

Achat, D. L., Bakker, M. R., and Trichet, P. (2008). Rooting patterns and fine root biomass of *Pinus pinaster* assessed by trench wall and core methods. *J. For. Res.* 13, 165–175. doi: 10.1007/s10310-008-0071-y

Adams, H. D., Zeppel, M. J. B., Anderegg, W. R. L., Hartmann, H., Landhäusser, S. M., Tissue, D. T., et al. (2017). A multi-species synthesis of physiological mechanisms in drought-induced tree mortality. *Nat. Ecol. Evol.* 1, 1285–1291. doi: 10.1038/s41559-017-0248-x

Allen, C. D., Macalady, A. K., Chenchouni, H., Bachelet, D., McDowell, N., Vennetier, M., et al. (2010). A global overview of drought and heat-induced tree mortality reveals emerging climate change risks for forests. *Forest Ecol. Manag.* 259, 660–684. doi: 10.1016/j.foreco.2009.09.001

Barnard, R. L., Bello, F. D., Gilgen, A. K., and Buchmann, N. (2006). The $\delta^{18}O$ of root crown water best reflects source water $\delta^{18}O$ in different types of herbaceous species. *Rapid Commun. Mass Sp.* 20, 3799–3802. doi: 10.1002/rcm.2778

Barron-Gafford, G. A., Knowles, J. F., Sanchez-Cañete, E. P., Minor, R. L., Lee, E., Sutter, L., Scott, R. L., et al. (2021). Hydraulic redistribution buffers climate variability and regulates grass-tree interactions in a semiarid riparian savanna. *Ecohydrology* 14, e2271. doi: 10.1002/eco.2271

Cai, G., Ahmed, M. A., Abdalla, M., and Carminati, A. (2022). Root hydraulic phenotypes impacting water uptake in drying soils. *Plant Cell Environ.* 45, 650–663. doi: 10.1111/pce.14259

Cao, R., Jia, X., Huang, L., Zhu, Y., Wu, L., and Shao, M. (2018). Deep soil water storage varies with vegetation type and rainfall amount in the Loess Plateau of China. *Sci. Rep.* 8, 12346. doi: 10.1038/s41598-018-30850-7

Cardinael, R., Mao, Z., Prieto, I., Stokes, A., Dupraz, C., Kim, J. H., et al. (2015). Competition with winter crops induces deeper rooting of walnut trees in a Mediterranean alley cropping agroforestry system. *Plant Soil* 391, 219–235. doi: 10.1007/s11104-015-2422-8

Carrière, S. D., Ruffault, J., Cakpo, C. B., Olioso, A., Doussan, C., Simioni, G., et al. (2020a). Intra-specific variability in deep water extraction between trees growing on a Mediterranean karst. *J. Hydrol.* 590, 125428. doi: 10.1016/j.jhydrol.2020.125428

Carrière, S. D., Ruffault, J., Pimont, F., Doussan, C., Simioni, G., Chalikakis, K., et al. (2020b). Impact of local soil and subsoil conditions on inter-individual variations in tree responses to drought: insights from Electrical Resistivity Tomography. *Sci. Total Environ.* 698, 134247. doi: 10.1016/j.scitotenv.2019.134247

Chapotin, S. M., Razanameharizaka, J. H., and Holbrook, N. M. (2006). Water relations of baobab trees (*Adansonia* spp. L.) during the rainy season: does stem water buffer daily water deficits? *Plant Cell Environ.* 29, 1021–1032. doi: 10.1111/j.1365-3040.2005.01456.x

Chen, Y.-J., Cao, K.-F., Schnitzer, S. A., Fan, Z.-X., Zhang, J.-L., and Bongers, F. (2014). Water-use advantage for lianas over trees in tropical seasonal forests. *New Phytol.* 205, 128–136. doi: 10.1111/nph.13036

Cui, Y.-Q., Ma, J.-Y., Feng, Q., Sun, J.-H., and Sun, W. (2017). Water sources and water-use efficiency of desert plants in different habitats in Dunhuang, NW China. *Ecol. Res.* 32, 243–258. doi: 10.1007/s11284-017-1433-8

Curt, T., and Prévosto, B. (2003). Rooting strategy of naturally regenerated beech in silver birch and Scots pine woodlands. *Plant Soil* 255, 265–279. doi: 10.1023/A:1026132021506

Danalatos, N. G., Kosmas, C. S., Moustakas, N. C., and Yassouglou, N. (1995). Rock fragments II Their impact on soil physical properties and biomass production under Mediterranean conditions. *Soil Use Manage.* 11, 121–126. doi: 10.1016/0148-9062(96)85003-0

Ding, Y., Nie, Y., Schwinning, S., Chen, H., Yang, J., Zhang, W., et al. (2018). A novel approach for estimating groundwater use by plants in rock-dominated habitats. *J. Hydrol.* 565, 760–769. doi: 10.1016/j.jhydrol.2018.08.033

Diochon, A., Kellman, L., and Beltrami, H. (2009). Looking deeper: an investigation of soil carbon losses following harvesting from a managed northeastern red spruce (*Picea rubens Sarg.*) forest chronosequence. *For. Ecol. Manage.* 257, 413–420. doi: 10.1016/j.foreco.2008.09.015

Doussan, C., Pierret, A., Garrigues, E., and Pagès, L. (2006). Water uptake by plant roots: ii—modelling of water transfer in the soil root-system with explicit account of flow within the root system—comparison with experiments. *Plant Soil* 283, 99–117. doi: 10.1007/s11104-004-7904-z

Dudgeon, D. (2010). Prospects for sustaining freshwater biodiversity in the 21st century: linking ecosystem structure and function. *Curr. Opin. Env. Sust.* 2, 422–430. doi: 10.1016/j.cosust.2010.09.001

Eggemeyer, K. D., Awada, T., Harvey, F. E., Wedin, D. A., Zhou, X. H., and Zanner, C. W. (2009). Seasonal changes in depth of water uptake for encroaching trees *Juniperus virginiana* and *Pinus ponderosa* and two dominant C_4 grasses in a semiarid grassland. *Tree Physiol.* 29, 157–169. doi: 10.1093/treephys/tpn019

Ehleringer, J. R., and Dawson, T. E. (1992). Water uptake by plants: perspectives from stable isotope composition. *Plant Cell Environ.* 15, 1073–1082. doi: 10.1111/j.1365-3040.1992.tb01657.x

Fort, F., Volaire, F., Guilioni, L., Barkaoui, K., Navas, M. L., and Roumet, C. (2017). Root traits are related to plant water-use among rangeland Mediterranean species. *Funct. Ecol.* 31, 1700–1709. doi: 10.1111/1365-2435.12888

Frazer, G. W., Canham, C. D., and Lertzman, K. P. (1999). *Gap light analyzer (GLA), version 2.0: imaging software to extract canopy structure and gap light transmission indices from true-color fisheye photographs* (Millbrook, New York: Copyright 1999: Simon Fraser University, Burnaby, BC, and the Institute of Ecosystem Studies). Available at: http://www.rem.sfu.ca/forestry/index.htmhttp://www.ecostudies.org.

Gargiulo, L., Mele, G., and Terribile, F. (2016). Effect of rock fragments on soil porosity: a laboratory experiment with two physically degraded soils. *Eur. J. Soil Sci.* 67, 597–604. doi: 10.1111/ejss.12370

Gulihanati, B., Chang, L., Li, H., Bahejiavinaer, T., and Zhang, Y. (2022). Differences in water sources of four main shrubs of Tianshan Mountains in summer. *Acta Ecol. Sin.* 42, 5471–5480. doi: 10.5846/stxb202102030366

Guo, D., Mitchell, R. J., and Hendricks, J. J. (2004). Fine root branch orders respond differentially to carbon source-sink manipulations in along leaf pine forest. *Oecologia* 140, 450–457. doi: 10.1007/s00442-004-1596-1

Hepworth, C., Turner, C., Landim, M. G., Cameron, D., and Gray, J. E. (2016). Balancing water uptake and loss through the coordinated regulation of stomatal and root development. *PLoS One* 11, e0156930. doi: 10.1371/journal.pone.0156930

Illuminati, A., Querejeta, J. I., Pías, B., Escudero, A., and Matesanz, S. (2022). Coordination between water uptake depth and the leaf economic spectrum in a Mediterranean shrubland. *J. Ecol.* 110, 1844–1856. doi: 10.1111/1365-2745.13909

Jia, Y., and Shao, M. (2014). Dynamics of deep soil moisture in response to vegetational restoration on the Loess Plateau of China. *J. Hydrology* 519, 523–531. doi: 10.1016/j.jhydrol.2014.07.043

Jiang, P., Chen, N., Zhang, X., Yan, H., Chen, Y., and Fan, S. (2023). Functional traits and its variation linked to species' degree of isohydry in subtropical regions with high heterogeneity. *Plant Soil* 482, 277–296. doi: 10.1007/s11104-022-05688-8

Jiang, Z., Ma, K., Liu, H., and Tang, Z. (2018b). A trait-based approach reveals the importance of biotic filter for elevational herb richness pattern. *J. Biogeogr.* 45, 2288–2298. doi: 10.1111/jbi.13398

Jiang, P., Meinzer, F. C., Wang, H., Kou, L., Dai, X., and Fu, X. (2020a). Belowground determinants and ecological implications of shrub species' degree of isohydry in subtropical pine plantations. *New Phytol.* 226, 1656–1666. doi: 10.1111/nph.16502

Jiang, P., Wang, H., Fu, X., Dai, X., Kou, L., and Wang, J. (2018a). Elaborate differences between trees and understory plants in the deployment of fine roots. *Plant Soil* 431, 433–447. doi: 10.1007/s11104-018-3778-3

Jiang, P., Wang, H., Meinzer, F. C., Kou, L., Dai, X., and Fu, X. (2020b). Linking reliance on deep soil water to resource economy strategies and abundance among coexisting understorey shrub species in subtropical pine plantations. *New Phytol.* 225, 222–233. doi: 10.1111/nph.16027

Jobbagy, E., and Jackson, R. B. (2001). The distribution of soil nutrients with depth: Global patterns and the imprint of plants. *Biogeochemistry* 53, 51–77. doi: 10.2307/1469627

Jobbagy, E. G., and Jackson, R. B. (2004). The uplift of soil nutrients by plants: biogeochemical consequences across scales. *Ecology* 85, 2380–2389. doi: 10.2307/3450236

Klinka, K., Green, R. N., Trowbridge, R. L., et al. (1981). Taxonomic classification of humus forms in ecosystems of British Columbia: first approximation. Land Management Report 8. *J. Ecol.* 70, 566–575. doi: 10.2307/2259944

Kong, F., Yu, R., Xu, Z., and Zhou, M. (2012). Application of excel in calculation of biodiversity indices. *Mar. Sci.* 36, 57–62.

Ksenzhek, O. S., and Volkov, A. G. (1998). Plant energetics (Elsevier Inc.). New York, USA: Academic Press 243–266. doi: 10.1016/B978-012427350-4/50012-1

Le Roux, X., Bariac, T., and Mariotti, A. (1995). Spatial partitioning of the soil water resource between grass and shrub components in a West African humid savanna. *Oecologia* 104, 147–155. doi: 10.1007/BF00328579

Li, H., Liu, B., McCormack, M. L., Ma, M., and Guo, D. (2017). Diverse belowground resource strategies underlie plant species coexistence and spatial distribution in three grasslands along a precipitation gradient. *New Phytol.* 216, 1140–1150. doi: 10.1111/nph.14710

Li, B., Zhang, W., Li, S., Wang, J., Liu, G., and Xu, M. (2021). Severe depletion of available deep soil water induced by revegetation on the arid and semiarid Loess Plateau. *For. Ecol. Manage.* 491, 119156. doi: 10.1016/j.foreco.2021.119156

Liu, Y., Gao, G., Wang, D., Jiao, L., Li, Z., Tian, L., et al. (2023). Water use characteristics of *Robinia pseudoacacia* plantations under different thinning intensities in the loess hilly region. *Acta Ecol. Sin* 303, 2845–2855. doi: 10.5846/stxb202204221107

Liu, B., Li, H., Zhu, B., Koide, R. T., Eissenstat, D. M., and Guo, D. (2015). Complementarity in nutrient foraging strategies of absorptive fine roots and arbuscular mycorrhizal fungi across 14 coexisting subtropical tree species. *New Phytol.* 208, 125–136. doi: 10.1111/nph.13434

Love, D., Venturas, M., Sperry, J., Brooks, P., Pettit, J. L., Wang, Y., et al. (2019). Dependence of aspen stands on a subsurface water subsidy: Implications for climate change impacts. *Water Resour. Res.* 55, 1833–1848. doi: 10.1029/2018WR023468

Luo, Y.-H., Cadotte, M. W., Burgess, K. S., Liu, J., Tan, S.-L., Xu, K., et al. (2019). Forest community assembly is driven by different strata-dependent mechanisms along an elevational gradient. *J. Biogeogr.* 46, 2174–2187. doi: 10.1111/jbi.13669

Maestre, F. T., Bautista, S., and Cortina, J. (2003). Positive, negative, and net effects in grass-shrub interactions in mediterranean semiarid grasslands. *Ecology* 84, 3186–3197. doi: 10.1890/02-0635

Matjaž, Č., and Primož, S. (2010). Root distribution of under-planted European beech (*Fagus sylvatica* L.) below the canopy of a mature Norway spruce stand as a function of light. *Eur. J. For. Res.* 129 (4), 531–539. doi: 10.1007/s10342-009-0352-9

McElrone, A. J., Pockman, W. T., Martínez-Vilalta, J., and Jackson, R. B. (2004). Variation in xylem structure and function in stems and roots of trees to 20 m depth. *New Phytol.* 163, 507–517. doi: 10.2307/1514454

McIvor, I. R., Sloan, S., and Pigem, L. R. (2014). Genetic and environmental influences on root development in cuttings of selected Salix and Populus clones–a greenhouse experiment. *Plant Soil* 377, 25–42. doi: 10.1007/s11104-013-1770-5

Meinzer, F. C., Andrade, J. L., Goldstein, G., Holbrook, M. N., Cavelier, J., and Wright, S. J. (1999). Partitioning of soil water among canopy trees in a seasonally dry tropical forest. *Oecologia* 121, 293–301. doi: 10.1007/s004420050931

Mi, M., Shao, M., and Liu, B. (2016). Effect of rock fragments content on water consumption, biomass and water-use efficiency of plants under different water conditions. *Ecol. Eng.* 94, 574–582. doi: 10.1016/j.ecoleng.2016.06.044

Miyatani, K., Mizusawa, Y., Okada, K., Tanikawa, T., Makita, N., and Hirano, Y. (2016). Fine root traits in *Chamaecyparis obtusa* forest soils with different acid buffering capacities. *Trees-Struct. Funct.* 30, 415–429. doi: 10.1007/s00468-015-1291-3

Moreira, M. Z., Sternberg, L. D. L., and Nepstad, D. C. (2000). Vertical patterns of soil water uptake by plants in a primary forest and an abandoned pasture in the eastern Amazon: an isotopic approach. *Plant Soil* 222, 95–107. doi: 10.1023/A:1004773217189

Nie, Y. P., Chen, H. S., Wang, K. L., Tan, W., Deng, P. Y., and Yang, J. (2011). Seasonal water use patterns of woody species growing on the continuous dolostone outcrops and nearby thin soils in subtropical China. *Plant Soil* 341, 399–412. doi: 10.1007/s11104-010-0653-2

Noguchi, K., Matsuura, Y., Morishita, T., Toriyama, J., and Kim, Y. (2021). Fine root growth of black spruce trees and understory plants in a permafrost forest along a north-facing slope in Interior Alaska. *Front. Plant Sci.* 12. doi: 10.3389/fpls.2021.769710

Novák, V., and Knava, K. (2012). The influence of stoniness and canopy properties on soil water content distribution: simulation of water movement in forest stony soil. *Eur. J. For. Res.* 131, 1727–1735. doi: 10.1007/s10342-011-0589-y

Oliva Carrasco, L., Bucci, S. J., Di Francescantonio, D., Lezcano, O. A., Campanello, P. I., Scholz, F. G., et al. (2015). Water storage dynamics in the main stem of subtropical tree species differing in wood density, growth rate and life history traits. *Tree Physiol.* 35, 354–365. doi: 10.1093/treephys/tpu087

Pabin, J., Lipiec, J., Wlodek, S., Biskupski, A., and Kaus, A. (1998). Critical soil bulk density and strength for pea seedling root growth as related to other soil factors. *Soil Till. Res.* 46, 203–208. doi: 10.1016/S0167-1987(98)00098-1

Padilla, F. M., Miranda, J. D., and Pugnaire, F. I. (2007). Early root growth plasticity in seedlings of three Mediterranean woody species. *Plant Soil* 296, 103–113. doi: 10.1007/s11104-007-9294-5

Pate, J. S., Jeschke, W. D., and Aylward, M. J. (1995). Hydraulic architecture and xylem structure of the dimorphic root systems of South-West Australian species of the Proteaceae. *J. Exp. Bot.* 46, 907–915. doi: 10.1093/jxb/46.8.907

Pate, J. S., Jeschke, W., Dawson, T. E., Raphael, C., Hartung, W., and Bowen, B. J. (1998). Growth and seasonal utilisation of water and nutrients by *Banksia prionotes*. *Aust. J. Bot.* 46, 511–532. doi: 10.1071/BT97045

Phillips, D. L., Newsome, S. D., and Gregg, J. W. (2005). Combining sources in stable isotope mixing models: alternative methods. *Oecologia* 144, 520–527. doi: 10.1007/s00442-004-1816-8

Pivovaroff, A. L., McDowell, N. G., Rodrigues, T. B., Brodribb, T., Cernusak, L. A., Choat, B., et al. (2021). Stability of tropical forest tree carbon-water relations in a rainfall exclusion treatment through shifts in effective water uptake depth. *Global Change Biol.* 27, 6454–6466. doi: 10.1111/gcb.15869

Pregitzer, K. S., DeForest, J. L., Burton, A. J., Allen, M. F., Ruess, R. W., and Hendrick, R. L. (2002). Fine root architecture of nine North American trees. *Ecol. Monogr.* 72, 293–309. doi: 10.1890/0012-9615(2002)072[0293:FRAONN]2.0.CO;2

Prieto, I., Roumet, C., Cardinael, R., Dupraz, C., Jourdan, C., Kim, J. H., et al. (2015). Root functional parameters along a land-use gradient: evidence of a community-level economics spectrum. *J. Ecol.* 103, 361–373. doi: 10.1111/1365-2745.12351

Querejeta, J. I., Estrada-Medina, H., Allen, M. F., and Jimenez-Osornio, J. J. (2007). Water source partitioning among trees growing on shallow karst soils in a seasonally dry tropical climate. *Oecologia* 152, 26–36. doi: 10.1007/s00442-006-0629-3

Quesada, C. A., Hodnett, M. G., Breyer, L. M., Santos, A. J. B., Andrade, S., Miranda, H. S., et al. (2008). Seasonal variations in soil water in two woodland savannas of central Brazil with different fire histories. *Tree Physiol.* 28, 405–415. doi: 10.1093/treephys/28.3.405

Ripullone, F., Camarero, J. J., Colangelo, M., and Voltas, J. (2020). Variation in the access to deep soil water pools explains tree-to-tree differences in drought-triggered dieback of Mediterranean oaks. *Tree Physiol.* 40, 591–604. doi: 10.1093/treephys/tpaa026

Rolo, V., and Moreno, G. (2012). Interspecific competition induces asymmetrical rooting profile adjustments in shrub-encroached open oak woodlands. *Trees* 26, 997–1006. doi: 10.1007/s00468-012-0677-8

Romero-Aranda, R., Soria, T., and Cuartero, J. (2001). Tomato plant-water uptake and plant-water relationships under saline growth conditions. *Plant Sci.* 160, 265–272. doi: 10.1016/S0168-9452(00)00388-5

Schall, P., Lödige, C., Beck, M., and Ammer, C. (2012). Biomass allocation to roots and shoots is more sensitive to shade and drought in European beech than in Norway spruce seedlings. *For. Ecol. Manage.* 266, 246–253. doi: 10.1016/j.foreco.2011.11.017

Schwartz, M. W., Brigham, C. A., Hoeksema, J. D., Lyons, K. G., Mills, M. H., and van Mantgem, P. J. (2000). Linking biodiversity to ecosystem function: implications for conservation ecology. *Oecologia* 122, 297–305. doi: 10.1007/s004420050035

Schwinning, S. (2010). The ecohydrology of roots in rocks. *Ecohydrology* 3, 238–245. doi: 10.1002/eco.134

Šenfeldr, M., Urban, J., Maděra, P., and Kučera, J. (2016). Redistribution of water via layering branches between connected parent and daughter trees in Norway spruce clonal groups. *Trees* 30, 5–17. doi: 10.1007/s00468-015-1157-8

Strock, C. F., Burridge, J. D., Niemiec, M. D., Brown, K. M., and Lynch, J. P. (2021). Root metaxylem and architecture phenotypes integrate to regulate water use under drought stress. *Plant Cell Environ.* 44, 49–67. doi: 10.1111/pce.13875

Sun, T., Dong, L., Mao, Z., and Li, Y. (2015). Fine root dynamics of trees and understorey vegetation in a chronosequence of *Betula platyphylla* stands. *For. Ecol. Manage.* 346, 1–9. doi: 10.1016/j.foreco.2015.02.035

Szota, C., Veneklaas, E. J., Koch, J. M., and Lambers, H. (2007). Root architecture of jarrah (*Eucalyptus marginata*) trees in relation to post-mining deep ripping in Western Australia. *Restor. Ecol.* 15, 65–73. doi: 10.1111/j.1526-100X.2007.00294.x

Tetegan, M., Korboulewsky, N., Bouthier, A., Samouëlian, A., and Cousin, I. (2015). The role of pebbles in the water dynamics of a stony soil cultivated with young poplars. *Plant Soil* 391, 307–320. doi: 10.1007/s11104-015-2429-1

Vadez, V. (2014). Root hydraulics: the forgotten side of roots in drought adaptation. *Field Crops Res.* 165, 15–24. doi: 10.1016/j.fcr.2014.03.017

Valladares, F., and Pearcy, R. W. (2002). Drought can be more critical in the shade than in the sun: a field study of carbon gain and photo-inhibition in a Californian shrub during a dry El Nino year. *Plant Cell Environ.* 25, 749–759. doi: 10.1046/j.1365-3040.2002.00856.x

Walker, B. H., and Noy-Meir, I. (1982). Aspects of the stability and resilience of savanna ecosystems. In Ecology of Tropical Savannas. *Ecol. Stud.* 42, 556–590. doi: 10.1007/978-3-642-68786-0

Wang, J., Fu, B. J., Lu, N., and Zhang, L. (2017). Seasonal variation in water uptake patterns of three plant species based on stable isotopes in the semi-arid Loess Plateau. *Sci. Total Environ.* 609, 27–37. doi: 10.1016/j.scitotenv.2017.07.133

Wen, X., Lee, X., Sun, X., Wang, J., Hu, Z., Li, S., et al. (2012). Dew water isotopic ratios and their relationships to ecosystem water pools and fluxes in a cropland and a grassland in China. *Oecologia* 168, 549–561. doi: 10.1007/s00442-011-2091-0

West, A. G., Hultine, K. R., Burtch, K. G., and Ehleringer, J. R. (2007). Seasonal variations in moisture use in a pinion-juniper woodland. *Oecologia* 153, 787–798. doi: 10.1007/s00442-007-0777-0

Wu, Z., Behzad, H. M., He, Q., Wu, C., Bai, Y., and Jiang, Y. (2021). Seasonal transpiration dynamics of evergreen Ligustrum lucidum linked with water source and water-use strategy in a limestone karst area, southwest China. *J. Hydrol.* 597, 126199. doi: 10.1016/j.jhydrol.2021.126199

Wu, X., Niu, Y., Xun, M., Jin, J., Li, N., Tang, Y., et al. (2022). Responses of water source to seasonal drought of dominant afforestation tree species in the loess hilly region of China. *Acta Ecol. Si.* 42, 4101–4112. doi: 10.5846/stxb202106221657

Yang, B., Wen, X., and Sun, X. (2015). Seasonal variations in depth of water uptake for a subtropical coniferous plantation subjected to drought in an East Asian monsoon region. *Agr. For. Meteorol.* 201, 218–228. doi: 10.1016/j.agrformet.2014.11.020

Yang, F., Feng, Z., Wang, H., Dai, X., and Fu, X. (2017). Deep soil waterextraction helps to drought avoidance but shallow soil water uptake during dry season controls the inter-annual variation in tree growth in four subtropical plantations. *Agr. For. Meteorol* 234, 106–114. doi: 10.1016/j.agrformet.2016.12.020

Yu, K. L., and D'Odorico, P. (2015). Hydraulic lift as a determinant of tree–grass coexistence on savannas. *New Phytol.* 207, 1038–1051. doi: 10.1111/nph.13431

Zhu, W., Li, W., Shi, P., Cao, J., Zong, N., and Geng, S. (2021). Intensified interspecific competition for water after afforestation with *Robinia pseudoacacia* into a native shrubland in the Taihang Mountains, Northern China. *Sustainability* 13, 807. doi: 10.3390/su13020807

frontiers | Frontiers in Plant Science

TYPE Original Research
PUBLISHED 21 September 2023
DOI 10.3389/fpls.2023.1254395

OPEN ACCESS

EDITED BY
Qingpeng Yang,
Chinese Academy of Sciences (CAS), China

REVIEWED BY
Xiran Li,
Central China Normal University, China
Jerry Lee Hatfield,
United States Department of Agriculture, United States

*CORRESPONDENCE
Naifeng Lin
1669733424@qq.com
Changxin Zou
zcx@nies.org

†These authors have contributed equally to this work

RECEIVED 07 July 2023
ACCEPTED 01 September 2023
PUBLISHED 21 September 2023

CITATION
Xu X, Liu J, Jiao F, Zhang K, Yang Y, Qiu J, Zhu Y, Lin N and Zou C (2023) Spatial variations and mechanisms for the stability of water use efficiency in China. *Front. Plant Sci.* 14:1254395. doi: 10.3389/fpls.2023.1254395

Spatial variations and mechanisms for the stability of water use efficiency in China

Xiaojuan Xu[1†], Jing Liu[1†], Fusheng Jiao[2], Kun Zhang[1], Yue Yang[1], Jie Qiu[1], Yingying Zhu[1], Naifeng Lin[1*] and Changxin Zou[1*]

[1]Nanjing Institute of Environmental Sciences, MEE, Nanjing, China, [2]School of Geography, Nanjing Normal University, Nanjing, China

A clearer understanding of the stability of water use efficiency (WUE) and its driving factors contributes to improving water use efficiency and strengthening water resource management. However, the stability of WUE is unclear. Based on the EEMD method, this study analyses the spatial variations and mechanisms for the stability of WUE in China, especially in the National Forest Protection Project (NFPP) areas. It is found that the stable WUE was dominated by non-significant trends and increasing trends in China, accounting for 33.59% and 34.19%, respectively. The non-significant trend of stable WUE was mainly located in the Three-North shelterbelt program area, and the increasing trend of stable WUE was in Huaihe and Taihu, Taihang Mountains, and Pearl River shelterbelt program areas. Precipitation and soil moisture promoted the stable WUE in these project areas. The unstable WUE was dominated by positive reversals or negative reversals of WUE trends. The positive reversals of unstable WUE were mainly located in the Yellow River shelterbelt program areas, which was promoted by temperature and radiation, while the negative reversals of unstable WUE were mainly distributed in the Yangtze River and Liaohe shelterbelt program areas, which were mainly induced by saturation water vapor pressure difference (VPD). Our results highlight that some ecological restoration programs need to be improved to cope with the negative climate impact on the stability of WUE.

KEYWORDS

ecological restoration, water use efficiency, climate change, stability, driving factors

1 Introduction

Water use efficiency (WUE) is an objective evaluation index of water-carbon coupling for an ecosystem, which is defined as the ratio of carbon sequences (i.e., gross primary production (GPP)) to water loss (i.e., evapotranspiration (ET)) (Beer et al., 2009; Jiang et al., 2019; Ma J. et al., 2019; Liu et al., 2020). WUE is not only an important index of the coupled terrestrial carbon-water cycle, but also one of the important parameters reflecting the impact of global changes on terrestrial ecosystems (Hatfield and Dold, 2019; Yang L. et al., 2022). Uncovering the changes in the stability of the ecosystem WUE can provide

important technical and policy implications for water conservation and carbon budgets (Cao et al., 2020). A large interannual variable in water use efficiency can lead to the instability of ecosystem functions and pose a serious challenge to nature-based climate solutions (Xue et al., 2015; Zhang et al., 2016; Wang et al., 2022). Thus, spatial variations and mechanisms for water use efficiency stability have become a foregrounded and topical issue for ecosystems.

The interannual variables of WUE are stable in the absence of climate and human drivers of change (Rödenbeck et al., 2018; Piao et al., 2020). However, the driving factors and their interactive effects influence GPP and ET in different ways, making the interannual variables in WUE threaten the stability of WUE (Ma J. et al., 2019). The instability in WUE considerably challenges the sustainability of the carbon-water cycle (Yu et al., 2021). The essence of WUE instability is that WUE has weak resistance to climate fluctuation (Wang et al., 2022). Both climate and ecosystems have obvious spatial differences, thus, WUE trends are nonlinear and their stability has a significant spatial variation (Piao et al., 2020). In areas with severe climate fluctuations or where WUE is sensitive to climate fluctuations, the stability of WUE is usually low (Liu et al., 2017; Ma J. et al., 2019). It provides a rare opportunity to explore the response of ecosystem functioning to climate change (Piao et al., 2020). However, there still exists uncertainty on the WUE stability response to climate change (Belmecheri et al., 2021). Thus, reducing the uncertainty is critical for an accurate future carbon-water cycle and its response to climate change (Belmecheri et al., 2021; Migliavacca et al., 2021).

Previous studies have shown that WUE change is influenced by climate change, such as CO_2, solar radiation, temperature, precipitation, saturated water vapor pressure, and soil moisture (Liu et al., 2020; Gonsamo et al., 2021; Wang M. et al., 2021). Precipitation is one of the principal indirect driving factors affecting WUE variables (Zhang et al., 2020). Precipitation changes directly affect the transpiration and evaporation of the ecosystem, and indirectly affect the carbon uptake process of plants by regulating the soil water content (Piao et al., 2020; Zhang et al., 2020). In addition, drought-induced reduction in vegetation production and WUE was offset by driving factors, such as warming climate and ecological restoration projects (Huang J. et al., 2015; Zhang et al., 2016; Ma J. et al., 2019). Numerous studies have shown that vapor pressure difference (VPD) is a key factor and has been demonstrated to have negative influences on the WUE (Beer et al., 2009; Ma J. et al., 2019). It is revealed that the increase in CO_2 concentration will increase the photosynthetic rate, while the transpiration rate will be weakened or have no significant effect, which will lead to the increase of vegetation WUE, with a significant CO_2 fertilization effect (El Masri et al., 2019; Ma J. et al., 2019; Gonsamo et al., 2021). Both photosynthesis and transpiration are affected by temperature, and show an opposite trend with increasing temperature (Huang J. et al., 2015). When the temperature was low, the photosynthetic rate increased with the increase of temperature, and then gradually weakened after it reached the maximum (Hatfield and Dold, 2019). The main reason was that the enzyme activity was significantly affected when the optimum temperature was reached (Hatfield and Dold, 2019). On the contrary, the increase in temperature will cause an increase in VPD and then increase the transpiration rate of vegetation (Cao et al., 2020). The radiation is one of the important factors of plant photosynthesis, and it also impacts plant WUE (Jiang et al., 2019; Wang et al., 2020). Nevertheless, the driving mechanisms underlying the stability of WUE remain unclear.

The National Forest Protection Project (NFPP) in China is one of the world's largest ecological restoration projects (Tong et al., 2017; Lu et al., 2018; Huang et al., 2019). It is a major initiative by the Chinese government to mitigate some of the environmental damage caused by rapid economic development through the implementation of a rigorous and creative policy of large-scale conservation (Cai et al., 2020; Ding et al., 2021; Xu et al., 2022a). Currently, some researchers believe that the implementation of the NFPP has led to an increase in vegetation cover in some areas, thus improving the carbon and water cycle and the ecological environment (Tong et al., 2018; Huang et al., 2019; Yang Y. et al., 2022). Another group of scholars believe that the implementation of the NFPP, especially afforestation in some areas, has led to a reduction in soil moisture due to strong forest transpiration and the increased precipitation cannot compensate for the consumption of evapotranspiration, which places a burden on local water resources (Yang et al., 2013; Hai et al., 2022). Therefore, there is an urgent need to reveal the actual trend and stability of WUE and its driving factors in NFPP areas and to provide scientific advice for the implementation of ecological projects.

In this study, we investigated the spatial variations and mechanisms for the stability of water use efficiency in China. Specifically, we aimed to propose three key issues: (1) What are the nonlinear trends of WUE in China, especially in NFPP areas? (2) What is the stability of WUE in China over recent years? (3) Which driving factors are important in determining the stability of WUE in China?

2 Materials and methods

2.1 Data sources

The terrestrial gross primary production (GPP) data was downloaded from the Global Land Surface Satellite (GLASS) program (http://www.resdc.cn/) (Jiao et al., 2022). It is generated using the Bayesian algorithm ensemble of eight widely-used light-use efficiency models and has been widely used in global carbon cycle assessment (Xu et al., 2022a). The dataset is a global composite product that spans from 1982 to 2015 with a spatial resolution of 0.05°.

The terrestrial evapotranspiration (ET) data was downloaded by the National Science & Technology Infrastructure (http://www.nesdc.org.cn/), with a 0.1° spatial resolution from 1981–2015. To obtain more accurate data, ET data is simulated by a nonlinear complementary Relational model and verified with 13 vorticity covariance measurements and 10 river basin Nash Sutcliffe efficiency measurements, with a range of 0.72-0.94 (Ma N. et al., 2019).

The WUE was calculated as follows:

$$WUE = GPP/ET \quad (1)$$

In this study, six driving factors were used to reveal the driving mechanism of the stability of WUE. The soil moisture (SM) and downward shortwave radiation (RAD) were downloaded by the Climatology Lab from 1981 to 2015 with a spatial resolution of 1/24°. Temperature and precipitation were downloaded from WorldCom (https://www.worldclim.org/) from 1981 to 2015 with a spatial resolution of 1 km. Vapor pressure deficit (VPD) was provided by Xu et al. (2021) (http://dx.doi.org/10.1016/j.scitotenv.2022.155086) from 1981 to 2015 with a spatial resolution of 0.1°. CO_2 was downloaded from the Emissions Database for Global Atmospheric Research (EDGAR) (https://edgar.jrc.ec.europa.eu/) from 1981 to 2015 with a spatial resolution of 0.1°.

2.2 Nonlinear method

The linear trends of NEP show an increasing trend with a constant rate of increase. However, the rate of NEP decomposed by EEMD increases with time. Therefore, the EEMD method can reveal the nonlinear trends in WUE (Pan et al., 2018; Xu et al., 2022b). Ensemble Empirical Mode Decomposition (EEMD) is an extension of the Empirical Mode Decomposition (EMD) method (Wu et al., 2007). The decomposition process of EMD is as follows:

First, the discrete extreme points of $X(t)$ are interpolated to the entire period with a cubic spline function to obtain the maximum and minimum envelopes, and the arithmetic mean of the upper and lower envelopes ($g_1(t)$) is calculated.

$$g_1(t) = X(t) - m_1(t) \quad (2)$$

Since $g_1(t)$ is not stable, continue to repeat the above steps:

$$g_{11}(t) = g_1(t) - m_{11}(t) \quad (3)$$

If the standard deviation (SD) is less than a given value (usually 0.2), the above iterative process is terminated:

$$SD = \sum_{t=1}^{N} \frac{|g_{1k}(t) - g_{1(k-1)}(t)|^2}{g^2_{1(k-1)}(t)} \quad (4)$$

In this way, we extracted the first Intrinsic Mode Function IMF (IMF) component (c_1=$g_{1k}(t)$) from the original data:

$$g_{1k}(t) = g_{1(k-1)(t)-m_{1k}(t)} \quad (5)$$

k is the number of iterations and the rest of the original data is:

$$r_1 = X(t) - c_1 \quad (6)$$

Since r_1 still contains fluctuations of a longer period, the above iterative process is still repeated, and the r_i is as follows:

$$r_i = r_{i-1} - c_i, i = 2, 3 \cdots n \quad (7)$$

Which is

$$X(t) = \sum_{i=1}^{n} c_i + r_n \quad (8)$$

c_i is the i-th IMF component, and r_n is the residual.

Due to the phenomenon of frequency mixing in the EMD method, the EEMD method was developed (Wu and Huang, 2009). The EEMD method introduces white noise with a certain signal-to-noise ratio into the original time series for EMD decomposition, and the IMFs obtained by each decomposition are then aggregated. The EEMD method not only greatly improves the modal aliasing defect of EMD, but also avoids the instantaneous noise that the original data may carry.

Repeat equations 2-8, with different Gaussian white noise series assed to $X(t)$, Finally, the original signal is decomposed into a series of $IMF_i(c_i)$ components with frequencies from high to low and a residual r_n.

The EEMD trends in WUE as a specific time t is defined as the value increase in r_n since the start time, that is trend(t)=$r_n(t)$-r_n (*1981*). The trends as their changing rates can be calculated (Pan et al., 2018):

$$Rate_{trend}(t) = Trend(t) - Trend(t-1) \quad (9)$$

The number of Gaussian white noises was set to 100 times, and the amplitude of these noises was set to 0.2 standard deviations of the raw data after considering the take-off between the decomposition robustness and the required computing time.

To test whether the trend is significant, the EEMD decomposition of Gaussian white noise is verified based on the Monte Carlo method (Pan et al., 2018). The non-significant trend of WUE is assumed to show no trend over time. The significantly nonlinear trend of the WUE is divided into the following four categories: increasing trends (Figure 1A), decreasing trends (Figure 1B), negative reversals (Figure 1C), and positive reversals (Figure 1D).

2.3 Stability method

Based on nonlinear trends detected by EEMD, excluding the trends with insignificant changes, we computed the interannual anomalies of WUE by removing their nonlinear trends. The standard deviation of interannual anomalies of WUE was identified as the stability of WUE (Wang et al., 2022). A higher standard deviation suggested lower stability. Additionally, the stability of WUE was classified into 6 classes (nonsignificant stable, stable, relatively stable, generally stable, relatively unstable, and unstable) based on natural breaks. The natural interval method is based on natural groupings inherited from the data. When creating classification intervals, similar values are grouped most appropriately and differences between classes are maximized. Elements are divided into classes, for which their boundaries are set at locations where the differences in data values are relatively large.

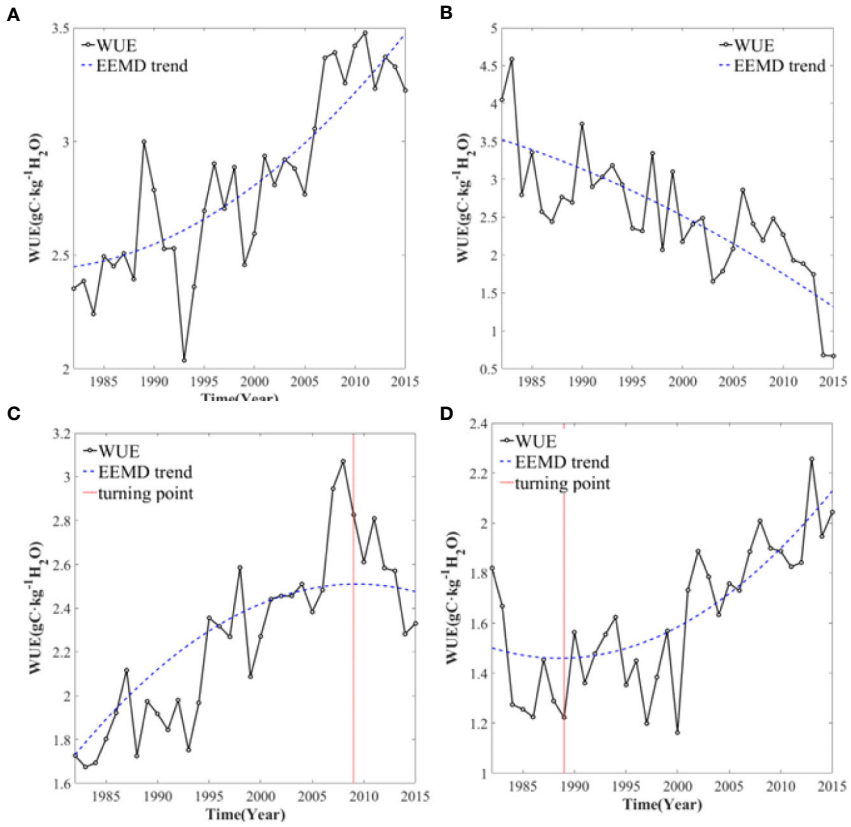

FIGURE 1
The nonlinear trends of WUE. **(A)** increasing trends; **(B)** decreasing trends; **(C)** negative reversals; **(D)** positive reversals.

2.4 Attribution analysis method

Multiple regression analysis was used to extract the impacts of the main drivers on the stability of WUE (Sun et al., 2015; Liu et al., 2018; Chu et al., 2019). We select 6 driving factors (CO_2, temperature (TEM), precipitation (PRE), soil moisture (SOIL), radiation (RAD), and vapor pressure deficit (VPD)) as the explanatory variables (Cai et al., 2015; Sun et al., 2015). Based on min-max normalization, all the driving factors were standardized in advance. The multiple regression analysis method is as follows:

$$SWUE_{pre} = aSWUE^{CO2} + bSWUE^{TEM} + cSWUE^{PRE} + dSWUE^{RAD} + eSWUE^{SOIL} + fSWUE^{VPD} + g \quad (10)$$

Where $SWUE_{pre}$ indicates the predicted stability of WUE, $SWUE^{CO2}$, $SWUE^{TEM}$, $SWUE^{PRE}$, $SWUE^{RAD}$, $SWUE^{SOIL}$, $SWUE^{VPD}$ represent SWUE variations that are driven by CO_2, TEM, PRE, RAD, SOIL, VPD, which were also standard deviations of the interannual anomalies without long-term nonlinear trends (Wang et al., 2022). *a–f* are the regression coefficients. The absolute value of the regression coefficient can represent the relative importance of the driving factors, and *g* is the regression constant. In this study, the largest regression coefficient of the multiple regression is the main driving factor on the stability of *SWUE*.

3 Result

3.1 The WUE trend in China and eight ecological restoration areas

Based on the linear method (Figure 2), WUE had an increasing trend from 1982 to 2015 with an average rate of 0.0135gC/kgH_2O/yr. WUE also had a nonlinear trend detected by EEMD and the increased rate was beyond the linear rate after 2005. In the National Forest Protection Project (NFPP) area (Figure 3), the WUE had increasing trends, the growth rate of WUE was the fastest in the Yellow River (at a rate of 0.0127 gC/kgH_2O/yr) and Taihang Mountains (at a rate of 0.0108 gC/kgH_2O/yr) shelterbelt program areas. It was the slowest in the Three-North shelterbelt program areas (at a rate of 0.0023 gC/kgH_2O/yr) and the Yangtze River shelterbelt program areas (at a rate of 0.0030 gC/kgH_2O/yr). There is a tendency for WUE to increase, with the rate of increase peaking around 2000-2005 and decreasing thereafter. It indicated that although ecological restoration projects has significantly improved water use efficiency, there is a risk of WUE reduction in the future.

In China (Figure 4), 33.59% of WUE was nonsignificant, which is assumed to be no trend over time and was mainly located in the Northwest, Northeast, and Tibetan Plateau. 34.19% and 19.72% of WUE had increasing trends and positive reversals, which are mainly distributed in the North China Plain and the Pearl River Basin

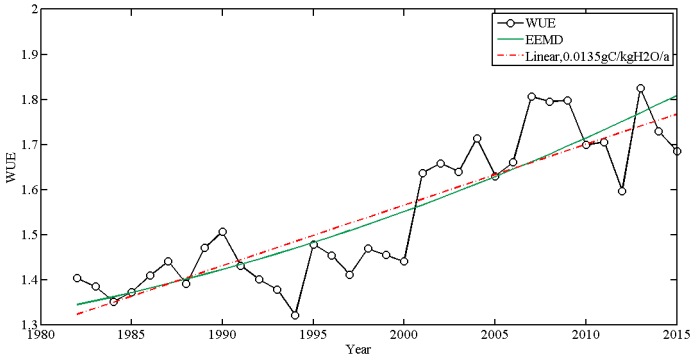

FIGURE 2
The linear and nonlinear trend of WUE in the whole of China based on linear regression method and EEMD method.

(Table 1). The decreasing trends and negative reversals of WUE only accounted for 1.86% and 10.64%, respectively, located in the Yangtze River basin. In eight NFPP areas, WUE was dominated by increasing trends in the Pearl River, Taihang Mountains, Huaihe, and Taihu shelterbelt program areas, accounting for 57.90%, 69.42%, and 72.25%, respectively. It had positive reversals in the Yellow River shelterbelt program areas, accounting for 44.63%. However, in the Yangtze River, the WUE was dominated by negative reversals, which accounted for 51.35%.

3.2 The spatial distribution of the WUE stability

EEMD decomposes WUE into four interannual variations and a residual (Figure 5), with periods of 2.7, 6.5, 27, and 38-year time scales. The SWUE (standard deviation of interannual variation) ranged from 0.30 to 0.67. The SWUE were relatively stable (ranging from 0.30-0.40) with small interannual fluctuations before 2000. There was a large instability of WUE after 2000. To be more specific, it increased sharply in 2000, 2001, and 2007, with the greatest volatility in 2007.

The six classes of SWUE, namely non-significant stable, stable, relatively stable, generally stable, relatively unstable, and unstable in China, account for 33.59%, 15.09%, 12.88%, 19.39%, 12.14%, and 6.91%, respectively (Figure 6 and Table 2). Overall, WUE was stable in the northwest and Tibetan Plateau, where the trend was mainly nonsignificant; while it was unstable in the northeast, southwest, and Yangtze River basin, where the WUE trends were dominated by negative reversals. In NFPP areas, the WUE was stable in Three-North shelterbelt program areas and the stable and relatively stable WUE accounted for 17.57% and 12.03%, respectively. the relatively stable WUE accounted for 32.81% in Coastal shelterbelt program areas. However, in the Liaohe and Taihang Mountains shelterbelt programs areas, the percentage of the relatively unstable and unstable WUE accounted for 57.00% and 45.62%, respectively. In Taihang Mountains shelterbelt program areas, the WUE was dominated by monotonically increasing trends and positive

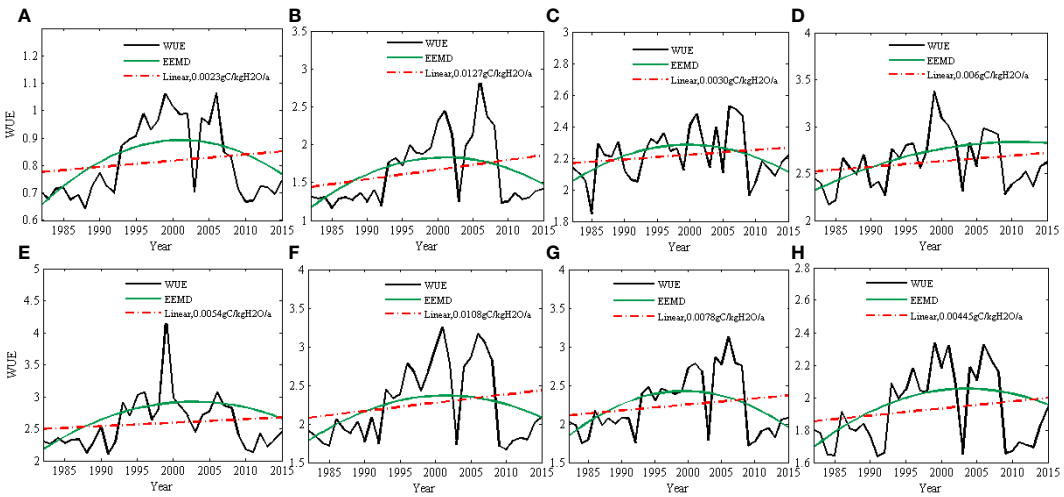

FIGURE 3
The linear and nonlinear trend of WUE in eight NFPP areas based on linear regression method and EEMD method (**A**: Three-north areas; **B**: Yellow River areas; **C**: Yangtze River shelterbelt program areas; **D**: Pearl River areas; **E**: Liaohe River areas; **F**: Taihang Mountains areas; **G**: Huaihe and Taihu areas; **H**: coastal areas).

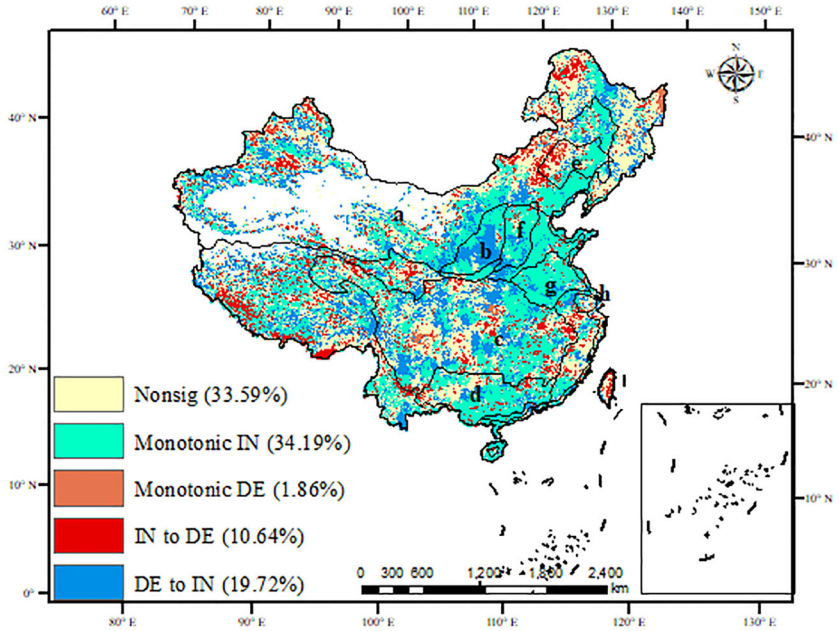

FIGURE 4
The spatial distribution of the nonlinear trend of WUE in China (Monotonical IN: increasing trends; IN to DE: decreasing trends; IN to DE: negative reversals; DE to IN: positive reversals; A: Three-north areas; B: Yellow River areas; C: Yangtze River shelterbelt program areas; D: Pearl River areas; E: Liaohe River areas; F: Taihang Mountains areas; G: Huaihe and Taihu areas; H: coastal areas).

reversals, while the WUE usually experienced negative reversals in Liaohe River areas. It is indicated that WUE with nonlinear trends (positive reversals and negative reversals) are generally unstable, which may be influenced by climatic or anthropogenic factors, leading to positive shifts or negative feedback.

3.3 The dominant climatic factors on the SWUE

To investigate the mechanism of climate fluctuations on SWUE in different regions of China, we analyzed the spatial distribution of the main climatic factors on the SWUE in China (Figure 7). The results show that the spatial variation of SWUE was mainly influenced by VPD in southwestern and northeastern China and along the Yangtze River, where the WUE was unstable. Temperature and solar radiation were the dominant factors for interannual fluctuations of WUE in the North China Plain and central Yangtze River, where the WUE was relatively unstable. In the NFPP areas, VPD was the main driving factor for the interannual variables of WUE in the Yangtze River, Pearl River, and Liaohe River shelterbelt program areas, accounting for 38.25%, 49.38%, and 65.85%, respectively (Table 3). This indicates that the WUE was affected by atmospheric drought in these ecological project areas, which led to low SWUE. Precipitation and soil moisture were the main driving factors for the interannual variables of WUE in the Yellow River and Tibetan Plateau, where the WUE was stable. Temperature and radiation

TABLE 1 The percentage of nonlinear trends of WUE in China and eight NFPP areas.

Region	Nonsig	Monotonical IN	Monotonical DE	IN to DE	DE to IN
Whole China	33.59	34.19	1.86	10.64	19.72
Three-North	35.10	29.75	2.63	10.28	22.24
Yellow River	6.89	47.45	0	1.02	44.63
Yangtze River	18.54	17.94	0.89	51.35	11.28
Pearl River	23.92	57.90	0.05	8.03	10.10
Liaohe River	35.96	38.94	2.92	14.53	7.62
Taihang Mountains	8.20	69.42	0.06	3.65	18.68
Huaihe and Taihu	10.33	72.25	0.96	3.36	13.10
Coastal	23.12	51.50	0.73	9.92	14.72

* Nonsig, nonsignificant trends; Monotonical IN, increasing trends; IN to DE, decreasing trends; IN to DE, negative reversals; DE to IN, positive reversals.

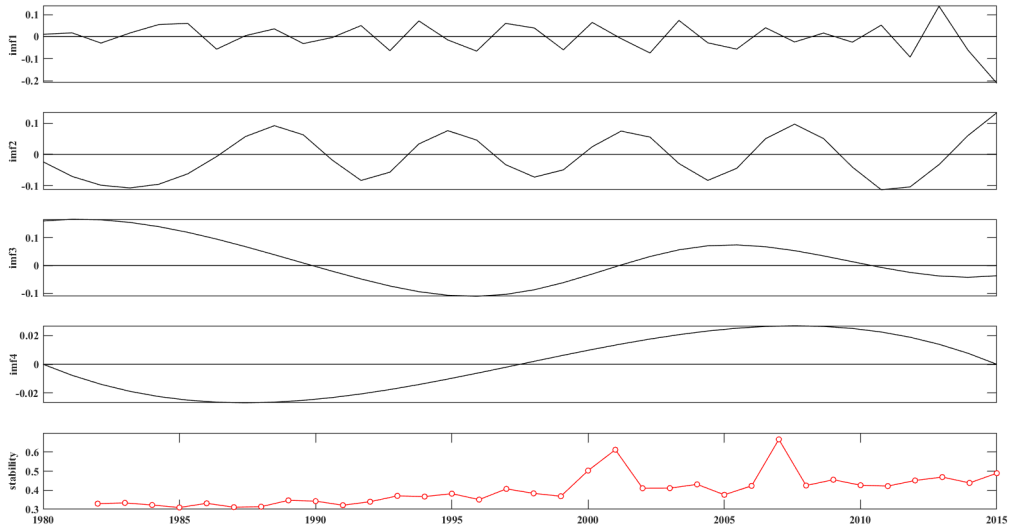

FIGURE 5
EEMD decomposition for averaged WUE in China (interannual anomalies (IMF1-IMF4); residual trend; stability).

promoted interannual variables of WUE in the Taihang Mountains and Yangtze River shelterbelt program areas, where the WUE was relatively unstable. The overall contribution of CO_2 to SWUE was low in eight NFPP areas. It indicated that VPD, temperature, and radiation lead to unstable changes in WUE, while precipitation and soil moisture lead to stable changes. Therefore, differences in the dominant climate factors in different regions need to be considered when exploring the influence of climate on the SWUE in China.

4 Discussion

4.1 The nonlinear trend of WUE

The core meaning of WUE can be summarized as the ratio of productivity to water consumption (El Masri et al., 2019; Jiao et al., 2022). A deep understanding of the WUE trend is an important entry point for coupling the water-carbon cycle, energy conversion, resource use, and climate change issues, especially in the ecological

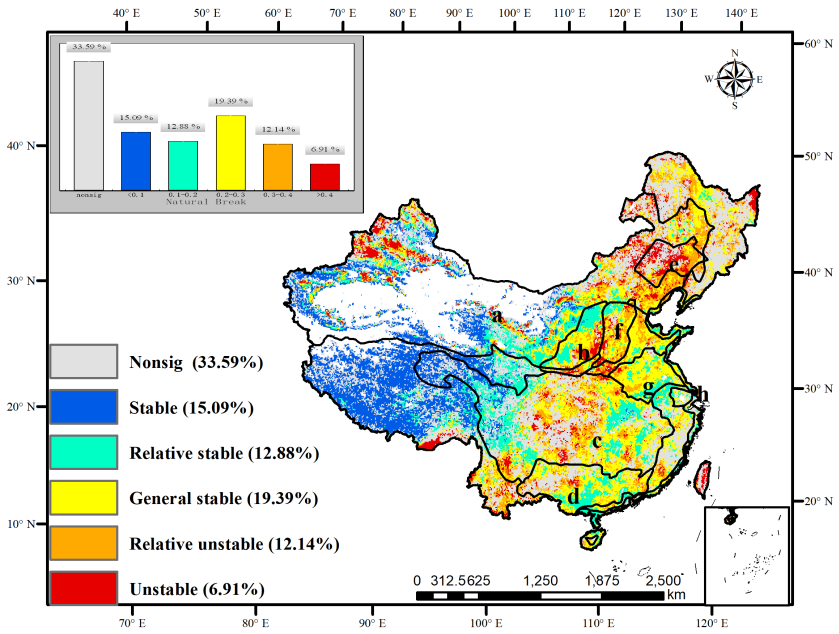

FIGURE 6
The spatial distribution of stability in WUE in China (non sig: non-significant stability of WUE. A: Three-north areas; B: Yellow River areas; C: Yangtze River shelterbelt program areas; D: Pearl River areas; E: Liaohe River areas; F: Taihang Mountains areas; G: Huaihe and Taihu areas; H: coastal areas).

TABLE 2 The percentage of stability of WUE in China and eight NFPP areas.

Region	Nonsig	Stable	Relative stable	General stable	Relative unstable	Unstable
Whole China	33.59	15.09	12.88	19.39	12.14	6.91
Three-North	35.41	17.57	12.03	13.56	12.00	9.70
Yellow River	6.89	0.67	28.89	34.24	17.55	11.77
Yangtze River	34.47	7.89	16.62	23.48	13.16	4.38
Pearl River	23.95	0.03	19.10	41.21	13.44	2.27
Liaohe River	35.93	0.00	0.39	6.68	25.98	31.02
Taihang Mountains	8.25	0.00	10.65	35.47	32.79	12.83
Huaihe and Taihu	10.38	0.00	22.8	55.46	10.42	1.26
Coastal	22.74	2.54	32.81	34.47	6.45	0.98

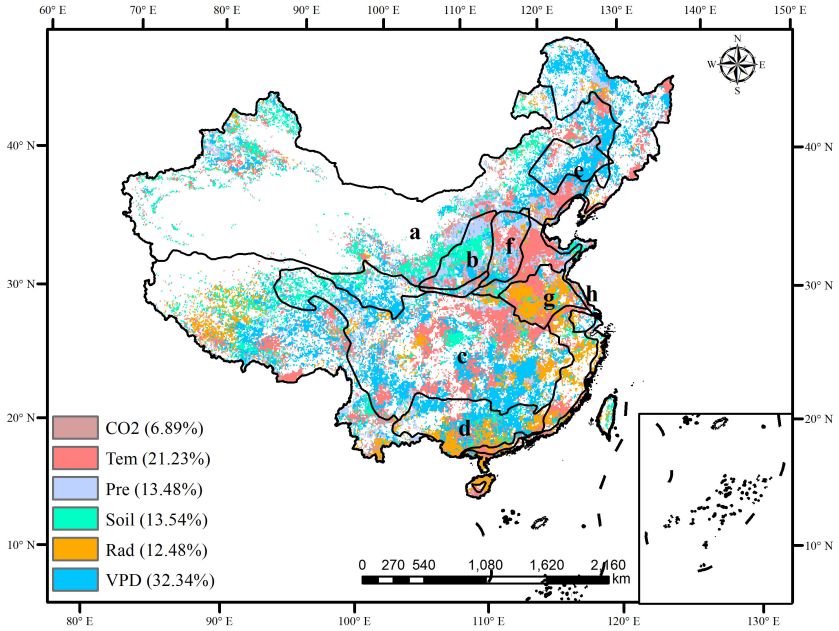

FIGURE 7
The dominant driving factors of WUE in China (A: Three-north areas; B: Yellow River areas; C: Yangtze River shelterbelt program areas; D: Pearl River areas; E: Liaohe River areas; F: Taihang Mountains areas; G: Huaihe and Taihu areas; H: coastal areas).

TABLE 3 The percentage of driving factors of WUE in China and eight NFPP areas.

Region	CO_2	Tem	Pre	Soil	Rad	VPD
Whole China	6.89	21.23	13.48	13.54	12.48	32.34
Three-North	7.18	16.54	16.29	28.17	4.27	27.55
Yellow River	8.48	12.54	32.56	25.83	1.64	18.95
Yangtze River	4.18	27.21	8.89	9.82	11.65	38.25
Pearl River	5.95	13.88	5.54	5.25	25.54	49.38
Liaohe River	5.26	12.56	12.54	1.53	2.25	65.86
Taihang Mountains	3.92	32.86	33.79	4.89	6.26	18.28
Huaihe and Taihu	8.15	26.75	4.89	4.15	43.87	12.19
Coastal	3.59	35.57	11.53	8.89	25.29	15.16

* Tem, temperature; Pre, precipitation; Soi, soil moisture; Rad, radiation; VPD, vapor pressure deficit.

restoration areas (Jiao et al., 2022). Basing on linear method, previous studies revealed that the WUE shows an increasing trend with a rate of 0.0025 gC kg/H_2O/yr globally (Xue et al., 2015; Yang L. et al., 2022; Zhao et al., 2022). In this study, the WUE was also dominated by increasing trends (34.19%) in China, while decreasing trends only accounted for 1.86%. Additionally, the nonlinear trends of WUE were detected by the EEMD method. 19.72% of WUE had positive reversals while 10.64% exhibited negative reversals, which is rarely explored by the linear methods (Jiao et al., 2022). Ignoring non-linear changes in WUE may lead to an overestimation of ecosystem productivity and an underestimation of water deficit (Hatfield and Dold, 2019). Thus, revealing the nonlinear trends of WUE provided a deep understanding of ecosystem functioning (Jiao et al., 2022). In eight NFPP areas, WUE was dominated by increasing trends or positive reversals. The time of turning points mainly occurred in 2000-2005, aligning well with the implementation of the NFPP (Chen et al., 2019). The restoration project has increased the area of forest and scrub at high WUE levels, and significantly reduced the area of farmland and grassland at low WUE levels, thus increased the overall WUE. This shows that the implementation of ecological restoration projects will improve the sustainability of WUE to a certain extent (Ding et al., 2021). However, in the Yangtze River shelterbelt program areas, the negative reversals of WUE accounted for 51.35%, indicating that the Yangtze River basin is facing reduced productively and drought risks, which limits crop production and triggers grassland fires secondary disasters, such as grassland fires and crop pests and diseases (Venkatappa et al., 2021).

4.2 The stability of WUE

Although the spatial distribution of the WUE trend has been determined using linear or nonlinear trends in previous studies, the stability of WUE remained unclear (Rödenbeck et al., 2018; Jiao et al., 2022). Jiao et al. (2022) obtained the WUE stability through the contribution of inter-annual variables to the secular trend, and revealed that the WUE was strongly stable in the north and Loess Plateau while interannual variables were found in the southwest. The trend itself can reflect the stability of the WUE. In this study, based on the EEMD method, the standard deviation of residual trends of WUE is used as the indicator of stability, and the spatial variations of SWUE were compared and analyzed. The change in WUE experienced large inter-annual fluctuations after 2000, especially from 2000 to 2005. Overall, compared to northwestern China and the Tibetan Plateau, the WUE in eastern China was much more unstable. A previous study showed that most of the ecological functioning has been improved in China (Jin et al., 2018). In this study, the unstable WUE experienced positive reversals or negative reversals. The traditional linear methods that ignore non-linear trends exaggerate the stability of WUE (Hao et al., 2021). Thus, there are hidden risks beneath apparent ecosystem degradation, and ecosystem improvement or degradation may be limited and exaggerated (Pan et al., 2018).

Previous studies have revealed that ecological restoration promotes the improvement of ecosystem functioning (Yang et al., 2017; Song et al., 2022). In this study, the WUE was stable with increasing trends in the Pearl River, Huaihe and Taihu, coastal shelterbelt program areas. Although WUE was unstable in the Yellow River and Taihang Mountains shelterbelt program areas, it experienced positive shifts. Previous studies have shown that the ecological restoration program contributed to a significant increase in vegetation productivity in the Yellow River and Taihang Mountains shelterbelt program areas (Xue et al., 2022). It is indicated that most ecological restoration projects in China enhance carbon sequestration thus leading to increasing trends or positive shifts in WUE (Xue et al., 2022). However, some ecological restoration may inhibit or reverse the trend in WUE (Lu et al., 2018). Our result demonstrated that WUE was unstable and may be easily altered from increasing to decreasing in the Yangtze River shelterbelt program areas. In the Yangtze River shelterbelt program area, the massive planting of trees stimulates an increase in the water demand of the forest, which in turn absorbs large amounts of soil water and stimulates increased evapotranspiration (Zhang et al., 2016). The simultaneous increase in productivity and evapotranspiration can lead to fluctuating changes in WUE, especially during the implementation phase of the ecological project from 2000-2005 (Tong et al., 2019). In addition, the Yangtze River is in the East Asian monsoon climate zone and is significantly influenced by the monsoon, with frequent drought disasters (Hong et al., 2014). Studies have shown that drought events in the Yangtze River have begun to increase and intensify in recent years, which deeply affected vegetation productivity (Horion et al., 2016). In areas with significant human influence and stable WUE, such as the southeastern coast, there is little room for further improvement of WUE stability. Therefore, achieving the sustainability of WUE may depend on reducing anthropogenic carbon emissions in these areas (Wang et al., 2022). Therefore, the spatial heterogeneity in WUE stability underscores the importance of implementing management strategies according to the local condition.

4.3 Driving mechanism of WUE

Climate change has a profound impact on the functioning of ecosystems and, as a result, on the coupled cycles of carbon and water (Liu et al., 2020). Some climatic factors influence the trend and stability of WUE, such as CO_2 concentration, VPD, temperature, precipitation, soil moisture, etc. (Cheng et al., 2017; Hatfield and Dold, 2019). In our study, the stability variation of WUE is mainly caused by precipitation and soil moisture, while instability is mainly induced by saturation water vapor pressure difference, temperature, and solar radiation in China.

Previous studies suggested that the atmospheric water demand, represented by VPD overrode other climatic factors exerting dominantly negative effects on WUE change in alpine meadow ecosystems (Cheng et al., 2017). In this study, the VPD played a dominant role in controlling the instability of the WUE trend in the Yangtze River and Liaohe River shelterbelt program areas, where the WUE experienced negative reversals. By controlling plant stomatal activity, atmospheric drought can affect carbon

acquisition and water transpiration losses (Konings et al., 2017). In recent years, China has undergone an increase in atmospheric vapor pressure deficit (Lopez et al., 2021). VPD plays a dominant role in controlling ET in these areas, with higher VPD leading to a dramatic increase in ET (Liu et al., 2020). Additionally, high VPD should lead to partial stomatal closure and suppression of photosynthetic rates (Ding et al., 2018). All these effects could lead to a negative response of WUE to changes in VPD (Cao et al., 2020). This negative impact is becoming stronger in terms of the severity and extent of the effects, indicating that atmospheric drought is becoming increasingly harmful to productivity (Ding et al., 2018). Therefore, in areas where VPD has led to a decline in WUE, the impact of atmospheric drought on vegetation should be closely monitored and the negative impact of atmospheric drought on vegetation should be reduced through artificial measures, such as artificial rainfall and irrigation.

Temperature and radiation are the dominant controlling factors on the instability of WUE in the Taihu and Huaihe and coastal shelterbelt program areas. In the Taihu Lake and Huaihe River shelterbelt program area, the increase of temperature promotes the increase in WUE, while in some coastal areas, the increase of temperature suppresses the increase in WUE and shifts it from decreasing to increasing. The appropriate increase in temperature prolongs the growth period of plants, leading to a higher increase in GPP than ET, resulting in a monotonic increase in WUE in the Huaihe and Taihu shelterbelt program areas. However, in coastal areas, especially in subtropical areas, the temperature increase promotes ET much more than GPP, resulting in negative reversals and large interannual fluctuations in WUE. There is a threshold for the effect of temperature on water utilization and a too high or too low temperature can harm plant WUE (Hatfield and Dold, 2019). When the temperature is below the threshold, WUE increases with increasing temperature, while when the temperature is above the threshold, WUE shows a negative relationship with temperature (Hatfield and Dold, 2019). The main reason is that enzyme activity is significantly affected when the optimum temperature is reached (Huang M. et al., 2015). Conversely, an increase of temperature causes an increase in VPD and thus increases the transpiration rate of vegetation (Xue et al., 2015). Xue et al. (2015) found that globally, WUE tended to increase linearly with temperature in the cooler regions, reaching a maximum at 18.5°C and decreasing thereafter. Therefore, high temperatures can cause instability in WUE with negative reversals. Thus, more attention should be paid to the high temperature, especially heat waves. In addition, with the economically developed eastern coast and the rapid expansion of urbanization, vegetation productivity is dominated by decreasing or increasing to decreasing trends, leading to negative reversals and instability in WUE (Liu et al., 2023).

Precipitation and soil moisture promoted the stability of WUE in the Yellow River shelterbelt program areas. Precipitation and soil moisture in these areas are relatively low and are crucial elements determining ecosystem composition, structure, and function (Zhang et al., 2020). Interannual variation in vegetation productivity in semi-arid regions is closely related to interannual variables of drought and precipitation (Zhang et al., 2020; Yang L. et al., 2022). Moderate rainfall could offset the effect of drought and keep the stability of WUE in the Yellow River program area (Cai et al., 2020; Wang M. et al., 2021). Previous studies revealed that WUE was positively correlated with precipitation and specific humidity (Xue et al., 2015; Wang H. et al., 2021). Liu et al. (2020) suggested that increased soil moisture contributed to a positive trend in WUE in humid and high latitudes of northern China, which could also enhance carbon sequestration because of the increased water availability (Liu et al., 2020). In addition, the Yellow River basin is the most effective area for ecological restoration projects in China, such as Natural Forest protection, afforestation, economic compensation, etc., which enhance carbon accumulation and greatly contribute to the increasing trends and stability in WUE (Kou et al., 2021; Zhang et al., 2022).

5 Conclusions

The stable WUE was dominated by nonsignificant trends and increasing trends, accounting for 33.59% and 34.19%, respectively. The nonsignificant trend of stable WUE was mainly located in Three-North shelterbelt program areas, and the increasing trend of stable WUE was in Huaihe and Taihu, Taihang Mountains, and Pearl River shelterbelt program areas. Precipitation and soil moisture promoted stable WUE in these project areas. The unstable WUE was dominated by positive reversals or negative reversals of WUE trends. The positive reversals of unstable WUE were mainly located in the Yellow River shelterbelt program areas, which was promoted by temperature and radiation, while the negative reversals of unstable WUE were mainly distributed in the Yangtze River and Liaohe shelterbelt program areas, which was mainly induced by VPD.

Data availability statement

The original contributions presented in the study are included in the article/Supplementary Material. Further inquiries can be directed to the corresponding authors.

Author contributions

XX: Conceptualization, Data curation, Funding acquisition, Investigation, Project administration, Resources, Software, Validation, Visualization, Writing – original draft, Writing – review & editing. JL: Investigation, Methodology, Software, Supervision, Resources, Visualization, Writing – original draft. FJ: Investigation, Methodology, Software, Supervision, Resources, Visualization, Writing – original draft. KZ: Methodology, Supervision, Conceptualization, Investigation, Software, Writing – review & editing. YY: Data curation, Formal Analysis, Methodology, Project administration, Supervision, Validation, Writing – original draft. JQ: Writing – original draft. YZ: Data curation, Methodology, Supervision, Writing – original draft,

Writing – review & editing. NL: Funding acquisition, Resources, Visualization, Writing – review & editing. CZ: Conceptualization, Funding acquisition, Resources, Visualization, Writing – review & editing.

Funding

This study was supported by the National Key R&D Program of China (2021YFB3901104). The Special Fund of the Jiangsu for Carbon Peak and Carbon Neutralization Science and Technology Innovation (BK20220021), and the Special Fund of the Chinese Central Government for Basic Scientific Research Operations in the commonweal Research Institute (GYZX210405).

Conflict of interest

The authors declare that the research was conducted in the absence of any commercial or financial relationships that could be construed as a potential conflict of interest.

Publisher's note

References

Beer, C., Ciais, P., Reichstein, M., Baldocchi, D., Law, B. E., Papale, D., et al. (2009). Temporal and among-site variability of inherent water use efficiency at the ecosystem level. *Global Biogeochem. Cycles* 23, 1–13. doi: 10.1029/2008gb003233

Belmecheri, S., Maxwell, R. S., Taylor, A. H., Davis, K. J., Guerrieri, R., Moore, D. J. P., et al. (2021). Precipitation alters the CO(2) effect on water-use efficiency of temperate forests. *Glob. Chang. Biol.* 27, 1560–1571. doi: 10.1111/gcb.15491

Cai, D., Ge, Q., Wang, X., Liu, B., Goudie, A. S., and Hu., S. (2020). Contributions of ecological programs to vegetation restoration in arid and semiarid China. *Environ. Res. Lett.* 15, 1–11. doi: 10.1088/1748-9326/abbde9

Cai, H., Yang, X., and Xu., X. (2015). Human-induced grassland degradation/restoration in the central Tibetan Plateau: The effects of ecological protection and restoration projects. *Ecol. Eng.* 83, 112–119. doi: 10.1016/j.ecoleng.2015.06.031

Cao, R., Hu, Z., Jiang, Z., Yang, Y., Zhao, W., Wu, G., et al. (2020). Shifts in ecosystem water use efficiency on China's loess plateau caused by the interaction of climatic and biotic factors over 1985–2015. *Agric. For. Meteorol.* 291 (1), 1–9. doi: 10.1016/j.agrformet.2020.108100

Chen, J. M., Ju, W., Ciais, P., Viovy, N., Liu, R., Liu, Y., et al. (2019). Vegetation structural change since 1981 significantly enhanced the terrestrial carbon sink. *Nat. Commun.* 10, 4259. doi: 10.1038/s41467-019-12257-8

Cheng, L., Zhang, L., Wang, Y. P., Canadell, J. G., Chiew, F. H. S., Beringer, J., et al. (2017). Recent increases in terrestrial carbon uptake at little cost to the water cycle. *Nat. Commun.* 8, 110. doi: 10.1038/s41467-017-00114-5

Chu, H., Venevsky, S., Wu, C., and Wang., M. (2019). NDVI-based vegetation dynamics and its response to climate changes at Amur-Heilongjiang River Basin from 1982 to 2015. *Sci. Total Environ.* 650, 2051–2062. doi: 10.1016/j.scitotenv.2018.09.115

Ding, Z., Liu, Y., Wang, L., Chen, Y., Yu, P., Ma, M., et al. (2021). Effects and implications of ecological restoration projects on ecosystem water use efficiency in the karst region of Southwest China. *Ecol. Eng.* 170, 1–9. doi: 10.1016/j.ecoleng.2021.106356

Ding, J., Yang, T., Zhao, Y., Liu, D., Wang, X., Yao, Y., et al. (2018). Increasingly important role of atmospheric aridity on Tibetan Alpine grasslands. *Geophys. Res. Lett.* 45, 2852–2859. doi: 10.1002/2017gl076803

El Masri, B., Schwalm, C., Huntzinger, D. N., Mao, J., Shi, X., Peng, C., et al. (2019). Carbon and water use efficiencies: A comparative analysis of ten terrestrial ecosystem models under changing climate. *Sci. Rep.* 9, 14680. doi: 10.1038/s41598-019-50808-7

Gonsamo, A., Ciais, P., Miralles, D. G., Sitch, S., Dorigo, W., Lombardozzi, D., et al. (2021). Greening drylands despite warming consistent with carbon dioxide fertilization effect. *Glob. Chang. Biol.* 27, 3336–3349. doi: 10.1111/gcb.15658

Hai, X., Li, J., Li, J., Liu, Y., Dong, L., Wang, X., et al. (2022). Variations in plant water use efficiency response to manipulated precipitation in a temperate grassland. *Front. Plant Sci.* 13. doi: 10.3389/fpls.2022.881282

Hao, X., Zhang, J., Fan, X., Hao, H., and Li., Y. (2021). Quantifying soil moisture impacts on water use efficiency in terrestrial ecosystems of China. *Remote Sens.* 13 (21), 4257. doi: 10.3390/rs13214257

Hatfield, J. L., and Dold, C. (2019). Water-use efficiency: advances and challenges in a changing climate. *Front. Plant Sci.* 10. doi: 10.3389/fpls.2019.00103

Hong, X., Guo, S., Zhou, Y., and Xiong., L. (2014). Uncertainties in assessing hydrological drought using streamflow drought index for the upper Yangtze River basin. *Stoch. Env. Res. Risk A* 29, 1235–1247. doi: 10.1007/s00477-014-0949-5

Horion, S., Prishchepov, A. V., Verbesselt, J., de Beurs, K., Tagesson, T., and Fensholt., R. (2016). Revealing turning points in ecosystem functioning over the Northern Eurasian agricultural frontier. *Glob. Chang. Biol.* 22, 2801–2817. doi: 10.1111/gcb.13267

Huang, M., Piao, S., Sun, Y., Ciais, P., Cheng, L., Mao, J., et al. (2015). Change in terrestrial ecosystem water-use efficiency over the last three decades. *Glob. Chang. Biol.* 21, 2366–2378. doi: 10.1111/gcb.12873

Huang, L., Wang, B., Niu, X., Gao, P., and Song., Q. (2019). Changes in ecosystem services and an analysis of driving factors for China's Natural Forest Conservation Program. *Ecol. Evol.* 9, 3700–3716. doi: 10.1002/ece3.4925

Huang, J., Yu, H., Guan, X., Wang, G., and Guo., R. (2015). Accelerated dryland expansion under climate change. *Nat. Climate Change* 6, 166–171. doi: 10.1038/nclimate2837

Jiang, Y., Still, C. J., Rastogi, B., Page, G. F. M., Wharton, S., Meinzer, F. C., et al. (2019). Trends and controls on water-use efficiency of an old-growth coniferous forest in the Pacific Northwest. *Environ. Res. Lett.* 14 (7), 1–12. doi: 10.1088/1748-9326/ab2612

Jiao, F., Xu, X., Zhang, M., Gong, H., Liu, H., and Wang., K. (2022). Contributory factors of the secular trends to changes in ecosystem water-use efficiency in China. *J. Hydro.l* 615, 128690. doi: 10.1016/j.jhydrol.2022.128690

Jin, N., Ren, W., Tao, B., He, L., Ren, Q., Li, S., et al. (2018). Effects of water stress on water use efficiency of irrigated and rainfed wheat in the Loess Plateau, China. *Sci. Total Environ.* 642, 1–11. doi: 10.1016/j.scitotenv.2018.06.028

Konings, A. G., Williams, A. P., and Gentine., P. (2017). Sensitivity of grassland productivity to aridity controlled by stomatal and xylem regulation. *Nat. Geosci.* 10, 284–288. doi: 10.1038/ngeo2903

Kou, P., Xu, Q., Jin, Z., Yunus, A. P., Luo, X., and Liu., M. (2021). Complex anthropogenic interaction on vegetation greening in the Chinese Loess Plateau. *Sci. Total Environ.* 778, 146065. doi: 10.1016/j.scitotenv.2021.146065

Liu, J., Bowman, K. W., Schimel, D. S., Parazoo, N. C., Jiang, Z., Lee, M., et al. (2017). Contrasting carbon cycle responses of the tropical continents to the 2015-2016 El Nino. *Science* 358 (6360), eaam5690. doi: 10.1126/science.aam5690

Liu, X., Feng, X., and Fu., B. (2020). Changes in global terrestrial ecosystem water use efficiency are closely related to soil moisture. *Sci. Total Environ.* 698, 134165. doi: 10.1016/j.scitotenv.2019.134165

Liu, H., Wang, Z., Wang, Z., Zeng, Y., Xue, P., and Zhang., M. (2023). Stability of the ecosystem gross primary productivity increasing in Chinese forestry ecological engineering area. *Agricult. Ecosyst. Environ.* 356, 108636. doi: 10.1016/j.agee.2023.108636

Liu, R., Xiao, L. L., Liu, Z., and Dai., J. C. (2018). Quantifying the relative impacts of climate and human activities on vegetation changes at the regional scale. *Ecol. Indic.* 93, 91–99. doi: 10.1016/j.ecolind.2018.04.047

Lopez, J., Way, D. A., and Sadok., W. (2021). Systemic effects of rising atmospheric vapor pressure deficit on plant physiology and productivity. *Glob. Chang. Biol.* 27, 1704–1720. doi: 10.1111/gcb.15548

Lu, F., Hu, H., Sun, W., Zhu, J., Liu, G., Zhou, W., et al. (2018). Effects of national ecological restoration projects on carbon sequestration in China from 2001 to 2010. *Proc. Natl. Acad. Sci. U.S.A.* 115, 4039–4044. doi: 10.1073/pnas.1700294115

Ma, J., Jia, X., Zha, T., Bourque, C. P. A., Tian, Y., Bai, Y., et al. (2019). Ecosystem water use efficiency in a young plantation in Northern China and its relationship to drought. *Agric. For. Meteorol.* 275, 1–10. doi: 10.1016/j.agrformet.2019.05.004

Ma, N., Szilagyi, J., Zhang, Y., and Liu., W. (2019). Complementary-relationship-based modeling of terrestrial evapotranspiration across China during 1982–2012: validations and spatiotemporal analyses. *J. Geophys. Res.: Atmos.* 124, 4326–4351. doi: 10.1029/2018jd029850

Migliavacca, M., Musavi, T., Mahecha, M. D., Nelson, J. A., Knauer, J., Baldocchi, D. D., et al. (2021). The three major axes of terrestrial ecosystem function. *Nature* 598, 468–472. doi: 10.1038/s41586-021-03939-9

Pan, N., Feng, X., Fu, B., Wang, S., Ji, F., and Pan., S. (2018). Increasing global vegetation browning hidden in overall vegetation greening: Insights from time-varying trends. *Remote Sens. Environ.* 214, 59–72. doi: 10.1016/j.rse.2018.05.018

Piao, S., Wang, X., Wang, K., Li, X., Bastos, A., Canadell, J. G., et al. (2020). Interannual variation of terrestrial carbon cycle: Issues and perspectives. *Glob. Chang. Biol.* 26, 300–318. doi: 10.1111/gcb.14884

Rödenbeck, C., Zaehle, S., Keeling, R., and Heimann., M. (2018). How does the terrestrial carbon exchange respond to inter-annual climatic variations? A quantification based on atmospheric CO<sub<2</sub< data. *Biogeosciences* 15, 2481–2498. doi: 10.5194/bg-15-2481-2018

Song, W., Feng, Y., and Wang., Z. (2022). Ecological restoration programs dominate vegetation greening in China. *Sci. Total Environ.* 848, 157729. doi: 10.1016/j.scitotenv.2022.157729

Sun, Y. L., Yang, Y. L., Zhang, L., and Wang., Z. L. (2015). The relative roles of climate variations and human activities in vegetation change in North China. *Phys. Chem. Earth* 87-88, 67–78. doi: 10.1016/j.pce.2015.09.017

Tong, X., Brandt, M., Yue, Y., Horion, S., Wang, K., Keersmaecker, W. D., et al. (2018). Increased vegetation growth and carbon stock in China karst *via* ecological engineering. *Nat. Sustain.* 1, 44–50. doi: 10.1038/s41893-017-0004-x

Tong, X., Mu, Y., Zhang, J., Meng, P., and Li., J. (2019). Water stress controls on carbon flux and water use efficiency in a warm-temperate mixed plantation. *J. Hydrol.* 571, 669–678. doi: 10.1016/j.jhydrol.2019.02.014

Tong, X., Wang, K., Yue, Y., Brandt, M., Liu, B., Zhang, C., et al. (2017). Quantifying the effectiveness of ecological restoration projects on long-term vegetation dynamics in the karst regions of Southwest China. *Int. J. Appl. Earth Observ. Geoinform.* 54, 105–113. doi: 10.1016/j.jag.2016.09.013

Venkatappa, M., Sasaki, N., Han, P., and Abe., I. (2021). Impacts of droughts and floods on croplands and crop production in Southeast Asia - An application of Google Earth Engine. *Sci. Total Environ.* 795, 148829. doi: 10.1016/j.scitotenv.2021.148829

Wang, M., Ding, Z., Wu, C., Song, L., Ma, M., Yu, P., et al. (2021). Divergent responses of ecosystem water-use efficiency to extreme seasonal droughts in Southwest China. *Sci. Total Environ.* 760, 143427. doi: 10.1016/j.scitotenv.2020.143427

Wang, L., Li, M., Wang, J., Li, X., and Wang., L. (2020). An analytical reductionist framework to separate the effects of climate change and human activities on variation in water use efficiency. *Sci. Total Environ.* 727, 138306. doi: 10.1016/j.scitotenv.2020.138306

Wang, H., Li, X., Xiao, J., and Ma., M. (2021). Evapotranspiration components and water use efficiency from desert to alpine ecosystems in drylands. *Agric. For. Meteorol.*, 298–299, 108283. doi: 10.1016/j.agrformet.2020.108283

Wang, K., Piao, S., He, Y., Liu, Y., and He., H. (2022). Spatial variations and mechanisms for the stability of terrestrial carbon sink in China. *Sci. China Earth Sci.* 66, 227–236. doi: 10.1007/s11430-021-1003-5

Wu, Z., and Huang, N. E. (2009). Ensemble emprirical mode decomposition: A noise-assisted data analysis method. *Adv. Adaptive Data Anal.* 01, 1–40. doi: 10.1142/S1793536909000047

Wu, Z., Huang, N. E., Long, S. R., and Peng., C. K. (2007). On the trend, detrending, and variability of nonlinear and nonstationary time series. *Proc. Natl. Acad. Sci. U.S.A.* 104, 14889–14894. doi: 10.1073/pnas.0701020104

Xu, X., Jiao, F., Liu, H., Gong, H., Zou, C., Lin, N., et al. (2022a). Persistence of increasing vegetation gross primary production under the interactions of climate change and land use changes in Northwest China. *Sci. Total Environ.* 834, 155086. doi: 10.1016/j.scitotenv.2022.155086

Xu, X., Liu, J., Jiao, F., Zhang, K., Ye, X., Gong, H., et al. (2022b). Ecological engineering induced carbon sinks shifting from decreasing to increasing during 1981-2019 in China. *Sci. Total Environ.* 864, 161037. doi: 10.1016/j.scitotenv.2022.161037

Xue, B.-L., Guo, Q., Otto, A., Xiao, J., Tao, S., and Li., L. (2015). Global patterns, trends, and drivers of water use efficiency from 2000 to 2013. *Ecosphere* 6 (10), 1–13. doi: 10.1890/es14-00416.1

Xue, Y., Liang, H., Zhang, B., and He., C. (2022). Vegetation restoration dominated the variation of water use efficiency in China. *J. Hydro.l* 612, 128257. doi: 10.1016/j.jhydrol.2022.128257

Yang, L., Feng, Q., Wen, X., Barzegar, R., Adamowski, J. F., Zhu, M., et al. (2022). Contributions of climate, elevated atmospheric CO2 concentration and land surface changes to variation in water use efficiency in Northwest China. *Catena* 213, 106220. doi: 10.1016/j.catena.2022.106220

Yang, W., Liu, W., Vina, A., Luo, J., He, G., Ouyang, Z., et al. (2013). Performance and prospects of payments for ecosystem services programs: evidence from China. *J. Environ. Manage* 127, 86–95. doi: 10.1016/j.jenvman.2013.04.019

Yang, Y., Shi, Y., Sun, W., Chang, J., Zhu, J., Chen, L., et al. (2022). Terrestrial carbon sinks in China and around the world and their contribution to carbon neutrality. *Sci. China Life Sci.* 65, 861–895. doi: 10.1007/s11427-021-2045-5

Yang, H. F., Yao, L., Wang, Y. B., and Li., J. L. (2017). Relative contribution of climate change and human activities to vegetation degradation and restoration in North Xinjiang, China. *Rangeland J.* 39, 289–302. doi: 10.1071/rj16069

Yu, L., Zhao, X., Gao, X., Jia, R., Yang, M., Yang, X., et al. (2021). Effect of natural factors and management practices on agricultural water use efficiency under drought: A meta-analysis of global drylands. *J. Hydrol.*, 594, 125977. doi: 10.1016/j.jhydrol.2021.125977

Zhang, L., Xiao, J., Zheng, Y., Li, S., and Zhou., Y. (2020). Increased carbon uptake and water use efficiency in global semi-arid ecosystems. *Environ. Res. Lett.* 15 (3), 034022. doi: 10.1088/1748-9326/ab68ec

Zhang, L., Xiao, J., Zhou, Y., Zheng, Y., Li, J., and Xiao., H. (2016). Drought events and their effects on vegetation productivity in China. *Ecosphere* 7 (12), e01591. doi: 10.1002/ecs2.1591

Zhang, C.-y., Zhao, L., Zhang, H., Chen, M.-n., Fang, R.-y., Yao, Y., et al. (2022). Spatial-temporal characteristics of carbon emissions from land use change in Yellow River Delta region, China. *Ecol. Indic.* 136, 108623. doi: 10.1016/j.ecolind.2022.108623

Zhao, F., Wu, Y., Ma, S., Lei, X., and Liao., W. (2022). Increased water use efficiency in China and its drivers during 2000–2016. *Ecosystems* 25, 1476–1492. doi: 10.1007/s10021-021-00727-4

frontiers | Frontiers in Plant Science

TYPE Original Research
PUBLISHED 20 November 2023
DOI 10.3389/fpls.2023.1279963

OPEN ACCESS

EDITED BY
Qingpeng Yang,
Institute of Applied Ecology, Chinese Academy of Sciences (CAS), China

REVIEWED BY
Songzhu Zhang,
Shenyang Agricultural University, China
Wenhua Xu,
Jilin Academy of Agricultural Sciences (CAAS), China

*CORRESPONDENCE
Wenxu Dong
dongwx@sjziam.ac.cn
Lianhong Gu
lianhong-gu@ornl.gov

RECEIVED 19 August 2023
ACCEPTED 25 October 2023
PUBLISHED 20 November 2023

CITATION
Liu X, Qiao Y, Zhou W, Dong W and Gu L (2023) Determinants of photochemical characteristics of the photosynthetic electron transport chain of maize. *Front. Plant Sci.* 14:1279963. doi: 10.3389/fpls.2023.1279963

Determinants of photochemical characteristics of the photosynthetic electron transport chain of maize

Xiuping Liu[1], Yunzhou Qiao[1], Wangming Zhou[2], Wenxu Dong[1]* and Lianhong Gu[3]*

[1]Key Laboratory of Agricultural Water Resources, Hebei Key Laboratory of Soil Ecology, Center for Agricultural Resources Research, Institute of Genetics and Developmental Biology, Chinese Academy of Sciences, Shijiazhuang, China, [2]School of Life Sciences, Anqing Normal University, Anqing, China, [3]Environmental Sciences Division and Climate Change Science Institute, Oak Ridge National Laboratory, Oak Ridge, TN, United States

Introduction: The photosynthetic electron transport chain (ETC) is the bridge that links energy harvesting during the photophysical reactions at one end and energy consumption during the biochemical reactions at the other. Its functioning is thus fundamental for the proper balance between energy supply and demand in photosynthesis. Currently, there is a lack of understanding regarding how the structural properties of the ETC are affected by nutrient availability and plant developmental stages, which is a major roadblock to comprehensive modeling of photosynthesis.

Methods: Redox parameters reflect the structural controls of ETC on the photochemical reactions and electron transport. We conducted joint measurements of chlorophyll fluorescence (ChlF) and gas exchange under systematically varying environmental conditions and growth stages of maize and sampled foliar nutrient contents. We utilized the recently developed steady-state photochemical model to infer redox parameters of electron transport from these measurements.

Results and discussion: We found that the inferred values of these photochemical redox parameters varied with leaf macronutrient content. These variations may be caused either directly by these nutrients being components of protein complexes on the ETC or indirectly by their impacts on the structural integrity of the thylakoid and feedback from the biochemical reactions. Also, the redox parameters varied with plant morphology and developmental stage, reflecting seasonal changes in the structural properties of the ETC. Our findings will facilitate the parameterization and simulation of complete models of photosynthesis.

KEYWORDS

photosynthesis, photosynthetic electron transport, redox parameters, leaf characteristics, plant growth stages, maize

1 Introduction

The photosynthetic electron transport chain (ETC) between photosystem II (PSII) and photosystem I (PSI) is a key bridge in photosynthesis. It links photophysical reactions at one end and biochemical reactions at the other, while photochemical reactions occur on this bridge (Kamen, 1963; Gu et al., 2023a). The photophysical reactions are responsible for photon harvesting, exciton transfer to reaction centers, and the dissipation of excess energy as heat and fluorescence. The photochemical reactions convert the excitons into free electrons and transport them down the ETC, resulting in water splitting in the lumen, proton translocation from the stroma to the lumen, and the synthesis of NADPH and ATP. The biochemical reactions use the NADPH and ATP produced to reduce CO_2 to sugars and to oxygenate RuBP (Kamen, 1963; Gu et al., 2023a). Because the three stages of the reactions are sequentially connected, the balance between them is crucial for the photosynthetic machinery to operate productively and safely in fluctuating environments.

Among the three reaction stages of photosynthesis at the leaf scale, the photochemical reactions at the ETC are the least studied. The photophysical reactions have long been probed with Pulse Amplitude-Modulated (PAM) fluorometry (Baker, 2008), whereas extensive research has been conducted on the biochemical reactions with the gas exchange technique (von Caemmerer and Farquhar, 1981). In contrast, there has been a lack of a technique that can be used to directly and quantitatively monitor the ETC and the photochemical reactions that occur on it. This lack of quantitative study of the ETC and the photochemical reactions has hindered progress on multiple fronts. For example, many components of the photophysical and biochemical reactions have been targeted for bioengineered modification to improve the efficiency of photosynthesis, including the size of the light-harvesting antenna complex (Kirst et al., 2017; Cardona et al., 2018), nonphotochemical quenching (Kromdijk et al., 2016; De Souza et al., 2022), and Rubisco kinetics (Lin et al., 2014). Currently, it is not clear whether the ETC will be capable of supporting these proposed modifications in such a way that the modified photosynthetic machinery will operate as expected under field conditions. This issue is of relevance for crop bioengineering because the ETC is likely suboptimal under current environmental conditions (Chida et al., 2007; Simkin et al., 2017; Ermakova et al., 2019) and may also need to be modified to support increased electron transport demand without suffering from excessive photooxidative stress (Sonoike, 2011; Vass, 2012). Resolving this issue will require a better understanding of the ETC and the factors that control photochemical reactions (Gu, 2023b).

Another example of areas that call for increased research on the ETC is applications of sun-induced chlorophyll fluorescence (SIF) to monitor CO_2 assimilation in real time under field conditions (Sun et al., 2023a; Sun et al., 2023b). SIF is emitted during the photophysical reactions as one of the dissipation pathways of photon energy harvested by antenna complexes, while CO_2 assimilation is part of the biochemical reactions. Using SIF to infer CO_2 assimilation requires a complete model of photosynthesis that integrates the photophysical, photochemical, and biochemical reactions. To make this complete model of photosynthesis a reality, knowledge of electron transport along the ETC is essential (Gu et al., 2019).

Recently, we developed a mechanistic photochemical model of electron transport that relates the rate of linear electron transport to the redox state of PSII (Gu et al., 2023a). This model can be coupled with the photophysical model of Gu et al. (2019) and the biochemical model of Farquhar et al. (1980) to form a complete model of photosynthesis. However, before such a complete model of photosynthesis can be applied, it is necessary to determine the variabilities of the parameters of the photochemical model and which biotic and abiotic factors may affect these variabilities. This is analogous to the study of parameter variabilities in the biochemical model of photosynthesis (*e.g.*, Walker et al., 2014). The parameters of the photochemical model reflect the characteristics of the redox reactions, which are controlled by the structural properties of the ETC. In this study, we conducted PAM fluorometry and gas exchange measurements on maize leaves at different developmental stages and canopy depths. After these measurements, leaf samples were taken for laboratory analyses of nutrient content and morphology. We inferred photochemical parameters from PAM fluorometry measurements and related them to foliar nutrient content and morphological indices to answer the following questions: How variable are the photochemical parameters of the ETC? Are photochemical parameters affected by leaf nutrient contents and morphology? How are variations in photochemical parameters related to each other? As the first study in this area, the answers to these questions should guide future research on other species.

2 Materials and methods

2.1 Site description and plant material

The study was conducted at the Luancheng Agro-ecological Experimental Station (37°53′ N, 114°41′ E, elevation 50.1 m). The dominant cropping system in this region is winter wheat (*Triticum aestivum* L.) and summer maize (*Zea mays* L.) rotations without fallow. Summer maize is planted from mid-June to early October, and winter wheat is cultivated from late October to early June of the following year. The climate is a warm temperate semi-humid monsoon, with cold winters and warm summers. The mean annual air temperature and precipitation for the period 1984 - 2016 were 12.6°C and 438.3 mm, and in 2022, 25.3°C and 492 mm occurred in the summer maize season (June-September), respectively. The soils are mainly cinnamon soils, containing 23.4 g kg^{-1} organic matter, 1.42 g kg^{-1} total N, 135 mg kg^{-1} available N, 18.9 mg kg^{-1} available P, and 98.4 mg kg^{-1} available K in the topsoil (0-20 cm).

Summer maize, Zhengdan 958, was sown on 18 June 2022 at 60 cm row spacing and 25 cm plant spacing, and harvested on 4 October 2022. Before sowing, winter wheat was harvested, and the straw was chopped and returned to the field. Subsequently, summer maize was planted with a no-till seeder equipped with a fertilizer distributor, and 600 kg ha^{-1} compound fertilizer (N: P_2O_5: K_2O =

30:5:5) was applied as basal fertilizer. On the fifth day after sowing, the plants were fully irrigated to ensure even germination. With the exception of a herbicide application in early July, no other management measures were applied during plant growth.

2.2 Gas exchange and chlorophyll fluorescence measurements

Using fully expanded leaves from the bottom to the top of the canopy, combined gas exchange and chlorophyll fluorescence (ChlF) measurements of summer maize were conducted at the seedling (8 July), jointing (17 July), flowering (29 July, 11 August), filling (20 August), and maturity (7 September, 21 September) stages. Measurements were made between 9:00 and 16:00 using a LI-6400XT portable photosynthesis system (Li-Cor, Lincoln, NE, USA) fitted with a LI-6400-40 fluorescence leaf chamber. It is important to note that photosynthetic light response and CO_2 response curves were measured together with ChlF on one leaf without moving the leaf chamber in between. Minimum fluorescence (F_o) and maximum fluorescence (F_m) in the dark-adapted state were measured pre-dawn. To produce light response curves and ChlF, the portable photosynthesis system was set to 400 μmol mol^{-1} CO_2, airflow at 500 μmol s^{-1}, photosynthetically active radiation (*PAR*) at 1800 μmol m^{-2} s^{-1}, and leaf temperature and relative humidity at ambient levels. Once net photosynthesis rate (A) and stomatal conductance (g_s) were stable, *PAR* was lowered sequentially to 1600, 1400, 1200, 1000, 800, 600, 400, 200, 150, 100, 50, 20, and 0 μmol m^{-2} s^{-1}, and measurements were taken at each *PAR* as A reached steady state. Following completion of the light response curves, *PAR* was switched to 1600 μmol m^{-2} s^{-1}, and CO_2 response curves and ChlF were measured using the following sequence of CO_2 concentrations: 400, 300, 200, 150, 100, 50, 400, 400, 600, 800, 1000, and 1200 μmol mol^{-1}. Before each measurement, the CO_2 and water vapor concentrations were automatically matched between the leaf and reference chambers. Finally, a total of 22 ChlF and gas exchange data were obtained for parameter calculation.

2.3 Leaf characteristics

After gas exchange measurements, leaves were harvested for the determination of leaf area with an electronic area meter (LI-3000A, Li-Cor, Lincoln, NE), leaf thickness with a digital micrometer (Mitutoyo, Japan), and dry mass after drying at 60°C to a constant mass. Specific leaf weight was then calculated as the ratio of leaf dry weight to leaf area. Subsequently, dried leaf samples were ground, nitrogen content (N) was determined by the Kjeldahl method (Kjeltec 8400, Foss, Sweden), phosphorus content (P) was measured by the molybdate colorimetric method (UV-2450, Shimadzu, Japan), and potassium (K) and calcium (Ca) contents were determined by a flame atomic absorption spectrophotometer (Analytik Jena, Germany). In total, six leaf characteristics were quantified: leaf thickness, specific leaf weight, foliar N, P, K, and Ca contents.

2.4 Inference of redox reaction parameters

Gu et al. (2023a) derived a steady-state redox model to study the relationship between electron transport and the redox state of the ETC. According to this model, the linear electron transport (LET) rate from PSII to PSI (J_{PSII}) is photochemically related to the fraction of open PSII reaction centers (q) via the following equations:

$$J_{PSII} = \frac{2Uf_T f_s f_q (q_r - q)q}{(R_1 + 2R_2 f_s f_q - 1)q + q_r}, \quad (1)$$

$$U = uN_{PQ_T}N_{cyt_T}, \quad (2)$$

$$R_1 = \frac{r_r}{r_d}, \quad (3)$$

$$R_2 = \frac{u}{r_d} \times \frac{N_{cyt_T}}{N_{PSII}}, \quad (4)$$

$$f_T = \sqrt{\frac{T_0}{T}} e^{E_T\left(\frac{1}{T_0} - \frac{1}{T}\right)}, \quad (5)$$

$$f_s = \frac{v}{v_{max}} = \frac{1}{1 + c_s e^{-b_s \times \alpha PAR}}, \quad (6)$$

$$f_q = \frac{1 + a_q}{1 + a_q \times q}, \quad (7)$$

where U is the maximum oxidation potential of the combined mobile plastoquinone/plastoquinol (PQ/PQH_2) pool by the cytochrome b_6f complex (Cyt). R_1 and R_2 are the first and second electron transport resistances, respectively. u is the second-order rate constant for the oxidation of PQH_2 by the RieskeFeS protein of Cyt. r_d and r_r are the second-order rate constants for the electron transfer from the reduced acceptor to PQ to form PQH_2 and for the reverse reaction, respectively. N_{PSII}, N_{PQ_T}, and N_{cyt_T} are the total foliar concentrations of PSII, the combined PQ and PQH_2 pool, and Cyt for linear electron transport, respectively. q_r is the fraction of reversible PSII reaction centers, which may be less than unity due to the presence of inhibited and Q_B-nonreducing PSII reaction centers and the two-electron gate.

Equation 1 also contains three function modifiers, f_T, f_s, and f_q. f_T (Equation 5) is the standardized temperature (T) response function for modifying redox reactions derived from the Marcus theory of electron transfer in proteins. E_T is a composite temperature sensitivity parameter related to the Gibbs free energy of activation. T_0 = 298.15 K is the reference temperature. f_s (Equation 6) is the light-induced thylakoid ultrastructure dynamic function, which quantifies the degree of thylakoid ultrastructural control over electron transport. This ultrastructural control is achieved by regulating the effect of macromolecular crowding on the diffusion of mobile electron carriers and the effective availability of Cyt for linear electron transport (LET) (Gu et al., 2022). v is the total thylakoid volume at a given *PAR* level and swells/shrinks in response to osmotic water fluxes into and out of the lumen, similar

to the guard cell turgor pressure dynamics. v_{max} is the maximum thylakoid volume when it is fully swollen. b_s controls the speed of light-induced swelling/shrinking, while c_s inversely determines the maximum net impact of macromolecular crowding on the effective availability of Cyt for LET. f_s varies between a value determined by c_s (thylakoid minimally shrunk in the dark) and 1 (thylakoid maximally expanded in full light). f_q is the photosynthetically controlled redox poise balance function between Cyt and PSII, with a_q as the redox poise stoichiometry parameter. This function relates the fraction of Cyt available for LET, denoted by h_{Cyt}, to the fraction of PSII open reaction centers (*i.e.*, q) via $h_{Cyt} = f_q \times q$. $a_q = 0$ gives the redox isocline between Cyt and PSII ($h_{Cyt} = q$, Gu et al., 2023a), and is a special case that has been assumed in previous studies (*e.g.*, Johnson and Berry, 2021). If $a_q > 0$, $h_{Cyt} > q$, it indicates that PSII is more strained than Cyt for LET. If $a_q < 0$, $h_{Cyt} < q$, it indicates that Cyt is more strained than PSII for LET.

It should be noted that the photochemical model of the $J_{PSII} - q$ relationship of Gu et al. (2023a) is complementary to, but fundamentally different from, the corresponding photophysical J_{PSII} - q relationship of Gu et al. (2019). The former is a consequence of redox reactions at the ETC, while the latter reflects the partitioning of the absorbed energy into different dissipation pathways according to the principle of energy conservation. These two models can be used together to couple the photophysics with the photochemistry of photosynthesis. A detailed discussion of this topic is available in Gu et al. (2023a).

Using the steady-state photochemical model in conjunction with ChlF and gas exchange data, we can infer the redox parameters of summer maize at different growth stages. To do so, we calculated J_{PSII} (μmol m^{-2} s^{-1}) with $J_{PSII} = \Phi_{PSII} \times \alpha\beta PAR$. Here, $\Phi_{PSII} = 1 - \frac{F_s}{F_m'}$ is the photochemical yield of PSII, PAR (μmol m^{-2} s^{-1}) is the incident photosynthetically active radiation, $\alpha = 0.85$ is the leaf absorptance in PAR, and $\beta = 0.5$ is the fraction of absorbed PAR allocated to PSII. We assumed a lake model of photosynthetic unit connectivity and calculated q as $q_l = \frac{F_m' - F_s}{F_m' - F_o'} \times \frac{F_o'}{F_s}$ (Kramer et al., 2004), $F_o' = \frac{F_o}{\frac{F_v}{F_m} + \frac{F_o}{F_m'}}$ (Oxborough and Baker, 1997) and F_m' are minimum, maximum fluorescence yield in the light-adapted state, and F_o and F_m are minimum, maximum fluorescence yield in the dark-adapted state, respectively, and F_s is the steady-state fluorescence yield. As explained in Gu et al. (2023a), the form of Equation 1 is independent of any assumption regarding the connectivity of the photosynthetic unit, but its parameter values may depend on whether the lake or puddle model is assumed, as the value of q (but not Φ_{PSII} and therefore J_{PSII}, Kramer et al., 2004) will be different.

Equation 1 contains eight independent composite redox parameters in total (U, R_1, R_2, q_r, E_T, c_s, b_s, and a_q). We estimated these eight redox reaction parameters by fitting the modeled J_{PSII} as closely as possible to the measured values with the Tool for Optimizing the Open-Closed Redox Model (TOOCRM) of photosynthetic electron transport developed by and provided in Gu et al. (2023a). TOOCRM is a convenient Excel spreadsheet-based tool that uses the evolutionary method for parameter optimization.

2.5 Statistical analyses

We evaluated model performance by comparing predicted and measured $J_{PSII} - q$ relationships at different growth stages and canopy heights and examining their correlation. The relationships between redox parameters (U, R_1, R_2, q_r, a_q, E_T, b_s, and c_s) and leaf characteristics (specific leaf weight, leaf thickness, N, P, K, and Ca), in addition to the relationships among these redox parameters, were examined by multiple regression. The goodness of fit of the model was evaluated by the coefficient of determination (R^2) and analysis of variance (p-value). Multivariate partial least squares regression, including leave-one-out cross-validation and jackknife estimation of regression coefficients, was performed to examine the associations between redox parameters and specific leaf weight, leaf thickness, N, P, K, and Ca. Additionally, we analyzed the temporal variation of redox parameters and leaf characteristics at different growth stages.

3 Results

3.1 Model performance

As shown in Figures 1, 2, we found close agreement between the observed and modeled $J_{PSII} - q$ relationships at different growth stages and canopy heights and almost perfect correlations between modeled and measured J_{PSII}. Table 1 summarizes the test statistics for model performance. Our evaluation is consistent with that reported by Gu et al. (2023a), and indicated that the steady-state photochemical model performed well in reproducing the relationship between the linear electron transport rate and the fraction of open PSII reaction centers and that our use of the $J_{PSII} - q$ equation to infer redox parameters was warranted.

3.2 Relationships between redox parameters and leaf characteristics

We examined all 48 relationships between the eight redox parameters and six leaf characteristic parameters ($8 \times 6 = 48$). 18 of the 48 relationships were statistically significant and are shown in Figures 3–13. U decreased with leaf thickness and Ca (Figures 3A, B) but increased with leaf N and K (Figures 3C, D). Power functions can reflect the relationships between U and leaf thickness (Figure 3A, $R^2 = 0.489$, $p = 0.000$) and between U and N (Figure 3C, $R^2 = 0.023$, $p = 0.014$), while a linear function and a quadratic polynomial can fit the relationship between U and Ca (Figure 3B, $R^2 = 0.201$, $p = 0.036$), and that between U and K (Figure 3D, $R^2 = 0.745$, $p = 0.000$), respectively. Partial least squares regression revealed that specific leaf weight (negative, p=0.031), N (positive, $p = 0.015$), P (negative, p=0.013), and K (positive, $p = 0.041$) significantly influenced U ($R^2 = 0.566$, Figures 4A, 5A). R_1 decreased with leaf K, and an exponential function can describe the relationship between them (Figure 6, $R^2 = 0.122$, p = 0.033). R_2

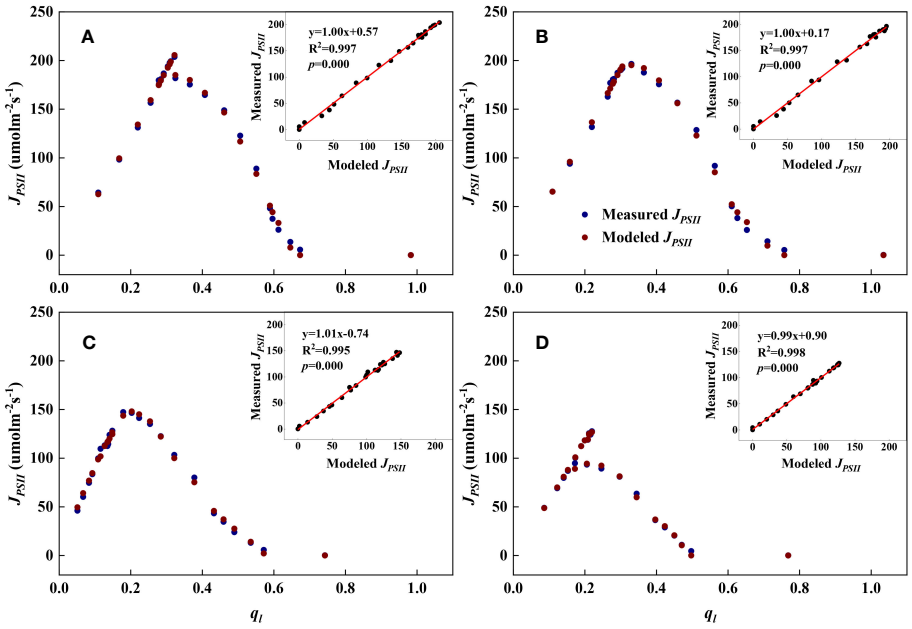

FIGURE 1
Examples demonstrating the performance of the steady-state photochemical model for predicting the linear electron transport rate (J_{PSII}) as a function of the fraction of open PSII reaction centers (q_l) for top canopy leaves at different growth stages. Inset: Comparison of measured vs. modeled J_{PSII}. **(A)**: Jointing (17 July); **(B)**: Flowering (29 July); **(C)**: Filling (20 August); **(D)**: Maturity (7 September).

decreased with specific leaf weight, leaf thickness, leaf N, P, and Ca (Figures 7A–E). Linear relationships were found between R_2 and specific leaf weight (Figure 7A, R^2 = 0.293, p = 0.009), leaf N (Figure 7C, R^2 = 0.183, p = 0.047), and P (Figure 7D, R^2 = 0.262, p = 0.015), while exponential relationships were found between R_2 and leaf thickness (Figure 7B, R^2 = 0.113, p = 0.019) and leaf Ca (Figure 7E, R^2 = 0.081, p = 0.027). Partial least squares regression revealed that specific leaf weight (p = 0.047) and N (p = 0.025) were negatively related to R_2 (R^2 = 0.073, Figures 4B, 5B). q_r appeared to be a peaked function of specific leaf weight, leaf N, and P, with both low and high values of these leaf characteristics lowering q_r (Figures 8A–C). As a result, quadratic polynomial functions can describe the relationships between q_r and specific leaf weight (Figure 8A, R^2 = 0.512, p = 0.008), between q_r and N (Figure 8B,

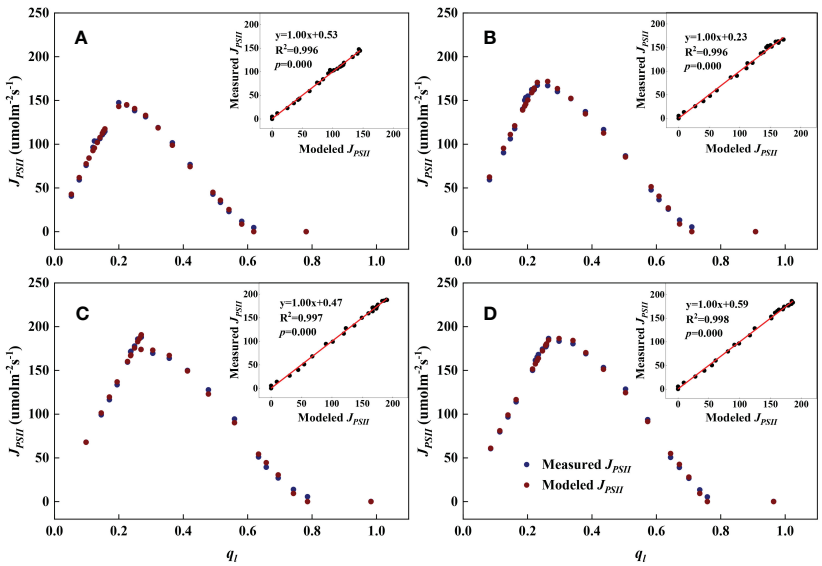

FIGURE 2
Examples demonstrating the performance of the steady-state photochemical model for predicting the linear electron transport rate (J_{PSII}) as a function of the fraction of open PSII reaction centers (q_l) at the flowering stage. Inset: Comparison of measured vs. modeled J_{PSII}. **(A)**: Bottom; **(B)**: Lower middle; **(C)**: Upper middle; **(D)**: Top.

10.3389/fpls.2023.1279963

TABLE 1 The correlation between modeled and measured linear electron transport rate (J_{PSII}).

Date	Position	Equation	R^2	*p*
8 July		y=1.00x+0.34	0.987	0.000
17 July	Bottom	y=1.00x+0.29	0.996	0.000
	Top	y=1.00x+0.57	0.997	0.000
29 July	Bottom	y=1.00x+0.35	0.997	0.000
	Middle	y=1.00x+0.10	0.995	0.000
	Top	y=1.00x+0.17	0.997	0.000
11 August	Bottom	y=1.00x+0.53	0.996	0.000
	Lower middle	y=1.00x+0.23	0.995	0.000
	Upper middle	y=1.00x+0.47	0.997	0.000
	Top	y=1.00x+0.59	0.998	0.000
20 August	Bottom	y=1.02x-1.48	0.986	0.000
	Lower middle	y=1.00x+0.56	0.996	0.000
	Upper middle	y=0.99x+0.68	0.996	0.000
	Top	y=1.01x-0.74	0.995	0.000
7 September	Bottom	y=1.01x-0.49	0.995	0.000
	Lower middle	y=0.99x+0.60	0.998	0.000
	Upper middle	y=0.99x+0.82	0.998	0.000
	Top	y=0.99x+0.90	0.999	0.000
21 September	Bottom	y=1.00x-0.23	0.987	0.000
	Lower middle	y=1.00x-0.15	0.991	0.000
	Upper middle	y=1.00x+0.45	0.997	0.000
	Top	y=1.00x-0.60	0.997	0.000

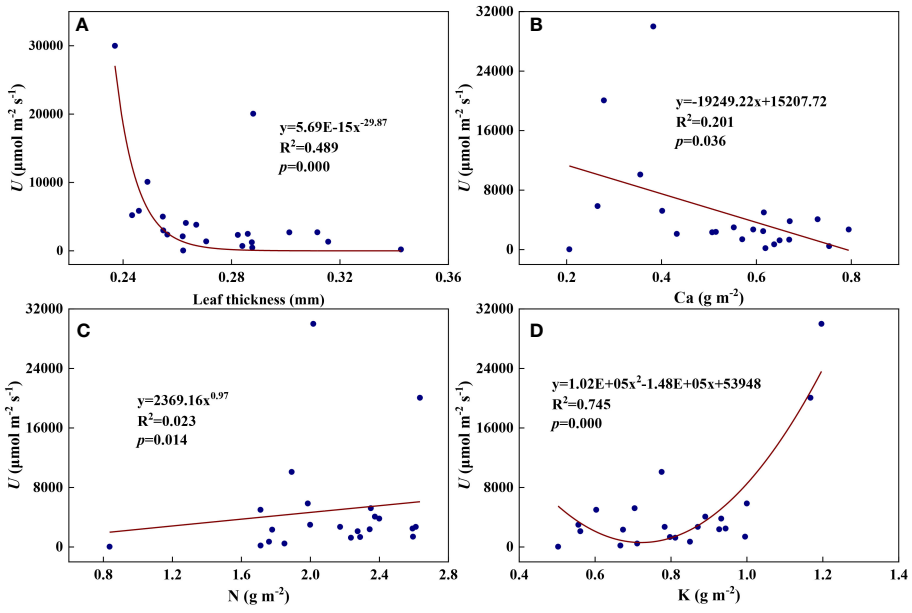

FIGURE 3
The relationships between the redox parameter *U* and leaf characteristics during summer maize growth. **(A)**: *U*-leaf thickness; **(B)**: *U*-Ca; **(C)**: *U*-N; **(D)**: *U*-K.

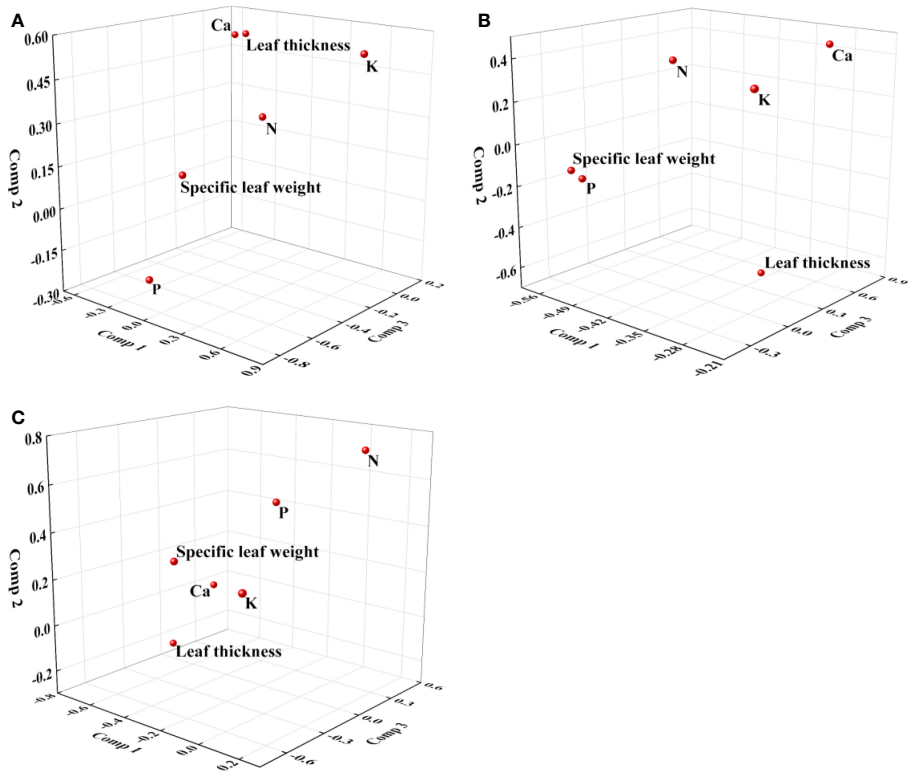

FIGURE 4
Loading plot of partial least squares regression for redox parameters and leaf characteristics. **(A)**: *U*; **(B)**: R_2; **(C)**: c_s.

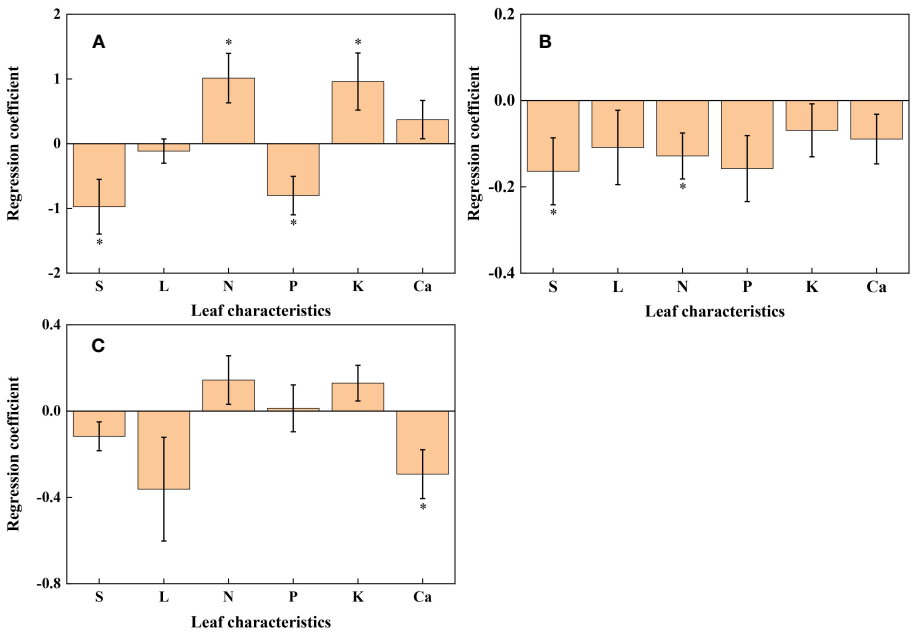

FIGURE 5
Histogram of regression coefficients of leaf characteristics affecting redox parameters. **(A)**: *U*; **(B)**: R_2; **(C)**: c_s. S: Specific leaf weight; L: Leaf thickness. ∗ Significant impact at $p< 0.05$.

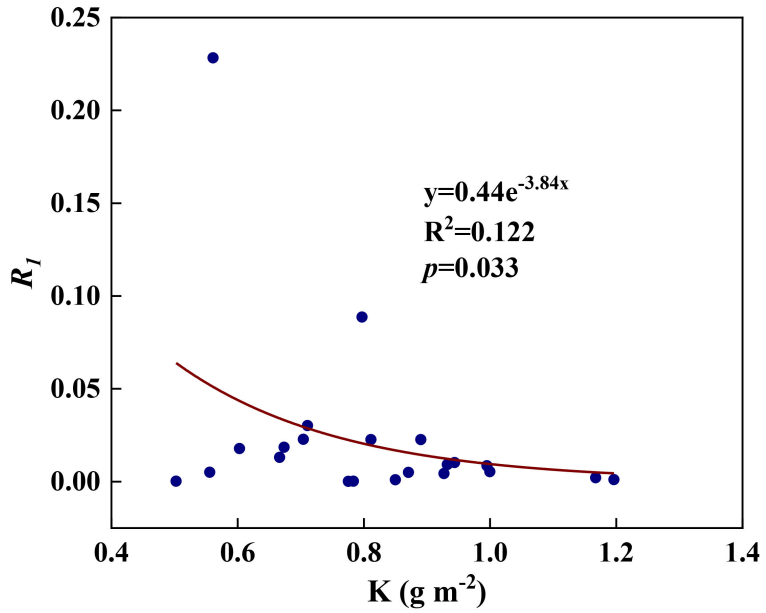

FIGURE 6
The relationships between redox parameter R_1 and leaf K content during summer maize growth.

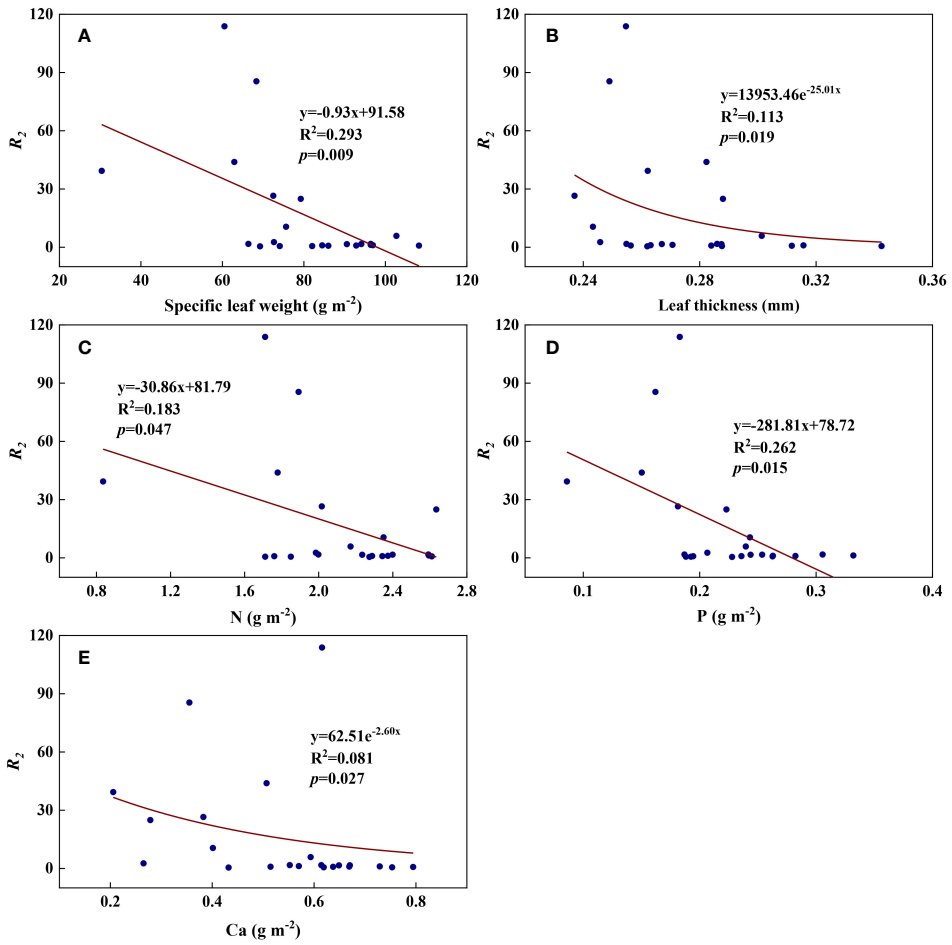

FIGURE 7
The relationships between redox parameter R_2 and leaf characteristics during summer maize growth. **(A)**: R_2-specific leaf weight; **(B)**: R_2-leaf thickness; **(C)**: R_2-N; **(D)**: R_2-P; **(E)**: R_2-Ca.

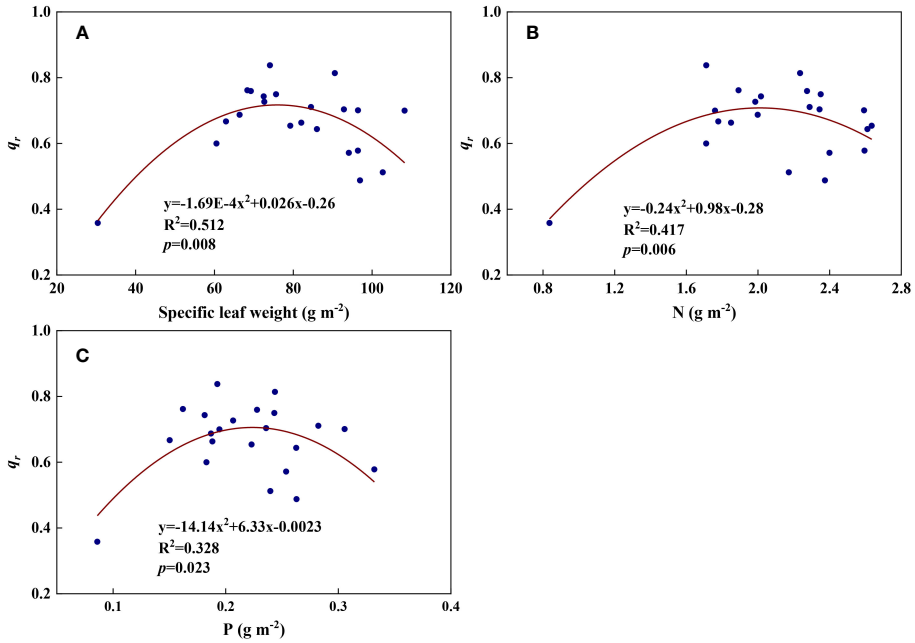

FIGURE 8
The relationships between redox parameter q_r and leaf characteristics during summer maize growth. **(A)**: q_r-specific leaf weight; **(B)**: q_r-N; **(C)**: q_r-P.

R^2 = 0.417, p = 0.006), and between q_r and P (Figure 8C, R^2 = 0.328, p = 0.023). a_q increased with specific leaf weight (Figure 9), and E_T and b_s increased with leaf P (Figures 10, 11). Quadratic polynomial functions can model the relationships between a_q and specific leaf weight (Figure 9, R^2 = 0.342, p = 0.023), between E_T and P (Figure 10, R^2 = 0.396, p = 0.008), and between b_s and P (Figure 11, R^2 = 0.299, p = 0.041). c_s decreased with leaf thickness and leaf Ca (Figures 12A, B). Linear functions can fit the relationships between c_s and leaf thickness (Figure 12A, R^2 = 0.318, p = 0.006) and between c_s and Ca (Figure 12B, R^2 = 0.243, p = 0.020). Partial least squares regression revealed that Ca was negatively correlated with c_s (R^2 = 0.079, p = 0.017, Figures 4C, 5C). As shown in Figure S1, the remaining 30 of the 48 relationships are highly scattered and are not statistically significant; these plots will not be discussed here.

3.3 Relationships between redox parameters

We examined all 28 relationships between any two of the eight redox parameters (8×7/2 = 28). Eight of the 28 relationships were statistically significant and are shown in Figure 12. a_q decreased with U, R_2, b_s, and c_s (Figures 13A–D). Logarithmic functions can describe the relationships between a_q and U (Figure 13A, R^2 = 0.260, p = 0.015) and between a_q and R_2 (Figure 13B, R^2 = 0.211, p = 0.031), while quadratic polynomial functions can describe the relationships between a_q and b_s (Figure 13C, R^2 = 0.658, p = 0.000) and between a_q and c_s (Figure 13D, R^2 = 0.464, p = 0.003). b_s decreased with q_r but increased with c_s (Figures 13E, F). A power function can fit the relationship between b_s and q_r (Figure 13E, R^2 = 0.168, p = 0.000), while a quadratic polynomial function can model the relationship between b_s and c_s (Figure 13F, R^2 = 0.285, p = 0.049). E_T increased with R_1 and a linear function fit the relationship between them well (Figure 13G, R^2 = 0.456, p = 0.000). U increased with R_2 and a logarithmic function can describe the relationship between them (Figure 13H, R^2 = 0.236, p = 0.022). As shown in Figure S2, the remaining 20 of the 28 relationships did not reach statistical significance.

3.4 Temporal variations of redox parameters

Redox parameters varied significantly from seedling to maturity. U increased significantly from the seedling to the jointing stage and then decreased rapidly to the filling stage but remained almost constant at the maturity stage (Figure 14A). R_1 increased from the seedling to the flowering stage and then decreased with grain maturation (Figure 14B). R_2 fluctuated at high levels until the flowering stage and then remained nearly constant during the maturity stages (Figure 14C). q_r increased steeply at the jointing stage and then fluctuated at relatively high levels until maturity (Figure 14D). E_T fluctuated at low levels until the flowering period and increased steeply at the filling stage but decreased with grain maturation (Figure 14E). a_q remained nearly constant until the flowering period and then gradually increased during the maturity stages (Figure 14F). b_s was highest in seedlings, and remained relatively constant throughout the growth period, but decreased at the end of late maturation (Figure 14G). c_s remained nearly constant until the flowering period and then decreased in a fluctuating way until maturity (Figure 14H).

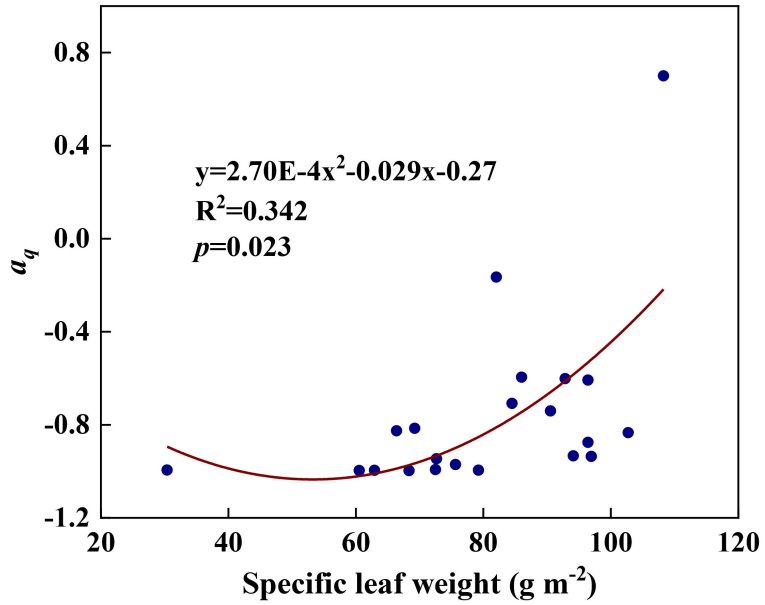

FIGURE 9
The relationships between redox parameter a_q and specific leaf weight during summer maize growth.

3.5 Temporal variations of leaf characteristics

Leaf physical traits and nutrient contents varied dynamically between different growth stages (Figure 15). Specific leaf weight increased gradually with the growth of summer maize (Figure 15A). Leaf thickness remained relatively stable before flowering and increased thereafter (Figure 15B). Leaf N content increased significantly from seedling to jointing stages and then remained almost constant throughout the growth period (Figure 15C). Leaf P and Ca contents increased with the growth of summer maize and decreased at the late stages of grain maturation (Figures 15D, E). Leaf K content increased rapidly at the jointing stage, decreased at the flowering stage, and then remained relatively constant at the filling stage until maturity (Figure 15F).

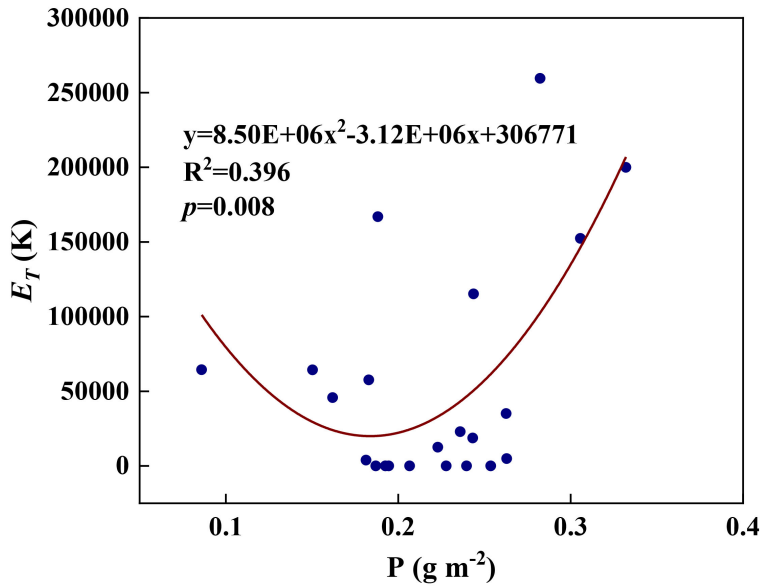

FIGURE 10
The relationships between redox parameter E_T and leaf P content during summer maize growth.

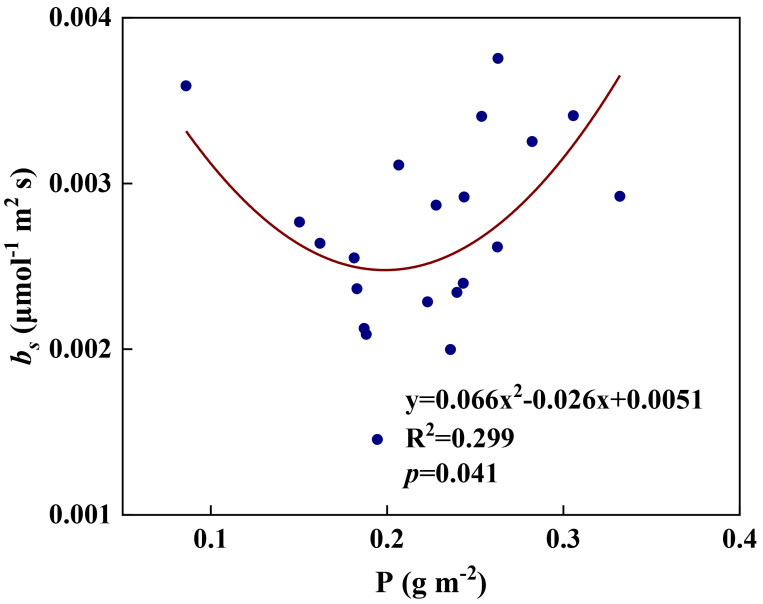

FIGURE 11
The relationships between redox parameter b_s and leaf P content during summer maize growth.

4 Discussion and conclusion

Our study found that there is considerable variation in photochemical redox parameters inferred from PAM fluorometry measurements in maize. Part of these variations may be due to measurement noise and a lack of data constraints on parameter optimization (*i.e.*, overfitting), while statistically significant relationships between these parameters and independently measured leaf macronutrient content and morphology, as well as their systematic variations with developmental stage, suggest that at least part of these variations may be due to changes in the structure of the ETC. All parameters in the photochemical model of electron transport are composite parameters that are influenced by multiple components of the ETC. For example, U is the main parameter that determines the capacity of the ETC. It is the product of the rate constant for the oxidation of PQH_2 by the RieskeFeS protein of Cyt and the abundances of the PQ and Cyt pools. Although PQ does not contain nitrogen, Cyt contains nitrogen in its hemes (Tikhonov, 2023). Therefore, the positive correlation between U and leaf nitrogen probably reflects the higher abundance of Cyt at higher leaf nitrogen contents. The positive correlation between U and leaf nitrogen contributes to the balance between electron transport and CO_2 assimilation, which is catalyzed by Rubisco, a dominant sink of leaf nitrogen (Evans and Clarke, 2019). Potassium is not involved in the structure of organic macromolecules. However, it is the most important inorganic osmotic ion in plant cells and plays an important role in controlling stomatal conductance and in maintaining the structural integrity of granal thylakoids, where photosynthetic macromolecules are located (Tränkner et al, 2018), which likely explains the positive correlation between U and potassium.

The resistance parameters R_1 and R_2 are given by $R_1 = \frac{r_r}{r_d}$ and $R_2 = \frac{u}{r_d} \times \frac{N_{cytT}}{N_{PSII}}$, respectively. r_d and r_r are the second-order rate constants for the forward and reverse reactions between the reduced acceptor of PSII and PQ, respectively, while u is the second-order rate constant for the oxidation of PQH_2 by the RieskeFeS protein of

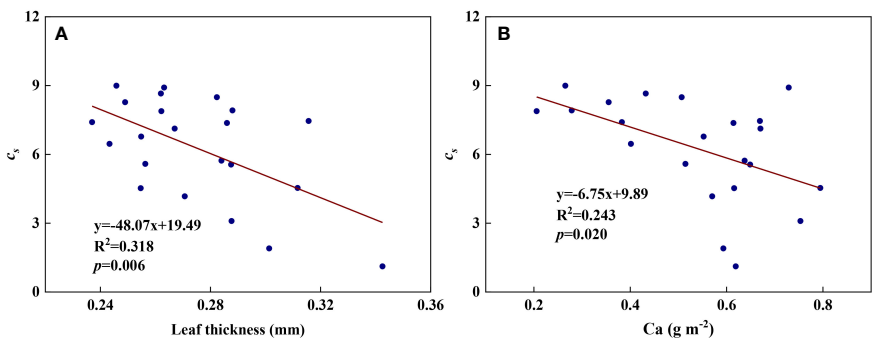

FIGURE 12
The relationships between redox parameter c_s and leaf characteristics during summer maize growth. **(A)**: c_s- leaf thickness; **(B)**: c_s-Ca.

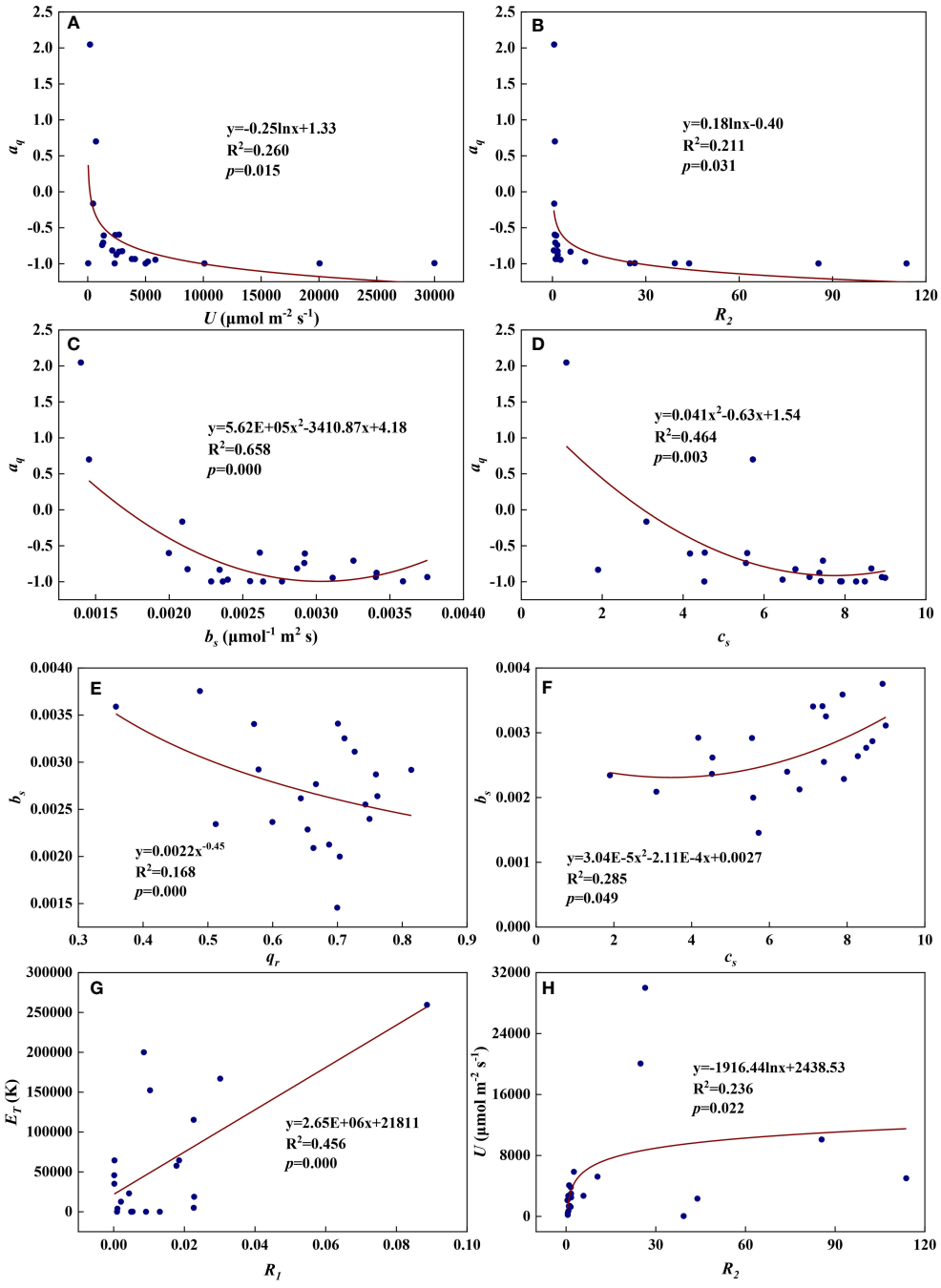

FIGURE 13
The relationships among redox parameters during summer maize growth. **(A)**: a_q-U; **(B)**: a_q-R_2; **(C)**: a_q-b_s; **(D)**: a_q-c_s; **(E)**: b_s-q_r; **(F)**: b_s-c_s; **(G)**: E_T-R_1; **(H)**: U-R_2.

Cyt. Thus, R_1 is inversely related to the efficiency of PQ to take away electrons from PSII, and R_2 is inversely related to the capacity of PSII to supply electrons relative to the capacity of Cyt to oxidize PQH_2. The smaller the values of R_1 and R_2, the higher the efficiency of the ETC. Thus, the decrease of R_1 with potassium and R_2 with nitrogen and phosphorus is consistent with the expected impact of these nutrients on electron transport.

A significant fraction of PSII reaction centers may be Q_B-nonreducing (Tomek et al., 2003; Schansker and Strasser, 2005; Vredenberg et al., 2006; Vredenberg, 2011), which can result in q_r being significantly less than 1. Currently, little is known about why such reaction centers exist at all and what their photochemical functions may be. The significant correlation between q_r and leaf nitrogen may suggest that the fraction of Q_B-nonreducing centers is affected by leaf nitrogen content.

Any factors that affect the relative abundances of PSII and Cyt can affect the value of the parameter a_q. A negative a_q indicates that there is a greater constraint on Cyt than on PSII for electron transport, whereas

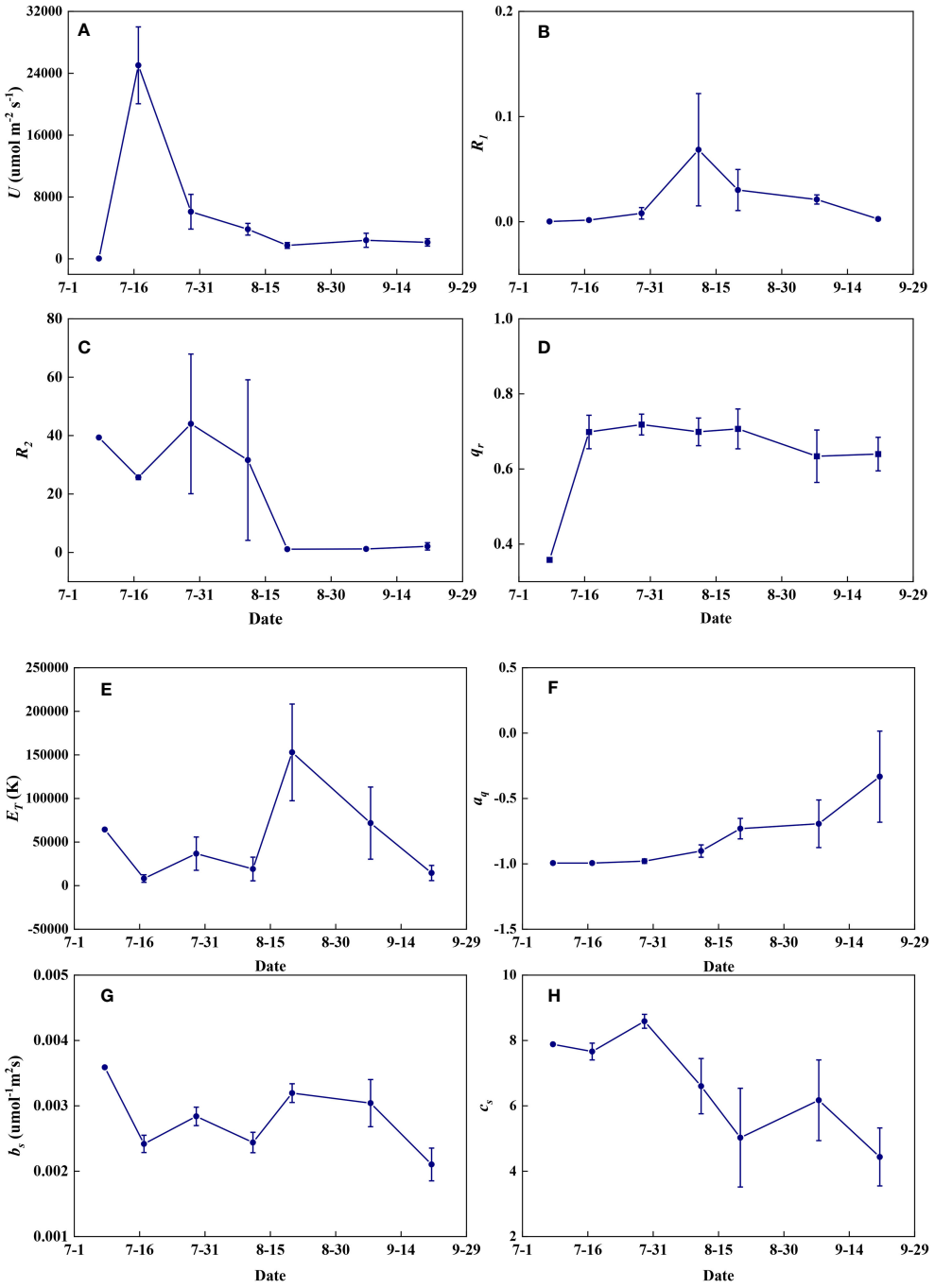

FIGURE 14
The temporal variations of redox parameters during summer maize growth. **(A)**: U; **(B)**: R_1; **(C)**: R_2; **(D)**: q_r; **(E)**: E_T; **(F)**: a_q; **(G)**: b_s; **(H)**: c_s.

a positive a_q indicates the opposite (Gu et al., 2023a). The increase in a_q with specific leaf weight likely indicates that the relative abundance of PSII vs. Cyt in a leaf depends on leaf-specific weight. Variations in b_s and c_s may reflect systematic changes in thylakoid structure. Such changes may include the number of grana per thylakoid, the height of a granum, and the density of ion channels, which affect ion exchange between the lumen and stroma and, therefore, osmotic water fluxes. These changes can affect the degree and speed of thylakoid swelling/shrinking and, therefore, the values of b_s and c_s. Variations in E_T can be caused by changes in the Gibbs free energy of activation (Gu et al., 2023a), which in turn can be caused by changes in the reduction potentials of redox reactions (Silverstein, 2012; Bostick et al., 2018). Thus, the variation of E_T with leaf phosphorus content may indicate that the latter affects the reduction potentials of redox reactions along the ETC.

Currently, it is difficult to provide an in-depth discussion of all the relationships reported in this study. There are very few previous studies that have investigated how the structures and redox reactions of the ETC may be affected by nutrient contents and plant developmental stages, and thus may provide guidance for our analysis. Nevertheless,

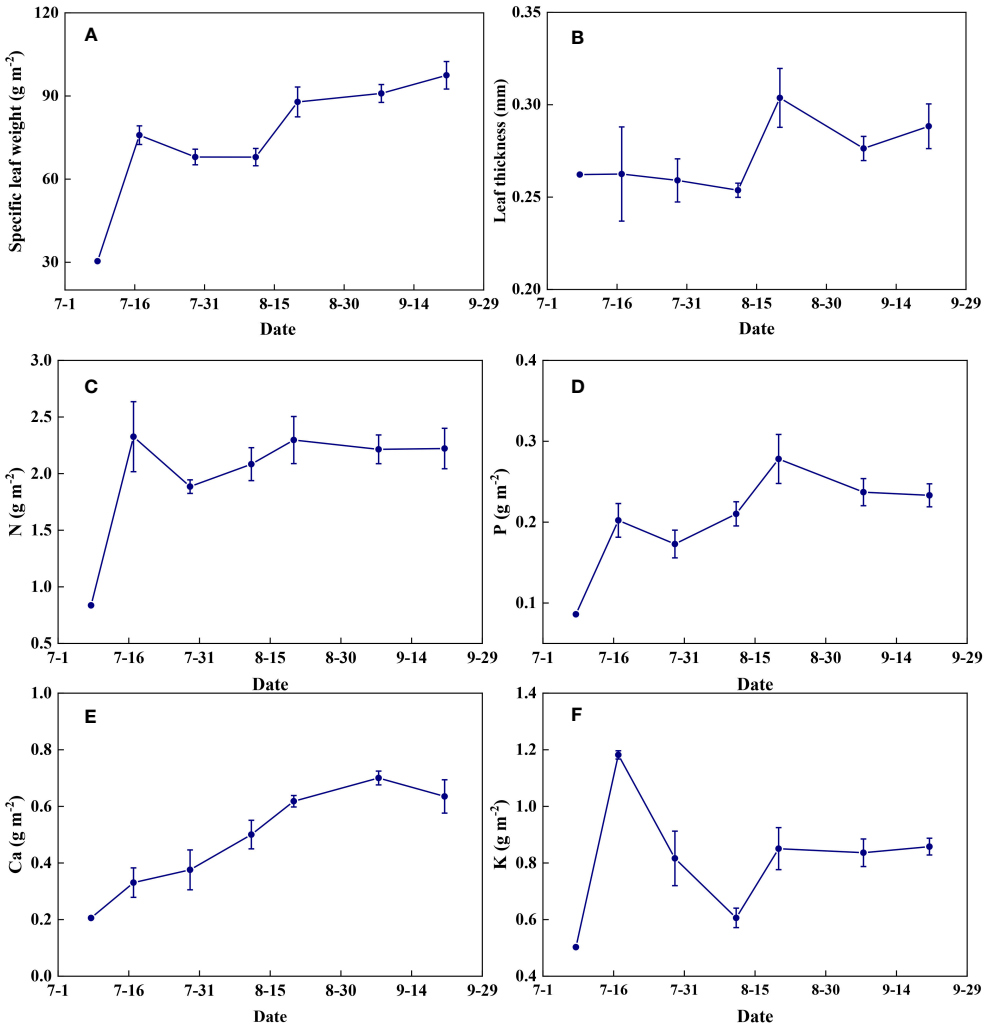

FIGURE 15
The temporal variations of leaf characteristics during summer maize growth. **(A)**: specific leaf weight; **(B)**: leaf thickness; **(C)**: N; **(D)**: P; **(E)**: Ca; **(F)**: K.

our study provides conclusive evidence that the structural properties of the electron transport chain are not static and may vary with plant growth conditions and developmental stages, allowing the photophysical, photochemical, and biochemical reactions to be balanced on seasonal time scales. Our findings also show that it may be possible to parameterize photochemical parameters of electron transport with leaf nutrient content and morphological properties for large-scale modeling applications.

Author's note

This manuscript was co-authored by UT-Battelle, LLC under contract number DE-AC05-00OR22725 with the U.S. Department of Energy. The publisher, by accepting the article for publication, acknowledges that the United States Government retains a non-exclusive, paid-up, irrevocable, worldwide license to publish or reproduce, or allow others to do so, the published form of this manuscript for the purposes of the United States Government. The Department of Energy will provide public access to these results of federally sponsored research in accordance with the DOE Public Access Plan (http://energy.gov/downloads/doe-public-access-plan).

Data availability statement

The raw data supporting the conclusions of this article will be made available by the authors, without undue reservation.

Author contributions

XL: Investigation, Formal analysis, Writing – original draft. YQ: Investigation, Writing – review & editing. WZ: Investigation, Writing – review & editing. WD: Supervision, Writing – review & editing. LG: Methodology, Writing – original draft.

Funding

The author(s) declare financial support was received for the research, authorship, and/or publication of this article. This research

was supported by the National Key Research and Development Program of China (2021YFD1901104, 2022YFD1901604), the "Strategic Priority Research Program" of the Chinese Academy of Sciences (XDA28020303, XDA26040103), and the Key Research and Development Program of Hebei Province (22326412D). LG is supported by the U.S. Department of Energy (DOE), Office of Science, Biological and Environmental Research Program. ORNL is managed by UT-Battelle, LLC, for DOE under contract DE-AC05-00OR22725.

Conflict of interest

The authors declare that the research was conducted in the absence of any commercial or financial relationships that could be construed as a potential conflict of interest.

Publisher's note

Supplementary material

The Supplementary Material for this article can be found online at: https://www.frontiersin.org/articles/10.3389/fpls.2023.1279963/full#supplementary-material

References

Baker, N. R. (2008). Chlorophyll fluorescence: a probe of photosynthesis *in vivo*. *Annu. Rev. Plant Biol.* 59, 89–113. doi: 10.1146/annurev.arplant.59.032607.092759

Bostick, C. D., Mukhopadhyay, S., Pecht, I., Sheves, M., Cahen, D., and Lederman, D. (2018). Protein bioelectronics: a review of what we do and do not know. *Rep. Prog. Phys.* 81, 026601. doi: 10.1088/1361-6633/aa85f2

Cardona, T., Shao, S., and Nixon, P. J. (2018). Enhancing photosynthesis in plants: the light reactions. *Essays Biochem.* 62, 85–94. doi: 10.1042/EBC20170015

Chida, H., Nakazawa, A., Akazaki, H., Hirano, T., Suruga, K., Ogawa, M., et al. (2007). Expression of the algal cytochrome c_6 gene in *Arabidopsis* enhances photosynthesis and growth. *Plant Cell Physiol.* 48, 948–957. doi: 10.1093/pcp/pcm064

De Souza, A. P., Burgess, S. J., Doran, L., Hansen, J., Manukyan, L., Maryn, N., et al. (2022). Soybean photosynthesis and crop yield are improved by accelerating recovery from photoprotection. *Science* 377, 851–854. doi: 10.1126/science.adc9831

Ermakova, M., Lopez-Calcagno, P. E., Raines, C. A., Furbank, R. T., and von Caemmerer, S. (2019). Overexpression of the RieskeFeS protein of the Cytochrome b_6f complex increases C_4 photosynthesis in *Setaria viridis*. *Commun. Biol.* 2, 314. doi: 10.1038/s42003-019-0561-9

Evans, J. R., and Clarke, V. C. (2019). The nitrogen cost of photosynthesis. *J. Exp. Bot.* 70, 7–15doi: 10.1093/jxb/ery366

Farquhar, G. D., von Caemmerer, S., and Berry, J. A. (1980). A biochemical model of photosynthetic CO_2 assimilation in leaves of C_3 species. *Planta* 149, 78–90. doi: 10.1007/BF00386231

Gu, L. (2023b). Optimizing the electron transport chain to sustainably improve photosynthesis. *Plant Physiol.*, kiad490. doi: 10.1093/plphys/kiad490

Gu, L., Grodzinski, B., Han, J., Marie, T., Zhang, Y.-J., Song, Y. C., et al. (2022). Granal thylakoid structure and function: Explaining an enduring mystery of higher plants. *New Phytol.* 236, 319–329. doi: 10.1111/nph.18371

Gu, L., Grodzinski, B., Han, J., Marie, T., Zhang, Y.-J., Song, Y. C., et al. (2023a). An exploratory steady-state redox model of photosynthetic linear electron transport for use in complete modelling of photosynthesis for broad applications. *Plant Cell Environ.* 46, 1540–1561. doi: 10.1111/pce.14563

Gu, L., Han, J., Wood, J. D., Chang, C. Y. Y., and Sun, Y. (2019). Sun-induced Chl fluorescence and its importance for biophysical modeling of photosynthesis based on light reactions. *New Phytol.* 223, 1179–1191. doi: 10.1111/nph.15796

Johnson, J. E., and Berry, J. A. (2021). The role of Cytochrome b_6f in the control of steady-state photosynthesis: a conceptual and quantitative model. *Photosynth. Res.* 148, 101–136. doi: 10.1007/s11120-021-00840-4

Kamen, M. (1963). *Primary processes in photosynthesis* (New York: Academic Press).

Kirst, H., Gabilly, S. T., Niyogi, K. K., Lemaux, P. G., and Melis, A. (2017). Photosynthetic antenna engineering to improve crop yields. *Planta* 245, 1009–1020. doi: 10.1007/s00425-017-2659-y

Kramer, D. M., Johnson, G., Kiirats, O., and Edwards, G. E. (2004). New fluorescence parameters for the determination of Q_A redox state and excitation energy fluxes. *Photosynth. Res.* 79, 209–218. doi: 10.1023/B:PRES.0000015391.99477.0d

Kromdijk, J., Głowacka, K., Leonelli, L., Gabilly, S. T., Iwai, M., Niyogi, K. K., et al. (2016). Improving photosynthesis and crop productivity by accelerating recovery from photoprotection. *Science* 354, 857–861. doi: 10.1126/science.aai8878

Lin, M. T., Occhialini, A., Andralojc, P. J., Parry, M. A. J., and Hanson, M. R. (2014). A faster Rubisco with potential to increase photosynthesis in crops. *Nature* 513, 547–550. doi: 10.1038/nature13776

Oxborough, K., and Baker, N. R. (1997). Resolving chlorophyll a fluorescence images of photosynthetic efficiency into photochemical and non-photochemical components – calculation of *qP* and Fv'/Fm'without measuring Fo'. *Photosynth. Res.* 54, 135–142. doi: 10.1023/A:1005936823310

Schansker, G., and Strasser, R. J. (2005). Quantification of non-Q_B-reducing centers in leaves using a far-red pre-illumination. *Photosynth. Res.* 84, 145–151. doi: 10.1007/s11120-004-7156-z

Silverstein, T. P. (2012). Marcus theory: thermodynamics can control the kinetics of electron transfer reactions. *J. Chem. Educ.* 89, 1159–1167. doi: 10.1021/ed1007712

Simkin, A. J., McAusland, L., Lawson, T., and Raines, C. A. (2017). Overexpression of the RieskeFeS protein increases electron transport rates and biomass yield. *Plant Physiol.* 175, 134–145. doi: 10.1104/pp.17.00622

Sonoike, K. (2011). Photoinhibition of photosystem I. *Physiol. Plant* 142, 56–64. doi: 10.1111/j.1399-3054.2010.01437.x

Sun, Y., Gu, L., Wen, J., van der Tol, C., Porcar-Castell, A., Joiner, J., et al. (2023a). From remotely sensed solar-induced chlorophyll fluorescence to ecosystem structure, function, and service: Part I—Harnessing theory. *Glob. Change Biol.* 29, 2926–2952. doi: 10.1111/gcb.16634

Sun, Y., Wen, J., Gu, L., Joiner, J., Chang, C. Y., van der Tol, C., et al. (2023b). From remotely-sensed solar-induced chlorophyll fluorescence to ecosystem structure, function, and service: Part II—Harnessing data. *Glob. Change Biol.* 29, 2893–2925. doi: 10.1111/gcb.16646

Tikhonov, A. N. (2023). The cytochrome b_6f complex: plastoquinol oxidation and regulation of electron transport in chloroplasts. *Photosynth. Res.* doi: 10.1007/s11120-023-01034-w

Tomek, P., Ilík, P., Lazár, D., Štroch, M., and Nauš, J. (2003). On the determination of Q_B-non-reducing photosystem II centers from chlorophyll a fluorescence induction. *Plant Sci.* 164, 665–670. doi: 10.1016/S0168-9452(03)00029-3

Tränkner, M., Tavakol, E., and Jákli, B. (2018). Functioning of potassium and magnesium in photosynthesis, photosynthate translocation and photoprotection. *Physiol. Plant* 163, 414–431. doi: 10.1111/ppl.12747

Vass, I. (2012). Molecular mechanisms of photodamage in the photosystem II complex. *Biochim. Biophys. Acta* 1817, 209–217. doi: 10.1016/j.bbabio.2011.04.014

von Caemmerer, S., and Farquhar, G. D. (1981). Some relationships between the biochemistry of photosynthesis and the gas exchange of leaves. *Planta* 153, 376–387. doi: 10.1007/BF00384257

Vredenberg, W. (2011). Kinetic analyses and mathematical modeling of primary photochemical and photoelectrochemical processes in plant photosystems. *Biosystems* 103, 138–151. doi: 10.1016/j.biosystems.2010.10.016

Vredenberg, W., Kasalicky, V., Durchan, M., and Prasil, O. (2006). The chlorophyll a fluorescence induction pattern in chloroplasts upon repetitive single turnover excitations: Accumulation and function of Q_B-nonreducing centers. *Biochim. Biophys. Acta* 1757, 173–181. doi: 10.1016/j.bbabio.2006.02.006

Walker, A. P., Beckerman, A. P., Gu, L., Kattge, J., Cernusak, L. A., Domingues, T. F., et al. (2014). The relationship of leaf photosynthetic traits – V_{cmax} and J_{max} – to leaf nitrogen, leaf phosphorus, and specific leaf area: a meta-analysis and modeling study. *Ecol. Evol.* 4, 3218–3235. doi: 10.1002/ece3.1173

frontiers | Frontiers in Plant Science

TYPE Original Research
PUBLISHED 27 November 2023
DOI 10.3389/fpls.2023.1271262

OPEN ACCESS

EDITED BY
Qingpeng Yang,
Chinese Academy of Sciences (CAS), China

REVIEWED BY
Liuyang Yu,
Northwest A & F University, China
Pengfei Wu,
Fujian Agriculture and Forestry University, China
Fengxia Zhao,
Shanxi Normal University, China

*CORRESPONDENCE
Lihua Hao
haolihua_000@sina.com
Yunxin Zhang
zyx14315@163.com

†These authors have contributed equally to this work

RECEIVED 02 August 2023
ACCEPTED 06 November 2023
PUBLISHED 27 November 2023

CITATION
Li F, He C, Chang Z, Ma C, Yu J, Liu L, Zhang Y and Hao L (2023) Effects of elevated carbon dioxide on plant growth and leaf photosynthesis of annual ryegrass along a phosphorus deficiency gradient. *Front. Plant Sci.* 14:1271262. doi: 10.3389/fpls.2023.1271262

Effects of elevated carbon dioxide on plant growth and leaf photosynthesis of annual ryegrass along a phosphorus deficiency gradient

Fei Li[1†], Chunlin He[2†], Zhijie Chang[3†], Chao Ma[1], Jingjin Yu[4], Liang Liu[1], Yunxin Zhang[1*] and Lihua Hao[1*]

[1]School of Water Conservancy and Hydropower, Hebei University of Engineering, Handan, China, [2]Jiangsu Provincial Flood Control and Drought Relief Center, Nanjing, China, [3]College of Water Resources and Architectural Engineering, Northwest A&F University, Yangling, China, [4]School of Agro-Grassland Science, Nanjing Agricultural University, Nanjing, China

Introduction: Soil phosphorus (P) deficiency limits plant growth and productivity in grassland ecosystems and may moderate the growth-promoting effects of "carbon dioxide (CO_2) fertilization effect".

Methods: To evaluate the interactive effects of these two factors on the growth and physiology for annual ryegrass (*Lolium multiflorum* Lam.), plants were grown in controlled growth chambers with a range of P supply (0.004, 0.012, 0.02, 0.06, 0.1 and 0.5 mM) under two levels of CO_2 (400 and 800 μmol mol^{-1}, respectively).

Results: Elevated [CO_2] dramatically increased the aboveground biomass and net photosynthetic rates of annual ryegrass by 14.5% and 25.3% under sufficient P supply (0.5 mM), respectively, whereas decreased the belowground biomass and net photosynthetic rates under lower P supply of $P_{0.004}$, $P_{0.02}$, and $P_{0.06}$. Two-way ANOVA results showed that CO_2 × P ($p < 0.001$) significantly affected stomatal traits, leaf photosynthesis and biomass. The stimulation of growth and photosynthesis by elevated CO_2 concentration (e[CO_2]) was reduced or highly suppressed, indicating that the sensitivity of annual ryegrass to P deficiency was enhanced under e[CO_2].

Discussion: These results indicated that P limitation may offset the positive effects of e[CO_2] on plant growth by altering stomatal traits, leaf photochemical processes and biochemical composition in annual ryegrass.

KEYWORDS

elevated CO_2 concentration, P limitation, stomatal traits, leaf photosynthesis, biochemical

Introduction

Global atmospheric carbon dioxide concentration ([CO_2]) has dramatically been accelerated with an average growth rate of about 1.6 μmol mol^{-1} from 280 μmol mol^{-1} to 400 μmol mol^{-1} in recent past five decades (IPCC, 2013). Meanwhile, many climate models have also predicted that the atmospheric [CO_2] would go up to 800 μmol mol^{-1} by the end of this century (IPCC, 2013). It has been well demonstrated that *e*[CO_2] stimulated plant growth (Suter et al., 2002; Ainsworth, 2008; Wang and Taub, 2010; Yu et al., 2012b) through the "CO_2 fertilization effect" by affecting physiological and biochemical processes (Taub and Wang, 2008; Yu et al., 2012a; Arndal et al., 2014) such as photosynthesis (Leakey et al., 2006; Leakey et al., 2009; Zhang et al., 2010; Zheng et al., 2018) and respiration (Crous et al., 2011; Tan et al., 2013), especially for the C_3 plants (Lee et al., 2001; Ainsworth and Rogers, 2007; Zheng et al., 2019). Nevertheless, plants in response to *e*[CO_2] varied with nutrient availability, and the CO_2 fertilization effect generally declined in parallel with the decreases of nutrient availability (Menge and Field, 2007; McCarthy et al., 2010; Norby et al., 2010; Lenka and Lal, 2012; Pandey et al., 2015; Zhang et al., 2017). Thereby, the CO_2 fertilization effect on plant growth might be mitigated or even counteracted by the limitation of nutrient availability due to the higher nutrient demand of plants with rising atmospheric CO_2 (Lenka and Lal, 2012; Pandey et al., 2014; Jin et al., 2015; Ellsworth et al., 2017). For instance, Lewis et al. (2010) analyzed the data from *Populus deltoides* and pointed out that increasing CO_2 nearly doubled the total biomass under 0.5 mM P supply, while it increased by only 7% under the heaviest P deficiency (0.004 mM). Overall, elevated [CO_2] and nutrient availability may have confounding impacts on plant growth and biomass allocation, and thus investigating the potential processes by which nutrient supply regulate the CO_2 fertilization effect on plant growth is critical to predicting the impacts of future climate change on the net primary productivity (NPP) of terrestrial ecosystems, particularly in the natural ecosystems such as forests and grasslands, which are limited by nutrient availability (Kimball et al., 2002; Sakurai et al., 2014; Deng et al., 2017).

Phosphorus (P) is an extremely critical nutrient for sustaining plant growth, development and reproduction (Chiera et al., 2002; Nord and Lynch, 2009; Peñuelas et al., 2013; Jin et al., 2015; Zhan et al., 2017). Because P plays a vital role not only in diverse biochemical processes, such as cell and lipid metabolism (Vance et al., 2003), but also serves as an essential source of energy for numerous biological functions (Almeida et al.,1999; Abel et al., 2002; Lambers et al., 2006). However, soil P deficiency is common in terrestrial ecosystems and is also most likely to become worse under future climate change, where rising [CO_2] may increase the required amount of P for sustaining plant growth (Elser et al., 2007; Richardson et al., 2009). Meanwhile, soil P availability is becoming lower as global reserves deplete (Fay et al., 2015; Jin et al., 2015). The diminishing P availability may gradually become a major limiting nutrient on plant growth in managed and natural ecosystems under elevated [CO_2] (Vance et al., 2003; Lewis et al., 2010; Lenka and Lal, 2012; Singh et al., 2013a). While most of previous studies investigating the effects of nutrient supply on plant responses to elevated [CO_2] have focused primarily on nitrogen (N) limitation for leaf photosynthesis (Hungate et al., 2003; Lewis et al., 2004; Ainsworth and Long, 2005; Reich et al., 2006; Xu et al., 2013), P availability in response to elevated [CO_2] is likely to be particularly important (Jin et al., 2015).

It is well demonstrated that P supply regulates the plant response to *e*[CO_2] and is intrinsically triggered by leaf photosynthesis (Duchein et al., 1993; Norisada et al., 2006; Singh et al., 2013b; Sinhg and Reddy, 2014), which is highly related to the changes in stomatal diffusion processes as well as the biochemical and photochemical processes under higher [CO_2] (Jacob and Lawlor, 1991; Singh et al., 2013b). Previous research have established that the responses of leaf photosynthesis to *e*[CO_2] may be affected by low P availability through decreasing stomatal conductance (Kirschbaum and Tompkins, 1990; Singh et al., 2013a). Moreover, low P limitation may also affect the biochemical and photochemical processes of leaf photosynthesis in response to elevated [CO_2] by the regeneration of triose-phosphate utilization (TPU) during ribulose bisphosphate (RuBP) regeneration (Rogers et al., 1993; Wissuwa et al., 2005; Pandey et al., 2015). Meanwhile, soil P deficiency may lower the activity of Calvin cycle enzymes, thus directly limit photosynthetic capacity under rising [CO_2] (Palma et al., 2000). Additionally, the photosynthetic responses to elevated [CO_2] can also be affected by low soil P supply through limiting plant growth and biomass allocation between source and sink tissues (Fredeen et al., 1989; Pandey et al., 2015). Understanding the potential mechanisms that low P availability affects photosynthetic responses to rising [CO_2] is critical for assessing the impacts of elevated [CO_2] on the structure and function of terrestrial ecosystems limited by low P supply under future climate change scenarios.

Grasslands hold a significant position within terrestrial ecosystems, as their responses to elevated [CO_2] play a pivotal role in the global carbon-water cycling (Coleman et al., 1993; Steffen and Canadell, 2005). The plant coverage and net primary production of grasslands are usually limited by soil P availability under elevated [CO_2] (Elser et al., 2007; Fay et al., 2015; Ceulemans et al., 2017). Annual ryegrass (*Lolium multiflorum* Lam.) is one of the most important principal forages with considerable ecological and economic significances due to high yield and quality in temperate grasslands and pastures (Li et al., 2007; Wang et al., 2013; Castanheira et al., 2014). In these contexts, low soil P supply may be a major factor limiting the CO_2 fertilization effect on plant growth and leaf photosynthesis of annual ryegrass under future climate change (Byrne et al., 2011; Xu, 2015; Zheng et al., 2018). Nevertheless, most of previous studies regarding the plant responses to elevated [CO_2] and P supply are primarily focused on trees (Lewis et al., 2010; Duan et al., 2019) and crops (Wissuwa et al., 2005). Thus, it is necessary to quantify whether P supply will affect grass growth and photosynthesis through altering the physiological and biochemical processes under enriched [CO_2]. Consequently, it is unclear whether grasses response to rising [CO_2] vary with P supply, even few studies have examined the responses of plant growth and leaf photosynthesis to elevated [CO_2] in grass species with P deficiency (Edwards et al., 2006). Understanding the underlying mechanisms and processes of low soil P availability on plant growth and biomass allocation of annual ryegrass with changes in stomatal traits, leaf photosynthesis and plant

biochemistry under elevated [CO_2] may have important significance on projecting the net primary productivity (NPP) and guiding the formulation of adaptation policies for grasslands.

The aims of this study are to: (1) examine the combined effects of *e*[CO_2] and soil P deficiency on the annual ryegrass growth and biomass allocation.; (2) investigate the potential processes that low P availability affecting photosynthetic responses to elevated [CO_2] in annual ryegrass; (3) explore the underling mechanisms that soil P deficiency regulating CO_2 fertilization effect on annual ryegrass growth with changes in stomatal traits, leaf photosynthesis and biochemistry.

Materials and methods

Growth chamber experiments

A golf hole cutter was utilized to eliminate the effect of errors in initial aboveground and belowground biomass (10 cm diameter × 20 cm long). Annual ryegrass was transplanted in the experimental farm at Hebei University of Engineering, Handan City, Hebei Province, China. Then, the collected grasses were transplanted into pots (10 cm diameter × 100 cm long) filled with fritted clay and moved to artificial climate chambers (Model BDP-2000, Ningbo Prandt Instrument Co., Ltd, China). We trimmed grasses every 30 days to a 5-cm canopy height during the 90 days experimental treatments to keep grass plants in good growth condition (Yu et al., 2012b).

Eight artificial climate chambers were utilized to automatically monitor and control CO_2, four of which were set as modern CO_2 (*a*[CO_2]; 400 μmol mol^{-1}) and the remaining four were set as elevated CO_2 (*e*[CO_2]; 800 μmol mol^{-1}). The environmental settings for all eight environmental growth chambers were at 25/20°Cday/night temperature, 800 μmol m^{-2} s^{-1} PAR canopy light intensity, 65% relative humidity, and a 12-h photoperiod of 7:00-19:00. To minimize confounding effects of environmental variation between two chambers, we changed the [CO_2] of each growth chamber every 7 days, and then relocated the CO_2 treated annual ryegrass plants to the growth chambers with corresponding [CO_2] during the whole experiment. In each artificial climate chamber, six randomly selected pots of annual ryegrass plants were watered to through-flow twice a week with half-strength Hoagland's solution modified to generate six P concentration treatments of 0.004, 0.012, 0.02, 0.06, 0.1-, and 0.5-mM P as KH_2PO_4, respectively. To ensure that all grasses have the same amount of potassium kalium (K) in the nutrient solution at each watering, we add an additional moderate amount of KCL to supplement the K in the half-strength Hoagland's solution. Four artificial climate chambers with *a*[CO_2] or *e*[CO_2] are biological replications (n = 4).

Measuring stomatal density, morphological traits and distribution pattern of stomata

To characterize the maximum stomatal pore size of annual ryegrass, we selected recently expanded leaves for sampling stomatal imprints from the middle section on the abaxial surface using colorless nail varnish in artificial climate chambers on the 30th, 60th, and 90th days after CO_2 treatment and P treatments (Zheng et al., 2013; Xu, 2015). We observed and photographed the collected imprints using the method of Zheng et al. (2013) and measured the stomatal aperture length (SAL), stomatal aperture width (SAW), stomatal aperture circumference (SAC) and stomatal aperture area (SAA) using the Image J quantification software (NH, Bethesda, MD). Stomata on each surface were counted and combined for calculating stomatal density (SD) (Ceulemans et al., 1995) and the stomatal aperture shape index (SASI) was also calculated as $\sqrt{SAA}/SAC \times 100\%$. The morphological traits of stomata were visualized and photographed with a scanning electron microscopy (FEI Corp, USA). We randomly selected four images (a magnification of 100) from each treatment to estimate the stomatal spatial distribution pattern. The selected images were digitized with a GIS software (ArcGIS 10.0; ESRI Inc., Redlands, CA). In this study, the center of each stoma was treated as a single point. Then the point pattern analysis was conducted with the Ripley's *K*-function (Ripley, 1976). Comprehensive guidelines for the analysis of stomatal spatial distribution pattern can be found in Xu (2015) and Zheng et al. (2020).

Measuring leaf gas exchange

A portable LI-6400 photosynthesis system (Li-Cor Inc., Lincoln, NE, USA) was utilized to determine the net photosynthetic rate (P_n), stomatal conductance (G_s) and transpiration rate (T_r) on recently expanded leaves on the 30th, 60th, 90th days after CO_2 treatment and P treatments. All measurements were performed in the standard cuvette chamber (2 cm × 3 cm) with the CO_2 concentration of 400 μmol mol^{-1}, the saturating light at 1000 μmol photons m^{-2} s^{-1}, the leaf-to-air vapor pressure deficit (VPD) of 1.5 KPa and the temperature of 20°C. The intrinsic water use efficiency (*WUE*) was calculated as P_n/T_r.

Measuring plant biomass and analyzing tissue carbon, nitrogen and phosphorus contents

The aboveground and belowground biomass were harvested using the physical cutting at the end of the 90-day experiment and oven-dried the separated tissues at 80°C to a constant weight. Finally, the data of biomass were weighed using an electronic scale. The aboveground and belowground portions were grinded to fine powder using a ball mill (MM2, Fa. Retsch, Haan, Germany). The tissue phosphorus (P), carbon (C), and nitrogen (N) contents of shoots and roots were determined using an elemental analyzer (Vario Max CN; Elemnetar Corp., Germany). All the biochemical analyses were repeated four times (n = 4).

Statistical analysis

Two-way analysis of variance (ANOVA) was utilized to test the interactive effects of P concentration and [CO_2] on plant biomass,

stomatal traits, and leaf gas exchange as well as the contents of P, C, and N among different treatments ($p < 0.05$). Additionally, a three-way analysis of variance (ANOVA) was also used to estimate the interactive effects of $[CO_2] \times P \times$ plant tissues on P, C, N contents ($p < 0.05$). Furthermore, we used linear and non-linear regressions to analyze the relationship between biomass and other variables ($p < 0.05$). All statistical analyses were conducted using the SPSS 20.0 software (Chicago, IL, USA).

Results

Effects of P supply and $[CO_2]$ on the plant biomass of annual ryegrass

Our results showed that the total plant biomass, aboveground biomass, belowground biomass and below/above biomass ratio of annual ryegrass were substantially changed by P supply (all $p < 0.001$), while $e[CO_2]$ only remarkably affected the aboveground biomass ($p = 0.014$) and belowground biomass ($p = 0.024$; Figure 1). Specifically, $e[CO_2]$ marginally decreased the total plant biomass by 6.6% at $P_{0.004}$ ($p < 0.05$), but the total plant biomass under the P concentrations of 0.02 Mm ($P_{0.02}$) and 0.06 mM ($P_{0.06}$) was obviously increased by 7.1% ($p < 0.05$) and 10.4% ($p < 0.01$) (Figure 1A). Moreover, elevated $[CO_2]$ dramatically increased the aboveground biomass by 14.5% ($p < 0.001$) under the highest P concentration of 0.5 mM ($P_{0.5}$) (Figure 1B). By contrast, rising $[CO_2]$ decreased the belowground biomass by 13.7% ($p < 0.01$), 9.2% ($p < 0.05$), and 11.1% ($p < 0.05$) under the P concentrations of 0.004 mM ($P_{0.004}$), 0.012 mM ($P_{0.012}$), and 0.5 mM ($P_{0.5}$) (Figure 1C). Similar to the changes in belowground biomass, elevated $[CO_2]$ also changed the allocation of plant biomass between belowground and aboveground (below/above biomass ratio) with decreasing the below/above biomass ratio by 11.9%, 11.4%, and 18.5% at $P_{0.004}$ ($p < 0.05$), $P_{0.012}$ ($p < 0.01$), and $P_{0.5}$ ($p < 0.05$), while the below/above biomass ratio of annual ryegrass at $P_{0.006}$ was substantially enhanced by 31.5% under elevated $[CO_2]$ ($p < 0.001$; Figure 1D). Moreover, our one-way ANOWA results revealed that the total biomass ($p < 0.001$), aboveground biomass ($p < 0.001$), belowground biomass ($p < 0.001$), and the ratio of below/above biomass ($p < 0.001$) were significantly changed by the P deficiency, while $e[CO_2]$ only marginally effected the aboveground biomass ($p = 0.014$) and belowground biomass ($p = 0.024$) of annual ryegrass (Figure 1). Additionally, the remarkably interactive effects of P and $[CO_2]$ were found on the total plant biomass, aboveground biomass, belowground biomass, and below/above biomass ratio of annual ryegrass (Figure 1).

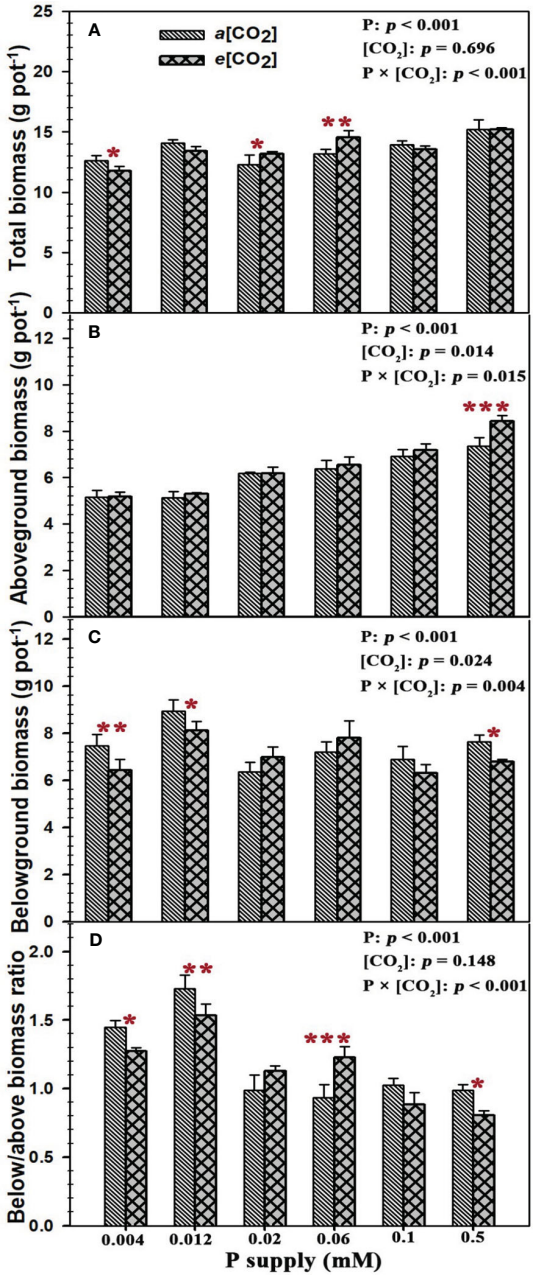

FIGURE 1
Effects of elevated $[CO_2]$ on plant biomass and its allocation of annual ryegrass under P deficits. Note that the grey bars represent ambient CO_2 concentration (Ca) and the black bars represent elevated CO_2 concentration (Ce). The symbols *, **, and *** indicate that the significant differences between Ca and Ce under the same P treatment. The part labels are mean that ANOVA p-values for P and $[CO_2]$ and interactive effects of $[CO_2]$ and P on annual ryegrass biomass.

Effects of P supply and $[CO_2]$ on leaf gas exchange of annual ryegrass

Sufficient P supply ($P_{0.5}$) had a strong CO_2 fertilization effect on the net photosynthetic rates of annual ryegrass, as evidenced by the 25.3% increase of net photosynthetic rates ($p < 0.001$) (Figure 2A). By contrast, the net photosynthesis rates of annual ryegrass at lower P supply of $P_{0.004}$, $P_{0.02}$, and $P_{0.06}$ were significantly decreased by 13.6% ($p < 0.01$), 19.8% ($p < 0.001$) and 16.9% ($p < 0.001$) under elevated $[CO_2]$. Meanwhile, elevated $[CO_2]$ substantially reduced the stomatal conductance by 54.2% ($p < 0.001$), 56.0% ($p < 0.001$), 39.6% ($p < 0.01$), 47.3% ($p < 0.01$), and 36.7% ($p < 0.05$) at the P treatments of $P_{0.012}$, $P_{0.02}$, $P_{0.06}$, $P_{0.1}$, and $P_{0.5}$ except for the stomatal conductance under the P supply of $P_{0.004}$ (Figure 2B). However, elevated $[CO_2]$ only increased the leaf transpiration rate at $P_{0.06}$ by 14.1% ($p < 0.01$),

10.3389/fpls.2023.1271262

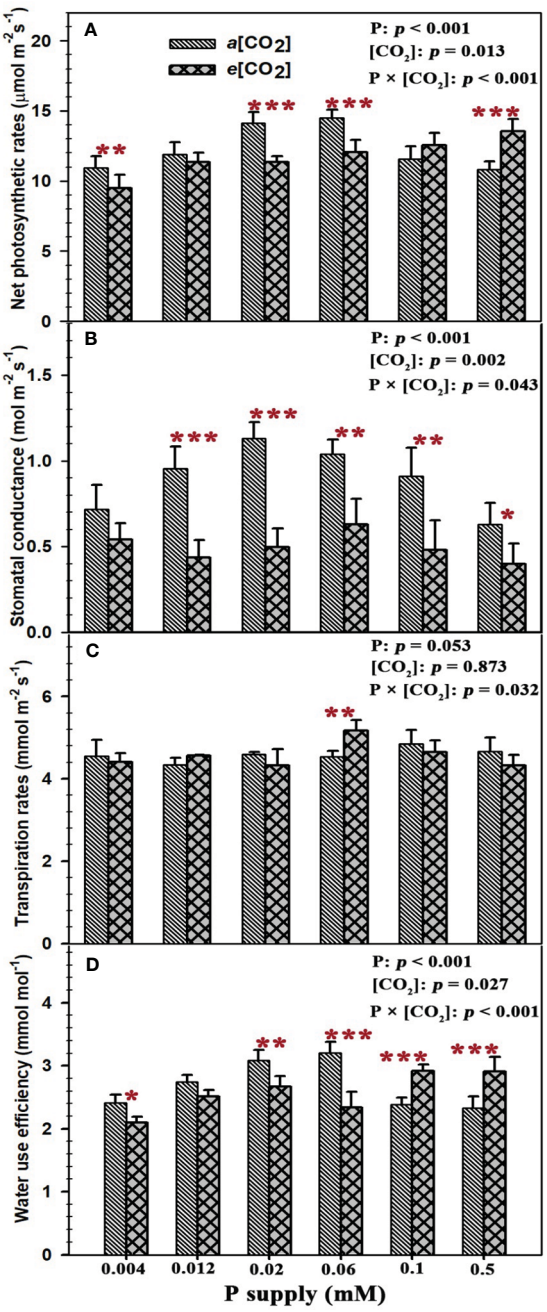

FIGURE 2
Effects of elevated [CO_2] on leaf gas exchange of annual ryegrass under P deficits. Note that the grey bars represent ambient CO_2 concentration (Ca) and the black bars represent elevated CO_2 concentration (Ce). The symbols *, **, and *** indicate that the significant differences between Ca and Ce under the same P treatment. The part labels are mean that ANOVA p-values for P and [CO_2] and interactive effects of [CO_2] and P on leaf exchange of annual ryegrass.

and barely affected the leaf transpiration rates under other P treatments (Figure 2C). Consequently, e[CO_2] dramatically reduced the water use efficiency of annual ryegrass by 13.1% ($p < 0.05$), 13.5% ($p < 0.01$), and 27.1% ($p < 0.001$) under lower P treatments of $P_{0.004}$, $P_{0.02}$ and $P_{0.06}$ (Figure 2D), whereas the water use efficiency at higher P treatments of $P_{0.1}$ and $P_{0.5}$ was significantly enhanced by 22.3% ($p < 0.001$) and 24.8% ($p < 0.001$; Figure 2D). Moreover, the significantly interactive effects of P supply and e[CO_2] were also found on the net photosynthetic rates ($p < 0.001$), stomatal conductance ($p = 0.043$), transpiration rates ($p = 0.032$) and water use efficiency ($p < 0.001$) of annual ryegrass (Figure 2).

Effects of P supply and [CO_2] on the morphological traits of individual stoma and the spatial distribution pattern of stomata on annual ryegrass leaves

Elevated [CO_2] substantially affected the stomatal density (SD) of annual ryegrass regardless of P supply (Table 1). Specifically, e[CO_2] dramatically increased the SD by 72.3%, 34.8% and 25.6% under $P_{0.012}$, $P_{0.1}$, and $P_{0.5}$, whereas obviously decreased the SD by 17.1%, 27.1%, and 35.5%, respectively, at the P supply of $P_{0.004}$, $P_{0.02}$, and $P_{0.06}$ (all $p < 0.05$; Table 1; Figure 3). Moreover, elevated [CO_2] dramatically decreased the stomatal area (SA) by 13.7%, 12.5% and 11.5% at $P_{0.004}$, $P_{0.1}$, and $P_{0.5}$ (all $p < 0.05$), which may be due to the smaller stomatal length and width (Table 1; Figure 4), and the minimum and maximum values of the stomatal area were occurred at $P_{0.012}$ and $P_{0.1}$, respectively (Table 1; Figure 4). Our two-way ANOVA results showed that the SD of annual ryegrass was substantial changed by [CO_2] or P supply (Table 2). Additionally, [CO_2] × P supply also significantly affected the SD, SAL, SAW, SAA, and SAA (all $p < 0.05$), but barely changed the SAC (Table 2).

The spatial distribution pattern of annual ryegrass was also changed by P supply and e[CO_2] (Figure 5). In general, the spatial pattern of stomata distributed on leaves of annual ryegrass followed a regular pattern at small scales (<150 μm) and a random distribution at larger scales (>200 μm) regardless of [CO_2] and P supply (Figure 5). Interestingly, the most regular pattern both at the scale of *c.* 110 μm regardless of the [CO_2] concentration was observed in the current study, as evidenced by the average minimum Lhat(d) values of -9.24 under a[CO_2] and -8.00 under e[CO_2] (Figure 5). Moreover, e[CO_2] produced more regular spatial patterns of stomata at small scales when annual ryegrass was subjected to three higher P supply of $P_{0.06}$, $P_{0.1}$, and $P_{0.5}$, due to the lower Lhat(d) values at the same spatial scales (Figure 5). Meanwhile, elevated [CO_2] also increased the range scale of regular pattern of stomata (Figure 5).

Effects of P supply and [CO_2] on tissue phosphorus (P), carbon (C), and nitrogen (N) contents of annual ryegrass

Elevated [CO_2] generally reduced phosphorus contents in both shoots and roots of annual ryegrass (Table 3). Specifically, elevated [CO_2] significantly decreased the phosphorus in shoots by 33.9%, 15.2%, 18.9% and 12.7% under $P_{0.012}$, $P_{0.06}$, $P_{0.1}$ and $P_{0.5}$ (all $p < 0.05$; Table 3). However, e[CO_2] only obviously reduced the phosphorus content in roots by 19.9% under $P_{0.06}$ ($p < 0.05$; Table 3). In addition, e[CO_2] significantly decreased shoots N by 25.8% and 20.6% under $P_{0.004}$ and $P_{0.06}$ (both $p < 0.05$; Table 3), but increased shoots N by 19.1% under $P_{0.5}$ ($p < 0.05$; Table 3).

TABLE 1 Effects of elevated [CO_2] on the stomatal morphology of annual ryegrass under P deficits.

Stomatal morphology	$a[CO_2]$						$e[CO_2]$					
	$P_{0.004}$	$P_{0.012}$	$P_{0.02}$	$P_{0.06}$	$P_{0.1}$	$P_{0.5}$	$P_{0.004}$	$P_{0.012}$	$P_{0.02}$	$P_{0.06}$	$P_{0.1}$	$P_{0.5}$
Stomatal density (No. mm^{-2})	24.6 ± 1.5c	19.9 ± 1.7e	20.8 ± 1.4de	20.7 ± 2.3de	20.7 ± 2.3de	22.8 ± 2.4cd	20.4 ± 1.0de	34.2 ± 0.2a	15.2 ± 1.8f	13.3 ± 0.3f	19.7 ± 1.9e	28.6 ± 0.3b
Stomatal length (μm)	42.6 ± 2.4bcd	44.8 ± 1.7bc	44.4 ± 1.7bc	42.6 ± 2.9bcd	48.4 ± 4.3a	42.6 ± 2.8bcd	41.3 ± 2.1bcd	40.0 ± 2.9d	41.2 ± 1.0bcd	45.1 ± 0.4ab	43.6 ± 1.4bcd	40.9 ± 2.6cd
Stomatal width (μm)	4.2 ± 0.1cde	4.2 ± 0.3cde	4.2 ± 0.2cde	4.1 ± 0.3de	5.1 ± 0.4a	4.6 ± 0.1b	4.0 ± 0.2e	4.3 ± 0.1bcde	4.5 ± 0.4bc	3.9 ± 0.2e	4.5 ± 0.3bcd	4.3 ± 0.1bcde
Stomatal perimeter (μm)	87.2 ± 6.7b	91.7 ± 2.6b	94.3 ± 6.5b	90.1 ± 4.6b	105.8 ± 8.3a	93.4 ± 6.7b	87.1 ± 4.7b	86.3 ± 5.9b	85.6 ± 2.8b	90.0 ± 4.3b	94.7 ± 3.3b	86.4 ± 5.7b
Stomatal area (μm^2)	182.3 ± 7.8b	151.3 ± 11.2de	154.2 ± 13.3d	156.5 ± 11.1d	201.1 ± 12.7a	182.3 ± 10.7b	157.3 ± 14.7d	136.7 ± 8.4e	158.1 ± 7.4d	166.6 ± 3.8bcd	175.9 ± 4.1bc	161.2 ± 9.8cd
Stomatal shape index	0.16 ± 0.01a	0.13 ± 0.006c	0.13 ± 0.004c	0.14 ± 0.006c	0.13 ± 0.01c	0.15 ± 0.011b	0.14 ± 0.008c	0.14 ± 0.005c	0.15 ± 0.006b	0.14 ± 0.007c	0.14 ± 0.005c	0.15 ± 0.008b

Different lowercase letters indicate significant differences between P deficits treatments at 0.05 level.

Consequently, the C/N ratio in shoot was enhanced by 29.2% and 25.0% under $P_{0.004}$ ($p < 0.05$) and $P_{0.06}$ ($p < 0.05$; Table 3) but lowered by 17.9% under $P_{0.5}$ ($p<0.05$; Table 3). Additionally, the shoot C ($p > 0.05$), root C ($p > 0.05$), N ($p > 0.05$) and C/N ratio in roots ($p > 0.05$) were barely changed by $e[CO_2]$ regardless of P supply (Table 3).

The tissue P contents were substantially affected by [CO_2] ($p < 0.05$) or P supply ($p < 0.001$) from the results of three-way ANOVA (Table 4). However, we found statistical differences in the contents of phosphorus ($p < 0.001$), C ($p < 0.001$) and N ($p < 0.001$) as well as the C/N ratio ($p < 0.001$) between tissues (shoot and root) of annual ryegrass (Table 4). Moreover, there were obviously interactive effects of [CO_2] × P supply on the tissue N ($p < 0.001$) and P contents ($p < 0.05$) as well as the C/N ratio ($p < 0.001$; Table 4), whereas P supply × tissue only changed the phosphorus content of annual ryegrass ($p < 0.001$; Table 4). In addition, our results also showed that [CO_2] × P supply × tissue significantly changed the contents of N, P and the C/N ratio of annual ryegrass (all $p < 0.05$; Table 4).

Relationships of plant biomass among photosynthesis as well as shoot P and N contents

The aboveground ($R^2 = 0.80$, $p = 0.017$; Figure 6D) and total biomass ($R^2 = 0.86$, $p = 0.008$; Figure 6F) demonstrated a linear increase with the elevation of leaf photosynthesis at $e[CO_2]$. However, no linear or parabolic relationships were found between leaf photosynthesis and aboveground biomass ($R^2 = 0.13$, $p = 0.815$; Figure 6A), as well as total biomass at $a[CO_2]$ ($R^2 = 0.31$, $p = 0.252$; Figure 6C). Similarly, we found linear relationships of shoot phosphorus content between aboveground ($R^2 = 0.73$, $p = 0.031$; Figure 7A) and total biomass ($R^2 = 0.59$, $p = 0.076$; Figure 7C) at $a[CO_2]$, as well as aboveground ($R^2 = 0.64$, $p = 0.055$; Figure 7D) and total biomass ($R^2 = 0.89$, $p = 0.005$; Figure 7F) at $e[CO_2]$. Nevertheless, there is no obvious correlation between belowground biomass and leaf photosynthesis (Figure 6), shoot phosphorus content (Figure 7), or shoot nitrogen content (Figure 8) regardless of CO_2 concentration. Moreover, we also found parabolic relationship of shoot nitrogen content with leaf photosynthesis, irrespective of CO_2 concentration (Figure 9).

Discussion

P deficit lowers the CO_2 fertilization effect on the growth of annual ryegrass

Previous studies have established that since the current atmospheric [CO_2] is suboptimal for the Rubisco enzyme involved in leaf photosynthesis (Ainsworth and Rogers, 2007; Pandey et al., 2015). As a result, the "CO_2 fertilization effect" would benefit crops, given the enriched atmospheric [CO_2], leading to plant growth and crop yield (Sakurai et al., 2014; Xu, 2015). For example, a study on winter wheat indicated that increasing [CO_2] had a maximum boost of more than 50% on its biomass (Butterly et al., 2015). However, it should be noted that most of these studies focused on the effects of $e[CO_2]$ on plant growth and physiological processes were conducted under sufficient nutrition supplies (Li et al., 2007). Therefore, this CO_2 fertilization effect is likely to be required more essential nutrients for sustaining plant growth (Plénet et al., 2000; Lee et al., 2011; Menge et al., 2012; Pandey et al., 2015; Zheng et al., 2017). Increasing CO_2 from 400 to 800 μmol mol^{-1} only substantially enhanced the aboveground biomass of annual ryegrass by 14.5% at $P_{0.5}$, indicating that $e[CO_2]$ indeed boosts the plant growth of annual ryegrass with sufficient P supply. However, the aboveground biomass of annual ryegrass subjected to P deficiency was barely affected by elevated CO_2 and total biomass even obviously decreased by 6.6% at $P_{0.004}$, which suggested that soil P deficiency down regulated the favorable impacts of CO_2 fertilization effect on annual ryegrass. Moreover, we also found that the belowground biomass was

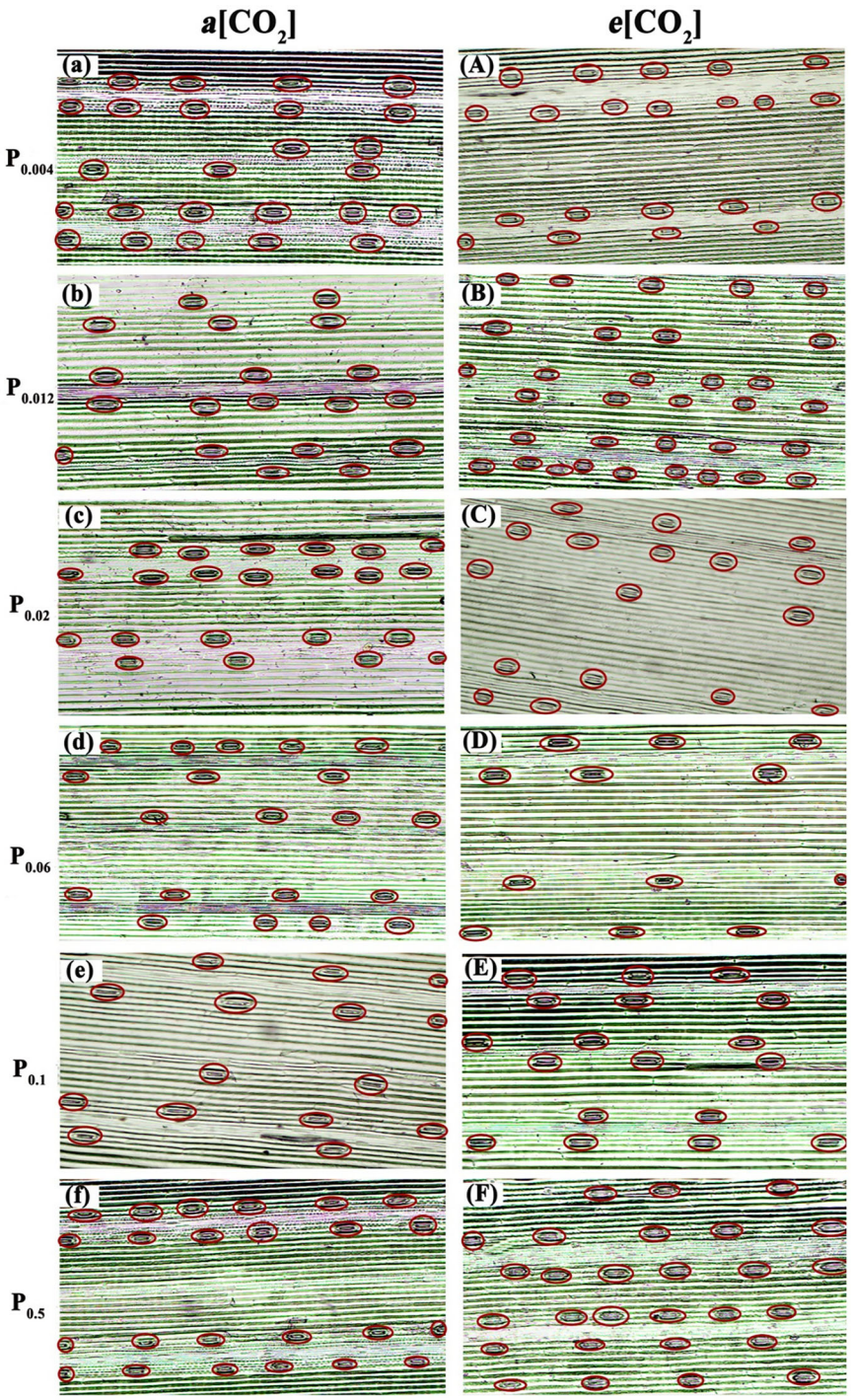

FIGURE 3
Observation on stomatal density of annual ryegrass under light microscopy. The P supply are 0.004 **(a)**, 0.012 **(b)**, 0.02 **(c)**, 0.06 **(d)**, 0.1 **(e)**, and 0.5 **(f)** mM under ambient CO_2, respectively;the P supply are 0.004 **(A)**, 0.012 **(B)**, 0.02 **(C)**, 0.06 **(D)**, 0.1 **(E)**, and 0.5 **(F)** mM under elevated [CO_2], respectively.

substantially increased under P deficiency, indicating that plants may preferentially distribute more biomass to the roots for nutrient uptake when subjected to P limitation, which is consistent with the conclusions from previous studies that P deficiency may favor root growth more than shoot growth, and thus result in a higher below/above biomass ratio (Péret et al., 2011; Pandey et al., 2015). Additionally, the pronounced interactive effect of CO_2 concentration and P supply on the aboveground, belowground and the total biomass of annual ryegrass was evident in two-way ANOVA results. The total biomass and aboveground biomass also increased with the increase of P supply, suggesting that the positive CO_2 fertilization effect on the growth of annual ryegrass was triggered by P supply and the stimulation of biomass accumulation by CO_2 depends on the P status.

10.3389/fpls.2023.1271262

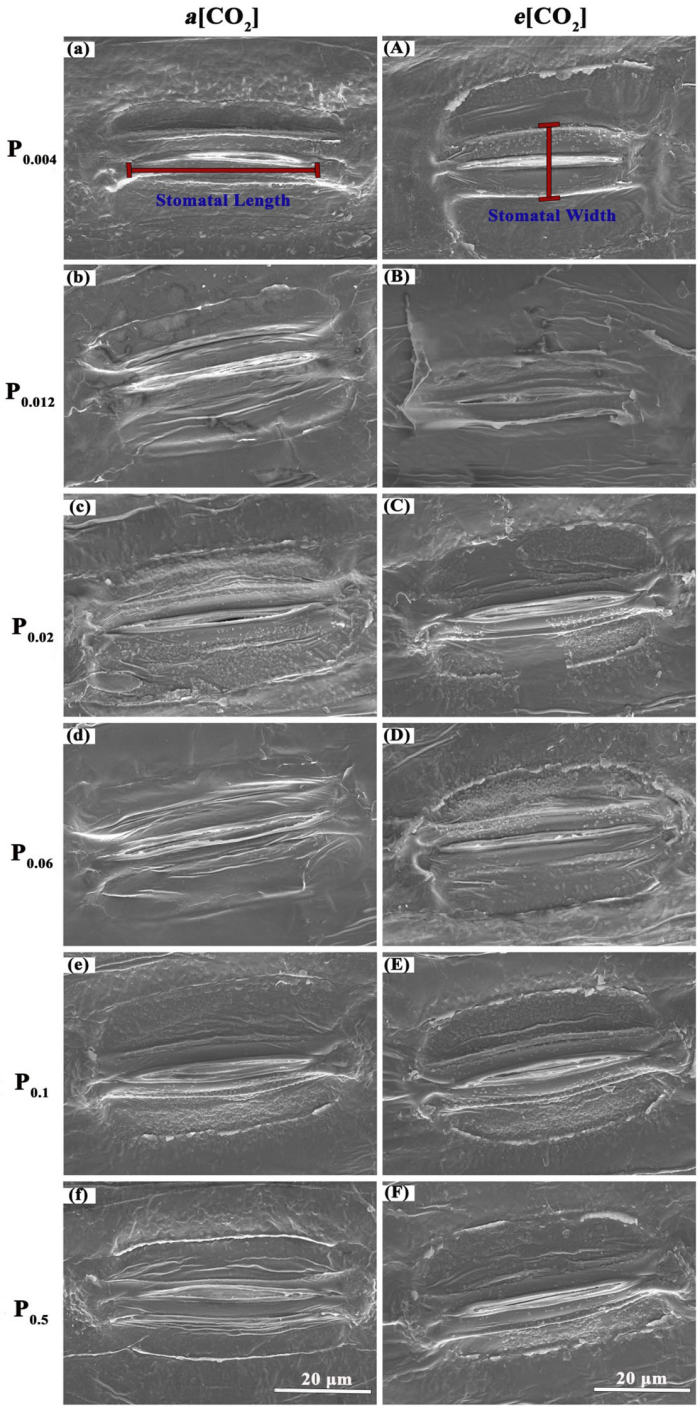

FIGURE 4
Micrographs of stomatal morphology photographed with Scanning Electrical Microscopy (SEM). The P supply are 0.004 **(a)**, 0.012 **(b)**, 0.02 **(c)**, 0.06 **(d)**, 0.1 **(e)**, and 0.5 **(f)** mM under ambient CO_2, respectively;the P supply are 0.004 **(A)**, 0.012 **(B)**, 0.02 **(C)**, 0.06 **(D)**, 0.1 **(E)**, and 0.5 **(F)** mM under elevated [CO_2], respectively.

TABLE 2 ANOVA *p*-values for the effects of P and CO_2 and interactive effects of P and [CO_2] on the stomatal morphology of annual ryegrass.

Stomatal traits	Stomatal density	Stomatal length	Stomatal width	Stomatal perimeter	Stomatal area	Stomatal shape index
[CO_2]	***p*<0.05**	***p*<0.05**	*p*=0.09	***p*<0.05**	***p*<0.001**	***p*=0.19**
P supply	***p*<0.001**	***p*<0.05**	***p*<0.001**	***p*<0.05**	***p*<0.001**	***p*<0.05**
[CO_2] × P supply	***p*<0.001**	***p*<0.05**	***p*<0.05**	*p*=0.261	***p*<0.05**	***p*<0.05**

P<0.05 were considered significant and highlighted in bold.

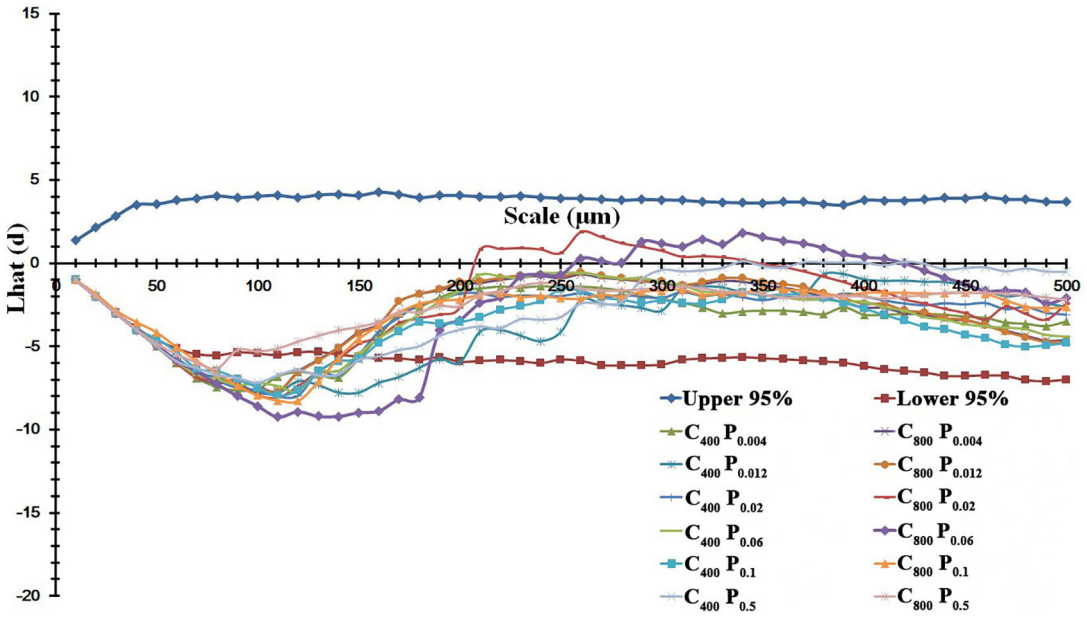

FIGURE 5
Effects of elevated [CO_2] on the spatial distribution pattern of stomata under P deficits. Note: that the more regular distribution pattern of stomata featured with a lower Lhat(d) value. The upper and lower 95% boundaries were obtained by Monte Carlo simulation of 1000 replicates.

The CO_2 fertilization effect on leaf gas exchange under P deficiency

It is well known that CO_2 is one of the key reactants needed by plants to engage in the biochemical process of photosynthesis, and elevated CO_2 stimulates leaf photosynthesis (Kimball et al., 2002). However, several lines of evidence suggest that the increased photosynthesis associated with $e[CO_2]$ may be diminished during prolonged exposure, particularly in plants limited by nutrient availability (Lauer et al., 1989; Campbell and Sage, 2006; Reich et al., 2006; Pandey et al., 2015). In this study, $e[CO_2]$ substantially enhanced the net photosynthetic rate at $P_{0.1}$ and $P_{0.5}$ was observed, whereas the net photosynthetic rate of annual ryegrass subjected to P deficit was barely affected or even obviously decreased by elevated CO_2 concentration, indicating that the stimulating effect of $e[CO_2]$ on the photosynthetic response of plants is weakened as the P concentration decreased. This result may be explained by the fact that high CO_2 improves uptake efficiency in the presence of adequate

TABLE 3 Effects of elevated [CO_2] on the tissue phosphorus (P), carbon (C), and nitrogen (N) contents of annual ryegrass under P deficits.

Elements (mg g^{-1})		$a[CO_2]$						$e[CO_2]$					
		$P_{0.004}$	$P_{0.012}$	$P_{0.02}$	$P_{0.06}$	$P_{0.1}$	$P_{0.5}$	$P_{0.004}$	$P_{0.012}$	$P_{0.02}$	$P_{0.06}$	$P_{0.1}$	$P_{0.5}$
Shoots	P	0.21 ± 0.02d	0.26 ± 0.03c	0.24 ± 0.02c	0.32 ± 0.02b	0.32 ± 0.02b	0.35 ± 0.01a	0.25 ± 0.01c	0.17 ± 0.01e	0.26 ± 0.02c	0.27 ± 0.01c	0.26 ± 0.02c	0.31 ± 0.02b
	C	40.9 ± 1.5a	39.4 ± 0.4b	39.0 ± 0.8ab	39.5 ± 1.8ab	39.4 ± 1.2b	40.0 ± 1.3b	39.4 ± 1.0ab	39.4 ± 0.4ab	39.0 ± 0.8b	39.5 ± 1.8ab	39.4 ± 1.2ab	40.0 ± 1.3ab
	N	3.5 ± 0.3a	2.7 ± 0.2bc	2.7 ± 0.2bc	3.0 ± 0.4a	2.5 ± 0.4bc	2.5 ± 0.2c	2.6 ± 0.2bc	2.8 ± 0.2bc	2.8 ± 0.3bc	2.4 ± 0.3c	2.7 ± 0.2bc	3.0 ± 0.2ab
	C/N	11.9 ± 0.9d	14.7 ± 1.4abc	14.7 ± 1.6abc	13.5 ± 1.7cd	15.7 ± 2.2abc	16.3 ± 0.9ab	15.4 ± 0.9abc	13.9 ± 0.9cd	14.3 ± 1.7bc	16.9 ± 1.9a	14.8 ± 1.1abc	13.4 ± 0.9cd
Roots	P	3.92 ± 0.24bc	3.91 ± 0.15bc	3.95 ± 0.25bc	4.21 ± 0.37b	4.11 ± 0.22b	4.76 ± 0.18a	3.92 ± 0.09bc	3.88 ± 0.20bc	3.63 ± 0.20cd	3.37 ± 0.34d	3.83 ± 0.18bc	5.10 ± 0.25a
	C	41.2 ± 0.3a	41.6 ± 0.2a	41.4 ± 0.1a	41.2 ± 0.4a	41.6 ± 0.4a	41.4 ± 0.3a	41.4 ± 0.7a	41.2 ± 0.4a	41.4 ± 0.4a	41.7 ± 0.2a	41.4 ± 0.3a	41.6 ± 0.3a
	N	1.8 ± 0.1a	1.8 ± 0.1a	1.8 ± 0.1a	1.8 ± 0.1a	1.8 ± 0.1a	1.7 ± 0.1a	1.8 ± 0.1a	1.8 ± 0.1a	1.8 ± 0.1a	1.8 ± 0.1a	1.8 ± 0.1a	1.8 ± 0.1a
	C/N	23.4 ± 0.3a	22.7 ± 1.1a	23.2 ± 0.6a	22.7 ± 0.8a	22.7 ± 1.1a	23.8 ± 0.8a	22.8 ± 0.9a	23.3 ± 0.3a	23.3 ± 0.6a	22.6 ± 0.5a	23.0 ± 0.3a	22.8 ± 0.6a

Different lowercase letters indicate significant differences between P deficits treatments at 0.05 level.

TABLE 4 ANOVA *p*-values for the effects of P and CO_2 and interactive effects of P and [CO_2] on the phosphorus, carbon, and nitrogen contents in tissues of annual ryegrass.

Treatments	Phosphorus	Carbon	Nitrogen	C/N ratio
[CO_2]	***p*<0.05**	*p*=0.549	*p*=0.488	*p*=0.678
P supply	***p*<0.001**	*p*=0.447	*p*=0.265	*p*=0.523
Tissue	***p*<0.001**	***p*<0.001**	***p*<0.001**	***p*<0.001**
[CO_2] × P supply	***p*<0.05**	*p*=0.178	***p*<0.001**	***p*<0.001**
[CO_2] × tissue	*p*=0.188	*p*=0.759	*p*=0.368	*p*=0.362
P supply × tissue	***p*<0.001**	*p*=0.224	*p*=0.143	*p*=0.115
[CO_2] × P supply × tissue	***p*<0.05**	*p*=0.067	***p*<0.001**	***p*<0.001**

P<0.05 were considered significant and highlighted in bold.

P supply (Nilsson et al., 2010; Jin et al., 2011; Pandey et al., 2015). Moreover, Duchein et al. (1993) found in a research on clover (*Trifolium subterraneum* L.) that *e*[CO_2] obviously increased its net photosynthetic rate under a P concentration supply of 2 mM, while it was inhibited when subjected to P limitation, which was similar to our study. In addition, we found that the highest P supply (0.5 mM) further enhanced the photosynthetic rate under *e*[CO_2], as evidenced by the higher increase of net photosynthetic rate at $P_{0.5}$ than that of

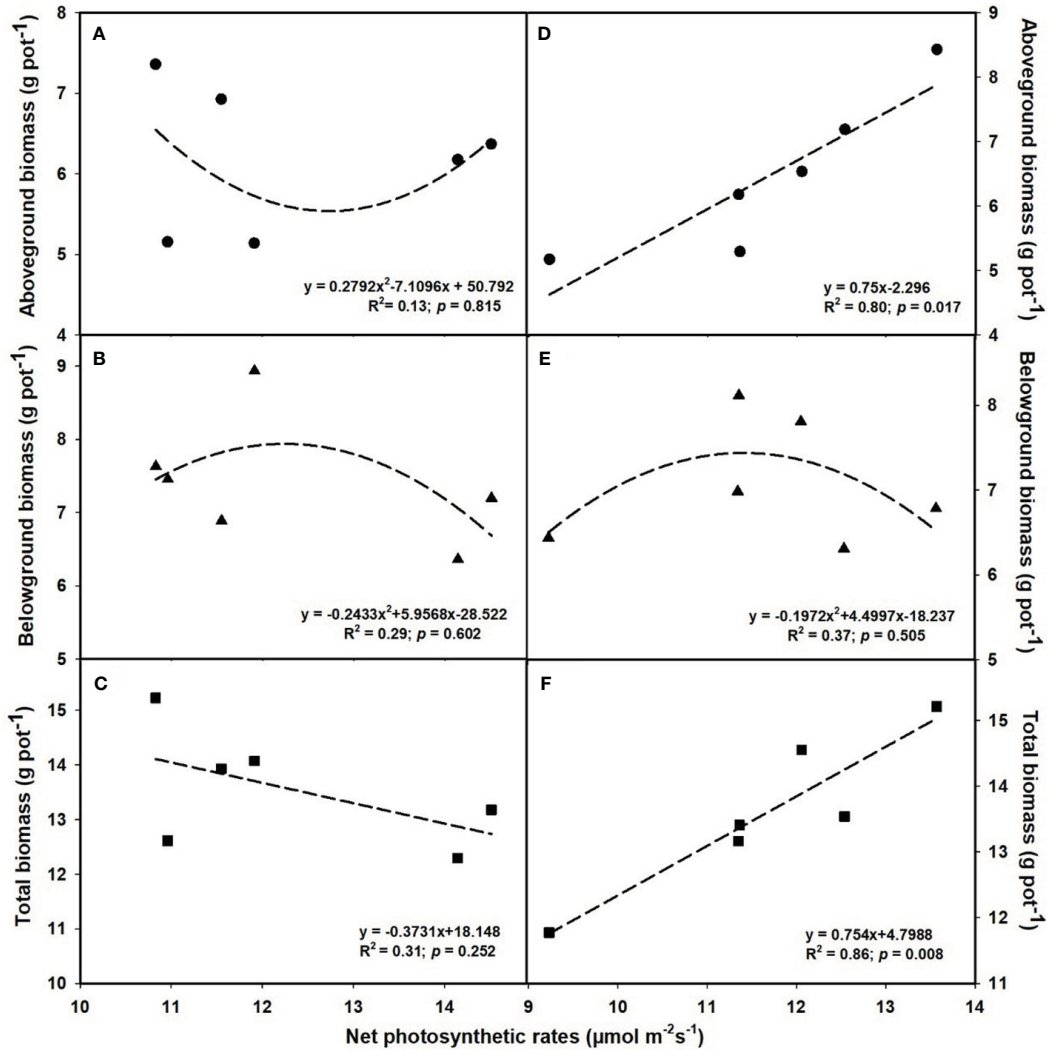

FIGURE 6
The relationships between net photosynthetic rates and aboveground biomass **(A, D)**, belowground biomass **(B, E)**, and total biomass **(C, F)**. Values are means ± SD (n = 4). The circle symbols represent aboveground biomass, the triangle symbols represent belowground biomass, and the square symbols represent total biomass.

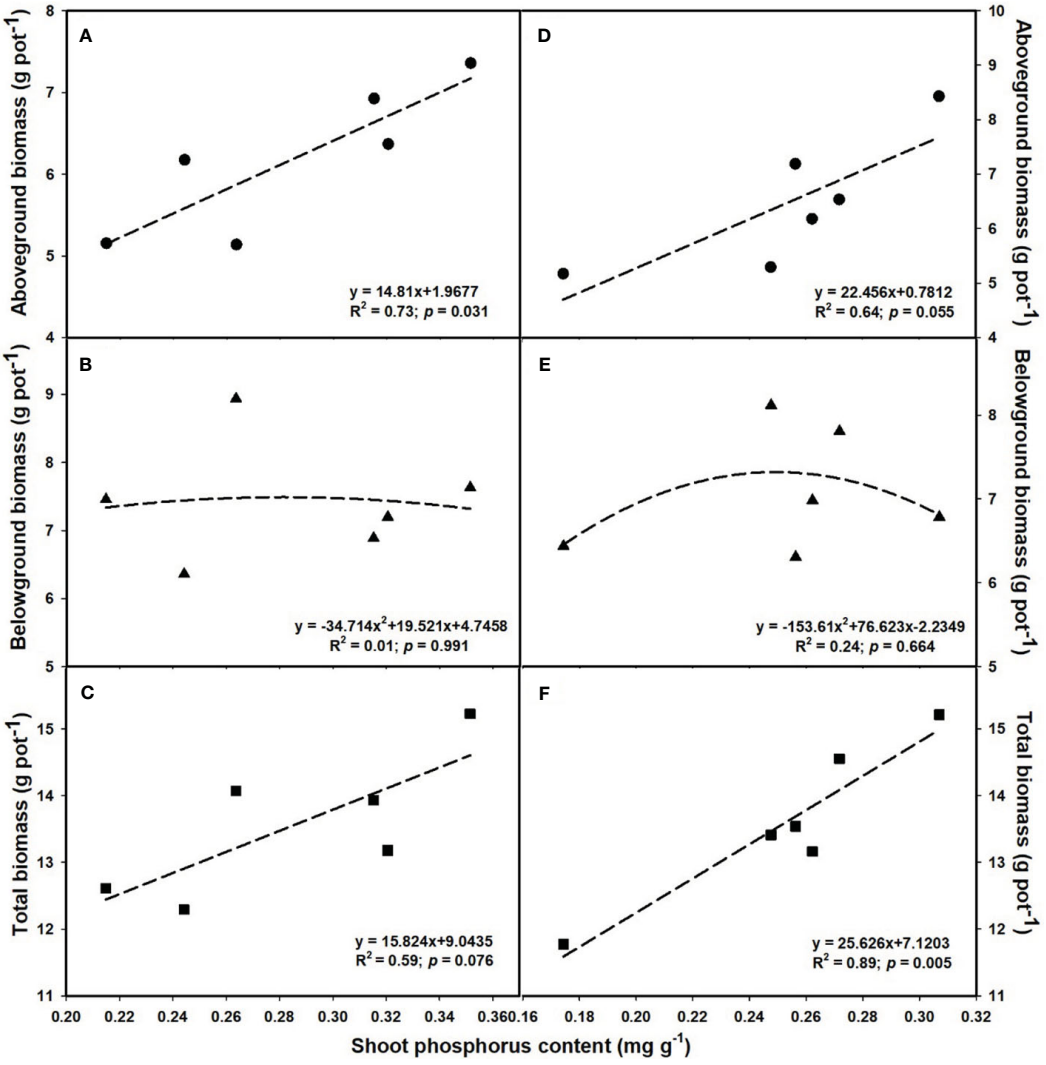

FIGURE 7
The relationships between leaf phosphorus content and aboveground biomass **(A, D)**, belowground biomass **(B, E)**, and total biomass **(C, F)**. Values are means ± SD (n = 4). The circle symbols represent aboveground biomass, the triangle symbols represent belowground biomass, and the square symbols represent total biomass.

plants treated with $P_{0.1}$, indicating that plants will probably demand ultra-optimal levels of P supply if they want to benefit from the general trend of increasing atmospheric CO_2 concentration in the future. Moreover, the aboveground biomass of annual ryegrass was barely affected by $e[CO_2]$ when the P supply was lower, although the net photosynthetic rates were higher under P deficit. This suggested that the CO_2 fertilization effect is more pronounced in stimulating the growth of annual ryegrass under sufficient P supply. Additionally, the obvious decrease in the net photosynthetic rate at elevated CO2, compared to ambient CO_2, under the lowest P supply (0.004 mM) likely indicates the crucial role of stomatal limitation on photosynthesis. Furthermore, one of the most consistent responses of plants to elevated atmospheric CO_2 is a decrease in stomatal conductance (Fleisher et al., 2012; Singh and Reddy, 2014; Zheng et al., 2019; Zheng et al., 2020). This aligned with our results, as we observed a remarkable decline in stomatal conductance with increasing CO_2 regardless of P supply. However, other nutrient studies have reported that reduced stomatal conductance under lower P supply did not seem to be the major reason for the limitation of photosynthesis (Jin et al., 2011; Singh et al., 2013a). From the above discussion, reduced photosynthesis may be a mechanism by which crops cope with soil phosphorus limitation, which may largely contribute to lower biomass.

Stomatal diffusion and tissue composition partially explain the decreasing benefit of $e[CO_2]$ to annual ryegrass under P deficiency

It has been reported that plant stomata normally exhibit a variety of short-term behavioral and long-term morphological reactions to CO_2 (Zheng et al., 2013; Xu, 2015), soil moisture (Sun et al., 2014), thus stomatal regulation is a potential mechanism for adaptation to

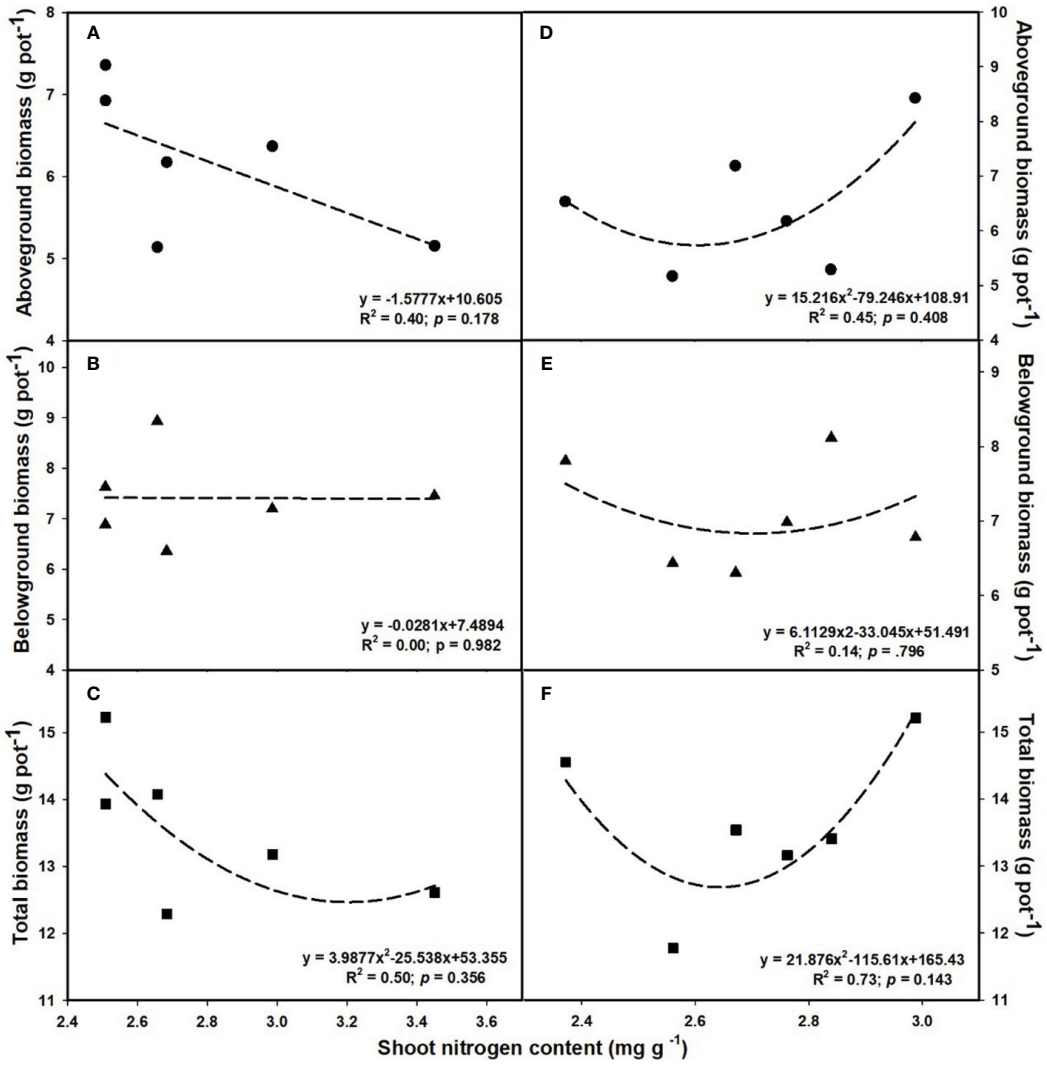

FIGURE 8
The relationships between leaf nitrogen content and aboveground biomass **(A, D)**, belowground biomass **(B, E)**, and total biomass **(C, F)**. Values are means ± SD (n = 4). The circle symbols represent aboveground biomass, the triangle symbols represent belowground biomass, and the square symbols represent total biomass.

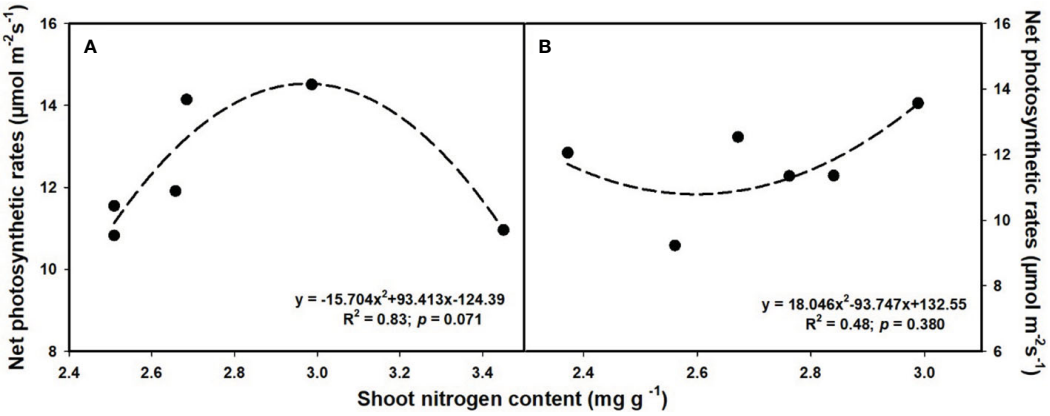

FIGURE 9
The relationships between leaf nitrogen content and net photosynthetic rates under ambiant **(A)** and elevated [CO^2] **(B)**.

the external environment during plant growth. In addition to CO_2 concentrations and soil moisture conditions, Sekiya and Yano (2008) also pointed out that phosphorus supply level can modulate the rate of stomatal production in plant epidermal cells, subsequentially influenced the SD. Our results have further confirmed that stomatal traits of annual ryegrass varied with the P supply and atmospheric CO_2 concentration. Our results showed that lower P supply reduced the stomatal width and stomatal area, suggesting that annual ryegrass improved their adaptability to different P situations through regulating their stomatal opening. We found that the response of annual ryegrass stomatal density under $e[CO_2]$ depended on P concentration, i.e., stomatal density increased at higher P concentrations and decreased at lower P supply. This CO_2-induced decrease of stomatal density under lower P supply may explain the downregulation of leaf photosynthesis, since the SD partially determines the efficiency of CO_2 diffusion from the atmosphere to the mesophyll tissues (Jin et al., 2011). However, observations from previous studies regarding the influence of elevated CO_2 concentration on SD differed (Ryle and Stanley, 1992; Woodward et al., 2002; Marchi et al., 2004). Regarding this inconsistency, Gray et al. (2000) pointed out that interspecific differences may play a role. However, it should be noted that, as revealed in this study, we cannot deny the strongly interactive effects between environmental variables. Furthermore, it has been well demonstrated that stomatal distribution patterns can affect the net photosynthetic rate and transpiration rate (Soares et al., 2008; Zheng et al., 2013). In the current research, we found that $e[CO_2]$ made the spatial distribution pattern of stomata more regular under sufficient P supply, while the opposite was true when annual ryegrass was subjected to P deficiency. This may partially explain why increasing CO_2 in this study did not enhance or even lowered the net photosynthetic rate under a lower P supply. This is because the spatial distribution of the stomata on the blade surface affects the diffusion distance of carbon dioxide between the stomata (Zheng et al., 2013; Xu, 2015), which means that the more regular the spatial distribution of the stomata, the more efficient the blade is in terms of gas exchange. Overall, these results implied that P supply partially decided the response of the stomatal distribution pattern to $e[CO_2]$.

It is now well established from a variety of studies that P limitation and $e[CO_2]$ are likely to alter the distribution patterns of tissue constituents as well (Taub and Wang, 2008; Singh et al., 2013a). However, previous studies on leaf P concentration have had contradictory results (Fangmeier et al., 1999; Lewis et al., 2010). For instance, Lewis et al. (2010) reported that leaf P content of *Populus deltoides* was reduced by 22.2-48.6% with increasing the CO_2 concentration from 350 to 700 μmol mol^{-1}. While Fangmeier et al. (1999) found that $e[CO_2]$ did not significantly lower the P concentration in the leaves of wheat. These inconsistencies suggested that the potential complexity of the effects of $e[CO_2]$ on P nutrition. In the current study, we found that the biomass - net photosynthetic rates relationship followed a similar linear or bell-shaped curve like the biomass-shoot P content relationship at the $e[CO_2]$ (Figures 6 and 7). It shows that $e[CO_2]$ did not enhance the net photosynthetic rate at a lower P supply, possibly owing to the decrease in leaf P content. Additionally, other studies also suggest that the decrease in nitrogen content in leaves may also be attributed to the decrease in photosynthesis, as the leaf N content is tightly correlated with the content of Rubisco enzymes (Zheng et al., 2019). Moreover, the P content in shoots dramatically decreased under P limitation, but the differences in roots under 0.001 mM - 0.1 mM P supply were mostly insignificant, indicating that shoots may be more sensitive to P limitation than roots.

Conclusion

We found that the growth enhancement effects of elevated CO_2 were trivial under the range of P treatments, as amply demonstrated by the reduction in leaf photosynthesis and plant biomass when annual ryegrass was subjected to P limitation. Consequently, P deficiency shifted biomass partitioning by decreasing aboveground production and increasing the root fraction of total biomass. The negative impacts of P limitation on the growth processes of plants benefiting from the effects of CO_2 fertilization can also be ascribed to the changes in the characteristics of individual stomatal morphology and the stomatal spatial distribution pattern, as well as the changes in tissue composition of annual ryegrass. Nevertheless, the increasing sensitivity of annual ryegrass growth to P supply with increasing $[CO_2]$ indicates that annual ryegrass will increase its requirements for P to support an aggressive growth response to future atmospheric conditions. Therefore, the role of annual ryegrass in grassland ecosystem responses to future climate change may be incrementally influenced by P supply.

Data availability statement

The original contributions presented in the study are included in the article/supplementary material. Further inquiries can be directed to the corresponding author.

Author contributions

FL: Writing – original draft. CH: Writing – original draft. ZC: Formal Analysis, Writing – original draft. CM: Data curation, Writing – original draft. JY: Data curation, Formal Analysis, Writing – review & editing. LL: Formal Analysis, Writing – review & editing. YZ: Data curation, Writing – review & editing. LH: Conceptualization, Writing – review & editing.

Funding

The author(s) declare financial support was received for the research, authorship, and/or publication of this article. This research was partially supported by the National Natural Science Foundation of China (32071608), the Natural Science Foundation of Hebei Province (E2021402031 and E2023402086), the Central Guidance on Local Science and Technology Development Funding of Hebei Province (226Z6401G), and the Handan Science and Technology Research and Development Program (19422011008-47).

Conflict of interest

The authors declare that the research was conducted in the absence of any commercial or financial relationships that could be construed as a potential conflict of interest.

The reviewer LY declared a shared affiliation with the author(s) ZC to the handling editor at the time of review.

Publisher's note

References

Abel, S., Ticconi, C. A., and Delatorre, C. A. (2002). Phosphate sensing in higher plants. *Physiol. Plantarum.* 115, 1–8. doi: 10.1034/j.1399-3054.2002.1150101.x

Ainsworth, E. A. (2008). Rice production in a changing climate: a meta-analysis of responses to elevated carbon dioxide and elevated ozone concentration. *Glob. Change Biol.* 14, 1642–1650. doi: 10.1111/j.1365-2486.2008.01594.x

Ainsworth, E. A., and Long, S. P. (2005). What have we learned from 15 years of free-air CO_2 enrichment (FACE)? A meta-analytic review of the responses of photosynthesis, canopy properties and plant production to rising CO_2. *New Phytol.* 165, 351–372. doi: 10.1111/J.1469-8137.2004.01224.X

Ainsworth, E. A., and Rogers, A. (2007). The response of photosynthesis and stomatal conductance to rising (CO_2): mechanisms and environmental interactions. *Plant Cell. Environ.* 30, 258–270. doi: 10.1111/j.1365-3040.2007.01641.x

Almeida, J. P. F., Lüscher, A., Frehner, M., Oberson, A., and Nösberger, J. (1999). Partitioning of P and the activity of root acid phosphatase in white clover (*Trifolium repens* L.) are modified by increased atmospheric CO_2 and P fertilization. *Plant Soil.* 210, 159–166. doi: 10.1023/A:1004625801141

Arndal, M. F., Schmidt, I. K., Kongstad, J., Beier, C., and Michelsen, A. (2014). Root growth and N dynamics in response to multi-year experimental warming, summer drought and elevated CO_2 in a mixed heath land-grass ecosystem. *Funct. Plant Biol.* 41, 1–10. doi: 10.1071/FP13117

Butterly, C. R., Armstrong, R., Chen, D. L., and Tang, C. X. (2015). Carbon and nitrogen partitioning of wheat and field pea grown with two nitrogen levels under elevated CO_2. *Plant Soil.* 391, 367–382. doi: 10.1007/s11104-015-2441-5

Byrne, S. L., Foito, A., Hedley, P. E., Morris, J. A., Stewart, D., and Barth, S. (2011). Early response mechanisms of perennial ryegrass (*Lolium perenne*) to phosphorus deficiency. *Ann. Bot.* 107, 243–254. doi: 10.1093/aob/mcq234

Campbell, C. D., and Sage, R. E. (2006). Interactions between the effects of atmospheric CO_2 content and P nutrition on photosynthesis in white lupin (*Lupinus albus* L.). *Plant Cell. Environ.* 29, 844–853. doi: 10.1111/j.1365-3040.2005.01464.x

Castanheira, N., Dourado, A. C., Alves, P. I., Cortés-Pallero, A. M., Delgado-Rodríguez, A. I., Prazeres, Â., et al. (2014). Annual ryegrass-associated bacteria with potential for plant growth promotion. *Microbiol. Res.* 169, 768–779. doi: 10.1016/j.micres.2013.12.010

Ceulemans, R., Praet, L. V., and Jiang, X. N. (1995). Effects of CO_2 enrichment, leaf position and clone on stomatal index and epidermal cell density in polar (*Populus*). *New Phytol.* 131, 99–107. doi: 10.1111/J.1469-8137.1995.TB03059.X

Ceulemans, T., Bodé, S., Bollyn, J., Harpole, S., Coorevits, K., Peeters, G., et al. (2017). Phosphorus resource partitioning shapes phosphorus acquisition and plant species abundance in grasslands. *Nat. Plants.* 3, 16224. doi: 10.1038/nplants.2016.224

Chiera, J., Thomas, J., and Rufty, T. (2002). Leaf initiation and development in soybean under phosphorus stress. *J. Exp. Bot.* 53, 473–481. doi: 10.1093/jexbot/53.368.473

Coleman, J. S., McConnaughay, K. D. M., and Bazzaz, F. A. (1993). Elevated CO_2 and plant nitrogen-use: is reduced tissue nitrogen concentration size-dependent? *Oecologia.* 93, 195–200. doi: 10.1007/BF00317671

Crous, K. Y., Zaragoz-Castells, J., Löw, M., Ellsworth, D. S., Tissue, D. T., Tjoelker, M. G., et al. (2011). Seasonal acclimation of leaf respiration in Eucalyptus saligna trees: Impacts of elevated atmospheric CO_2 and summer drought. Glob. *Change Biol.* 17, 1560–1576. doi: 10.1111/j.1365-2486.2010.02325.x

Deng, Q., Hui, D., Dennis, S., and Reddy, K. C. (2017). Responses of terrestrial ecosystem phosphorus cycling to nitrogen addition: a meta-analysis. *Glob. Ecol. Biogeogr.* 26, 713–728. doi: 10.1111/geb.12576

Duan, H. L., Ontedhu, J., Milham, P., Lewis, J. D., and Tissue, D. T. (2019). Effects of elevated carbon dioxide and elevated temperature on morphological, physiological and anatomical responses of Eucalyptus tereticornis along a soil phosphorus gradient. *Three Physiol.* 39 (11), 1821–1837. doi: 10.1093/treephys/tpz094

Duchein, M. C., Bonicel, A., and Betsche, T. (1993). Photosynthetic net CO_2 uptake and leaf phosphate concentrations in CO_2 enriched clover (*Trifolium subterraneum* L.) at three levels of phosphate nutrition. *J. Exp. Bot.* 44, 17–22. doi: 10.1093/jxb/44.1.17

Edwards, E. J., McCaffery, S., and Evans, J. R. (2006). Phosphorus availability and elevated CO_2 affect biological nitrogen fixation and nutrient fluxes in a clover-dominated sward. *New Phytol.* 169, 157–167. doi: 10.1111/J.1469-8137.2005.01568.X

Ellsworth, D. S., Anderson, I. C., Crous, K. Y., Cooke, J., Drake, J. E., Gherlenda, A. N., et al. (2017). Elevated CO_2 does not increase eucalypt forest productivity on a low-phosphorus soil. *Nat. Clim. Change.* 7, 279–282. doi: 10.1038/nclimate3235

Elser, J. J., Bracken, M. E. S., Cleland, E. E., Gruner, D. S., Harpole, W. S., Hillebrand, H., et al. (2007). Global analysis of nitrogen and phosphorus limitation of primary producers in freshwater, marine and terrestrial ecosystems. *Ecol. Letters.* 10, 1135–1142. doi: 10.1111/j.1461-0248.2007.01113.x

Fangmeier, A., Temmerman, L. D., Mortensen, L., Kemp, K., Burke, J., Mitchell, R., et al. (1999). Effects on nutrients and on grain quality in spring wheat crops grown under elevated CO_2 concentrations and stress conditions in the European, multiple-site experiment 'ESPACE-wheat'. *Eur. J. Agron.* 10, 215–229. doi: 10.1016/S1161-0301(99)00012-X

Fay, P. A., Prober, S. M., Harpole, W. S., Knops, J. M. H., Bakker, J. D., Borer, E. T., et al. (2015). Grassland productivity limited by multiple nutrients. *Nat. Plants.* 1, 15080. doi: 10.1038/nplants.2015.80

Fleisher, D. H., Wang, Q., Timlin, D. J., Chun, J. A., and Reddy, V. R. (2012). Response of potato gas exchange and productivity to phosphorus deficiency and carbon dioxide enrichment. *Crop Sci.* 52, 1803–1815. doi: 10.2135/cropsci2011.09.0526

Fredeen, A. L., Rao, I. M., and Terry, N. (1989). Influence of phosphorus nutrition on growth and carbon partitioning in *Glycine max*. *Plant Physiol.* 89, 225–230. doi: 10.1104/PP.89.1.225

Gray, J. E., Holroyd, G. H., Lee, V. D. F. M., Bahrami, A. R., Sijmons, P. C., Woodward, F. I., et al. (2000). The *HIC* signaling pathway links CO_2 perception to stomatal development. *Nature.* 408, 713–716. doi: 10.1038/35047071

Hungate, B. A., Dukes, J. S., Shaw, M. R., Luo, Y. Q., and Field, C. B. (2003). Nitrogen and climate change. *Science.* 302, 1512–1513. doi: 10.1126/science.1091390

IPCC (2013). *Climate change: the physical science basis, contribution of working group I to the fifth assessment report of the intergovernmental panel on climate change* (United Kingdom/New York, NY, USA: Cambridge University Press, Cambridge).

Jacob, J., and Lawlor, D. (1991). Stomatal and mesophyll limitations of photosynthesis in phosphate deficient sunflower, maize and wheat plants. *J. Exp. Bot.* 42, 1003–1011. doi: 10.1093/jxb/42.8.1003

Jin, S. H., Huang, J. Q., Li, X. Q., Zheng, B. S., Wu, J. S., Wang, Z. J., et al. (2011). Effects of potassium supply on limitations of photosynthesis by mesophyll diffusion conductance in *Carya cathayensis*. *Tree Physiol.* 31, 1142–1151. doi: 10.1093/treephys/tpr095

Jin, J., Tang, C. X., and Sale, P. (2015). Impact of elevated carbon dioxide on the phosphorus nutrition of plants: a review. *Ann. Bot.* 116, 987–999. doi: 10.1093/aob/mcv088

Jin, B., Wang, L., Wang, J., Jiang, K. Z., Wang, Y., Jiang, X. X., et al. (2011). The effect of artificial warming on leaf functional traits, leaf structure and leaf biochemistry in Arabidopsis thaliana. *BMC Plant Biol.* 11, 35. doi: 10.1186/1471-2229-11-35

Kimball, B. A., Kobayashi, K., and Bindi, M. (2002). Responses of agricultural crops to free-air CO_2 enrichment. *Adv. Agron.* 77, 293–368. doi: 10.1016/S0065-2113(02)77017-X

Kirschbaum, M. U. F., and Tompkins, D. (1990). Photosynthetic responses to phosphorus nutrition in Eucalyptus grandis seedlings. *Aust. J. Plant Physiol.* 17, 527–535. doi: 10.1071/pp9900527

Lambers, H., Shane, M. W., Cramer, M. D., Pearse, S. J., and Veneklaas, E. J. (2006). Root structure and functioning for efficient acquisition of phosphorus: matching morphological and physiological traits. *Ann. Bot-London.* 98, 693–713. doi: 10.1093/aob/mcl114

Lauer, M. J., Pallardy, S. G., Blevins, D. G., and Randall, D. D. (1989). Whole leaf carbon exchange characteristics of phosphate deficient soybeans (*Glycine max* L.). *Plant Physiol.* 91, 848–854. doi: 10.1104/PP.91.3.848

Leakey, A. D. B., Ainsworth, E. A., Bernacchi, C. J., Rogers, A., Long, S. P., Ort, D. R., et al. (2009). Elevated CO2 effects on plant carbon, nitrogen, and water relations: six important lessons from FACE. *J. Exp. Bot.* 60, 2859–2876.

Leakey, A. D. B., Uribelarrea, M., Ainsworth, E. A., Naidu, S. L., Rogers, A., Ort, D. R., et al. (2006). Photosynthesis, productivity, and yield of maize are not affected by open-air elevation of CO_2 concentration in the absence of drought. *Plant Physiol.* 140, 779–790. doi: 10.1104/pp.105.073957

Lee, J. S. (2011). Combined effect of elevated CO_2 and temperature on the growth and phenology of two annual C_3 and C_4 weedy species. *Agr. Ecosyst. Environ.* 140, 484–191. doi: 10.1016/j.agee.2011.01.013

Lee, T. D., Tjoelker, M. G., and Ellsworth, D. S. (2001). Leaf gas exchange responses of 13 prairie grassland species to elevated CO_2 and increased nitrogen supply. *New Phytol.* 150, 405–418. doi: 10.2307/1353746

Lenka, N. K., and Lal, R. (2012). Soil-related constraints to the carbon dioxide fertilization effect. Crit. *Rev. Plant Sci.* 31, 342–357. doi: 10.1080/07352689.2012.674461

Lewis, J. D., Lucash, M., Olszyk, D. M., and Tingey, D. T. (2004). Relationships between needle nitrogen concentration and photosynthetic responses of Douglas-fir seedlings to elevated carbon dioxide and temperature. *New Phytol.* 162, 355–364. doi: 10.1111/j.1469-8137.2004.01036.x

Lewis, J. D., Ward, J. K., and Tissue, D. T. (2010). Phosphorus supply drives nonlinear responses of cottonwood (*Populus deltoides*) to increases in CO_2 concentration from glacial to future concentrations. *New Phytol.* 187, 438–448. doi: 10.1111/j.1469-8137.2010.03307.x

Li, J., Zhou, J. M., Duan, Z. Q., Du, C. W., and Wang, H. Y. (2007). Effect of CO_2 enrichment on the growth and nutrient uptake of tomato seedlings. *Pedosphere.* 17, 343–351. doi: 10.1016/S1002-0160(07)60041-1

Marchi, S., Tognetti, R., Vaccari, F. P., Lanini, M., Kaligaric, M., Miglietta, F., et al. (2004). Physiological and morphological responses of grassland species to elevated atmospheric CO_2 concentrations in FACE-systems and natural CO_2 springs. *Funct. Plant Biol.* 31, 181–194. doi: 10.1071/FP03140

McCarthy, H. R., Oren, R., Johnsen, K. H., Gallet-Budynek, A., Pritchard, S. G., Cook, C. W., et al. (2010). Re-assessment of plant carbon dynamics at the Duke free-air CO_2 enrichment site: interactions of atmospheric [CO_2] with nitrogen and water availability over stand development. *New Phytol.* 185, 514–528. doi: 10.1111/j.1469-8137.2009.03078.x

Menge, D. N. L., and Field, C. B. (2007). Simulated global changes alter phosphorus demand in annual grassland. *Glob Change Biol.* 13, 2582–2591. doi: 10.1111/j.1365-2486.2007.01456.x

Menge, D. N. L., Hedin, L. O., and Pacala, S. W. (2012). Nitrogen and phosphorus limitation over long-term ecosystem development in terrestrial ecosystems. *PloS One* 7, 1–17. doi: 10.1371/journal.pone.0042045

Nilsson, L., Muller, R., and Nielsen, T. H. (2010). Dissecting the plant transcriptome and the regulatory responses to phosphate deprivation. *Physiol. Plant* 139, 129–143. doi: 10.1111/j.1399-3054.2010.01356.x

Norby, R. J., Warren, J. M., Iversen, C. M., Medlyn, B. E., and McMurtrie, R. E. (2010). CO_2 enhancement of forest productivity constrained by limited nitrogen availability. *Proc. Natl. Acad. Sci. U. S. A.* 107, 19368–19373. doi: 10.1073/pnas.1006463107

Nord, E. A., and Lynch, J. P. (2009). Plant phenology: a critical controller of soil resource acquisition. *J. Exp. Bot.* 60, 1927–1937. doi: 10.1093/jxb/erp018

Norisada, M., Motoshige, T., Kojima, K., and Tange, T. (2006). Effects of phosphate supply and elevated CO_2 on root acid phosphatase activity in *Pinus densiflora* seedlings. *J. Plant Nutr. Soil Sci.* 169, 274–279. doi: 10.1002/jpln.200520558

Palma, D. A., Blumwald, E., and Plaxton, W. C. (2000). Upregulation of vascular H$^{(+)}$-translocating pyrophosphatase by phosphate starvation of *Brassica napus* (rapeseed) suspension cell cultures. *FEBS Lett.* 486, 155–158. doi: 10.1016/S0014-5793(00)02266-3

Pandey, R., Dubey, K. K., Ahmad, A., Nilofar, R., Verma, R., Jain, V., et al. (2014). Elevated CO_2 improves growth and phosphorus utilization efficiency in cereal species under sub-optimal phosphorus supply. *J. Plant Nutr.* 38, 1196–1217. doi: 10.1080/01904167.2014.983116

Pandey, R., Zinta, G., AbdElgawad, H., Ahmad, A., Jain, V., and Janssens, I. A. (2015). Physiological and molecular alterations in plants exposed to high CO_2 under phosphorus stress. *Biotechnol. Adv.* 33, 303–316. doi: 10.1016/j.bioteChadv.2015.03.011

Peñuelas, J., Poulter, B., Sardans, J., Ciais, P., Velde, M. A. D., Bopp, L., et al. (2013). Human-induced nitrogen-phosphorus imbalances alter natural and managed ecosystems across the globe. *Nat. Commun.* 4, 2934. doi: 10.1038/ncomms3934

Péret, B., Clement, M., Nussaume, L., and Desnos, T. (2011). Root developmental adaptation to phosphate starvation: better safe than sorry. *Trends Plant Sci.* 16, 442–450. doi: 10.1016/j.tplants.2011.05.006

Plénet, D., Etchebest, S., Mollier, A., and Pellerin, S. (2000). Growth analysis of maize field crops under phosphorus deficiency. *Plant Soil.* 223, 117–130. doi: 10.1023/A:1004877111238

Reich, P. B., Hobbie, S. E., Lee, T., Ellsworth, D. S., West, J. B., Tilman, D., et al. (2006). Nitrogen limitation constrains sustainability of ecosystem response to CO_2. *Nature.* 440, 922–925. doi: 10.1038/nature04486

Richardson, A. E., Hocking, P. J., Simpson, R. J., and George, T. S. (2009). Plant mechanisms to optimise access to soil phosphorus. *Crop Pasture Sci.* 60, 124–143. doi: 10.1071/CP07125

Ripley, B. D. (1976). The second-order analysis of stationary point processes. *Appl. Probab.* 13, 255–266. doi: 10.1017/S0021900200094328

Rogers, G. S., Payne, L., Milham, P., and Conroy, J. (1993). Nitrogen and phosphorus requirements of cotton and wheat under changing atmospheric CO_2 concentrations. *Plant Soil.* 155, 155–156, 231-234. doi: 10.1007/BF00025026

Ryle, G. J. A., and Stanley, J. (1992). Effects of elevated CO_2 on stomatal size and distribution in perennial ryegrass. *Ann. Bot.* 69, 563–565. doi: 10.1093/oxfordjournals.aob.a088387

Sakurai, G., Lizumi, T., Nishimon, M., and Yokozawa, M. (2014). How much as the increase in atmospheric CO_2 directly affected past soybean production. *Sci. Rep.* 4, 4978. doi: 10.1038/srep04978

Sekiya, N., and Yano, K. (2008). Stomatal density of cowpea correlates with carbon isotope discrimination in different phosphorus, water and CO_2 environments. *New Phytol.* 179, 799–807. doi: 10.1111/j.1469-8137.2008.02518.x

Singh, S. K., Badgujar, G., Reddy, V. R., Fleisher, D. H., and Bunce, J. A. (2013b). Carbon dioxide diffusion across stomata and mesophyll and photo-biochemical processes as affected by growth CO_2 and phosphorus nutrition in cotton. *J. Plant Physiol.* 170, 801–813. doi: 10.1016/j.jplph.2013.01.001

Singh, S. K., Badgujar, G., Reddy, V. R., Fleisher, D. H., and Timlin, D. J. (2013a). Effect of phosphorus nutrition on growth and physiology of cotton under ambient and elevated carbon dioxide. *J. Agro. Crop Sci.* 199, 436–448. doi: 10.1111/jac.12033

Singh, S. K., and Reddy, V. R. (2014). Combined effects of phosphorus nutrition and elevated carbon dioxide concentration on chlorophyll fluorescence, photosynthesis, and nutrient efficiency of cotton. *J. Plant Nutr. Soil Sci.* 177, 892–902. doi: 10.1002/jpln.201400117

Soares, A. S., Driscoll, S. P., Olmos, E., Harbinson, J., Arrabaca, M. C., and Foyer, C. H. (2008). Adaxial/abaxial specification in the regulation of photosynthesis and stomatal opening with respect to light orientation and growth with CO_2 enrichment in the C_4 species *Paspalum dilatatum*. *New Phytol.* 177, 186–198. doi: 10.1111/j.1469-8137.2007.02218.x

Steffen, W. L., and Canadell, J. G. (2005). *Carbon dioxide fertilization and climate change policy. Department of Environment and Heritage* (AGO: Australian Greenhouse Office).

Sun, Y. Q., Yan, F., Cui, X. Y., and Liu, F. L. (2014). Plasticity in stomatal size and density of potato leaves under different irrigation and phosphorus regimes. *J. Plant Physiol.* 171, 1248–1255. doi: 10.1016/j.jplph.2014.06.002

Suter, D., Frehner, M., and Fischer, B. U. (2002). Elevated CO_2 increases carbon allocation to the roots of *Lolium perenne* under free-air CO_2 enhancement but not in a controlled environment. *New Phytol.* 154, 65–75. doi: 10.1046/j.1469-8137.2002.00368.x

Tan, K., Zhou, G. S., and Ren, S. X. (2013). Responses of leaf dark respiration of winter wheat to changes in CO_2 concentration and temperature. *Chin. Sci. Bull.* 58, 1795–1800. doi: 10.1007/s11434-012-5605-1

Taub, D. R., and Wang, X. (2008). Why are nitrogen concentrations in plant tissue lower under elevated CO_2? A critical examination of the hypotheses. *J. Integr. Plant Biol.* 50, 1365–1374. doi: 10.1111/j.1744-7909.2008.00754.x

Vance, C. P., Uhde-Stone, C., and Allan, D. L. (2003). Phosphorus acquisition and use: critical adaptations by plants for securing a nonrenewable resource. *New Phytol.* 15, 423–447. doi: 10.1046/J.1469-8137.2003.00695.X

Wang, S. R., Li, H. S., and Lin, C. X. (2013). Physiological, biochemical and growth responses of Italian ryegrass to butachlor exposure. *Pestic. Biochem. Physiol.* 106, 21–27. doi: 10.1016/j.pestbp.2013.03.007

Wang, X., and Taub, D. R. (2010). Interactive effects of elevated carbon dioxide and environmental stress on root mass fraction in plants: a meta-analytical synthesis using Pair wise techniques. *Oecologia.* 163, 1–11. doi: 10.1007/s00442-010-1572-x

Wissuwa, M., Gamat, G., and Ismail, A. M. (2005). Is root growth under phosphorus deficiency affected by source or sink limitations? *J. Exp. Bot.* 56, 1943–1950. doi: 10.1093/jxb/eri189

Woodward, F. I., Lake, J. A., and Quick, W. P. (2002). Stomatal development and CO_2: ecological consequences. *New Phytol.* 153, 477–484. doi: 10.1046/j.0028-646X.2001.00338.x

Xu, M. (2015). The optimal atmospheric CO_2 concentration for the growth of winter wheat (*Triticum aestivum*). *J. Plant Physiol.* 184, 89–97. doi: 10.1016/j.jplph.2015.07.003

Xu, M. Y., He, Z. L., Deng, Y., Wu, L. Y., Nostrand, J. D. V., Hobbie, S. E., et al. (2013). Elevated CO_2 influences microbial carbon and nitrogen cycling. *BMC Microbiol.* 13, 124. doi: 10.1186/1471-2180-13-124

Yu, J., Chen, L., Xu, M., and Huang, B. R. (2012b). Effects of elevated CO_2 on physiological responses of tall fescue to elevated temperature, drought stress, and the combined stress. *Crop Sci.* 52, 1848–1858. doi: 10.2135/cropsci2012.01.0030

Yu, J., Du, H., and Xu, M. (2012a). Metabolic responses to heat stress under elevated atmospheric CO_2 concentration in a cool-season grass species. *J. Am. Soc Hortic. Sci.* 137, 221–228. doi: 10.21273/JASHS.137.4.221

Zhan, S., Wang, Y., Zhu, Z., Li, W., and Bai, Y. (2017). Nitrogen enrichment alters plant N: P stoichiometry and intensifies phosphorus limitation in a steppe ecosystem. *Environ. Exp. Bot.* 134, 21–32. doi: 10.1016/j.envexpbot.2016.10.014

Zhang, Z., Lu, S., Wang, W., Lepo, J. E., Guan, C., Ismail, A. M., et al. (2017). Effect of elevated atmospheric CO_2 on nitrogen distribution and N utilization efficiency in winter rape (*Brassica napus* L.). *Pak. J. Bot.* 49, 1307–1315. doi: 10.1016/j.aquaculture.2005.05.014

Zhang, L., Yang, Y., and Zhan, X. (2010). Responses of a dominant temperate grass plant (*Leymus chinensis*) to elevated carbon dioxide and nitrogen addition in China. *J. Environ. Qual.* 39, 251–259. doi: 10.2134/jeq2009.0109

Zheng, Y. P., He, C. L., Guo, L. L., Cheng, D. J., Li, F., Peng, Z. P., et al. (2020). Soil water status triggers CO_2 fertilization effect on the growth of winter wheat (*Triticum aestivum*). *Agr. For. Meteorol.* 291, 108097. doi: 10.1016/j.agrformet.2020.108097

Zheng, Y. P., Li, R. Q., Hao, L. H., Cheng, D. J., Wu, H. X., Li, F., et al. (2017). Growth, physiological, and biochemical responses of three grass species to elevated carbon dioxide concentrations. *Pak. J. Bot.* 49. doi: 10.3389/fpls.2015.00321

Zheng, Y. P., Li, F., Hao, L. H., Sheday, A. A., Guo, L. L., Ma, C., et al. (2018). The optimal CO_2 concentrations for the growth of three perennial grass species. *BMC Plant Biol.* 18, 27. doi: 10.1186/s12870-018-1243-3

Zheng, Y. P., Li, F., Hao, L. H., Yu, J. J., Guo, L. L., Zhou, H. R., et al. (2019). Elevated CO_2 concentration induces photosynthetic down-regulation with changes in leaf structure, non-structural carbohydrates and nitrogen content of soybean. *BMC Plant Biol.* 19, 255. doi: 10.1186/s12870-019-1788-9

Zheng, Y. P., Xu, M., Hou, R. X., Shen, R. C., Qiu, S., and Ouyang, Z. (2013). Effects of experimental warming on stomatal traits in leaves of maize (*Zea may* L.). *Ecol. Evol.* 3, 3095–3111. doi: 10.1002/ece3.674

Frontiers in Plant Science

Cultivates the science of plant biology and its applications

The most cited plant science journal, which advances our understanding of plant biology for sustainable food security, functional ecosystems and human health.

Discover the latest Research Topics

See more →

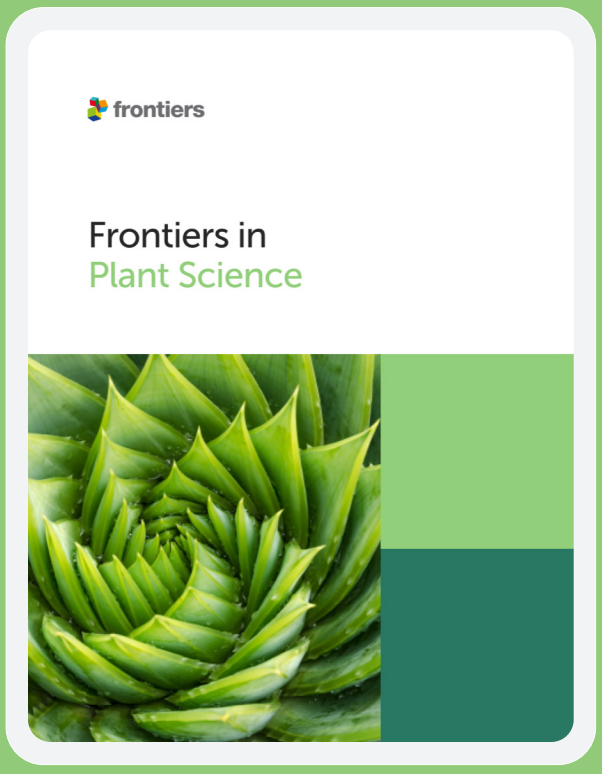

Frontiers

Avenue du Tribunal-Fédéral 34
1005 Lausanne, Switzerland
frontiersin.org

Contact us

+41 (0)21 510 17 00
frontiersin.org/about/contact